Università degli Studi di Urbino Carlo Bo

Department of Biomolecular Sciences

Ph.D. PROGRAMME IN BIOMOLECULAR AND HEALTH SCIENCES

CYCLE XXXVI

REDOX MODULATION OF ADIPOGENESIS:
Clozapine slows down the differentiation process and induces mitochondrial dysfunction by blunting early ROS formation

ACADEMIC DISCIPLINE: BIO/10

Coordinator: Prof. Marco Bruno Luigi Rocchi

Supervisor: Prof. Mara Fiorani

Co-Supervisor: Dr. Lucia Coppo

Ph.D. student: Dr. Giulia Blandino

ACADEMIC YEAR 2022/2023

SUMMARY

ABBREVIATIONS

- 2-Deoxy-D-glucose (2-DG)
- 3-(4, 5-dimethylthiazol-2-yl)-2, 5-diphenyltetrazolium bromide (MTT)
- 3-Isobutyl-1-methylxanthine (IBMX)
- Adipose Tissue (AT)
- Adipose-Derived Stem Cells (ASCs)
- Antioxidant response elements (ARE)
- Body mass index (BMI)
- Brown adipose tissue (BAT)
- CCAAT/enhancer-binding protein α (C/EBPα)
- CCAAT/enhancer-binding protein β (C/EBPβ)
- CCAAT/enhancer-binding protein δ (C/EBPδ)
- Central nervous system (CNS)
- Cholesteryl ester transfer protein (CTEP)
- Clozapine (CLZ)
- Clozapine-N-oxide (CNO)
- Coenzyme Q (CoQ)
- Differentiation medium (DM)
- Dynamin-related protein 1 (DRP1)
- Electron transport chain (ETC)
- Endoplasmic reticulum (ER)
- Estrogen related receptors (ERRs)
- Fission protein 1 (FIS1)
- Forkhead box O3 (FOXO3α)
- Glucocorticoid receptor (GR)
- Glutamate-Cysteine Ligase Catalytic Subunit (GCLC)
- Glutamate-Cysteine Ligase Modifier Subunit (GCLM)
- Glutaredoxins (Grxs)
- Glutathione (GSH)
- Glutathione peroxidase (GPx)
- Glutathione synthase (GS)
- Glutathione-S-transferase (GSTs)
- Heme oxygenase 1 (HO-1)
- Inner mitochondrial membrane (IMM)
- Insulin-like growth factor-1 (IGF-1)
- Kelch-like ECH-associated protein 1 (Keap1)
- Lipoprotein lipase (LPL)
- Metabolic syndrome (MetS)
- Mitochondrial carrier 2-oxoglutarate/malate (2-OGC)
- Mitochondrial DNA (mtDNA)
- Mitochondrial ROS (mtROS)
- Mitochondrial transcription factor A (TFAM)
- Mitochondrial transcription factors B2 (TFB2M)
- Mitofusin-1 (MFN1)

- Mitofusin-2 (MFN2)
- Mitotic clonal expansion (MCE)
- MitoTracker Green (MTG)
- Monocyte chemotactic protein 1 (MCP-1)
- N-acetylcysteine (NAC)
- NAD(P)H Quinone Dehydrogenase 1 (NQO1)
- NADPH-dependent glutathione reductase (GR)
- N-desmethylclozapine (NDC)
- Neuropeptide Y (NPY)
- Nitric oxide synthase (iNOS)
- NADPH oxidases (NOXs)
- Nuclear factor erythroid 2-related factor 2 (Nrf2)
- Nuclear respiratory factors 1 (NRF-1)
- Nuclear respiratory factors 2 (NRF-2)
- Optic atrophy 1 (OPA1)
- Peroxiredoxins (Prxs)
- Peroxisome proliferator activated receptor γ (PPARγ)
- Peroxisome proliferator-activated receptor α (PPARα)
- Peroxisome proliferator-activated receptor δ (PPARδ)
- Phosphodiesterase (PDE)
- Primary mouse embryonic fibroblasts (MEFs)
- Proliferator-activated receptor gamma coactivator −1 α (PGC1α)
- Protein tyrosine phosphatase 1 b (PTP1b)
- Quantitative Real Time PCR (qPCR)
- Reactive oxygen species (ROS)
- Rotenone (ROT)
- Second-generation antipsychotic drug (SGA)
- Stromal vascular fraction (SVF)
- Superoxide dismutase (SOD)
- Tetramethylrhodamine ethyl ester (TMRE)
- Thiazolidinediones (TZDs)
- Thioredoxin interacting protein (Txnip)
- Thioredoxin reductases (TrxRs)
- Thioredoxins (Trxs)
- Trichloroacetic acid (TCA)
- Triglycerides (TG)
- Tumour necrosis factor-α (TNF-α)
- Type 2 diabetes mellitus (T2DM)
- White adipose tissue (WAT)

STRUCTURE AND CONTENTS OF THE THESIS

The dissertation is composed of an abstract; an introduction, that leads the reader into the main topics of the thesis; two chapters relative to previously published articles (chapters 1 and 2); a third chapter containing unpublished data relative to the ongoing research that represents the continuation of the study; conclusions and an appendix including a published paper on *a latere* research project.

During the first period of my PhD course I primarily focused the study on the characterization of the differentiation process of human liposarcoma SW872 cells and identified an early formation of ROS, which is positively correlated to the conversion of preadipocytes into mature adipocytes. This early phase was followed by a late phase characterised, instead, by the generation of mitochondrial ROS and by the onset of mitochondrial dysfunction (chapter 1). Then, during the remaining period of my PhD course I centred my attention on the molecular mechanisms by which clozapine, a second-generation antipsychotic drug, can induce some metabolic effects.

By blunting early ROS formation, clozapine slowed down adipogenesis and anticipated the formation of mitochondrial ROS causing early mitochondrial dysfunction. This event might be critically connected with metabolic syndrome associated pathologies induced by clozapine (chapter 2 and 3).

ABSTRACT

The differentiation process of human SW872 preadipocytes to mature adipocytes is accompanied by morphological changes associated with lipid droplets (LDs) formation and progressive modifications in differentiation markers' expression, as well as by enhanced mitochondrial biogenesis and membrane potential. Under the same circumstances, NADPH oxidase (NOX2)-derived reactive oxygen species (ROS) production was consistent at days 3 and 10 of differentiation and hardly appreciable at day 6. No mitochondrial ROS (mtROS) were detected until the 6th day, most probably owing to the activation of nuclear factor erythroid 2-related factor 2 (Nrf2) antioxidant response. On the contrary, mtROS formation was observed at day 10, along with large cytosolic LDs, oxidation of both cardiolipin and thioredoxin 2, and significant drop in mitochondrial glutathione. Therefore, these results show that the morphological and biochemical changes occurring during the SW872 adipogenic process were paralleled by the discontinuous release of NOX2-derived ROS. The mtROS formation was detected only in the late phase of adipogenesis and has been connected to mitochondrial dysfunction.

The second generation antipsychotic drug Clozapine (CLZ) is considered a 'gold standard' for other treatment-resistant psychosis. However, it shows numerous disabling and serious side-effects which limits its clinical practice, such as an impairment of glucose, insulin, plasma lipid and body fat homeostasis, which can predispose CLZ-treated patients to Type 2 diabetes and cardiovascular disease and eventually to metabolic syndrome (MetS).

Exposure of SW872 differentiating cells to CLZ slowed down adipogenesis and caused an early inhibition (day 3) of the expression of crucial transcription factors implicated in the differentiation process. In addition, CLZ dropped NOX2-derived ROS formation, by both NOX2 inhibition and ROS scavenging mechanisms. This effect had an impact on Nrf2-dependent downstream antioxidant responses, triggering an anticipated mitochondrial superoxide formation, associated with signs of mitochondrial dysfunction.

Regarding this latter issue, the exposure of SW872 cells to CLZ negatively impacted on mitochondrial biogenesis, leading to decreased mitochondrial number and mass unexpectedly associated with an upregulation of the mitochondrial respiratory chain complexes.

Under the same conditions CLZ reduced the cellular ATP levels and affected the compensatory glycolytic response, an effect particularly evident after exposure to complex I inhibitor Rotenone. Finally, the drug impaired the mitochondrial dynamics; indeed under the same conditions a

significant downregulation of the main targets of fission and fusion (DRP1, FIS1, MFN1, MFN2 and OPA1) was detected in CLZ-treated cells.

In conclusion, the results reported in this thesis may help to shed light on the molecular mechanisms explaining some of the adverse metabolic effects induced by CLZ.

INTRODUCTION

1. ADIPOSE TISSUE

1.1 Physiology of adipose tissue

Two types of adipose tissue (AT) are present in mammals: white adipose tissue (WAT) and brown adipose tissue (BAT). WAT is responsible for lipid uptake, synthesis, and storage in the form of triglycerides (TG) [Scherer P.E., 2006]. Moreover, it is now considered also as a metabolic organ which secretes hormones and metabolites in order to regulate the body's energy balance. In fact, AT also play key roles acting as an endocrine and paracrine organ; for instance, it mediates several physiological and pathological functions by secreting factors that control glucose metabolism, appetite, immunological responses, inflammatory responses, angiogenesis, blood pressure regulation and reproductive function [Lefterova and Lazar, 2009; Ali A.T. *et al.,* 2013]. When the organism is under an energy-lacking condition, TG stored in WAT will be mobilised and divided into fatty acids and glycerol, used as an energy source. As mentioned above, WAT also works as a key endocrine organ that secretes adipokines and proinflammatory cytokines, including tumour necrosis factor-α (TNF-α), IL-1β, IL-6, IL-8, IL-10, and monocyte chemotactic protein 1 (MCP-1) under condition of obesity [Scherer P.E., 2006; Ouchi N. *et al.,* 2011; Galic S. *et al.,* 2010]. In addition to adipocytes, WAT are formed by macrophages, fibroblasts, pericytes, blood cells, endothelial cells, smooth muscle cells, mesenchymal stem cells and adipose precursor cells. These cell types are mainly present in the stromal vascular fraction (SVF) which composes 75% of the total cell population [Wang and Hai, 2015].

BAT is present mainly in newborns, protecting against exposure to cold temperature, and largely disappears during childhood [Garruti and Ricquier, 1992]; in addition, it is able also to maintain body temperature by dissipating stored energy as heat [Wang and Hai, 2015]. WAT and BAT have different functions and characteristics [Hansen and Kristiansen, 2006]: for instance, white adipocytes have a major and unilocular lipid droplet which fills the entire cytoplasm of the cells; instead brown adipocytes have several small and multilocular lipid droplets [Wang and Hai, 2015]. Finally, brown adipocytes also contain several mitochondria, in contrast to white adipocytes which contain only a small amount of these organelles [Wang and Hai, 2015].

1.2 Adipogenesis

Adipogenesis is a developmental process in which undifferentiated cells are converted into preadipocytes, then undergoes final differentiation steps becoming mature adipocytes, with the unique feature to contain only one large lipid droplet in their cytoplasm [Ali A.T. *et al.,* 2013].

Molecular mechanisms of adipocyte differentiation have been extensively studied, due to the increasing attention to obesity and other associated pathologies in our society [Ali A.T. *et al.,* 2013]. The possibility to work on these processes in good cellular systems permits detailed studies which are not possible in other models [Ali A.T. *et al.,* 2013]. Indeed, the capability to obtain homogenous populations of cells *in vitro* permits unequivocal responses to treatments, and the presence of stable sources of adipocytes can contribute to facilitating these studies [Ali A.T. *et al.,* 2013]. In literature, there are several evidence showing that 3T3-L1 preadipocytes and 3T3-F442A murine cell line are the mostly used; but they also have disadvantages [Rosen E.D. *et al.,* 2000; Gregoire F.M., 2001; Ali A.T. *et al.,* 2013]. However, in literature there are scarce data based on human preadipocytes [Ntambi and Yung-Cheul, 2000].

Briefly, adipocyte differentiation is divided into four phases, including initial growth arrest, mitotic clonal expansion (MCE), early differentiation, and terminal differentiation [Rosen E.D. *et al.,* 2000; Gregoire F.M. *et al.,* 1998]. As mentioned above, preadipocytes are similar to fibroblasts. After MCE, cells start to accumulate lipids inside their cytoplasm and they convert their shape to a more rounded one, and progressively acquire phenotype of mature adipocytes [Gregoire F.M. *et al.,* 1998; Wang and Hai, 2015]. The phases of the adipogenic differentiation are illustrated in Fig. 1.
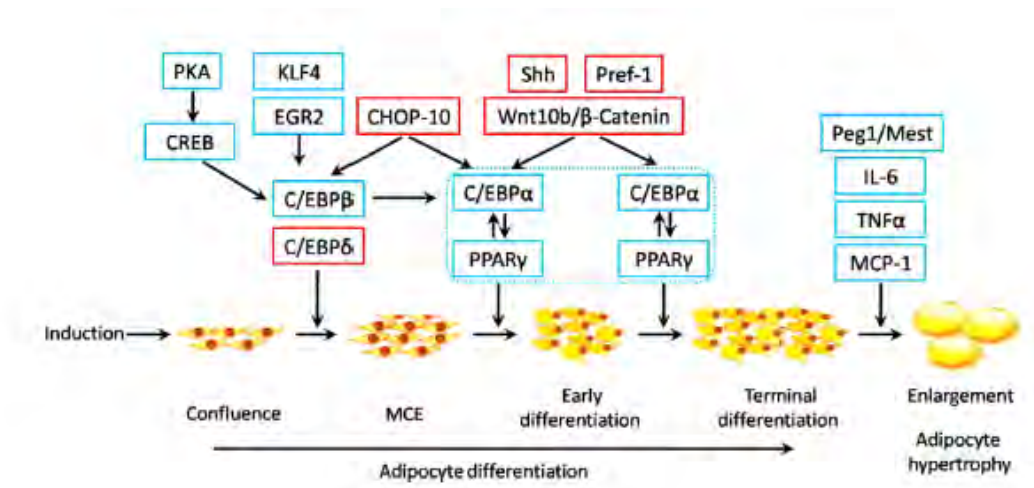

Figure 1. Main signalling network involved in the regulation of adipogenic differentiation [Wang and Hai, 2015]

1.3 Signalling pathways involved in the regulation of adipogenesis

Adipocyte differentiation is made by a complex process in which several transcription factors are involved, regulating a series of adipogenic downstream targets which promote formation of mature adipocytes. The master regulators of the adipogenic program are peroxisome proliferator activated receptor γ (PPARγ) and CCAAT/enhancer-binding protein α (C/EBPα) [Farmer S.R., 2006; Wang and Hai, 2015]. PPARγ is a primary regulator of adipogenesis, and its activation exerts important effects on the regulation of lipid metabolism in adipocytes and glucose homeostasis and adipogenesis in subcutaneous fat [Dutchak P.A. et al. 2012; Zhang Y. et al. 2018]. Moreover, several studies provided evidence supporting the notion that ectopic expression of PPARγ in undifferentiated mouse fibroblasts can initiate, alone, the adipogenic program and formation of mature adipocytes [Tontonoz P. *et al.*, 1994c]. For these reasons, PPARγ is one of the main adipogenic targets evaluated both in *in vitro* and *in vivo* studies [Farmer S.R., 2006]. Two different isoforms of PPARγ are present in adipose cells: PPARγ1, which can be expressed also in other tissues; and PPARγ2, which is mainly located in the AT [Farmer S.R., 2006]. Despite the different localization, both PPARγ1 and PPARγ2 [Mueller *et al.*, 2002] are capable of inducing adipocyte differentiation. Indeed, knockout mice for PPARγ2 developed insulin resistance and exhibited reduced fat formation; however, they still have an amount of adipose tissue, suggesting that PPARγ1 can compensate for PPARγ2 functions [Zhang J. *et al.*, 2004a]. In addition, this evidence supports the notion that PPARγ2 modulates insulin signalling [Farmer S.R., 2006].

The other adipogenic target which plays an important role during adipocyte differentiation is C/EBPα. Freytag *et al.*, showed that ectopic expression of C/EBPα in fibroblasts enhanced adipogenesis [Freytag S.O. *et al.*, 1994]. Moreover, PPARγ modulates adipogenesis in C/EBPα-deficient MEFs, but C/EBPα alone is not able to induce adipogenic program in absence of PPARγ [Rosen E.D. *et al.*, 2002]; suggesting that PPARγ acts as a dominant factor in the differentiation process [Farmer S.R., 2006].

Concerning the early phases of adipocyte differentiation, several research groups tried to investigate the key regulators of these events and established that a cascade of transcription factors leads to expression of PPARγ and C/EBPα [Farmer S.R., 2006]. However, it has been demonstrated in 3T3-L1 the expression of other genes related to C/EBP family, as C/EBPβ and C/EBPδ [Farmer S.R., 2006] at the early phases of the adipogenic process and that they might be key regulators of C/EBPα expression [Cao Z. *et al.*, 1991; Yeh W.C. *et al.*, 1995; Farmer S.R., 2006]. More specifically, some authors highlighted that C/EBPβ induces C/EBPα expression and, both together, they regulate PPARγ expression [Farmer S.R., 2006].

1.4. Adipogenic induction cocktail

To induce the *in vitro* adipogenic differentiation, several studies used a well established differentiation cocktail containing high glucose medium, FBS, glucocorticoids, 3-Isobutyl-1-methylxanthine (IBMX) and insulin. Thiazolidinediones (TZDs), such as rosiglitazone can also be added to the differentiation medium, since they promote and accelerate the adipogenic process [Styner M. et al. 2010; Wang and Hai, 2015].

1.4.1. Glucocorticoids

Dexamethasone is essential for the differentiation process. In fact, glucocorticoids directly bind glucocorticoid receptor (GR) and they translocate into the nucleus promoting the transcription of several genes, including C/EBPδ and C/EBPα [Wu Z. *et al.,* 1996; Tontonoz P. *et al.,* 1994c; Wang and Hai, 2015]. Moreover, some studies showed that glucocorticoids can also regulate the activation of C/EBPβ [Tomlinson J.J. *et al.,* 2006].

1.4.2. IBMX

IBMX is a compound which acts as an inhibitor of phosphodiesterase (PDE) and adenosine receptor antagonist; by increasing cAMP levels, activating PKA and promoting CREB phosphorylation it leads to the C/EBPβ increased expression [Zhang J.W. *et al.,* 2004; Petersen R.K. *et al.,* 2008; Wang and Hai, 2015].

1.4.3. Insulin

Insulin and insulin-like growth factor-1 (IGF-1) are also considered fundamental components of the adipogenic differentiation mixture, since some studies showed that insulin and/or IGF-1 -activated signalling pathway is important for both early and late adipogenesis through direct and indirect block of C/EBPα and PPARγ repressors [Rosen and MacDougald, 2006; Farmer S.R., 2006; Wang and Hai, 2015].

1.5 Cellular models of adipocyte differentiation

The most common cells used for *in vitro* studies on adipose tissue biology derived from rodents, although feline or porcine cells have been utilised [Ruiz-Ojeda F.J. *et al.,* 2016]. These models are particularly useful for understanding the mechanisms of the differentiation process, notwithstanding

their applicability in humans are restricted due to their physiologic and metabolic differences [Lee and Fried, 2014; Ruiz-Ojeda *et al.,* 2016].

Primary preadipocytes are also used as cellular models for studying adipocyte differentiation, showing several advantages with respect to continuous cell lines. Indeed, they can derive from different body depots and from different aged animals, giving the possibility to examine different conditions during the adipogenic process [Hausman G.J. *et al.,* 2014; Ruiz-Ojeda F.J. *et al.,* 2016]. However, it should be kept into consideration that, unlike continuous cell lines, primary cells more closely resemble the physiological conditions of the tissue from which they originated and the general state of the animals from which they are isolated [Wolins N.E. *et al.,* 2006; Ruiz-Ojeda F.J. *et al.,* 2016].

1.5.1 3T3-L1 Mouse Cell Line

The murine 3T3-L1 cells derived from Swiss 3T3 embryos [Green and Meuth, 1974] can be transformed to adipocytes by growing up to 12 days in a conventional differentiation mixture. One of the main advantages of using this cell line is the easy of manipulation and the affordability; moreover, it tolerates an high number of culture passages and provides an homogenous response following treatments and different experimental conditions [Poulos S.P. *et al.,* 2010; Ruiz-Ojeda F.J. *et al.,* 2016]. For all of these reasons, 3T3-L1 cells have been largely used to study the adipogenic process and evaluate the effects of various compounds or nutrients during the adipogenic differentiation [Okabe Y. *et al.,* 2014; Eseberri I. *et al.,* 2015; Patel R. *et al.,* 2013; Chang C.C. *et al.,* 2016].

Nevertheless, this cell model has several limitations due to the long period of differentiation and the inability of reproducing the primary cell features [Wolins N.E. *et al.,* 2006].

1.5.2 Primary mouse embryonic fibroblasts (MEFs)

MEFs originated from totipotent cells of early mouse embryos can differentiate into adipocytes with a variable efficiency (from 10% to 70%), if cultured in appropriate conditions [Rosen and MacDougald, 2006]. Moreover, these cells have a fast rate of proliferation and are easily manipulated [Ruiz-Ojeda F.J. *et al.,* 2016]. Nevertheless, MEFs show some limitations, such as the high percentage of cellular heterogeneity due to their origin [Garfield A.S., 2010].

1.5.3 Adipose-Derived Stem Cells (ASCs)

One of the main cell types present in the SVF of AT is adipose-derived stem cells (ASCs). ASC cells present some peculiar features such as their capability to be subcultured several times, an high expansion ability and the possibility to be cryopreserved for long time periods [Lee and Fried, 2014; Ruiz-Ojeda F.J. *et al.,* 2016]. In the last years, this cellular model has been widely used to evaluate the effect of some compounds during the adipogenic process [Kang I. *et al.,* 2016; Zhao L. *et al.,* 2015]; moreover, it has been used to investigate the role of specific genes on adipocyte differentiation and metabolism [Ruiz-Ojeda F. J. *et al.,* 2016; Ruiz-Ojeda F. J. *et al.,* 2016]. Finally, ASCs are also considered for the assessment of the browning process, since they are capable of conversion from white to brown adipocytes [Pisani D.F. *et al.,* 2011].

1.5.4 Human liposarcoma cell line SW872

Human liposarcoma cell line (SW872) has been developed quite recently and it represents an interesting cell model to induce the adipogenic differentiation process [Olivieri C. *et al.,* 2022]. SW872 cells are preadipocytes, which express several genes related to fatty acid metabolism, as lipoprotein lipase (LPL), cholesteryl ester transfer protein (CTEP), CD36 and PPARγ [Wassef H. *et al.,* 2004].

It is reported that the addition of 100 μM oleic acid alone to the SW872 cell culture medium stimulates the PPARγ transcription factor, which induces specific genes and thus stimulates adipocyte differentiation [Cicolari S. *et al.,* 2020]. However, other studies use traditional cocktails to induce the adipocyte differentiation [Fiorani M. *et al.,* 2021].

2. OXIDATIVE STRESS AND ADIPOGENESIS

Oxidative stress is triggered by a perturbation in the equilibrium between ROS production and their elimination by antioxidant defence systems. In the cells, ROS are mainly generated in the mitochondria by the electron transport chain (ETC) [Starkov A.A., 2008; Murphy M.P., 2009]; other cellular sites of ROS generation are NADPH oxidases (NOXs), nitric oxide (NO) synthases, Fenton reaction, microsomal cytochrome p450 oxidases, peroxisomal β-oxidation, prostaglandin synthesis and others [Halliwell B., 2006; Hohn A. *et al.,* 2013]. The electron transfer in the ETC produces superoxide (O_2^-) and other products and complexes I and III are considered the main source of ROS. In addition, under specific conditions, complex II and other sources can contribute to this pool [Masschelin P.M. *et al.,* 2020]. O_2^- is the most common ROS produced by the cells that

can react with Fe-containing proteins to generate hydrogen peroxide (H_2O_2). H_2O_2 is stable for a long time (up to minutes in solution but, *in vivo*, the half-life is shorter due to the presence of reducing enzymes) and can participate in various cellular signalling pathways [Castro J.P. *et al.*, 2016]. For instance, H_2O_2 can accumulate inside the cells contributing to the adipogenic and metabolic imbalance, leading to an excess of nutrients and onset of insulin resistance [Masschelin P.M. *et al.*, 2020; Anderson E.J. *et al.*, 2009; Akl M.G. *et al.*, 2017; Fazakerley D.J. *et al.*, 2018]. The homeostatic systems that balance oxidative stress inside cells are repressed in the condition of obesity, due to the accumulation of these oxidised molecules in WAT pool [Masschelin P.M. *et al.*, 2020]. Indeed, excessive ROS production damages DNA, lipids and proteins through direct and indirect pathways [Grimsrud P.A. *et al.*, 2008; Davies M.J., 2016]. More specifically, ROS can react with lipids and generate lipid aldehydes that can modify DNA, RNA, proteins and other lipid species [Esterbauer H. *et al.*, 1991; Uchida K., 2003]. Highly reactive hydroxyl radicals ($OH^.$) can also be generated when an excess of H_2O_2 reacts with ferrous iron [Masschelin P.M. *et al.*, 2020]. $OH^.$ has a very short half-life (about few nanoseconds) resulting in an immediate reaction after its formation causing damage on nearby biomolecules [Stadtman and Levine, 2000].

The production of ROS seems to play an important role in several cellular events, including adipocyte differentiation. Mouche *et al.*, showed that preadipocytes have lower production of extracellular and intracellular ROS in comparison with adipocytes [Mouche S. *et al.*, 2007]. Indeed, mouse 3T3-L1 cells display an increased ROS production that is abolished after treatment with the antioxidant agent N-acetylcysteine (NAC) [Hou Y. *et al.*, 2012]. OP6 pre-adipocyte cell model, after differentiation, showed an increased ROS formation in the cytosolic compartment, in parallel with lipid accumulation [Saitoh Y. *et al.*, 2010]. C/EBPβ and PPARγ, the main regulators of adipogenesis, are also involved in the adipogenic function of ROS. It has been shown that ROS induce adipogenesis by stimulating the induction of C/EBPβ [Hou Y. *et al.*, 2012]. More specifically, ROS activate C/EBPβ and the consequent DNA-binding activity [Tang and Lane, 2012]. Finally, there is evidence showing that when 3T3-L1 cells were treated with H_2O_2, adipogenesis was enhanced through the expression of PPARγ [Lee H. *et al.*, 2009].

The impact of oxidative stress on the adipocyte function is illustrated in Fig. 2.
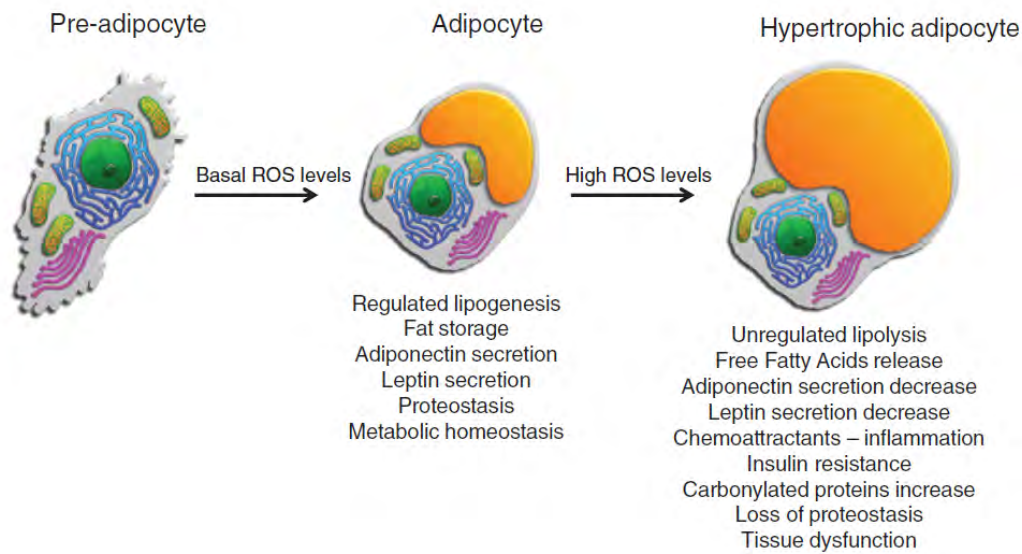
Figure 2. Effect of oxidative stress in adipose tissue [Castro J.P. *et al.*, 2016]

2.1 NADPH oxidases and adipocyte differentiation

2.1.1 General structure of NADPH oxidases

As mentioned before, in addition to mitochondria, several other enzymes can generate ROS, including NOXs, xanthine oxidase, nitric oxide synthase, and others [Soberman R.J., 2003; Lambeth J.D., 2004; Boveris and Chance, 1973; Turrens J.F. *et al.,* 1985].

NOXs are membrane-bound enzymes responsible for the single-electron reduction of O_2 to produce ROS, such as O_2^{-} and H_2O_2 [Brandes R.P. *et al.,* 2014]. As shown in Fig. 3, in *Homo sapiens*, the NOX family is made up of 7 members (or isoforms): NOX-1 to NOX-5 and Dual oxidase 1 (Duox1) and Duox2 [Brandes R.P. *et al.,* 2014; Nazari B. *et al.,* 2023]. NOXs are multi-subunit enzymes composed of two integral membrane proteins gp91^{phox} and p22^{phox} (corresponding to the heterodimeric cyt b$_{558}$) and cytosolic regulatory subunits p40^{phox}, p47^{phox}, p67^{phox} and Rac1/2 [Dang P.M. *et al.,* 2001; Babior B.M., 2004]. The NOX isoforms show different cellular localization and activation mechanism, but they share similar catalytic subunits [Vermot A. *et al.,* 2021]. NOX-2 was the first NOX isoform identified in mammalian peripheral blood phagocytes [Gabig and Babior, 1979]. Moreover, it has been shown to be relevant in immune defence, leading to the

destruction of pathogens through ROS production [Vermot A. et al. 2021]. Although its effect on innate immunity, NOX-2 has known to participate to various cellular processes, such as signalling transduction, angiogenesis or cell death [Ray P.D. *et al.*, 2012; Lamberth and Neish, 2014; Nathan and Cunningham-Bussel, 2013; Parvez S. *et al.,* 2018; Bedard and Krause, 2007]. NOX1 is considered the predominant isoform in the colon, prostate, uterus and vascular cells [Suh Y.A. *et al.,* 1999; Banfi B. *et al.,* 2001; Krause K.H., 2004]. NOX3 is typically expressed in the inner ear, in fact its expression in cochlea produces ROS that has been linked to hearing loss [Rybak L.P. *et al.,* 2012], while NOX3 located in the vestibule produces ROS involved in gravity perception [Krause K.H., 2004]. Low expression of NOX3 has also been identified in the brain and lungs, but the function in these tissues is still unclear [Cooney S.J. *et al.,* 2013; Zhang X. *et al.,* 2006; Ruwanpura S.M. *et al.,* 2006].

Under resting conditions, the heterodimeric cyt b_{558} does not interact with the cytosolic subunits. Upon stimulation, the cytoplasmic subunit p47[phox] is rapidly phosphorylated and gets in contact with p67[phox]. This complex migrates to the cell membrane and interacts with cyt b_{558} to form the active enzyme able to produce superoxide anion [Ago T. *et al.,* 1999; Groemping Y. *et al.,* 2003; Nakanishi A. *et al.,* 1992].
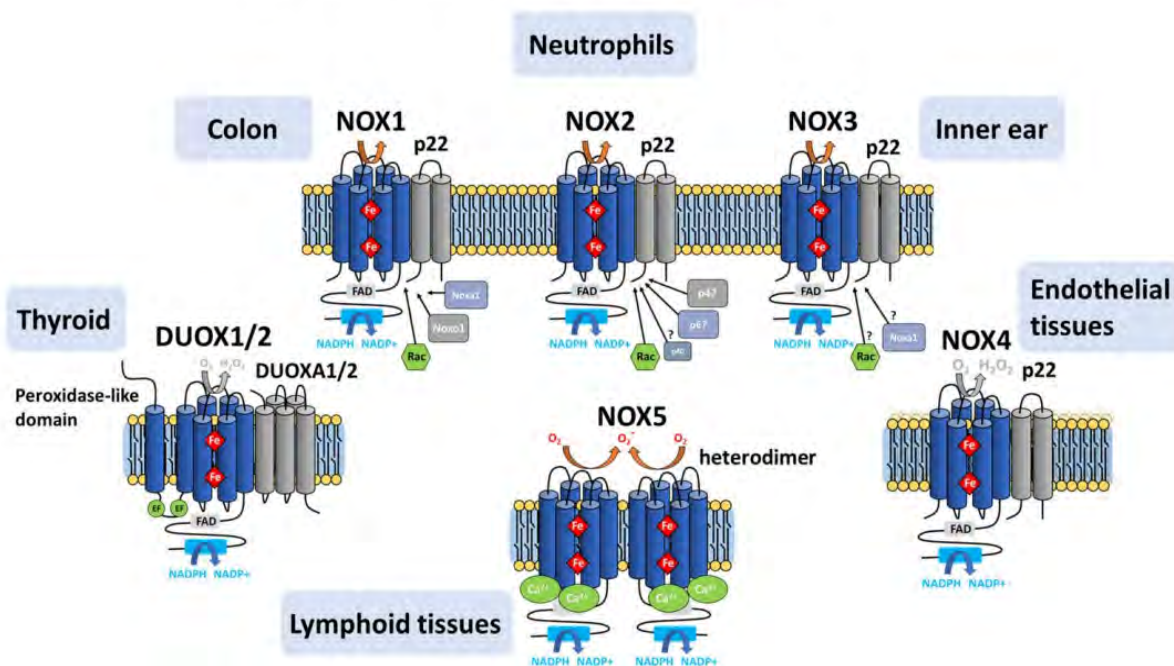

Figure 3. Illustration of the NADPH oxidase isoforms [Vermot A. *et al.,* 2021]

2.1.2 NADPH oxidases and adipogenesis

Among the different NOXs, NOX-4 is the most studied in adipocytes [Mahadev K. *et al.,*2004; Schroder K. *et al.,* 2009]. Only few reports deal with the changes in NOX-1 and 2 expressions during adipogenic programs [Sautin Y.Y. *et al.,* 2007; Schroder K. *et al.,* 2009]. It has been reported that, during adipocyte differentiation, NOX-4 mediates H_2O_2 production and the consequent stimulation of insulin signalling, through the inhibition of the protein tyrosine phosphatase 1 b (PTP1b), which promotes insulin receptor activation and glucose uptake [Mahadev K. *et al.,* 2004]. In addition, in preadipocytes, NOX-4-derived H_2O_2 increases insulin response through Akt activation, mediating the conversion of preadipocytes to mature adipocytes [Schroder K. *et al.,* 2009]. Moreover, some studies show that NOX-4 and p47[phox] are involved in the adipogenic differentiation; however, the exact role of NOX-4 during adipogenesis is yet to be clarified [Wang and Hai, 2015]. In conclusion, the available data show the involvement of NOXs and the consequent ROS formation during adipocyte differentiation, but which NOX isoform is involved in this process is currently unclear [Wang and Hai, 2015].

2.2 Antioxidant systems and adipocyte differentiation

The antioxidant machinery counteracts ROS and oxidant stimuli catalysing a series of redox reactions inside the cells. The most important antioxidant systems involved in the regulation of the adipogenic differentiation are illustrated in Fig. 4.
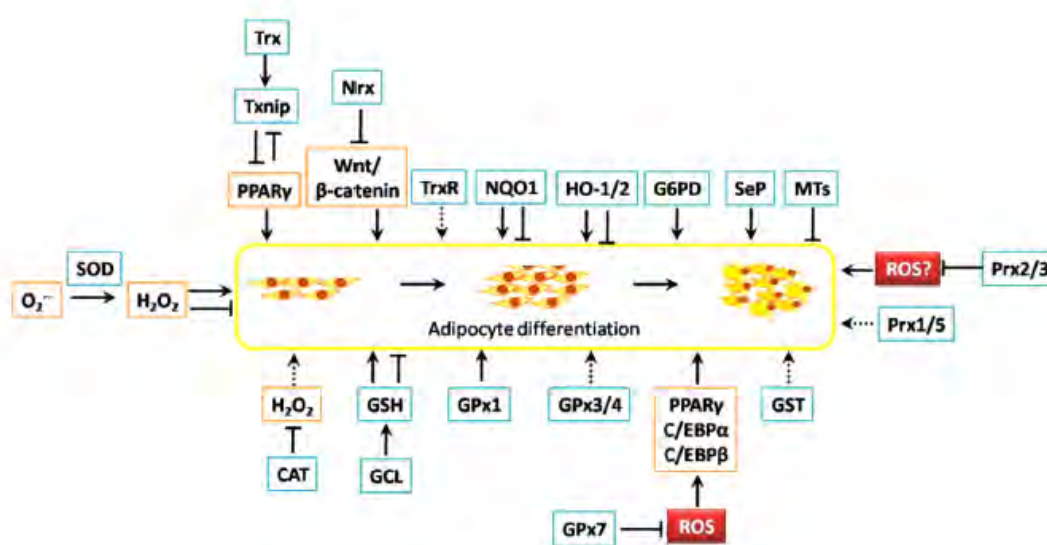

Figure 4. Effect of antioxidant system on adipogenic differentiation [Wang and Hai, 2015]

19

2.2.1 Nuclear factor erythroid 2-related factor 2 (Nrf2) and adipogenesis

Nrf2 is one of the most studied antioxidant transcription factors. In basal conditions, Nrf2 is totally inactivated by Kelch-like ECH-associated protein 1 (Keap1) which binds Nrf2 for the proteasomal degradation. In response to stimuli, Nrf2 binds the antioxidant response elements (ARE) encoding for more than 100 genes involved in response to oxidative stress [Wang X. *et al.,* 2011; Sporn and Liby, 2012]. Nrf2 can also regulate enzymes such as superoxide dismutase (SOD) and nitric oxide synthase (iNOS) [Zhu H. *et al.,* 2005; Dinkova-Kostova A.T. *et al.,* 2005]. The most important redox targets regulated by Nrf2 are: NAD(P)H Quinone Dehydrogenase 1 (NQO1), Glutamate-Cysteine Ligase Catalytic Subunit (GCLC), Glutamate-Cysteine Ligase Modifier Subunit (GCLM), glutathione peroxidase (GPx), NADPH-dependent glutathione reductase (GR), SOD, heme oxygenase 1 (HO-1), catalase, thioredoxins (Trxs), thioredoxin reductases (TrxRs) and peroxiredoxins (Prxs) [Zhu H. *et al.,* 2005; Kwak M.K. *et al.,* 2003; Wang and Williamson, 1994; Nguyen T. *et al.,* 2003; MacLeod A.K. *et al.,* 2009]. Since Nrf2 is involved in the regulation of the glutathione (GSH) synthesis, cellular GSH follows the same pattern of activation [Hou Y. *et al.,* 2012]. Moreover, several studies demonstrate that Nrf2 is not fundamental only for the antioxidant system, but it is involved also in other processes and conditions, such as the innate immunity response [Reddy N.M. *et al.,* 2009; Thimmulappa R.K. *et al.,* 2006], protection against inflammation [Innamorato N.G. *et al.,* 2008; Ruiz S. *et al.,* 2013], insulin resistance, diabetes [Aleksunes L.M. *et al.,* 2010] and cancer [Pearson K.J. *et al.,* 2008].

Regarding the role of Nrf2 during adipogenesis, results from studies employing Nrf2-KO (Nrf2$^{-/-}$) and WT (Nrf2$^{+/+}$) preadipocytes derived from mouse WAT [Hou Y. *et al.,* 2012] and knockdown 3T3L1 cells [Pi J. *et al.,* 2010] showed that this factor enhances adipogenesis by the transcriptional regulation of adipogenic genes, such as C/EBPβ, PPARγ1 e PPARγ2. Indeed, in conditions in which Nrf2 expression is lowered, the mRNA level of these adipogenic transcription factors is significantly less in comparison with control groups [Hou Y. *et al.,* 2012]. Moreover, Keap1 knockdown cells showed an opposite response, since C/EBPβ and PPARγ1 were rapidly activated [Hou Y. *et al.,* 2012].

However, other studies reported that Nrf2 could also have a negative impact on the regulation of the adipogenic program. Adipogenesis was inhibited in Keap1$^{-/-}$-primary MEFs in comparison with WT MEFs [Shin S. *et al.,* 2007]. Moreover, it was reported that an high fat diet diminished the Nrf2 expression and its related genes, as NQO1 and GSTm6 [Tanaka Y. *et al.,* 2008] and that Nrf2 slowed down lipid accumulation in mouse liver after a high fat diet treatment [Tanaka Y. *et al.,* 2008].

In conclusion, Nrf2 is an important transcription factor which regulates the main cellular antioxidant system and also the differentiation process; however, the mechanism by which Nrf2 modulates the adipocyte differentiation needs to be further examined [Wang and Hai, 2015].

2.2.2 Glutathione (GSH) and adipogenesis

GSH (γ-L-glutamyl-L-cysteinyl-glycine), is the main hydrophilic antioxidant present in cells. The glutamate-cysteine ligase (GCL) is the rate-limiting enzyme for the synthesis of GSH starting from cysteine, glutamate and glycine, in parallel with glutathione synthase (GS) [Wang and Hai, 2015; Lu S.C., 2013]. GCL is composed of a catalytic subunit (GCLC) and a modifier subunit (GCLM). The synthesis of GSH, starting from its constituent amino acids, involves two enzymatic reactions that require ATP.

The main function of GSH in the cells is to eliminate radicals in a non-enzymatic reaction as well as to be cofactor in enzymatic cycles; for example the reduction of hydroperoxides by GPx requires GSH [Wang and Hai, 2015]. In addition, glutathione-S-transferase (GSTs) is involved in the detoxification of xenobiotics by conjugating a molecule of GSH to non-polar substrates [Hayes J.D. *et al.,* 2005]. After these reactions, GSH is converted into GSSG (the oxidised form of GSH) or GSSR (the glutathionylated form of GSH). Glutathionylation is a reaction involving the binding of GSH to a reactive cysteine in proteins [Dominko and Dikic, 2018; Grek C.L. *et al.,* 2013; Scalcon V. *et al.,* 2022]. Glutaredoxins (Grxs) are enzymes controlling this reversible process. In fact, Grx has been discovered to regulate both the formation of the mixed disulphide between protein cysteine and GSH and catalyse the reverse oxido-reduction. The two principal and most studied dithiol isoforms of mammalian Grxs are Grx1, that mainly exists in the cytoplasm, and Grx2, which localises to mitochondria, cytoplasm or nucleus depending on gene splicing. More specifically, cysteine residues of mitochondrial proteins are more susceptible to Grx2 mediated glutathionylation [Scalcon V. *et al.,* 2022; Hurd T.R. *et al.,* 2005], facilitating the glutathionylation/de-glutathionylation of some target proteins [Scalcon V. *et al.,* 2022]. Two isoforms of Grx2 are present in cells: Grx2a (mitochondrial) and Grx2c (cytosolic) [Hudemann C. *et al.,* 2009; Lonn M.E. *et al.,* 2008; Scalcon V. *et al.,* 2022]. As reported by Scalcon V. *et al*, in absence of mitochondrial Grx2, mice fed with a standard diet showed a spontaneous increase in body weight and accumulation of lipid droplets in liver in comparison with WT, suggesting that this protein could be involved in some early changes in the lipid metabolism, which is associated with

the pathogenesis of metabolic dysfunction-associated fatty liver disease (MAFLD) [Scalcon V. *et al.,* 2022; Eslam M. *et al.,* 2020].

In particular, it has been reported that, in comparison with WT, GSH level is higher in adipose tissue of ob/ob mice [Kobayashi H. *et al.,* 2009]; and depletion of GSH in mice prevents diet-induced obesity [Findeisen H.M. *et al.,* 2011]. In line with this evidence, NAC decreases ROS level and slowed down adipocyte differentiation in 3T3-L1 cells [Lee H. *et al.,* 2009; Calzadilla P. *et al.,* 2011; Kim J.R. *et al.,* 2006; Cho K.J. *et al.,* 2003]; probably due to the inhibition of C/EBPβ and PPARγ [Kim J.R. *et al.,* 2006]. GCL expression modulates the adipocyte differentiation in ob/ob mice [Kobayashi H. *et al.,* 2009].

GPx1, 3, 4 and 7 are highly expressed during adipocyte differentiation [Kobayashi H. *et al.,* 2009]; it was observed an increased GPx activity in conditions in which lipid accumulation occurred [Caldazilla P. *et al.,* 2011]. For instance, mice overexpressing GPx1 are more susceptible to hyperglycemia, hyperinsulinemia and obesity [McClung J.P. *et al.,* 2004]; moreover, the increase in GPx3 expression is required for the PPARγ-mediated antioxidant effects [Chung S.S. *et al.,* 2009]. GPx system seems to be involved in regulation of early adipogenic marker such as C/EBPβ, since GPx7 deficiency stimulates C/EBPβ expression through the PKA signalling pathway which is also dependent on ROS production [Chang Y.C. *et al.,* 2013]. In addition, GPx7 deficiency promotes the expression of some of the key transcription factors which regulate the early and late adipogenesis, such as C/EBPβ, PPARγ and C/EBPα [Chang Y.C. *et al.,* 2013].

2.2.3 Thioredoxin (Trx) system and adipogenesis

The Trx system is composed of NADPH, Trx and TrxR. TrxR reduced the oxidised form of Trx. A member of the Trx family, the thioredoxin interacting protein (Txnip) is a negative modulator of the Trx [Wang and Hai, 2015]. This antioxidant system can be modulated during adipocyte differentiation and several studies described its role during the adipogenic program [Wang and Hai, 2015]. For instance, Rajalin *et al.,* showed that during the differentiation of 3T3-L1 cells TrxR1, TrxR2 and Trx2 protein levels were up-regulated [Rajalin A.M. *et al.,* 2014]. In case of Txnip protein, it has been shown to decrease during the first minutes after hormonal stimulation, suggesting that its degradation appears to be important for regulating the differentiation process [Chutkow and Lee, 2011]. Same results have been reported by Chutkow *et al.,* where in

Txnip-silenced preadipocytes and Txnip$^{-/-}$ MEFs, adipogenesis was clearly enhanced, whereas its overexpression impaired adipocyte differentiation [Chutkow W.A. *et al.,* 2010].

It has been observed that in MEFs, TrxR1 can influence glucose and lipid metabolism. This cell line can be differentiated into osteocytes, chondrocytes and adipocytes depending on the hormonal induction [Saeed H. *et al.,* 2012]. For instance, Peng X *et al.,* demonstrated that Txnrd1$^{-/-}$ MEFs show more propensity to undergo adipogenesis compared to the parental cells that have Txnrd1 gene [Peng X. *et al.,* 2016]. In fact, Txnrd1 depletion causes an acceleration of the mitotic clonal expansion and insulin signalling was also modulated after the induction of the differentiation process. Moreover, it has been shown that in absence of Txnrd1, the expression of PPARγ was higher than the parental cells; and this increase was even much more in presence of the differentiation stimuli [Peng X. *et al.,* 2016].

3. ANTIPSYCHOTIC DRUGS

3.1 Mechanism of action of antipsychotic drugs

Antipsychotics are drugs used for psychiatric and non-psychiatric disorders. The main molecular mechanism, apart from aripiprazole, is based on the blockage of D_2 receptors [Cikankova T. *et al.,* 2019]. The antagonism of this receptor in the mesolimbic region is responsible for the positive symptoms of schizophrenia; whereas the non-specific occupation of D_2 in central nervous system (CNS) causes a series of side effects, related to extrapyramidal syndrome and hyperprolactinemia [Stępnicki P. *et al.,* 2018]. This class of drug is divided into first generation (or typical) and second generation (or atypical) antipsychotic drugs.

First generation antipsychotic (FGAs) drugs antagonise mainly D_2 receptors in cortical and striatal areas of the brain; whereas second generation antipsychotic (SGAs) have a higher affinity for several systems (5-HT, dopamine, muscarinic, adrenergic and histamine receptors) [Kapur and Seeman, 2021; Seeman P., 2002]. These drugs are represented by clozapine (CLZ), olanzapine, zotepine and quetiapine. Aripiprazole differs for the partial agonism at D_2 receptors [Bolonna and Kerwin, 2005]; acting as a partial $5-HT_{1A}$ receptor agonist and $5-HT_{2A}$ receptor antagonist [Cikankova T. *et al.,* 2019]. Although SGAs are well tolerated, several side effects were also observed in patients treated with these drugs. For instance, hyperglycemia, dyslipidemia, weight gain and hypertension are the major risk factors of MetS [Masand P.S. *et al.,* 2005]. Furthermore, QT interval prolongation and cardiac effects were also observed [Cikankova T. *et al.,* 2019].

CLZ is the preferred drug used for the treatment of resistant psychosis [Swartz M.S. *et al.,* 2008; Remington G. *et al.,* 2017; Remington G. *et al.,* 2016; Lee L.H.N. *et al.,* 2018; Honer W.G. *et al.,* 2009], probably due to its unique and complex mechanism of action [Kim D.D. *et al.,* 2018]. Indeed, CLZ decreases violent behaviour in patients with schizophrenia [Frogley C. *et al.,* 2012; Grazler and Dickson, 1998]; but unfortunately, it is associated with an increased risk of immune, cardiovascular, metabolic and psychiatric complications. In fact, some adverse effects are related to neutropenia/agranulocytosis [Mijovic and MacCabe, 2020], myocarditis/cardiomyopathy, tachycardia [Yuen J.W.Y. *et al.,* 2018; Kim D.D. *et al.,* 2018; Kim D.D. *et al.,* 2017] and obsessive-compulsive symptoms [Kim D.D. *et al.,* 2020; Kim D.D. *et al.,* 2019].

3.2 Definition of Metabolic Syndrome

The clinical definition of MetS is based on the onset of several pathologies which include insulin resistance, obesity, cardiovascular anomalies, hypertension, dysglycemia and dyslipidemia [Alberti K.G. *et al.,* 2005]. Moreover, it also includes abnormalities in coagulation and inflammation [Grundy S.M., 2016]. In a clinical point of view, these metabolic risk factors are not considered for a diagnosis of MetS; therefore this diagnosis is made if three on the five following criteria are present: 1) waist circumference $\geq$ 102 cm in men and 88 cm in women; 2) triglyceride levels $\geq$ 150 mg/dl; 3) HDL cholesterol below 40 mg/dl in men and 50 mg/dl in women; 4) hypertension (blood pressure $\geq$ 130/85 mm Hg) and 5) glucose levels $\geq$ 100 mg/dl [Grundy S.M., 2004; Yuen J.W.Y. *et al.,* 2021].

3.3 Clozapine-induced Metabolic Syndrome

The propensity of CLZ to cause weight gain and obesity is already documented in several papers [Lamberti J.S. *et al.,* 2006; Allison and Casey, 2001]. For instance, in comparison with other antipsychotics, CLZ can induce the largest amount of weight gain during the first year of treatment, and the 30.5% of patients develop Type 2 diabetes mellitus (T2DM) after 46 months [Henderson D.C. *et al.,* 2000]. Consequently, significant weight gain can predispose patients to cardiovascular disease [Nasrallah H., 2003; Hubert H.B. *et al.,*1983]. Several risk factors can alter this response in patients such as sex, smoking status and baseline levels of body mass index (BMI) [Lau S.L. *et al.,* 2016].

Another theory regarding the CLZ-induced MetS consists in the inflammatory hypothesis, since there is some evidence showing that CLZ increases production of proinflammatory cytokines in insulin-responsive cells [Contreras-Shannon V. *et al.,* 2013]. Indeed, alterations in the levels of cytokines such as IL-6, TNF-α and adipokines as adiponectin, leptin and resistin, have been linked to these metabolic alterations [Klemettilä J.P. *et al.,* 2014; Klemettilä J.P. *et al.,* 2017].

Complexity in CLZ's pharmacology, related to blockage of multiple receptors, could contribute to the development of these effects, and H_1 receptor plays an important role in this process [Kroeze W.K. *et al.,* 2003]. Moreover, CLZ also affects release of hormones related to obesity as ghrelin and neuropeptide Y (NPY), since CLZ-treated patients show higher serum ghrelin levels compared to control groups [Esen-Danaci A. *et al.,* 2008]. Indeed, this imbalance in ghrelin release has been related to the action of receptors such as H_1, serotonin ($5HT_{2A}/_{2C}$) and dopamine (D_2) receptors [Esen-Danaci A. *et al.,* 2008].

In general, drugs which are used in co-treatment with CLZ may target only one or more symptoms associated to MetS, for example metformin is efficient for the treatment of obesity, hyperglycemia and hypertriglyceridemia [Siskind D.J. *et al.,* 2016].

As mentioned above, dyslipidemia has been considered as one of the diagnostic criteria for the MetS [Alberti K.G. *et al.,* 2005; Grundy S.M., 2004]. However, several studies showed that CLZ increased serum triglyceride levels in patients [Kim D.D. *et al.,* 2019; Whitney Z. *et al.,* 2015; Henderson D.C. *et al.,* 2005; Gaulin B.D. *et al.,* 1999; Procyshyn R.M. *et al.,* 2007], which can be independent of weight gain [Procyshyn R.M. *et al.,* 2007; Newcomer J.W., 2007].

Some options for treating CLZ-induced dyslipidemia are related to the use of statins [Tse L. *et al.,* 2014; Landry P. *et al.,* 2008]. In addition, peroxisome proliferator-activated receptor α (PPARα) agonists can manage the increase in circulating triglycerides and the decrease in HDL cholesterol [Berger J.P. *et al.,* 2005]. In conclusion, the mechanism by which CLZ induced dyslipidemia is still unknown, but there is some evidence showing that the activity of sympathetic nervous system can contribute to glucose dysregulation and also cardiovascular abnormalities [Bravo E.L.,1989; Tentolouris N. *et al.,* 2008; Boyda H.N. *et al.,* 2013].

3.4 Antioxidant properties of antipsychotic drugs

As mentioned above, SGAs show better efficiency in the management of positive symptoms, with few side effects [Seeman P., 2002]. In case of Risperidone, there are some data showing that in

adolescent mice, it was capable to inhibits iNOS expression and increase catalase and SOD activity in some brain areas [Casquero-Veiga M. *et al.,* 2019; Caruso G. *et al.,* 2020]. In addition, the antioxidant activity of Risperidone can be due to the ability to increase GSH levels and, at the same time, to decrease pro-oxidant effects of extracellular glutamate [Quincozes-Santos A. *et al.,* 2010; Caruso G. *et al.,* 2020]. In case of CLZ, a study published by Hendouei *et al.*, show that CLZ acts as a better antioxidant than Risperidone and Perphenazine, by increasing SOD and GSH serum levels and by reducing lipid peroxidation, another important marker of oxidative stress [Hendouei N. *et al.,* 2018]. The antioxidant effects of CLZ and Olanzapine are considered clinically relevant, since there is some evidence showing a lower risk to oxidative stress-induced damage, such as neurological symptoms observed in schizophrenic patients treated with SGAs [Singh O.P. *et al.,* 2008; Dietrich-Muszalska A. *et al.,* 2013; Caruso G. *et al.,* 2020]. Moreover, it has been suggested that their antioxidant activity can be due to the amino group part of their chemical structure [Brinholi F.F. *et al.,* 2016]. Other works provided evidence showing that the serotonergic metabolite 5-hydroxyindoleacetic acid could be the effective scavenger of hydroxyl and superoxide radicals which also contrasts lipid peroxidation [Blakely R.D. *et al.,* 1984]. Based on the above findings, we can conclude that these two drugs are considered the most effective for their ability to scavenge O_2^-, one of the main ROS [Brinholi F.F. *et al.,* 2016; Ribaudo G. *et al.,* 2020].

However, Shin *et al.* demonstrate a possible mechanism showing the involvement of CLZ on ROS production and oxidative stress; providing evidence on the inhibition of proton currents in microglia, essential for the maintenance of NADPH oxidase activity [Shin H. *et al.,* 2015; Caruso G. *et al.,* 2020]. Moreover, only CLZ was able to inhibit microglial proton currents in the brain at therapeutic doses [Caruso G. *et al.,* 2020]. In addition, also its metabolites can protect neurons from oxidative stress. In fact, Clozapine-N-oxide (CNO) and N-desmethylclozapine (NDC) were able to inhibit microglial NADPH oxidase [Jiang L. *et al.,* 2016]. In addition, some authors demonstrate that SGAs have a "local antioxidant action" in proximity to dopaminergic and serotonergic receptors, since their increasing concentration close to these receptors, resulting in a protective action against oxidation, nitration and chlorination of receptors themselves [Sadowska-Bartosz I. *et al.,* 2016].

4. SECOND-GENERATION ANTIPSYCHOTIC DRUGS, MITOCHONDRIAL DYSFUNCTION AND METABOLIC SYNDROME

4.1 Physiology of mitochondria

Mitochondria are small organelles which are formed by an outer mitochondrial membrane (OMM) and an inner mitochondrial membrane (IMM) separated by an intramembranous space [Prasun P., 2020]. As well known, mitochondria are considered the powerhouse of the cells, because of the ATP production, which corresponds to 90% of the total cellular ATP [Spinelli and Haigis, 2018]. ETC is located in the IMM and is composed of five complexes, Complex I to V [Prasun P., 2020]. Complex I receives electrons from NADH, while Complex II from $FADH_2$. Complex I and II donate electrons to coenzyme Q (CoQ) [Alcazar-Fabra *et al.,* 2016]. CoQ transfers electrons to Complex III which reduces cytochrome C (part of Complex III) that gets oxidised by Complex IV [Prasun P., 2020]. In the final part, electrons passed on to oxygen through Complex IV forming water. The electron flow along the respiratory chain creates free energy that is released and utilised for pump electrons, creating a proton gradient across the IMM [Sun F. *et al.,* 2013; Kühlbrandt W., 2015]. Finally, energy release from the proton is utilised to produce ATP from ADP by complex V (ATP synthase),[Watt I.N. *et al.,* 2010]. This event is called oxidative phosphorylation (OXPHOS) [Schatz G., 1967].

As mentioned in the previous paragraphs, mitochondria are also an important source of ROS [Brookes P.S., 2005]. Indeed, a small portion of electrons can directly reach oxygen and react with this, producing superoxide radicals [Prasun P., 2020]. Superoxide radicals can be converted to H_2O_2, which can be transformed through Fenton reaction into high reactive molecules such as hydroxyl radicals, that are considered deleterious for membranes, proteins, enzymes and DNA [Lipinski B., 2011]. To counteract this phenomenon, mitochondria have efficient antioxidant systems, such as SOD, which can convert superoxide radicals to H_2O_2. In turn, H_2O_2 can be converted into water by GPx, in presence of GSH [Prasun P., 2020; Murphy M.P., 2009].

Mitochondria dysfunction occurs when the antioxidant defence is not effective to scavenge ROS production, resulting in damage to macromolecules affecting cellular function and viability [Prasun P., 2020]. Mitochondria oxidative stress is considered to play a crucial role for the development of MetS [Bhatti J.S. *et al.,* 2017]. The involvement of mitochondria dysfunction on the onset of MetS will be discussed in the following paragraphs.

4.2 Mitochondrial biogenesis

Mitochondria have their own DNA which encodes only for a few components of ETC (13 proteins) and 22 species of mitochondrial tRNA [Wallace D.C., 2018]. The rest of ETC machinery (80 proteins) and the other mitochondrial components are nuclear encoded [Prasun P., 2020]. Peroxisome proliferator-activated receptor gamma coactivator −1 α (PGC1α) is considered one of the main transcription factors involved in mitochondrial biogenesis, by activation of several transcription factors involved in mitochondrial and nuclear gene expression [Islam H. *et al.,* 2018] such as nuclear respiratory factors 1 and 2 (NRF-1 and NRF-2), and estrogen related receptors (ERRs), which leads to induction of mitochondrial transcription factor A (TFAM) [Scarpulla R.C. *et al.,* 2012; Jornayvaz and Shulman, 2010]. TFAM can directly interact with mitochondrial transcription factors B2 (TFB2M), causing mitochondrial gene transcription [Barshad G. *et al.,* 2018]. Moreover, PGC1α increases mitochondrial fatty acid oxidation by PPARα and PPARδ which activate mitochondrial beta fatty oxidation genes [Scarpulla R.C. *et al.,* 2012; Vega R.B. *et al.,* 2000]. PGC1α has also been involved in substrate oxidation, resulting in increased $NAD^+/NADH$ ratio [Cantò and Auwerx, 2009]. Indeed, PGC1α activation can be related to an increase in NAD^+ mediated by Sirtuin-1 pathways [Kahn B.B. *et al.,* 2005; Dominy J.E. *et al.,* 2010].

Finally, PGC1α is also involved in reducing mitochondrial oxidative stress by enhancing expression of several mitochondrial antioxidant enzymes such as SOD [Prasun P., 2020; Valle I. *et al.,* 2005].

4.3 Role of mitochondria in the pathogenesis of Metabolic Syndrome

Oxidative stress in adipocytes plays an important role in the onset of insulin resistance, diabetes and MetS [Furukawa S. *et al.,* 2004; Henriksen E.J. *et al.,* 2011]. Indeed, mitochondrial dysfunction occurs during progression from insulin resistance to T2DM [Ma Z.A. *et al.,* 2012; Fex M. *et al.,* 2018], due to chronic hyperglycemia which leads to excessive ROS formation in pancreatic beta cells. This elevated ROS generation leads to apoptosis of beta cells and reduction in beta cell mass [Prasun P., 2020; Mulder and Ling, 2009].

Increase in H_2O_2 levels inhibits tricarboxylic cycle enzyme aconitase, resulting in citrate accumulation which is turned to fat synthesis [Prasun P., 2020]. In addition, it has been shown that morphological differences on mitochondrial networks occur in obese and diabetic patients [Zorzano A. *et al.,* 2009].

4.4 Mitochondrial dysfunction and second-generation antipsychotic drugs-induced Metabolic Syndrome

Imbalance on brain bioenergetics and disturbance in OXPHOS in specific brain regions of schizophrenic patients led to study the effect of antipsychotics on mitochondrial functionality [Maurer I. *et al.,* 2001]. Indeed, some patients showed significant reduction in the number of synaptic mitochondria in specific regions of the brain, in comparison with patients which are resistant to treatment with antipsychotics [Roberts R.C., 2017]. Moreover, there is evidence in literature showing that mitochondrial impairment induced by antipsychotic drugs seems to be related to inhibition of ETC [Cikankova T. *et al.,* 2019]. The metabolic side effects induced by SGAs could be connected with alterations on mitochondrial homeostasis, imbalance on mitochondrial fusion/fission ratio and to an inefficient mitochondrial phenotype in muscle cells [Del Campo A. *et al.,* 2018].

Olanzapine generates a down-regulation of genes related to mitochondrial enzymes of ETC, a decrease in mitochondrial enzyme activities, ATP synthesis and oxygen consumption in patients' blood cells with elevated risk for MetS [Scaini G. *et al.,* 2018; Cikankova T. *et al.,* 2019]. CLZ has also been involved to promote oxidation of mitochondrial protein related to energy metabolism in neuroblastoma cells and in lymphoblastoid cells of schizophrenic patients [Baig M.R. *et al.,* 2010; Walss-Bass C. *et al.,* 2008; Contreras-Shannon V. *et al.,* 2013]. Moreover, CLZ alters mitochondrial function, energy metabolism, expression of mitochondrial proteins related to ETC and oxidative phosphorylation pathway such as succinate dehydrogenase and cytochrome oxidase [Ji B. *et al.,* 2009; Streck E.L. *et al.,* 2007; Contreras-Shannon V. *et al.,* 2013]. In addition, it has been shown that SGAs increase production of ROS [Heiser P. *et al.,* 2010; Polydoro M. *et al.,* 2004; Reinke A. *et al.,* 2004; Contreras-Shannon V. *et al.,* 2013]. Finally, Paredes et colleagues showed that SGAs differ in their response on generating MetS due to differences in alterations of energy metabolism pathways, in which CLZ and olanzapine are associated with the higher imbalance?? [Paredes R.M. *et al.,* 2014].

In conclusion, the molecular mechanisms by which SGAs alter mitochondrial functionality and induce MetS are not fully understood; Scaini et colleagues proposed a possible mechanism(s) involving mitochondrial dysfunction and SGAs-induced MetS [Scaini G. *et al.,* 2018], as reported in Fig.5.
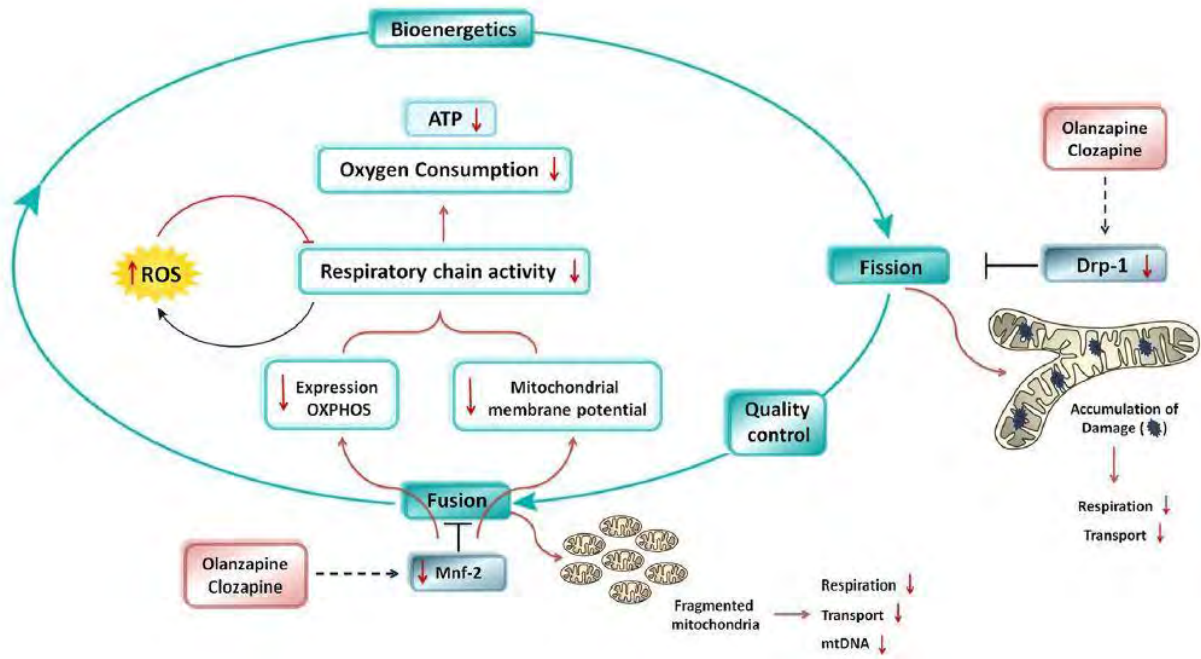
Figure 5. Mitochondrial dysfunction and SGAs [Scaini G. *et al.*, 2018]

AIM OF THE THESIS

The aim of this thesis has been first to characterise the morphological and biochemical changes occurring during the adipogenesis in human liposarcoma SW872 cell model with a particular focus on the role of ROS during this process (chapter 1).

Subsequently, the objective has been to investigate in the same cellular model the impact of CLZ on adipogenesis, in order to analyse the molecular mechanisms by which the drug can induce metabolic side effects (chapter 2).

Finally, the purpose of the thesis has been to connect the CLZ-induced mitochondrial dysfunction to the metabolic side effects observed in patients treated with the aforementioned drug (chapter 3).

CHAPTER 1: PAPER 1

RESEARCH COMMUNICATION

Temporal correlation of morphological and biochemical changes with the recruitment of different mechanisms of reactive oxygen species formation during human SW872 cell adipogenic differentiation

Mara Fiorani [ID] | Rita De Matteis | Barbara Canonico | Giulia Blandino | Alessandro Mazzoli | Mariele Montanari | Andrea Guidarelli | Orazio Cantoni [ID]

Department of Biomolecular Sciences, University of Urbino Carlo Bo, Urbino, Italy

Correspondence
Mara Fiorani, Dipartimento di Scienze Biomolecolari, Sezione di Biochimica e Biotecnologie, Università degli Studi di Urbino, Via Saffi 2, 61029 Urbino (PU), Italy.
Email: mara.fiorani@uniurb.it

Funding information
Ministero della Salute, Grant/Award Number: RF-2016-02363761

Abstract

Human SW872 preadipocyte conversion to mature adipocytes is associated with time-dependent changes in differentiation markers′ expression and with morphological changes accompanied by the accumulation of lipid droplets (LDs) as well as by increased mitochondriogenesis and mitochondrial membrane potential. Under identical conditions, the formation of reactive oxygen species (ROS) revealed with a general probe was significant at days 3 and 10 of differentiation and bearly detectable at day 6. NADPH oxidase (NOX)-2 activity determined with an immunocytochemical approach followed a very similar pattern. There was no evidence of mitochondrial ROS (mROS), as detected with a selective fluorescence probe, at days 3 and 6, possibly due to the triggering of the Nrf-2 antioxidant response. mROS were instead clearly detected at day 10, concomitantly with the accumulation of very large LDs, oxidation of both cardiolipin and thioredoxin 2, and decreased mitochondrial glutathione. In conclusion, the morphological and biochemical changes of differentiating SW872 cells are accompanied by the discontinuous formation of ROS derived from NOX-2, increasingly implicated in adipogenesis and adipose tissue dysfunction. In addition, mROS formation was significant only in the late phase of differentiation and was associated with mitochondrial dysfunction.

KEYWORDS
adipocyte differentiation, mitochondria, NADPH oxidase, ROS

1 | INTRODUCTION

Adipose tissue plays an essential role in maintaining lipid and glucose homeostasis. More specifically, healthy adipose tissue is actively engaged in the regulation of nutrient excess removal from the bloodstream as well as in storing/releasing of energy. This is in remarkable contrast with adipose tissue dysfunction that links obesity to related metabolic diseases.[1–3] These conditions, in which oxidative stress is increasingly implicated,[4,5] are particularly relevant for the human health, since associated with an increased risk for many chronic disorders, as hypertension, type II diabetes, cardiovascular diseases, and some types of cancer.[6,7]

A deeper understanding of the mechanisms involved in the process of adipogenesis and regulation of adipocyte function/malfunction is therefore critical for the comprehension of the molecular basis of these metabolic diseases. Based on the current knowledge, adipogenesis can be defined as a highly regulated-multistep process, mediating proliferation and differentiation of mesenchymal stem cells to lipid-laden mature adipocytes. It involves expression of genes and transcriptional factors, as the CAAT/enhancer-binding proteins (C/EBPs) family, peroxisome proliferator-activated receptor γ (PPARγ), cell cycle regulatory proteins, hormones, and growth factors.[8,9]

The formation of reactive oxygen species (ROS) is critical for adipocyte differentiation and, consistently, this process was inhibited or suppressed by antioxidants, as N-acetyl-L-cysteine or vitamin C.[10,11] The specific role of these species, however, is still controversial and in general poorly understood.[12,13] Excess of nutrients has been associated with an extensive mitochondrial ROS (mROS) formation[14,15] as well as with activation of NADPH oxidases (NOX) during adipogenesis.[15,16]

NOX-4, the most abundant NOX in mature adipocytes,[15,16] is constitutively active and independent of activator proteins,[13] redox regulated by its own product,[17] directly generates H_2O_2 under basal conditions and hence responsible for long-lasting effects.[18,19] Furthermore, preadipocytes and mature adipocytes express other NOX enzymes,[15,16] which include the phagocytic NOX-2, comprising six different subunits in part integrated in the plasma membrane and in part localized in the cytosol.[16] After appropriate stimuli, these subunits interact to release superoxide ($O_2^{-\cdot}$) in both intracellular and extracellular compartments. NOX-2 is also expressed in nonphagocytic cells, including human primary as well as rodent adipocytes.[20,21] Interestingly, NOX-2 deletion mitigates adiposopathy induced by a high fat diet in experimental animals,[22,23] in contrast to NOX-4 deficiency, which produced opposite effects.[24]

The process of adipogenesis has been extensively studied in primary cells in culture, an approach presenting the advantage of the biological relevance of the experimental results, and also some disadvantages in particular associated with the limited availability and renewal capacity of the cells.[25] In order to overcome these drawbacks, there has been a continuous increase in the use of cultured cells, in particular the murine 3T3-L1 cell line.[26] This well-characterized cellular model of adipogenesis, while conveniently utilized by numerous authors,[26–29] however, presents some limitations related to the translation of the experimental outcomes to humans.[12,30–33] Based on these considerations, it appears important to establish and characterize paradigms of adipogenesis using human cultured cells.

In recent years, there has been a growing interest in the use of SW872 cells, derived from a human liposarcoma,[31,34–38] which however remain poorly characterized for several aspects, in particular related to the identification of the specific mechanisms associated with ROS formation during adipogenesis.

Using this cell line, we performed a detailed characterization of the morphological and biochemical changes occurring during adipocyte differentiation and identified early events leading to NOX-2 activation followed by late mROS formation and dysfunction.

2 | MATERIALS AND METHODS

2.1 | Materials

Acrylamide 30%, glycine, sodium dodecyl sulfate (SDS), methanol, acetonitrile, insulin, dexamethasone, 3-isobutyl-1-methylxanthine (3-IBMX), oleic acid-albumin and linoleic acid-albumin, Oil Red O (ORO), glutathione (GSH), dithiobis-2-nitrobenzoic acid (DTNB), isopropanol, and most of the reagent-grade chemicals were purchased from Merck Life Science s.r.l. (Milan, Italy). Sodium chloride, ethylenediaminetetraacetic acid (EDTA), Na_2HPO_4, KH_2PO_4, and K_2HPO_4 were from Carlo Erba (Milan, Italy). Tween 20 and WesternBright ECL (K12045) were purchased from Advansta-Aurogenes s.r.l (Rome, Italy). Clarity Max was purchased from BioRad Laboratories s.r.l. (Milan, Italy).

2.2 | Cell culture conditions

Human liposarcoma SW872 cells were purchased from the American Type Culture Collection (Rockville, MD) and used between passages 3 and 10. Cells were maintained in Dulbecco's modified Eagle medium/

nutrient mixture F-12 (DMEM/F12) Merck Life Science s.r.l. (Milan, Italy), supplemented with 10% fetal bovine serum (FBS) (35-079-CV, Corning-S.I.A.L. s.r.l, Rome, Italy), 100 U/ml penicillin, 100 μg/ml streptomycin (P4333, Merck Life Science s.r.l. Milan, Italy), under a humidified 5% (vol/vol) CO_2 atmosphere at 37°C.

Postconfluent SW872 cells were induced to differentiation by changing the medium with the differentiation medium (DM) composed of 1 μM dexamethasone, 0.1 mM 3-IBMX, 30 μM bovine serum albumin (BSA)-bounded oleic acid/linoleic acid, and 10 μg/ml insulin in DMEM/F12 with 10% FBS). The DM was changed every 48 h and the differentiation process was followed up to day 10.[33] Morphological, immunocytochemical, and biochemical analyses were performed at different time points of SW872 cell differentiation.

2.3 | Cell culture preparation for morphological analysis

The SW872 cells were seeded onto 12-mm sterile glass microslides (Thermo Fisher Scientific, United Kingdom) placed inside the 12-well plates and differentiated, as described in the previous paragraph.

2.4 | ORO staining

In cellular preparations, neutral lipids were visualized using the soluble selective dye ORO.[39] Slides were washed with potassium phosphate-buffered saline (PBS: 136 mM NaCl, 10 mM Na_2HPO_4, 1.5 mM KH_2PO_4, 3 mM KCl; pH 7.4) and fixed for 1 h with 4% paraformaldehyde in PBS at 4°C, washed in the same buffer, and then incubated in 0.3% ORO solution, as previously described.[39]

The slides were incubated with the ORO working solution for 1 h at room temperature, washed twice with H_2O, counterstained with hematoxylin to visualize nuclei, and mounted in glycerol gel (Sigma-Aldrich-SIAL Rome, Italy).

2.5 | Western blot assay

Equal amounts (40 μg) of cell lysates were resolved in 8–12% SDS polyacrylamide gel and electrotransferred to polyvinyldiene difluoride (PVDF) membranes. Western blot analyses were performed using antibodies against actin, C/EBPβ, C/EBPδ, PPARγ, CD36, and nuclear factor (erythroid-derived 2)-like 2 (Nrf2) (Table S1). Details on the Western blotting apparatus and conditions are reported elsewhere.[40]

2.6 | Redox Western blot analysis

The thioredoxin2 (Trx2) redox state was estimated by redox Western blots, as described by Guidarelli et al.[41] Briefly, at the indicated time points, the cells were washed with PBS and detached from the culture dish in 200 μl urea lysis buffer (100 mM Tris/HCl, pH 8.2; urea 8 M; EDTA 1 mM) containing 10 mM iodoacetoamide. The samples were then incubated for 20 min at 37°C and centrifuged for 1 min at 14,000g. Ten volumes of cold acetone/1 M HCl (98:2) were added to the supernatants and the pellets were washed twice with acetone/1 M HCl/H_2O (98.2:10). The pellets were resuspended in 80 μl of urea lysis buffer containing 3.5 mM dithiothreitol, and, after a 30 min incubation at 37°C, incubated for a further 30 min at the same temperature in the presence of 30 mM iodoacetoamide. Samples were then subjected to urea polyacrylamide gel electrophoresis (7 M urea and 7% acrylamide), under nonreducing conditions, and blotted.[42]

2.7 | Isolation of mitochondria

Cells were processed to obtain a crude mitochondrial fraction, as described by Fiorani et al.[43] Briefly, the cells were washed twice in PBS and detached with pre-warmed trypsin/EDTA solution (2.5 g/L trypsin plus 0.2 g/L EDTA). The cells were then transferred to a centrifuge tube, washed with PBS, and resuspended in ice-cold homogenization buffer (HB, 225 mM mannitol, 75 mM sucrose, 0.1 mM EGTA, protease inhibitor cocktail, 5 mM Tris–HCl, pH 7.4). The cells were homogenized with 30–40 strokes in a glass potter placed in an ice-bath. The efficiency of the homogenization process was monitored under the microscope by counting the number of residual trypan blue negative cells. The homogenate was centrifuged at 1000g for 10 min at 4°C and the supernatant (S1) was collected for the final centrifugation. The pellet was rehomogenized and the supernatant (S2) was added to S1 and centrifuged at 12,000g for 30 min at 4°C. The corresponding pellet (mitochondrial fraction) was washed and processed for GSH analysis.

2.8 | Measurement of GSH content in cells and mitochondria by high-performance liquid chromatography

GSH content in SW872 cells and mitochondria was measured as described by Fiorani et al.[40] Briefly, the cellular or mitochondrial pellets were suspended in lysis buffer (0.1% Triton X-100; 0.1 M Na_2HPO_4; 5 mM Na-EDTA, pH 7.5), vortexed, and kept for 10 min on an ice bath.

Thereafter, 0.1 N HCl and precipitating solution (0.2 M glacial meta-phosphoric acid, 5 mM Na-EDTA, 0.5 M NaCl) were added to the samples. After centrifugation, the supernatants were collected and kept at −20°C until the high-performance liquid chromatography (HPLC) analyses. Just before analysis, DTNB (20 mg in 100 ml of 1% wt/vol sodium citrate) was added to the extracts. The samples were filtered through 0.22-μm-pore microfilter and finally analyzed for their GSH content by HPLC,[44] using a 15 cm × 4.6 mm, 5 μm Supelco Discovery® C18 column (Supelco, Bellefonte, PA). The UV absorption was detected at 330 nm. The injection volume was 20 μl. The retention time of GSH was ~15.7 min.

2.9 | Flow cytometric staining

Cells were labeled with one of the indicated fluorochromes. MitoSOX Red (5 μM, 10 min), a dye targeting the mitochondria of live cells, is selectively oxidized by O_2^{-} to produce red fluorescence,[45] chloromethyl-2′,7′-dichlorodihydrofluorescein diacetate (DCF, 5 μM, 30 min), a general probe for ROS detection.[46] The mitochondrial membrane potential was analyzed using tetramethylrhodamine (TMRE, 40 nM, 15 min), selectively taken up by mitochondria.[47] MitoTracker Green (MTG, 50 nM, 30 min) is taken up by mitochondria independently of their membrane potential.[47] The cardiolipin-sensitive probe 10-nonyl acridine orange (NAO, 100 nM, 15 min) was used to monitor mitochondrial lipid changes.[47] Nile Red (NR, 1 μg/ml in dimethylsulfoxide, 15 min) is a phenoxazine dye, which can be used to localize and quantify neutral and polar lipids in living cells. Polar lipids (i.e., phospholipids), mostly present in membranes, are stained in red (emission >590 nm), whereas neutral lipids (esterified cholesterol and triglycerides), present in lipid droplets (LDs), are stained in yellow (570–590 nm).[47] At least 10,000 events were acquired for each sample.

2.10 | DNA content analysis

The effects on cell cycle progression were investigated in differentiating SW872 cells by flow cytometry, as previously detailed by Benedetti et al.[48]

2.11 | Cytometric investigations

Cytometric experiments were carried out with a FACS Canto II flow cytometer equipped with an argon laser (blue, Ex 488 nm), a helium-neon laser (red, Ex 633 nm) and a solid-state diode laser (Violet, Ex 405 nm). Analyses were performed by using FACSDivaTM software; ~15,000 cell events were acquired for each sample.

2.12 | Immunofluorescence analysis

The cells were fixed for 1 min with 95% ethanol/5% acetic acid, washed with PBS, and blocked in PBS-containing BSA (2% wt/vol) (30 min at room temperature). The cells were subsequently incubated with rabbit polyclonal antiphosphorylated p47phox (Table S1), stored for 18 h at 4°C, washed, and then incubated for 3 h in the dark with fluorescein isothiocyanate (Santa Cruz Biotechnology)-conjugated secondary antibody diluted 1:100 in PBS. The cells were washed three times and fluorescence images were captured using a BX-51 microscope (Olympus, Milan, Italy), equipped with a SPOT-RT camera unit (Diagnostic Instruments, Delta Sistemi, Rome, Italy) using an Olympus LCAch 40 × 0.55 objective lens. The excitation and emission wavelengths were 488 and 515 nm with a 5-nm slit width for both emission and excitation.

2.13 | Immunocytochemistry

Cells grown on microslides were fixed in 4% formaldehyde in PBS (15 min), washed twice in PBS and permeabilized (10 min) in PBS containing 0.25% Triton-X 100, or washed in PBS when permeabilization was not required. After fixation and permeabilization, cells were blocked with 2% normal serum at room temperature for 20 min. Immunostaining was carried out with specific primary antibodies (Table S1). The immunoreaction was revealed with the avidin–biotin–peroxidase complex (ABC) method (Vector, Burlingame, CA, United States). Peroxidase activity was revealed by diaminobenzidine hydrochloride as chromogen (Sigma-Aldrich—SIAL, Rome, Italy). The cellular preparations were then counterstained with methyl green (Genetex-Prodotti Gianni, Milan, Italy) and mounted in Eukitt (Kindler, Freiburg, Germany).

Preparations were examined using a Nikon light microscope (Nikon Eclipse 80i microscope, Laboratory Imaging, Czech Republic) and an ACT-2U image analyzer linked to a Sony equipped with digital camera.

2.14 | Statistical analysis

Data are expressed as mean ± SD. Comparisons were made using a one-way analysis of variance (ANOVA)

followed by Dunnett's test for multiple comparison. All experiments were repeated at least three times. Differences were considered significant at $p < 0.05$ (*) and $p < 0.01$ (**).

3 | RESULTS

3.1 | Morphological changes of differentiating SW872 cells

Addition of the DM to confluent SW872 cells promoted adipogenesis associated with significant time-dependent changes in morphology. Cells, initially displaying a fibroblast-like morphology, virtually in the absence of detectable lipid accumulation (Figure 1A, T0), became more elongated at day 3 (T3), with some LDs in their cytoplasm. At day 6 of differentiation (T6), the cells featured a more rounded shape, with an increased number and size of LDs dispersed throughout the cytosol. At day 10 (T10), most cells appeared roundish with large LDs, thereby displaying the typical morphology of mature adipocytes.

The time-dependent conversion of preadipocytes to fully differentiated adipocytes can be well appreciated by the analysis of the results illustrated in Figure 1B, in which the LD total area per cell was quantified with the "analyse particles" function of the ImageJ software.[49] Spectrophotometric measurement of ORO eluted from the cells also provided an indication for a time-dependent increase of intracellular lipid content during differentiation, however with a slowdown of the lipid accumulation trend after the sixth day (Figure 1B).

It is important to note that the above changes were detected in the very last majority of the cells analyzed at the different time points of differentiation. However, a small proportion of cells at different stages of differentiation was detected in all of these conditions. An example is provided by cultures at T10, characterized by a large proportion of rounded cells with an abundant lipid accumulation, and also by other cells more elongated and with a significantly lower LD content (Figure 1A). This notion was more clearly established by comparing flow cytometric forward scatter (FSC) versus side scatter (SSC) dot plots in cells at T0 versus T10 (Figure 1C), using a procedure employed in other studies.[50] Quantification of these data (Figure 1D) demonstrates that at T6 most of the cells correspond to mature adipocytes, falling in the SSC zone (P2, about 80%), whereas the less differentiated phenotype accounted for the residual 20% of the cell population (P1). Remarkably similar results were obtained at day 10, thereby suggesting that differentiation was nearly completed at day 6 (Figure 1C,D).

Figure 1E depicts a representative histogram plot for NR staining in P2 cell population (i.e., blue area enclosed cells). Histogram overlay shows an increase in NR fluorescence intensities from blue events enclosed in the P2 area, highlighting the presence of scarce and dim-fluorescent cells at T0 (red histogram on the left). The lipid quantification of both P1- and P2-enclosed cells reported in Figure 1F reveals a similar lipid accumulation trend in both subpopulations, but a significantly higher amount of LDs in P2 cells. These results indicate that a flow of cells from P1 red to the P2 blue area occurred during differentiation (Figure 1C), and that the increase in the granulation/vacuolation of these cells is paralleled by an increased lipid content (Figure 1E).

3.2 | Cell cycle distribution and expression of adipogenic markers during SW872 cell differentiation

We measured the changes in DNA content and cell cycle distribution of differentiating SW872 cells. As indicated by the analysis of the flow cytometric DNA profiles reported in Figure 2A, there was evidence for a time-dependent reduction in the number of proliferating cells, which appeared well synchronized at T10, with a large prevalence of cells in the G0/G1 phase (>90%).

The expression patterns of specific transcription factors and differentiation markers were next analyzed by both Western immunoblotting (Figure 2B) and immunocytochemistry (Figure 2C).

We found that C/EBPβ, a "classical" early inducer of adipogenesis,[8,9] is constitutively expressed and largely localized in the nuclei of cells at T0, upregulated at T3 and T6, with a return to control levels at T10. Increased expression of C/EBPβ protein was in most cells associated with both nuclear and diffused cytoplasmic labeling.

C/EBP-δ was instead barely detectable at T0 and T3, but its expression eventually increased significantly (four times) at T6 and T10. Immunocytochemical analysis revealed that T0 cells exclusively express nuclear C/EBPδ, with a progressive decline at T3–T10, in parallel with a redistribution of the protein in the cytoplasm. Rounded T6 or T10 cells, in particular when associated with an elevated lipid accumulation, showed a weak cytoplasmic C/EBPδ staining.

PPARγ expression, very low at T0, was significantly increased at T3, to remain to similar levels throughout the entire course of the differentiation period. PPARγ was mainly localized in the nuclear compartment. CD36, a target gene of PPARγ,[8,9] followed the same expression pattern of PPARγ, but with a different subcellular distribution. CD36 immunoreactivity was indeed generally diffused and occasionally punctate or even reticular.
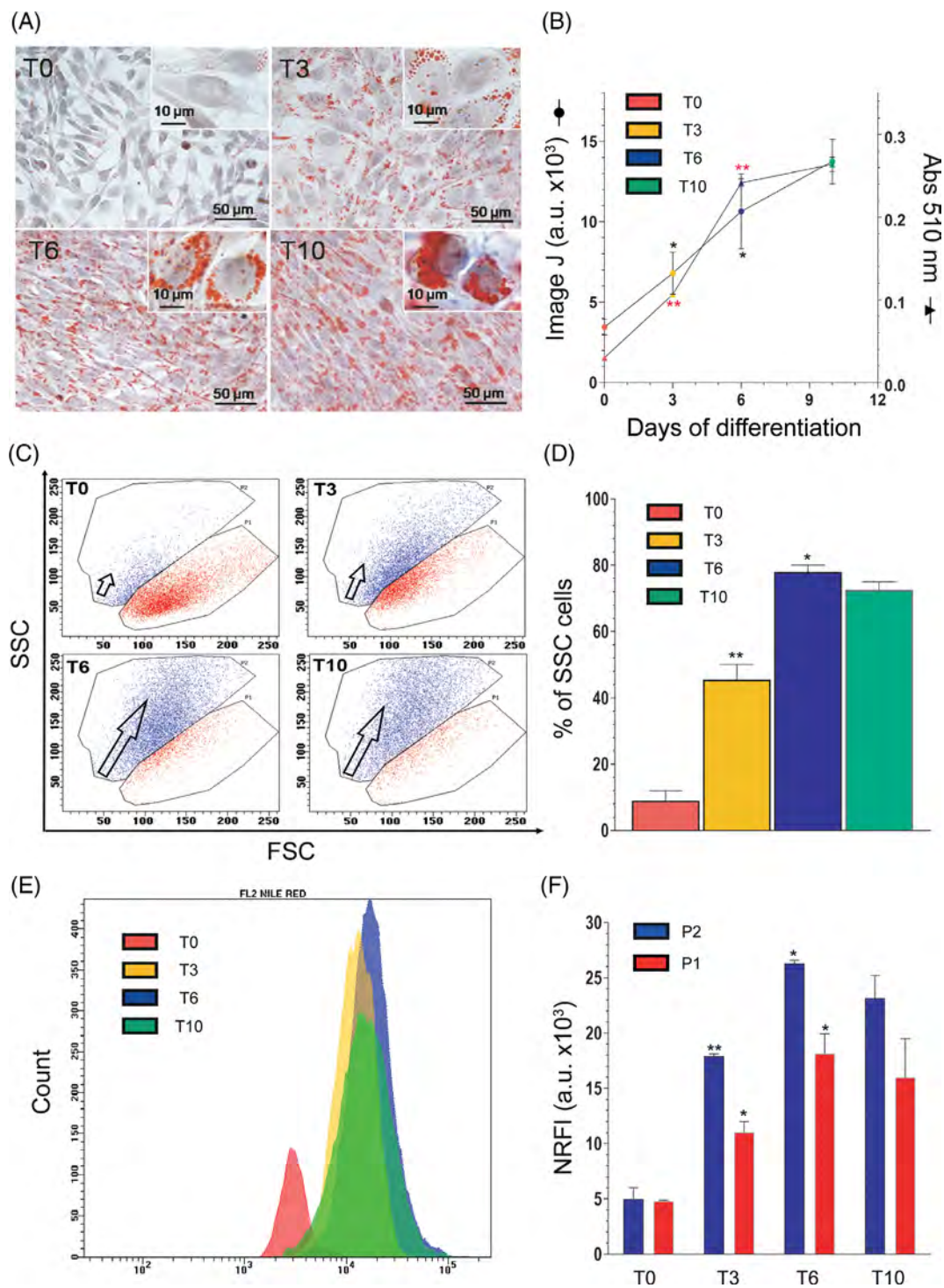
FIGURE 1 Morphological changes in differentiating SW872 cells. (A) Representative images of Oil Red O (ORO)-stained LDs (red) and hematoxylin-stained nuclei (blue), in differentiating SW872 cells. The higher enlargements (insets) allowed to analyze the differences of lipid accumulation in the cytoplasm of the cells: (T0) tiny LD accumulation; (T3) a substantial lipid accumulation as small LDs; (T6) numerous enlarged LDs; (T10) some large lipid vacuoles in fully differentiated adipocytes. Bars = 50 μm; inset = 10 μm. (B) Cellular ORO quantification performed by ImageJ software and by spectrophotometric analysis. (C) Forward scatter (FSC) versus side scatter (SSC) dot plots at the indicated differentiation times. The red area enclosed by gate P1 at T0 represents highly enriched events. Of note, the blue area (enclosed by gate P2) progressively becomes the main representative of total cells, particularly at T6 and T10. The blue area is characterized by an increase in SSC values, meaning an increase in granulations/vacuolations in each cell, as explained in the text. (D) Statistical analysis of the percentage of SSC cells (granulated/vacuolated cells) at the indicated differentiation times. (E) Representative histogram of Nile Red-labeled cells from P2 blue area. (F) Comparison between fluorescence intensities (NR FI) from blue events, enclosed in the P2 gate (more differentiated cells) and red events, enclosed in the P1 gate (less differentiated cells). Values reported are raw FI data of specific FL2 Nile Red fluorescence (revealing neutral lipid). Results represent the means ± SD calculated from at least three independent determinations. *$p < 0.05$, **$p < 0.01$, as compared to the previous time point (one-way analysis of variance followed by Dunnett's test)
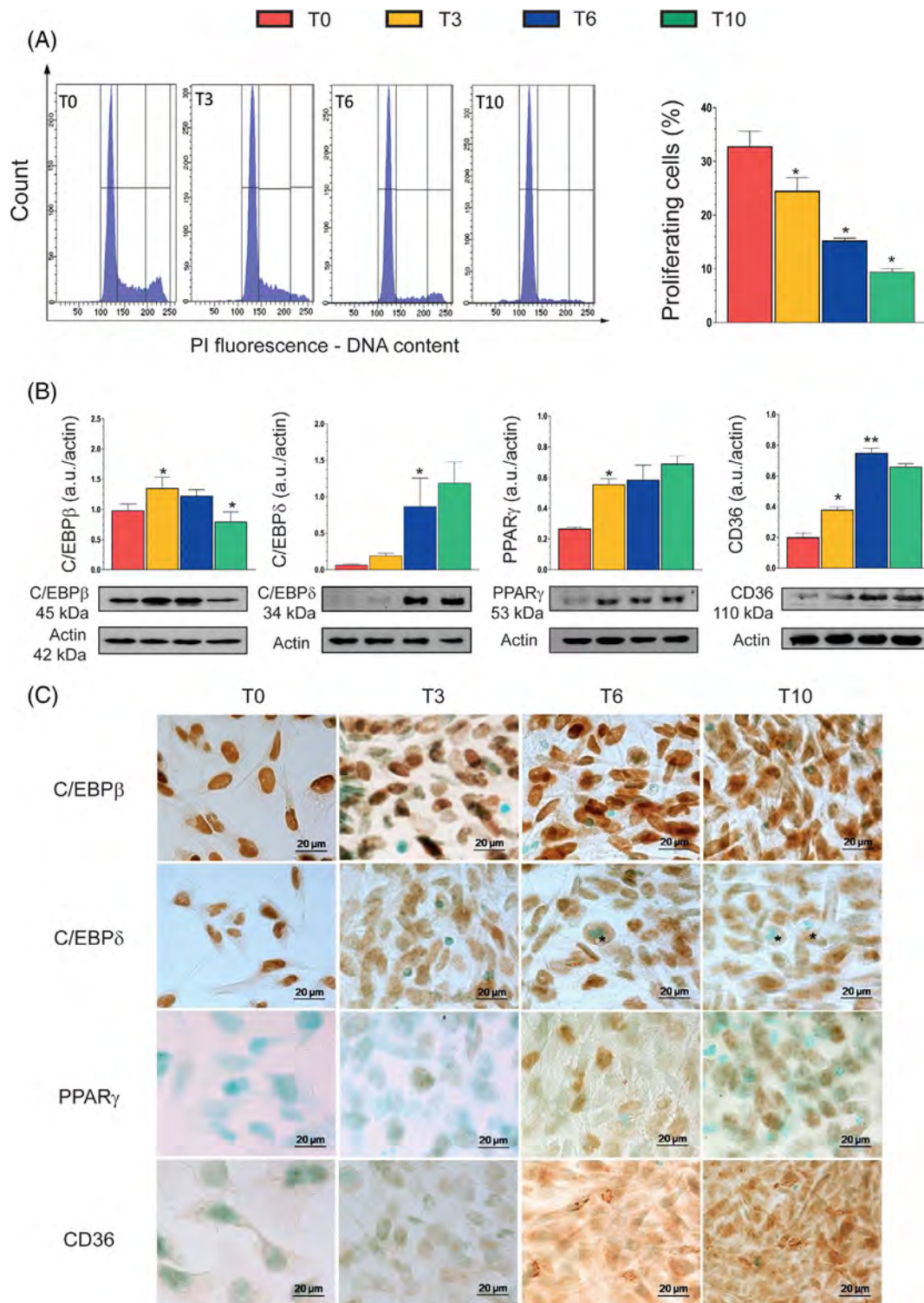
FIGURE 2 Proliferation state and expression of adipogenic markers during differentiation. (A) DNA content of cells at different stages of differentiation was evaluated by flow cytometry. Histogram profiles highlight the progressive loss of proliferating cells during the process of differentiation. Markers are posed in sequence to delineate (and quantitate) G0/G1, S, and G2/M phases. Events from S+G2/M phases (proliferating cells) were calculated and plotted in the statistic histogram. (B) Western immunoblotting analysis of the key adipocyte differentiation markers CAAT/enhancer-binding protein β (C/EBPβ), C/EBPδ, peroxisome proliferator-activated receptor γ (PPARγ), and CD36, at the indicated differentiation times. Actin was used as a loading control. (C) Immunohistochemical analysis of C/EBPβ, C/EBPδ, PPARγ, and CD36 at the indicated differentiation times. Immunolocalization was visualized using diaminobenzidine (brown) and nuclei were counterstained with methyl green. * indicates adipocyte with evident lipid accumulation. Magnification 100×; bar: 20 μm. Results represent the means ± SD calculated from at least three independent determinations. *$p < 0.05$, **$p < 0.01$, as compared to the previous time point (one-way analysis of variance followed by Dunnett's test)

3.3 | Increase in mitochondrial mass/number and membrane potential during SW872 cell differentiation

We simultaneously measured MTG and TMRE fluorescence in differentiating SW872 cells to obtain an indication of the relative mitochondrial mass/number and mitochondrial membrane potential, respectively. As indicated in Figure 3A, MTG exhibits fluorescence progressively, but moderately increased with time of differentiation. The TMRE fluorescence response was instead steeper and indicative of a significant rise in mitochondrial membrane potential.

In other experiments, the use of a different fluorescent probe, NAO, revealed a progressive increase in cardiolipin content from day 0 to day 6 (Figure 3B), consistently with the observed increase in mitochondrial mass/number (Figure 3A). However, a sudden drop of NAO fluorescence occurred at T10, which obviously does not fit with the data demonstrating a further increase in mitochondrial mass/number, and might rather provide an indication of cardiolipin oxidation.[51]
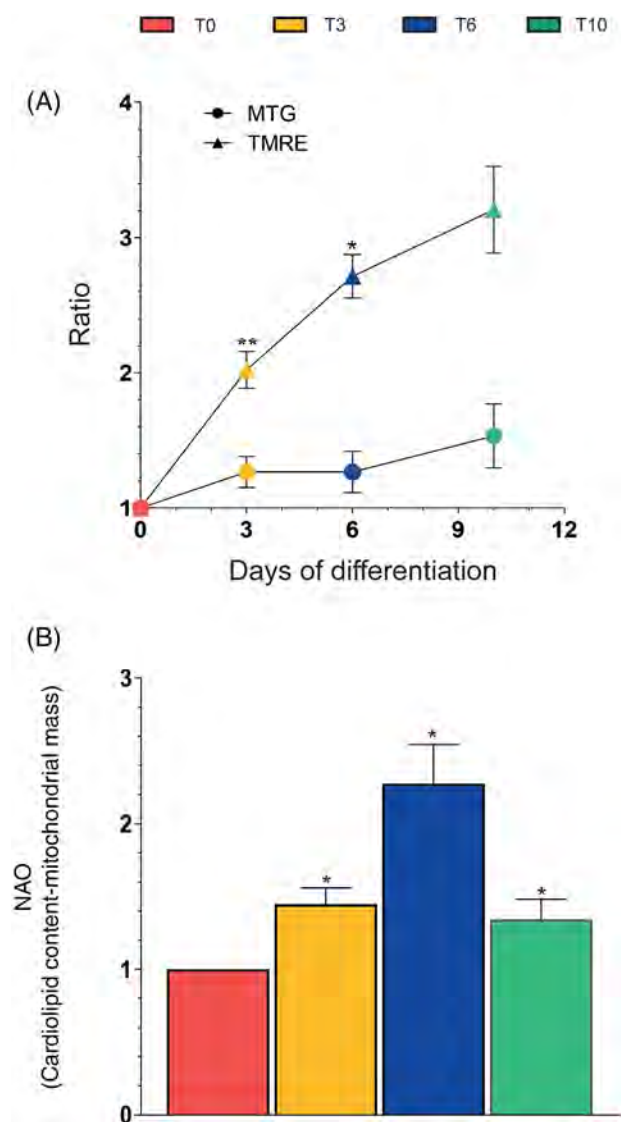
3.4 | ROS formation during SW872 cell differentiation

We measured ROS formation in differentiating SW872 cells using DCF. Figure 4A shows representative cytometric profiles for the DCF fluorescence detected at T0–T10, immediately giving a clue for a nonlinear rate of ROS formation during adipogenesis. This notion is more clearly established by the histograms depicted in Figure 4B, indicating an initial sudden increase in ROS formation at T3, followed by a marked decrease at T6 and a further increase at T10.

We next investigated the mechanism(s) of ROS formation associated with the different phases of the differentiation process and, for the reasons indicated in Section 1, tested the possibility of an involvement of NOX-2. This NOX enzyme, while predominant in macrophages, is also expressed in the adipose tissue[52] and animal studies document its importance in adipogenenesis.[16] As indicated in Figure 4C, immunocytochemical evidence of NOX-2 activation was detected at the same time points in which an increased DCF fluorescence response was also observed (Figure 4B).

In order to investigate whether NOX-2 activation was paralleled by a mitochondrial mechanism of ROS formation, we also performed experiments using MitoSOX Red. Interestingly, the resulting fluorescence responses, while absent or negligible at T0–T6, increased significantly at T10 (Figure 4D,E). An indication of mitochondrial $O_2^{-\cdot}$ formation is therefore obtained under conditions of maximal mitochondrial membrane hyperpolarization (Figure 3A) and cardiolipin oxidation (Figure 3B).

FIGURE 3 Flow cytometric analyses of mitochondrial mass and membrane potential during differentiation. (A) MitoTracker Green (MTG)- and tetramethylrhodamine (TMRE)-fluorescence intensity (FI) assays and (B) NAO-FI analysis at the indicated differentiation times. Results are the ratio T3-T10/T0 and represent the means ± SD calculated from at least three independent determinations. *$p < 0.05$, **$p < 0.01$, as compared to the previous time point (one-way analysis of variance followed by Dunnett's test)

3.5 | Consequences of ROS formation during SW872 cell differentiation

We investigated Nrf2 expression in differentiating SW872 cells (Figure 5A) and observed a response characterized by a bimodal trend, reminiscent of that obtained in
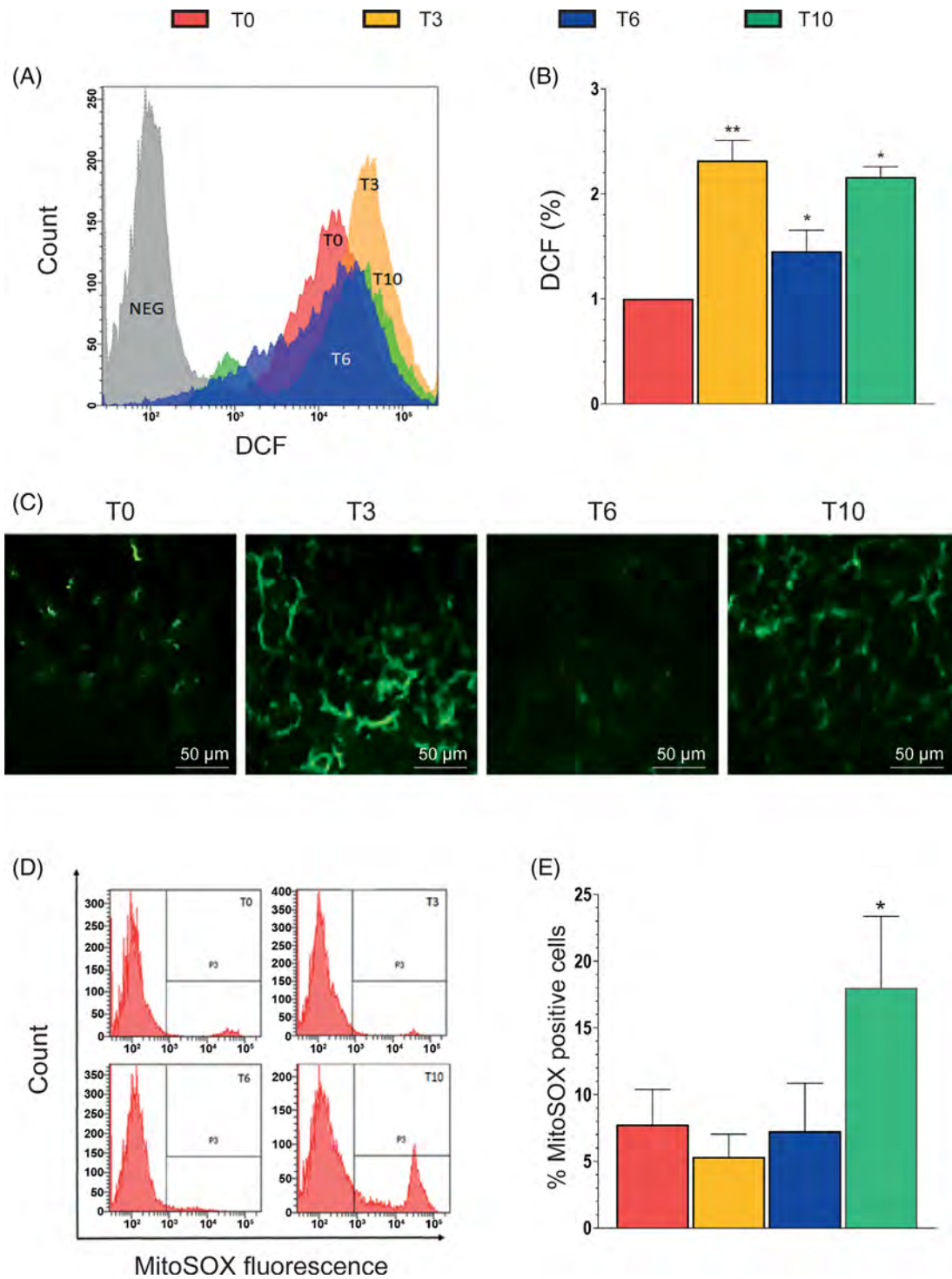
FIGURE 4   Reactive oxygen species (ROS) production during differentiation. (A) Representative flow cytometry histograms of cells treated with the ROS-sensitive probe chloromethyl-2′,7′-dichlorodihydrofluorescein diacetate (DCF). (B) Statistical analysis of the results obtained from different DCF flow cytometry assays. (C) Representative micrographs showing phosphorylated p47[phox] localization in SW872 cells. At the indicated times, the cells were fixed and analyzed for immunocytochemical detection of phosphorylated p47[phox]. (D) Representative flow cytometry histograms of cells treated with the mitochondrial ROS-sensitive probe MitoSOX Red. (E) Statistical analysis of the results from different MitoSOX Red flow cytometry analyses. Results represent the means ± SD calculated from at least three independent determinations. *$p < 0.05$, **$p < 0.01$, as compared to the previous time point (one-way analysis of variance followed by Dunnett's test)
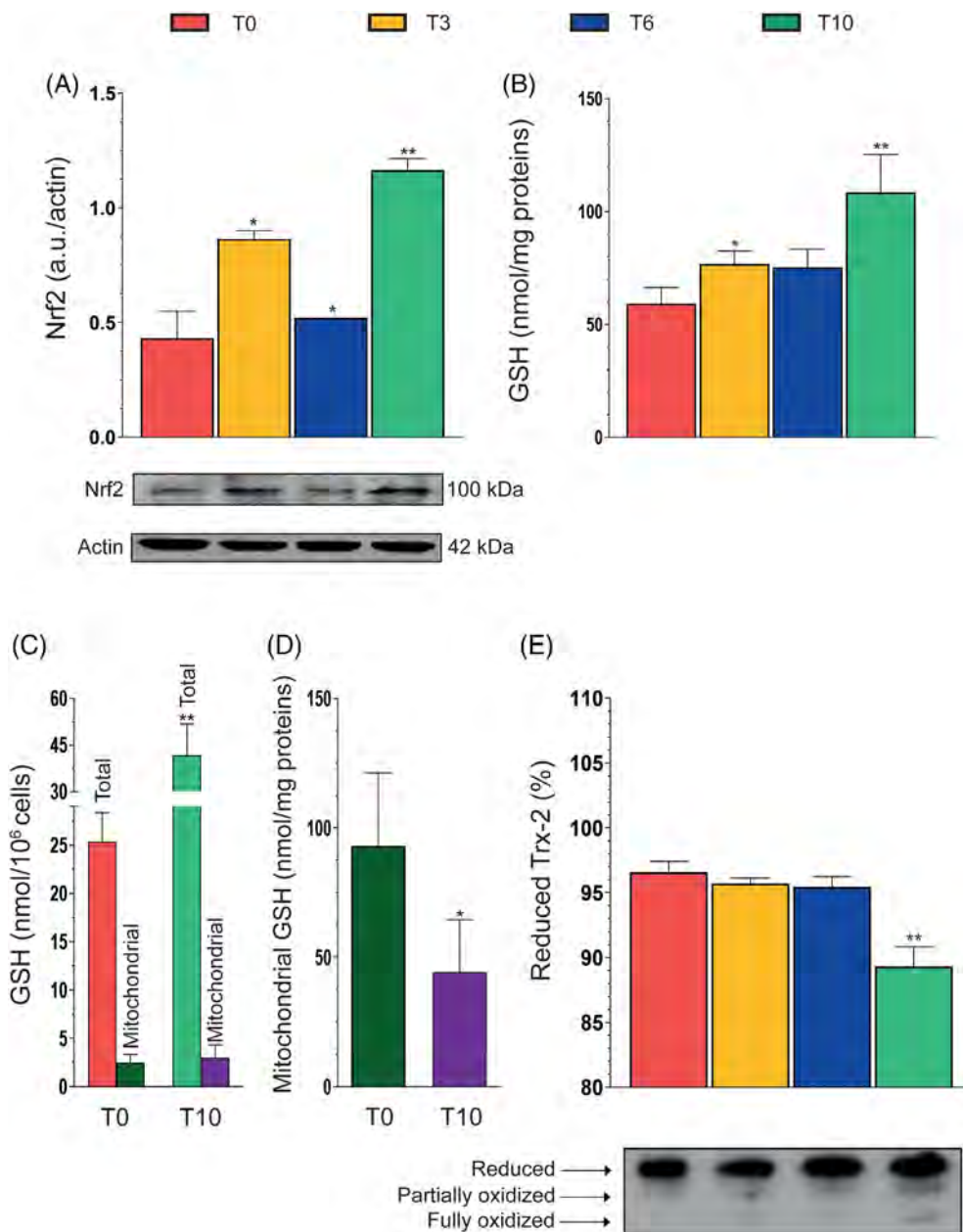
FIGURE 5 Nuclear factor (erythroid-derived 2)-like 2 (Nrf2) expression, cellular/mitochondrial glutathione content, and thioredoxin 2 redox state during differentiation. (A) Western immunoblotting analysis of Nrf2 expression in differentiating SW872 cells. Actin was used as loading control. (B) Total glutathione (GSH) content at the indicated differentiation times. (C) Total and mitochondrial GSH content at T0 and T10. (D) GSH content of mitochondria isolated from cells at T0 and T10. (E) Analysis of reduced, partially oxidized, and fully oxidized thioredoxin 2 (Trx2) thiol groups at the indicated differentiation times. The redox state of Trx2 was determined by urea polyacrylamide gel electrophoresis under nonreducing conditions. Results represent the means ± SD calculated from at least three independent determinations. $*p < 0.05$, $**p < 0.01$, as compared to the previous time point (one-way analysis of variance followed by Dunnett's test)

experiments measuring DCF fluorescence (Figure 4B). Consistently, an increase in total GSH was also observed at T3–T10 (Figure 5B), as γ-glutamine cysteine ligase, the rate-limiting enzyme of GSH biosynthesis, is over-expressed after Nrf2 activation.[53]

Based on the results shown in Figures 3B and 4E, respectively, providing evidence for a decline in cardiolipin expression and mitochondrial $O_2^{-\cdot}$ formation at T10, we compared the levels of total GSH and mitochondrial GSH (mGSH) at T0 versus T10.

It was interesting to observe that, when normalized on cell number, the increase in total GSH detected at T10 is not paralleled by a similar increase in mGSH, which actually remained virtually unchanged with respect to that detected at T0 (Figure 5C). Consistently, when the data

were expressed as nmol/mg proteins, mGSH was significantly lower at T10 versus T0 (Figure 5C). These results are therefore indicative of an extensive mitochondrial $O_2^{-\cdot}$ formation, a notion also consistent with the outcome of studies investigating the level of Trx2 oxidation, an important mitochondrial redox regulator.[42] We performed a redox gel using anti-Trx 2 antibodies and obtained evidence of significant Trx2 oxidation at T10, with hardly any effect being observed at T3 or T6 (Figure 5D).

4 | DISCUSSION

Adipocyte differentiation is a complex process characterized by a highly ordered and well-defined temporal

sequence. In this study, we performed a detailed characterization of the morphological changes associated with the differentiation of postconfluent human SW872 cells grown in a conventional DM. We obtained evidence for a time-dependent conversion of a very large proportion of the pre-adipocytes to fully differentiated adipocytes. This process, apparently completed at T6, was paralleled by the progressive accumulation of cells in the G0/G1 phase, and expression of specific transcription factors and differentiation markers was involved in the induction phase, as C/EBPβ and C/EBPδ, or the late phase, as PPARγ and CD36.

More specifically, we obtained evidence for a constitutive expression, further increased at T3 and T6, of C/EBPβ, which is associated with an intracellular redistribution of the protein, initially exclusively localized in nuclei. These results are in keeping with the findings from other studies.[54,55]

The kinetics of C/EBPδ expression was instead somewhat unexpected and different from those obtained in other studies using different models of adipogenesis.[54] Indeed, C/EBPδ was scarcely detectable at the early stages of differentiation (T0 and T3), and its expression increased significantly in the late stages of differentiation (T6 and T10), in parallel with a subcellular redistribution of the protein.

C/EBPβ, unlike C/EBPδ protein expression, seemed to precede the expression of PPARγ, which increased significantly at T3, with maintenance of similar levels at T6 and T10. CD36, a multifunctional protein and a target gene of PPARγ, presented an expression pattern similar to that of PPARγ.[56]

In short, SW872 cells well differentiate to mature adipocytes when grown in DM and the morphological changes observed during this process were accompanied by the expression of early and late markers of differentiation, which followed kinetics similar to the ones reported in other cellular model of adipocyte differentiation,[54,55] however with the exception of C/EBPδ.

The process of adipocyte differentiation is associated with an increased mitochondrial biogenesis, which is needed to support various key functions of the mature adipocytes.[57] Increased mitochondriogenesis is often associated with an increase in mitochondrial membrane potential.[58,59] Consistently, a progressive increase in mitochondrial mass/number was observed during the course of SW872 cell adipogenesis. We also observed a rather dramatic increase in mitochondrial membrane potential, indicative of an active mitochondrial formation of ROS.[60] Our data on cardiolipin expression, showing a progressive increase followed by a sudden drop at day 10, are therefore consistent with both the data on mitochondrial mass/number and with the robust increase in mitochondrial $O_2^{-\cdot}$ formation detected at T10.

The involvement of ROS in the adipogenic process is documented by numerous studies using different cellular models.[61–63] In this study, we obtained evidence for an intermittent formation of ROS during SW872 cell adipogenesis, likely attributable to NOX-2 activation, requiring interaction of the membrane and cytosolic subunits to generate $O_2^{-\cdot}$, rapidly converted to diffusible H_2O_2.[64] Indeed, our immunofluorescence studies using anti-p47[phox] antibodies were indicative of a significant NOX-2 activation at T3, virtual loss of activity at T6, and again activation at T10, that is, an intermittent activation pattern superimposable on the kinetic of ROS formation measured with DCF.

These results are therefore consistent with the possibility that early NOX-2 activation plays a role in SW872 cell adipogenic differentiation, a conclusion in keeping with the outcome of in vivo studies using NOX-2-deficient mice.[22,23]

In this study, we did not investigate NOX-4 expression and activity during differentiation, which in any case appears likely since this NOX enzyme displays enhanced expression in response to H_2O_2.[15] This suggests the possibility of a crosstalk between NOX-2 and NOX-4. However, a crosstalk is also likely to take place between the NOX enzymes and mROS.[15] We observed a late onset mitochondrial $O_2^{-\cdot}$ formation, thereby implying that at least two different mechanisms contribute to the DCF-fluorescence response detected at T10, one based on NOX-2 activation and another one associated with mitochondrial events. These results are consistent with the possibility that late NOX-2 activity participates in the triggering of late mitochondrial $O_2^{-\cdot}$ emission.

It is important to note that the apparent absence of mROS formation at T3 and T6 is rather surprising since other reports provided evidence for the formation of these species during the early phases of adipogenesis.[65] In addition, as indicated earlier, an excessive supply of energy substrates to metabolic pathways should induce the production of ROS and, more specifically, oversupply of electrons to the respiratory chain should increase mitochondrial $O_2^{-\cdot}$ formation.[14,15]

One good reason that might explain the absence of detectable mROS at T3 and T6 is, however, based on the increased expression of Nrf2, readily activated after ROS-dependent oxidation of the Nrf2 inhibitor Kelch-like ECH-associated protein 1.[66] Upregulated Nrf2 promotes the expression of multiple antioxidant genes involved in different functions, which include mitochondrial H_2O_2 detoxification.[67] One of these genes encodes for γ-glutamine cysteine ligase, the rate-limiting enzyme of GSH biosynthesis.[53] This event takes place in the cytosol and is followed by a subcellular distribution of the tripeptide in different compartments, for example, nuclei,

endoplasmic reticulum, and mitochondria.[68] Interestingly, the cytosolic and mitochondrial concentrations of GSH are remarkably similar (1–10 mM).[69] Cytosol-to-mGSH translocation takes place via poorly defined mitochondrial carriers,[70,71] in some studies identified in the dicarboxylate and 2-oxoglutarate carriers (rat liver and kidney),[71,72] or tricarboxylate carrier (rat brain).[73] mGSH represents a key player of the mitochondrial antioxidant defense, actively regulating the redox status of these organelles via different mechanisms, in particular by acting as a cofactor for glutathione peroxidase.[74] An additional important mitochondrial antioxidant defense is represented by the Trx 2/Trx reductase 2 system.[75]

In our experiments, Nrf2 activation was detected under the same conditions in which ROS were generated by early NOX-2-activation, and late events in which NOX-2 and mitochondria were concomitantly involved. Consistently, an increase in total GSH was also detected at T3 and T10. Based on these findings, the early Nrf2 response, while possibly stimulated by NOX-2-derived ROS, should provide a general protection to the differentiating adipocytes and may account for an efficient scavenging of mROS at T3 and T6.

The scenario drastically changed at T10, a time at which mROS formation was possibly associated with mitochondrial dysfunction. At T3 and T6, we observed parallel increases in cardiolipin levels and mitochondrial mass/number, but at T10 cardiolipin levels decreased despite the further increase in mitochondrial mass/number. This is indicative of cardiolipin oxidation, since this protein is highly susceptible to oxidative damage.[76] At T10, we also obtained evidence for a decline in mGSH levels, despite the significant rise in the overall cellular concentration of the tripeptide. This is also indicative of extensive mROS formation, apparently causing a decrease in mGSH, which cannot be compensated by the increased GSH biosynthesis driven by the Nrf2 response. The synthesis of GSH indeed takes place in the cytosol, and its transport in mitochondria limits the accumulation of the tripeptide in these organelles.[77]

The third observation providing indirect evidence of mROS formation at T10 is based on the extensive Trx2 oxidation detected at this time point. In addition, in keeping with the results of experiments using MitoSOX Red fluorescence to detect $O_2^{-\cdot}$ formation, there was no evidence of Trx2 oxidation at T3 or T6.

In conclusion, the results presented in this study provide a detailed characterization of the biochemical and morphological changes of differentiating SW872 cells as well as an indication for an intermittent release of ROS mediated by different mechanisms. Our results are indicative of a complex regulation of ROS formation during differentiation of these cells, with the NOX enzymes likely involved in the regulation of the adipogenic process. We provide evidence for an early increase in NOX-2 activity, which might imply a role of NOX-2-derived $O_2^{-\cdot}$ in adipogenesis, although a critical link between this event and delayed mROS formation is also likely to occur. This second mechanism of ROS formation, probably as a consequence of the Nrf2-dependent adaptive response, was uniquely detected at T10, and, at least in the conditions employed in this study, does not appear to play a major role in the induction of adipogenesis, apparently completed at T6. mROS are instead likely involved with the induction of mitochondrial dysfunction.

CONFLICT OF INTEREST
The authors declare no potential conflict of interest.

DATA AVAILABILITY STATEMENT
The data that support the findings of this study are available from the corresponding author upon reasonable request.

ORCID
Mara Fiorani https://orcid.org/0000-0003-0310-2670
Orazio Cantoni https://orcid.org/0000-0002-7182-802X

REFERENCES
1. Kojta I, Chacinska M, Blachnio-Zabielska A. Obesity, bioactive lipids, and adipose tissue inflammation in insulin resistance. Nutrients. 2020;12:1305.
2. Fuster JJ, Ouchi N, Gokce N, Walsh K. Obesity-induced changes in adipose tissue microenvironment and their impact on cardiovascular disease. Circ Res. 2016;118:1786–1807.
3. Corona-Meraz FI, Robles-De Anda JA, Madrigal-Ruiz P-M, Díaz-Rubio G-I, Castro-Albarrán J, Navarro-Hernández R-E. In: Çakmur H, editor. Obesity. London: Intechopen; 2020.
4. Manna P, Jain SK. Obesity, oxidative stress, adipose tissue dysfunction, and the associated health risks: causes and therapeutic strategies. Metab Syndr Relat Disord. 2015;13:423–444.
5. McMurray F, Patten DA, Harper ME. Reactive oxygen species and oxidative stress in obesity-recent findings and empirical approaches. Obesity (Silver Spring). 2016;24:2301–2310.
6. Haslam DW, James WP. Obesity. Lancet. 2005;366:1197–1209.
7. Grundy SM, Brewer HB Jr, Cleeman JI, Smith SC Jr, Lenfant C, American Heart Association, et al. Definition of metabolic syndrome: report of the National Heart, Lung, and Blood Institute/American Heart Association conference on scientific issues related to definition. Circulation. 2004;109:433–438.
8. Rangwala SM, Lazar MA. Transcriptional control of adipogenesis. Annu Rev Nutr. 2000;20:535–559.
9. Lefterova MI, Lazar MA. New developments in adipogenesis. Trends Endocrinol Metab. 2009;20:107–114.

10. Calzadilla P, Sapochnik D, Cosentino S, Diz V, Dicelio L, Calvo JC, et al. N-acetylcysteine reduces markers of differentiation in 3T3-L1 adipocytes. Int J Mol Sci. 2011;12:6936–6951.

11. Totan BR, Baygut H, Karada MG. Vitamin C physiology: the known and the unknown in obesity. J Food Nutr Res. 2019;7: 613–618.

12. de Villiers D, Potgieter M, Ambele MA, Adam L, Durandt C, Pepper MS. The role of reactive oxygen species in adipogenic differentiation. Adv Exp Med Biol. 2018;1083:125–144.

13. Castro JP, Grune T, Speckmann B. The two faces of reactive oxygen species (ROS) in adipocyte function and dysfunction. Biol Chem. 2016;397:709–724.

14. Wellen KE, Thompson CB. Cellular metabolic stress: considering how cells respond to nutrient excess. Mol Cell. 2010;40: 323–332.

15. Jankovic A, Korac A, Buzadzic B, Otasevic V, Stancic A, Daiber A, et al. Redox implications in adipose tissue (dys)function—a new look at old acquaintances. Redox Biol. 2015;6: 19–32.

16. DeVallance E, Li Y, Jurczak MJ, Cifuentes-Pagano E, Pagano PJ. The role of NADPH oxidases in the etiology of obesity and metabolic syndrome: contribution of individual isoforms and cell biology. Antioxid Redox Signal. 2019;31: 687–709.

17. Han CY. Roles of reactive oxygen species on insulin resistance in adipose tissue. Diabetes Metab J. 2016;40:272–279.

18. Schroder K, Wandzioch K, Helmcke I, Brandes RP. Nox4 acts as a switch between differentiation and proliferation in preadipocytes. Arterioscler Thromb Vasc Biol. 2009;29:239–245.

19. Liu GS, Chan EC, Higuchi M, Dusting GJ, Jiang F. Redox mechanisms in regulation of adipocyte differentiation: beyond a general stress response. Cell. 2012;1:976–993.

20. Catalán V, Gómez-Ambrosi J, Rodríguez A, Ramírez B, Rotellar F, Valentí V, et al. Increased levels of calprotectin in obesity are related to macrophage content: impact on inflammation and effect of weight loss. Mol Med. 2011;17:1157–1167.

21. Sakurai T, Izawa T, Kizaki T, Ogasawara JE, Shirato K, Imaizumi K, et al. Exercise training decreases expression of inflammation-related adipokines through reduction of oxidative stress in rat white adipose tissue. Biochem Biophys Res Commun. 2009;379:605–609.

22. Pepping JK, Freeman LR, Gupta S, Keller JN, Bruce-Keller AJ. NOX2 deficiency attenuates markers of adiposopathy and brain injury induced by high-fat diet. Am J Physiol Endocrinol Metab. 2013;304:E392–404.

23. Ronis MJ, Sharma N, Vantrease J, Borengasser SJ, Ferguson M, Mercer KE, et al. Female mice lacking p47phox have altered adipose tissue gene expression and are protected against high fat-induced obesity. Physiol Genomics. 2013;45:351–366.

24. Li Y, Mouche S, Sajic T, Veyrat-Durebex C, Supale R, Pierroz D, et al. Deficiency in the NADPH oxidase 4 predisposes towards diet-induced obesity. Int J Obes (Lond). 2012;36:1503–1513.

25. Ruiz-Ojeda FJ, Ruperez AI, Gomez-Llorente C, Gil A, Aguilera CM. Cell models and their application for studying adipogenic differentiation in relation to obesity: a review. Int J Mol Sci. 2016;17:1040.

26. Tung YC, Hsieh PH, Pan MH, Ho CT. Cellular models for the evaluation of the antiobesity effect of selected phytochemicals from food and herbs. J Food Drug Anal. 2017;25:100–110.

27. Burton GR, Nagarajan R, Peterson CA, Mcgehee RE Jr. Microarray analysis of differentiation-specific gene expression during 3T3-L1 adipogenesis. Gene. 2004;329:167–185.

28. Madsen L, Petersen RK, Sørensen MB, Jørgensen C, Hallenborg P, pridal L, et al. Adipocyte differentiation of 3T3-L1 preadipocytes is dependent on lipoxygenase activity during the initial stages of the differentiation process. Biochem J. 2003;375:539–549.

29. Samuni Y, Cook JA, Choudhuri R, DeGraff W, Sowers AL, Krishna MC, et al. Inhibition of adipogenesis by Tempol in 3T3-L1 cells. Free Radic Biol Med. 2010;49:667–673.

30. Qian SW, Li X, Zhang YY, Huang HY, Liu Y, Sun X, et al. Characterization of adipocyte differentiation from human mesenchymal stem cells in bone marrow. BMC Dev Biol. 2010; 10:47.

31. Yin C, Xiao Y, Zhang W, Xu E, Liu W, Yi X, et al. DNA microarray analysis of genes differentially expressed in adipocyte differentiation. J Biosci. 2014;39:415–423.

32. Lefterova MI, Haakonsson AK, Lazar MA, Mandrup S. PPARgamma and the global map of adipogenesis and beyond. Trends Endocrinol Metab. 2014;25:293–302.

33. Zhao XY, Chen XY, Zhang ZJ, Kang Y, Liao WM, Yu WH, et al. Expression patterns of transcription factor PPARgamma and C/EBP family members during in vitro adipogenesis of human bone marrow mesenchymal stem cells. Cell Biol Int. 2015;39:457–465.

34. Vassiliou G, Benoist F, Lau P, Kavaslar GN, Mcpherson R. The low density lipoprotein receptor-related protein contributes to selective uptake of high density lipoprotein cholesteryl esters by SW872 liposarcoma cells and primary human adipocytes. J Biol Chem. 2001;276:48823–48830.

35. Stratford EW, Castro R, Daffinrud J, Skarn M, Lauvrak S, Munthe E, et al. Characterization of liposarcoma cell lines for preclinical and biological studies. Sarcoma. 2012;2012:148614.

36. Nativel B, Marimoutou M, Thon-Hon VG, Gunasekaran MK, Andries J, Stanislas G, et al. Soluble HMGB1 is a novel adipokine stimulating IL-6 secretion through RAGE receptor in SW872 preadipocyte cell line: contribution to chronic inflammation in fat tissue. PLoS One. 2013;8:e76039.

37. Gauthier A, Vassiliou G, Benoist F, Mcpherson R. Adipocyte low density lipoprotein receptor-related protein gene expression and function is regulated by peroxisome proliferator-activated receptor gamma. J Biol Chem. 2003;278:11945–11953.

38. Greene DJ, Izem L, Morton RE. Defective triglyceride biosynthesis in CETP-deficient SW872 cells. J Lipid Res. 2015;56: 1669–1678.

39. Koopman R, Schaart G, Hesselink MK. Optimisation of oil red O staining permits combination with immunofluorescence and automated quantification of lipids. Histochem Cell Biol. 2001; 116:63–68.

40. Fiorani M, Guidarelli A, Capellacci V, Cerioni L, Crinelli R, Cantoni O. The dual role of mitochondrial superoxide in arsenite toxicity: signaling at the boundary between apoptotic commitment and cytoprotection. Toxicol Appl Pharmacol. 2018; 345:26–35.

41. Guidarelli A, Cerioni L, Fiorani M, Catalani A, Cantoni O. Arsenite-induced mitochondrial superoxide formation: time and concentration requirements for the effects of the metalloid on the endoplasmic reticulum and mitochondria. J Pharmacol Exp Ther. 2020;373:62–71.

42. Folda A, Citta A, Scalcon V, Calì T, Zonta F, Scutari G, et al. Mitochondrial thioredoxin system as a modulator of cyclophilin D redox state. Sci Rep. 2016;6:23071.

43. Fiorani M, Scotti M, Guidarelli A, Burattini S, Falcieri E, Cantoni O. SVCT2-dependent plasma and mitochondrial membrane transport of ascorbic acid in differentiating myoblasts. Pharmacol Res. 2020;159:105042.

44. Brundu S, Nencioni L, Celestino I, Coluccio P, Palamara AT, Magnani M, et al. Validation of a reversed-phase high performance liquid chromatography method for the simultaneous analysis of cysteine and reduced glutathione in mouse organs. Oxid Med Cell Longev. 2016;2016:1746985.

45. Kauffman ME, Kauffman MK, Traore K, Zhu H, Trush MA, Jia Z, et al. MitoSOX-based flow cytometry for detecting mitochondrial ROS. React Oxyg Species. 2016;2:361–370.

46. Wojtala A, Bonora M, Malinska D, Pinton P, Duszynski J, Wieckowski MR. Methods to monitor ROS production by fluorescence microscopy and fluorometry. Methods Enzymol. 2014; 542:243–262.

47. Canonico B, Cesarini E, Salucci S, Luchetti F, Falcieri E, di Sario G, et al. Defective autophagy, mitochondrial clearance and lipophagy in Niemann-pick type B lymphocytes. PLoS One. 2016;11:e0165780.

48. Benedetti S, Catalani S, Palma F, Canonico B, Luchetti F, Galati R, et al. Acyclovir induces cell cycle perturbation and apoptosis in Jurkat leukemia cells, and enhances chemotherapeutic drug cytotoxicity. Life Sci. 2018;215:80–85.

49. Mehlem A, Hagberg CE, Muhl L, Eriksson U, Falkevall A. Imaging of neutral lipids by oil red O for analyzing the metabolic status in health and disease. Nat Protoc. 2013;8:1149–1154.

50. Hagberg CE, Li Q, Kutschke M, Bhowmick D, Kiss E, Shabalina IG, et al. Flow cytometry of mouse and human adipocytes for the analysis of browning and cellular heterogeneity. Cell Rep. 2018;24:e2745.

51. Asumendi A, Morales MC, Alvarez A, Arechaga J, Perez-Yarza G. Implication of mitochondria-derived ROS and cardiolipin peroxidation in N-(4-hydroxyphenyl)retinamide-induced apoptosis. Br J Cancer. 2002;86:1951–1956.

52. Leloup C, Casteilla L, Carrière A, Galinier A, Benani A, Carneiro L, et al. Balancing mitochondrial redox signaling: a key point in metabolic regulation. Antioxid Redox Signal. 2011; 14:519–530.

53. Wild AC, Moinova HR, Mulcahy RT. Regulation of gamma-glutamylcysteine synthetase subunit gene expression by the transcription factor Nrf2. J Biol Chem. 1999;274:33627–33636.

54. Wu Z, Xie Y, Morrison RF, Bucher NL, Farmer SR. PPARgamma induces the insulin-dependent glucose transporter GLUT4 in the absence of C/EBPalpha during the conversion of 3T3 fibroblasts into adipocytes. J Clin Invest. 1998; 101:22–32.

55. Farmer SR. Transcriptional control of adipocyte formation. Cell Metab. 2006;4:263–273.

56. Gao H, Li D, Yang P, Zhao L, Wei L, Chen Y, et al. Suppression of CD36 attenuates adipogenesis with a reduction of P2X7 expression in 3T3-L1 cells. Biochem Biophys Res Commun. 2017;491:204–208.

57. Wilson-Fritch L, Burkart A, Bell G, Mendelson K, Leszyk J, Nicoloro S, et al. Mitochondrial biogenesis and remodeling during adipogenesis and in response to the insulin sensitizer rosiglitazone. Mol Cell Biol. 2003;23:1085–1094.

58. Hofmann AD, Beyer M, Krause-Buchholz U, Wobus M, Bornhäuser M, Rödel G. OXPHOS supercomplexes as a hallmark of the mitochondrial phenotype of adipogenic differentiated human MSCs. PLoS One. 2012;7:e35160.

59. Zhang Y, Marsboom G, Toth PT, Rehman J. Mitochondrial respiration regulates adipogenic differentiation of human mesenchymal stem cells. PLoS One. 2013;8:e77077.

60. Suski J, Lebiedzinska M, Bonora M, Pinton P, Duszynski J, Wieckowski MR. Relation between mitochondrial membrane potential and ROS formation. Methods Mol Biol. 2018;1782: 57–381.

61. Atashi F, Modarressi A, Pepper MS. The role of reactive oxygen species in mesenchymal stem cell adipogenic and osteogenic differentiation: a review. Stem Cells Dev. 2015;24:1150–1163.

62. Wang W, Zhang Y, Lu W, Liu K. Mitochondrial reactive oxygen species regulate adipocyte differentiation of mesenchymal stem cells in hematopoietic stress induced by arabinosylcytosine. PLoS One. 2015;10:e0120629.

63. Lee H, Lee YJ, Choi H, Ko EH, Kim JW. Reactive oxygen species facilitate adipocyte differentiation by accelerating mitotic clonal expansion. J Biol Chem. 2009;284:10601–10609.

64. Panday A, Sahoo MK, Osorio D, Batra S. NADPH oxidases: an overview from structure to innate immunity-associated pathologies. Cell Mol Immunol. 2015;12:5–23.

65. Tormos KV, Anso E, Hamanaka RB, Eisenbart J, Joseph J, Kalyanaraman B, et al. Mitochondrial complex III ROS regulate adipocyte differentiation. Cell Metab. 2011;14:537–544.

66. Kovac S, Angelova PR, Holmström KM, Zhang Y, Dinkova-Kostova AT, Abramov AY. Nrf2 regulates ROS production by mitochondria and NADPH oxidase. Biochim Biophys Acta. 2015;1850:794–801.

67. Dinkova-Kostova AT, Abramov AY. The emerging role of Nrf2 in mitochondrial function. Free Radic Biol Med. 2015;88:179–188.

68. Circu ML, Aw TY. Glutathione and modulation of cell apoptosis. Biochim Biophys Acta. 2012;1823:1767–1777.

69. Meister A, Anderson ME. Glutathione. Annu Rev Biochem. 1983;52:711–760.

70. Booty LM, King MS, Thangaratnarajah C, Majd H, James AM, Kunji ERS, et al. The mitochondrial dicarboxylate and 2-oxoglutarate carriers do not transport glutathione. FEBS Lett. 2015;589:621–628.

71. Bachhawat AK, Thakur A, Kaur J, Zulkifli M. Glutathione transporters. Biochim Biophys Acta. 2013;1830:3154–3164.

72. Mari M, Morales A, Colell A, Garcia-Ruiz C, Fernandez-Checa JC. Mitochondrial glutathione, a key survival antioxidant. Antioxid Redox Signal. 2009;11:2685–2700.

73. Kamga CK, Zhang SX, Wang Y. Dicarboxylate carrier-mediated glutathione transport is essential for reactive oxygen species homeostasis and normal respiration in rat brain mitochondria. Am J Physiol Cell Physiol. 2010;299:C497–505.

74. Handy DE, Loscalzo J. Redox regulation of mitochondrial function. Antioxid Redox Signal. 2012;16:1323–1367.

75. Jaganjac M, Milkovic L, Sunjic SB, Zarkovic N. The NRF2, thioredoxin, and glutathione system in tumorigenesis and anticancer therapies. Antioxidants. 2020;9:1151.

76. Paradies G, Paradies V, Ruggiero FM, Petrosillo G. Oxidative stress, cardiolipin and mitochondrial dysfunction in

nonalcoholic fatty liver disease. World J Gastroenterol. 2014;
20:14205–14218.

77. Calabrese G, Morgan B, Riemer J. Mitochondrial glutathione:
regulation and functions. Antioxid Redox Signal. 2017;27:1162–
1177.

SUPPORTING INFORMATION

Additional supporting information may be found online in the Supporting Information section at the end of this article.

Supplementary Material

Table S1. Antibodies used in the study.

Primary Antibodies	Host	Dilution	Company	Secondary antibody
C/EBPβ	Rabbit	*IC 1:100 WB 1:1000	Santa Cruz Biotech; sc-150	IC: Biotinylated anti-rabbit IgG-BA1000 (Vector Lab, CA) WB: goat anti-rabbit IgG-HRP (Santa Cruz sc-2004).
C/EBPδ	Rabbit Mouse	IC 1:100 WB 1:1000	Santa Cruz Biotech; sc-151 Santa Cruz Biotech; sc-365546	IC: Biotinylated anti-rabbit IgG-BA1000 (Vector Lab, CA) WB: m-IgGk BP-HRP (Santa Cruz, sc-516102)
PPARγ	Mouse Rabbit	IC 1:100 WB 1:1000	Santa Cruz Biotech; sc-7273 Cell Signaling 81B8	IC: Biotinylated anti-mouse IgG-BA2000 (Vector Lab, CA) WB: goat anti-rabbit IgG-HRP (Santa Cruz sc-2004).
CD36	Rabbit	IC 1:140 WB 1:1000	AbCam-ab78054;	IC: Biotinylated anti-rabbit IgG-BA1000 (Vector Lab, CA) WB: goat anti-rabbit IgG-HRP (Santa Cruz sc-2004).
Actin	Mouse	WB 1:1000	Biorad VMA00048	WB: m-IgGk BP-HRP (Santa Cruz, sc-516102)
Nrf2	Rabbit	WB 1:1000	Cell Signaling D1Z9C	WB: goat anti-rabbit IgG-HRP (Santa Cruz sc-2004).
p47^{phox}	Rabbit	IF 1:100	St. John's Laboratory, UK; S370	IF: goat anti-rabbit IgG-FITC sc-2012
Trx-2	Mouse	WB 1:1000	Santa Cruz Biotech; sc-133201	WB: m-IgGk BP-HRP (Santa Cruz, sc-516102)

*IC, Immunocitochemistry; IF, Immunofluorescence; WB, Western Blotting.

CHAPTER 2: PAPER 2

Clozapine suppresses NADPH oxidase activation, counteracts cytosolic H₂O₂, and triggers early onset mitochondrial dysfunction during adipogenesis of human liposarcoma SW872 cells

Giulia Blandino [a,1], Mara Fiorani [a,*,1], Barbara Canonico [a], Rita De Matteis [a], Andrea Guidarelli [a], Mariele Montanari [a], Gloria Buffi [a], Lucia Coppo [b], Elias S.J. Arnér [b,c], Orazio Cantoni [a]

[a] *Department of Biomolecular Sciences, University of Urbino Carlo Bo, Urbino, Italy*
[b] *Division of Biochemistry, Department of Medical Biochemistry and Biophysics, Karolinska Institutet, Stockholm, Sweden*
[c] *Department of Selenoprotein Research and the National Tumor Biology Laboratory, National Institute of Oncology, Budapest, Hungary*

A R T I C L E   I N F O

A B S T R A C T

Long-term treatment of schizophrenia with clozapine (CLZ), an atypical antipsychotic drug, is associated with an increased incidence of metabolic disorders mediated by poorly understood mechanisms. We herein report that CLZ, while slowing down the morphological changes and lipid accumulation occurring during SW872 cell adipogenesis, also causes an early (day 3) inhibition of the expression/nuclear translocation of CAAT/enhancer-binding protein β and peroxisome proliferator-activated receptor γ. Under the same conditions, CLZ blunts NADPH oxidase-derived reactive oxygen species (ROS) by a dual mechanism involving enzyme inhibition and ROS scavenging. These effects were accompanied by hampered activation of the nuclear factor (erythroid-derived2)-like 2 (Nrf2)-dependent antioxidant responses compared to controls, and by an aggravated formation of mitochondrial superoxide. CLZ failed to exert ROS scavenging activities in the mitochondrial compartment but appeared to actively scavenge cytosolic H₂O₂ derived from mitochondrial superoxide. The early formation of mitochondrial ROS promoted by CLZ was also associated with signs of mitochondrial dysfunction. Some of the above findings were recapitulated using mouse embryonic fibroblasts.

We conclude that the NADPH oxidase inhibitory and cytosolic ROS scavenging activities of CLZ slow down SW872 cell adipogenesis and suppress their Nrf2 activation, an event apparently connected with increased mitochondrial ROS formation, which is associated with insulin resistance and metabolic syndrome. Thus, the cellular events characterised herein may help to shed light on the more detailed molecular mechanisms explaining some of the adverse metabolic effects of CLZ.

1. Introduction

Second generation antipsychotics (SGAs) are fundamental drugs for the cure of schizophrenia and other psychiatric disorders. SGAs present important advantages with respect to first-generation antipsychotics, as they effectively control both the positive and negative symptoms of schizophrenia, with a significant reduction of extrapyramidal side effects. However, SGAs are not immune from severe reactions. Indeed, substantial evidence links SGA exposure to metabolic impairment, making patients more vulnerable to cardiovascular alterations, hypertension, hyperlipidaemia, body weight gain, insulin resistance and type 2 diabetes [1–4].

Clozapine (CLZ) is one of the most effective SGAs, frequently employed to treat psychosis resistant to other pharmacotherapies [5] and severely ill patients [6], which however also causes serious cardiovascular complications [7,8] and body weight gain [9,10].

The identification of the mechanism(s) mediating the metabolic effects of CLZ is complicated by the complexity of its pharmacological profile, characterised by antagonism to various subtypes of dopaminergic, serotoninergic, noradrenergic, muscarinic, and histaminergic receptors [10–12], as well as by other receptor-independent effects [13, 14]. Indeed, CLZ inhibits the activity of enzymes such as pyruvate kinase, mitochondrial malate dehydrogenase, succinate dehydrogenase

---

Abbreviations		NOX-2	NADPH oxidase-2
		NQO1	NAD(P)H: quinone oxidoreductase 1
C/EBPs	CAAT/enhancer-binding proteins	NR	Nile Red
CLZ	clozapine	Nrf2	nuclear factor (erythroid-derived2)-like 2
DCF	chloromethyl-2′,7′-dichlorodihydrofluorescein diacetate	ORO	Oil Red O
DM	differentiation medium	PMA	phorbol-12-myristate-13-acetate
DTNB	dithiobis-2-nitrobenzoic acid	PPARγ	peroxisome proliferator-activated receptor γ
GCL	glutamate-cysteine ligase	qPCR	quantitative real time PCR
Glut4	Glucose Transporter Type 4	ROS	reactive oxygen species
HPLC	high performance liquid chromatography	SDS	sodium dodecyl sulphate
IBMX	3-isobutyl-1-methylxanthine	SGAs	second generation antipsychotics
LD	lipid droplet	TrxR-1	thioredoxin reductase-1
MEF	mouse embryonic fibroblast	Trx-1	thioredoxin-1
NAO	nonyl acridine orange	Trx-2	thioredoxin-2

and cytochrome oxidase [15–17] and causes other effects which may potentially contribute to the induction of mitochondrial dysfunction [18], an event implicated in insulin resistance and more generally in metabolic syndrome [19,20]. As a final note, CLZ has been reported to induce mitochondrial dysfunction in cell types of different origin, through yet undefined mechanisms [18].

Although mitochondrial dysfunction is often associated with the formation of reactive oxygen species (ROS), CLZ can also counteract oxidative stress, for example through inhibition of NADPH oxidase-2 (NOX-2) [21,22] or by having a direct antioxidant activity [23–25]. The lipophilic nature of CLZ is critical to determine its final concentration in different cellular compartments and tissues. The sub-cellular compartmentalization of the drug should also represent a critical determinant of the redox signalling pathways affected. These important characteristics of CLZ have potential implications in numerous processes regulated by ROS, which also include adipogenesis [26–28].

Based on the above considerations, studies using cultured cells have attempted to address the issues of the direct effects of CLZ in processes associated with the conversion of pre-adipocytes to mature adipocytes, demonstrating that the SGA up-regulates fat-specific markers [29] and stimulates adipogenesis in murine 3T3L1 cells [30–32]. In a recent study, we characterised the differentiation process of human liposarcoma SW872 cells and identified an early formation of NOX-2 derived ROS, apparently associated with critical biochemical events regulating the conversion of pre-adipocytes to mature adipocytes [33]. This early phase was followed by a late phase instead characterised by the emission of mitochondrial ROS and by the onset of mitochondrial dysfunction.

Here we reasoned that the antioxidant and NOX-2 inhibitory properties of CLZ might impact on the early ROS signalling of differentiating SW872 cells, thereby affecting an array of downstream events during the adipogenic process. We report results consistent with this notion, establishing a link between these effects and a delay of the progression of adipogenesis. Most importantly, however, suppression of early ROS formation was associated with the inhibition of nuclear factor (erythroid-derived2)-like 2 (Nrf2)-dependent activation of antioxidant defense that was seen in control cells. Consequently, CLZ, apparently failing to induce ROS scavenging in the mitochondrial compartment, promoted an early formation of mitochondrial ROS and mitochondrial dysfunction.

2. Materials and methods

2.1. Materials

Acrylamide 30 %, glycine, sodium dodecyl sulphate (SDS), methanol, acetonitrile, insulin, dexamethasone, 3-isobutyl-1-methylxanthine (IBMX), DL-Dithiothreitol (DTT), oleic acid-albumin and linoleic acid-

albumin, Oil Red O (ORO), Glutathione (GSH), dithiobis-2-nitrobenzoic acid (DTNB), TWEEN 20, isopropanol, glacial *meta*-phosphoric acid as well most of the reagent-grade chemicals were purchased from Merck Life Science s.r.l. (Milan, Italy). Auranofin, Sodium arsenite, ATP, phorbol-12-myristate-13-acetate (PMA), catalase, H_2O_2 were purchased from Sigma-Aldrich (Milan, Italy). Glycerol, Sodium chloride, EDTA, Na_2HPO_4, KH_2PO_4 and K_2HPO_4 were from Carlo Erba (Milan, Italy). HRP was from SERVA. Luminol was from Alfa Aesar. NADPH tetrasodium salt was purchased from Saaven Werner. WesternBright™ ECL (K-12045-D20) was from Advansta-Aurogenes s.r.l (Rome, Italy). Clarity Max was from Biorad Laboratories s.r.l. (Milan, Italy). CLZ (S2459) was purchased from Selleckchem (Planegg, Germany).

2.2. Cell culture conditions

Human liposarcoma SW872 cells were purchased from the American Type Culture Collection (Rockville, Maryland, USA) and used between passages 3 and 14. Cells were maintained in Dulbecco's modified Eagle medium/nutrient mixture F-12 (DMEM/F12) Merck Life Science s.r.l., supplemented with 10 % foetal bovine serum (FBS) (35-079-CV, Corning-S.I.A.L. s.r.l, Rome, Italy), 100 U/ml penicillin and 100 μg/ml streptomycin. U937 human myeloid leukaemia cells were cultured in suspension in RPMI 1640 medium (Sigma Aldrich) supplemented with 10 % FBS, 100 U/ml penicillin and 100 μg/ml streptomycin. Post-confluent SW872 were induced to adipogenic differentiation by changing the regular growth medium to differentiation medium (DM), containing several differentiation factors including hormonal inducers such as dexamethasone and insulin, as described previously [33].

Primary mouse embryonic fibroblasts (MEFs) [34] were kindly provided by Prof Ester Zito (Istituto di Ricerche Farmacologiche Mario Negri IRCCS, Milan, Italy) and cultured in DMEM - high glucose (6546, Merck Life Science s.r.l.) supplemented with 2 mM L-glutamine (Euroclone), 100 U/ml penicillin, 100 μg/ml streptomycin and 10 % FBS. Post-confluent MEFs were induced to differentiate in a DM containing 0.5 mM IBMX, 830 nM insulin and 1 μM dexamethasone.

CLZ stock solution was prepared in dimethyl sulfoxide (DMSO) at a concentration of 10 mM. The final DMSO concentration never exceeded 0.15 %. CLZ was added to the DM at the concentrations reported in the legends to the figures and the same procedure was repeated after 48 h. Controls (CTR) received DMSO alone.

2.3. Oil Red O staining

SW872 cell neutral lipids were visualized using the soluble selective dye ORO, as described in Ref. [33]. Briefly, cells were washed with potassium phosphate-buffered saline (PBS: 136 mM NaCl, 10 mM Na_2HPO_4, 1.5 mM KH_2PO_4, 3 mM KCl; pH 7.4), fixed with 4 % formaldehyde in PBS (1 h, room temperature, RT), washed with PBS, and

incubated with isopropanol 60 % (1 min, RT). Then, samples were stained with 0.3 % ORO working solution (1 h, RT). The ORO working solution was freshly prepared and filtered before use. After several washes with PBS, lipid droplet formation was followed on an inverted microscope (Axio Vert.A1, Carl Zeiss, Germany) equipped with a Canon EOS 1100 D camera. Cellular ORO quantification was performed by eluting the dye with 100 % isopropanol and measuring the absorption at 510 nm.

ORO staining was performed in MEFs on glass slides, processed as described in Ref. [33]. The slides were incubated with the ORO working solution for 1 h at RT, washed twice with H_2O, counterstained with hematoxylin to visualize nuclei, and mounted in glycerol gel (Sigma-Aldrich-SIAL Rome, Italy).

2.4. Enzyme activities

Thioredoxin Reductase-1 (TrxR-1) activity was determined with the Thioredoxin (Trx) dependent insulin reduction assay, as described in Ref. [35]. Recombinant Trx and TrxR proteins were produced as described previously [36]. In short, total cell lysate protein was incubated with 0.275 mM human insulin, 1.3 mM NADPH and 20 μM human Trx for 30 min in 96-well plates at 37 °C in TE buffer (50 mM Tris-HCl, 2 mM EDTA, pH 7.5) [36]. Finally, a mixture of 6 M guanidine HCl and 1 mM DTNB was added to the plates and the absorbance at 412 nm was measured using a microplate spectrophotometer (TECAN Infinite M200 Pro). To measure Trx-1 activity, samples were incubated with the above-described mix, but replacing Trx-1 with 20 nM TrxR-1. The absorbance values were normalized by the protein concentrations measured using Pierce bicinchoninic acid assay protein assay kit (Thermo Fischer Scientific) according to the manufacturer's protocol.

2.5. RNA extraction and cDNA synthesis

Total RNA extraction was performed with the miRNeasy Mini Kit (Qiagen, Hilden, Germany) after direct lysis with 700 μl of QIAzol Lysis Reagent (Qiagen, Hilden, Germany). Extracted RNA was quantified with a Micro UV–Vis Spectrophotometer Nanoready (Life Real, Hangzhou, Zhejiang, China). Total RNA (500 ng) was reverse transcribed using PrimeScriptTM RT Master Mix (Perfect Real Time) (Takara Bio Inc.) according to the manufacturer instructions with a GeneExplorer Thermal Cycler (Hangzhou Bioer Technology Co., Ltd).

2.6. Quantitative real-time PCR (qPCR)

The gene expression was evaluated by qPCR as previously described [37]. Briefly, the qPCR reactions were carried out in duplicate in a final volume of 20 μl using TB Green PreMix ex Taq II Master Mix (Takara Bio Europe, France) and 200 nM primers listed in Fig. S10 in a RotorGene 6000 instrument (Corbett life science, Sydney, Australia). The amplification conditions were: 95 °C for 10 min, 40 cycles at 95 °C for 10 s and 60 °C for 50 s, followed by a melting curve analysis at the end of each run from 65 to 95 °C, to exclude the presence of non-specific products or primer dimers. A duplicate non-template control was included for each primer pair reaction as negative control. The relative expression levels were calculated by the $2^{-\Delta\Delta Ct}$ method [38] using GAPDH or HPRT as reference genes for SW872 cells or MEFs, respectively.

2.7. Western Blot

Western Blot analysis were performed as described in Ref. [33]. Briefly, cell lysate proteins (25/35 μg) were separated by SDS poly-acrylamide gel electrophoresis and then probed with anti-CAAT/enhancer-binding protein β (C/EBPβ) (1:1000; sc-150; Santa Cruz Biotech, Santa Cruz CA), anti-peroxisome proliferator-activated receptor γ (PPARγ) (1:1000; 81B8; Cell Signalling, USA), anti-Nrf2 (1:1000; D1Z9C; Cell Signalling, USA), anti- NAD(P)H:quinone oxidoreductase 1

(NQO1) (1:1000; A180; Cell Signalling, USA), anti-Trx-1 (1:1000; ATRX-03; IMCO Ltd), anti-GAPDH (1:1000; sc-47724, Santa Cruz Biotech, Santa Cruz CA), anti-Actin (1:1000; VMA00048, Biorad), anti-TrxR-1 (1:1000; sc-58444; Santa Cruz Biotech, Santa Cruz CA), anti-Trx-2 (1:1000; sc-133201; Santa Cruz Biotech, Santa Cruz CA) at 4 °C overnight. After washing 3 times with TBS-T, membranes were further probed with goat anti-rabbit IgG-HRP (1:5000; sc-2004; Santa Cruz Biotech, Santa Cruz CA), with m-IgGk BP-HRP (1:5000; sc-516102; Santa Cruz Biotech) or with rabbit anti-goat IgG (H + L)-HRP (1:5000; 6160-05; SouthernBiotech; UK) for 2 h at RT. Bands were detected using the chemiluminescence system (WesternBright™ ECL). The density of the corresponding bands was measured quantitatively using National Institutes of Health (NIH) Image software (http://rsb.info.nih.gov/nih-image). In Fig. S11 the uncut Western blot membranes are reported. Validation of Trx-1, TrxR-1 and NQO1, Nrf2 and Keap1 WB analyses by using KO cells was reported in Fig. S12.

2.8. Evaluation of DNA content and sub diploid peak by flow cytometry

Cells were harvested and fixed with 70 % cold (−20 °C) ethanol. Samples were washed twice with PBS and pellets were resuspended in PBS, containing 20 μg/ml propidium iodide (PI) and 100 μg/ml RNAse. Samples were kept at 37 °C in the dark for at least 30 min and analysed for cell cycle profile by means of a FACSCanto™ flow cytometer equipped with three lasers. Data were acquired and analysed by FACS-Diva™ flow cytometry software (Becton Dickinson, San Jose, CA).

2.9. Measurement of GSH content

Cellular GSH was measured by high performance liquid chromatography (HPLC) as described in Ref. [39]. Briefly, the cellular pellet was suspended in lysis buffer (0.1 % Triton X-100; 0.1 M Na_2HPO_4; 5 mM Na-EDTA, pH 7.5), vortexed and kept for 10 min on ice. Thereafter, 0.1 N HCl and the precipitating solution (0.2 M glacial *meta*-phosphoric acid, 5 mM sodium EDTA, 0.5 M NaCl) were added to the samples. After centrifugation, the supernatants were collected and kept at −80 °C until HPLC analyses. Just before analysis, DTNB (20 mg in 100 ml of 1 % w/v sodium citrate) was added to the extracts. The samples were filtered through 0.22 μm pore micro-filters and finally analysed for their GSH content by HPLC, using a 15 cm × 4.6 mm, 5 μm Supelco Discovery® C18 column (Supelco, Bellefonte, PA). The UV absorption was detected at 330 nm. The injection volume was 20 μl. The retention time of GSH was approximately 15.7 min.

2.10. BODIPY 493/503 staining of neutral lipid droplets for microscopy

After treatments, MEFs were incubated with 2 μM 4,4-difluoro-1,3,5,7,8-pentamethyl-4-bora-3a,4a-diaza-s-indacene (BODIPY 493/503) in medium with 0.25 % FBS in a cell culture incubator for 20 min. Cells were washed twice with PBS and fixed with 4 % formalin for 30 min at RT. Finally, images were visualized using a fluorescence microscope and the fluorescence intensity was quantified by ImageJ software [40].

2.11. Redox Western Blot

The mitochondrial Trx-2 redox state, having only one active site dithiol-disulfide motif without additional Cys residues, was measured by a redox Western blot approach as described by Guidarelli et al. [41]. Briefly, cells were washed with PBS and detached from the culture dish in 200 μl urea lysis buffer (100 mM Tris/HCl, pH 8.2; urea 8 M; EDTA 1 mM) containing 10 mM iodoacetamide. The samples were then incubated for 20 min at 37 °C and centrifuged for 1 min at 14,000g. Ten volumes of cold acetone/1 M HCl (98:2) were added to the supernatants and the pellets were washed twice with acetone/1 M HCl/H_2O (98.2:10). The pellets were resuspended in 80 μl of urea lysis buffer

containing 3.5 mM dithiothreitol and after 30 min incubation at 37 °C, samples were incubated for a further 30 min at the same temperature in the presence of 30 mM iodoacetic acid. Samples were then subjected to urea polyacrylamide gel electrophoresis (7 M urea and 7 % acrylamide), under non reducing conditions, and blotted [42]. In Fig. S11 the uncut Western blot membranes are reported.

2.12. Flow cytometric staining of fresh, unfixed cells for pan ROS detection

Cells were labelled with MitoSOX red (5 μM, 10 min) (Thermo Fisher Scientific, Milan, Italy), a dye targeting the mitochondria of live cells, selectively oxidized by O_2^- to produce red fluorescence [43]. Chloromethyl-2′,7′-dichlorodihydrofluorescein diacetate (DCF, 5 μM, 30 min) (Thermo Fisher Scientific), a general probe for ROS detection [44], was also used. The cardiolipin-sensitive probe 10-nonyl acridine orange (NAO) (Molecular Probes, Leiden, The Netherlands) was applied (15 min) at a final concentration of 100 nM, as indicated in Ref. [33].

2.13. Flow cytometric and confocal staining of fixed/permeabilised cells for NADPH oxidase subunits

SW872 cells were washed with PBS at RT and resuspended in 100 μl of Dako Intrastain Reagent A (Dako, Agilent, Santa Clara, CA). After 15 min of incubation, cells were washed and resuspended in 100 μl of Dako Intrastain Reagent B [45]. Anti-phosphorylated p47[phox] (STJ91180; St. John's Laboratory, UK), anti-p67[phox] (CQA1036; Cohesion Biosciences) and anti-p47[phox] (SAB4502810; Merck Life Science s.r.l) were incubated for 30 min at 4 °C; after a washing step, anti-rabbit IgG-FITC antibody was added (sc-2012; Santa Cruz Biotech, Santa Cruz CA), as indicated in the manufacturer's instructions. Finally, cells were incubated for 30 min at 4 °C before being processed for flow cytometric and/or confocal microscopy analysis. All cytometric experiments were carried out with a FACSCanto II flow cytometer (BD, Franklin, Lakes, NJ, USA) equipped with an argon laser (Blue, Excitation 488 nm), a helium-neon laser (Red, Excitation 633 nm), and a solid-state diode laser (Violet, Ex 405 nm). Analyses were performed with the FACSDiva™ software (BD); approximately 10,000 cell events were acquired for each sample. Negative controls for phosphorilated-p47[phox] were performed by in-parallel omission of the secondary antibody, as reported in Fig. S13.

2.14. Flow cytometric staining with Nile red (NR)

MEFs were labelled for 15 min with 1 μg/ml NR (1000X stock solution was dissolved in DMSO), as reported in Fiorani et al., 2021 [33]. At least 10,000 events were acquired for each sample.

2.15. Morphology of mitochondrial network by confocal analyses

To evaluate the mitochondrial morphology, the cells were grown on MatTek glass bottom chambers (MatTek Corporation) and stained with MitoTracker Deep red 50 nM (Molecular Probes, Leiden, The Netherlands) for 20 min at 37 °C in 5 % CO₂. Confocal microscopy analyses were performed with a Leica TCS SP5 II confocal microscope (Leica Microsystem, Germany), with 488, 543, and 633 nm illuminations and oil-immersed objectives. The images were further processed and analysed in ImageJ software (NIH, Bethesda, MD, USA).

2.16. Immunocytochemistry

Cells grown on microslides were fixed with 4 % formaldehyde in PBS (15 min), washed twice with PBS and eventually permeabilized (10 min) with PBS containing 0.25 % Triton-X 100. After fixation and permeabilization, cells were blocked with 2 % normal serum for 20 min at room temperature.

Immunostaining was carried out with anti-Nrf2, anti-C/EBPβ, anti-

PPARγ. The immunoreaction was revealed with the avidin–biotin–peroxidase complex (ABC) method (Vector, Burlingame, CA, United States). Peroxidase activity was revealed by diaminobenzidine hydrochloride as chromogen (Sigma-Aldrich, SIAL, Rome, Italy). Nuclei were counterstained with hematoxylin (VWR International, Milan, Italy) and mounted in Eukitt (Kindler, Freiburg, Germany). Antibody specificities were tested by in-parallel omission of the primary antibodies in the immunocytochemical staining (Fig. S14). Preparations were examined using a Nikon light microscope (Nikon Eclipse 80i microscope, Laboratory Imaging, Czech Republic) and an ACT-2U image analyser linked to a Sony equipped with digital camera.

2.17. Single cell DCF and MitoSOX-red fluorescence assays

Logarithmically growing U937, SW872 and MEFs were seeded in 35 mm tissue culture dishes. After CLZ exposure, the cells were incubated for 30 min with either 5 μM DCF or 5 μM MitoSOX red, washed twice with PBS, and finally treated with PMA, H_2O_2, or ATP/arsenite. After treatments, the cells were washed with PBS three times and the fluorescence images were visualized using a fluorescence microscope. The excitation and emission wavelengths were 488 and 515 nm (DCF) and 510 and 580 nm (MitoSOX red), with a 5-nm slit width for both emission and excitation. Images were collected with exposure times of 100–400 ms, digitally acquired and processed for fluorescence determination at the single cell level by ImageJ software. Mean fluorescence values were determined by averaging the fluorescence values of at least 50 cells/treatment condition/experiment.

2.18. Statistical analysis

Data are expressed as mean ± SEM. Statistical differences were analysed by unpaired *t*-test and one-way ANOVA followed by Dunnett's test for multiple comparison using Prism 6.01 software (GraphPad Software). A value of $p < 0.05$ was considered significant.

3. Results

3.1. Clozapine slows down SW872 cell adipogenesis

Post-confluent SW872 cells, characterised by a fibroblast like shape and the virtual absence of lipid droplets (LDs) (time zero sample, T0), undergo progressive changes in morphology when grown in DM for ten days (Fig. 1A). Under the same conditions, cells accumulate significant amounts of lipids in the forms of LDs, as it can be well appreciated by visual inspection of the cultures stained with ORO (Fig. 1A) and after ORO quantification (Fig. 1B). We investigated the effect of CLZ supplementation at the time of DM addition on lipid accumulation, and for this purpose employed concentrations of the SGA ≤ than 15 μM. These concentrations are slightly higher than those found in the bloodstream of treated patients [46–48] but are probably in the right range if one considers the accumulation of this lipophilic drug in the adipose tissue. Furthermore, these concentrations are much lower than those utilised in other studies [15,18,49,50].

As illustrated in Fig. 1A and B, addition of 15 μM CLZ at the time of DM supplementation significantly reduced the rate of lipid accumulation over the 10 days of growth. We decided to focus on the effects mediated by the SGA at the early times of differentiation, in which we previously detected significant redox changes [33]. We therefore performed our experiments at T3 and determined that the inhibitory effects of the drug on LD accumulation were concentration-dependent over a 5–15 μM concentration range (Fig. S1A). In addition, at this time point, flow cytometric analysis failed to reveal sub-diploid peaks in cells which did or did not receive 15 μM CLZ (Fig. S1B). Furthermore, the above inhibitory effects are detected under nontoxic conditions (Fig. S1C). Most of the experiments described below were therefore performed using 15 μM CLZ.
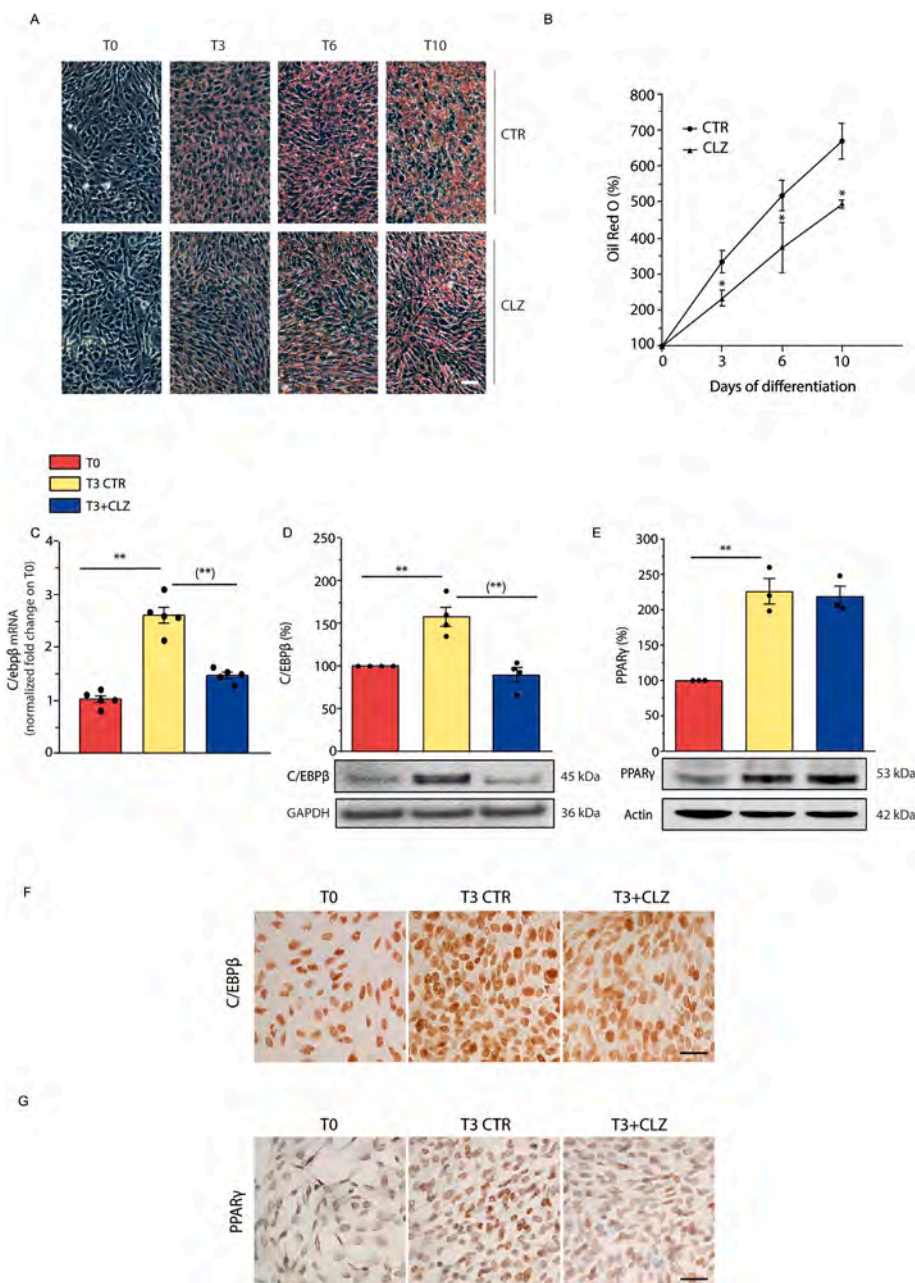
Fig. 1. Clozapine slows down the morphological and biochemical changes occurring during differentiation of SW872 cells.
(A) Representative images of ORO-stained LDs in differentiating SW872 cells grown for 10 days with or without CLZ (15 μM). Magnification 20X; scale bar represents 100 μm. (B) ORO quantification by spectrophotometric analysis at 510 nm. CTR samples received DMSO alone. Data are expressed in % respect to T0 condition. Results represent the means ± SEM calculated from at least three independent determinations, *p < 0.05, as compared to the CTR samples (Unpaired *t*-test). (C) Quantitative real time PCR of C/EBPβ expression after 3 days of differentiation (T3) with or without CLZ. The graph shows the normalized fold change compared to T0. GAPDH was used as housekeeping. (D) Western immunoblotting analysis of C/EBPβ. GAPDH was used as loading control. (E) Western immunoblotting analysis of PPARγ. Actin was used as loading control. T3 CTR received DMSO alone. Data are expressed in % respect to T0. Results represent the means ± SEM calculated from at least three independent determinations. **p < 0.01, as compared to T0; (**)p < 0.01, as compared to T3 (one-way ANOVA followed by Dunnett's test). (F–G) Immunocytochemical analysis of C/EBPβ and PPARγ expression at T3 with or without CLZ (Magnification 40X; scale bar represents 40 μm). Immunolocalization was visualized using diaminobenzidine (brown). Nuclei were counterstained with hematoxylin (blue grey). (For interpretation of the references to colour in this figure legend, the reader is referred to the Web version of this article.)

We found that expression of C/EBPβ, a master regulator of adipogenesis [51], detected at T3 at both the mRNA (Fig. 1C) and protein (Fig. 1D) levels, was abolished by CLZ. Consistently, under the same conditions, immunocytochemical analyses (Fig. 1F) provided evidence for increased nuclear C/EBPβ-immunostaining also sensitive to CLZ.

The effects were less prominent with PPARγ, another critical regulator of adipogenesis [52,53], since its increased expression, clearly detected at T3, was not affected by CLZ (Fig. 1E). However, the SGA

inhibited the translocation of PPARγ to the nuclear compartment (Fig. 1G). The percentage of PPARγ immunoreactive (i.r.) nuclei at T0 corresponded to 13.2 ± 2.4. This percentage remarkably increased at T3 (44.5 ± 5.4; p < 0.01) and CLZ significantly reduced this response (27.9 ± 2.4; p < 0.01).

The results presented here show that CLZ slows down lipid accumulation in differentiating SW872 cells and under the same conditions inhibits C/EBPβ and PPARγ expression and/or nuclear translocation. We

next addressed whether these effects of CLZ were redox related.

3.2. Clozapine suppresses early ROS formation and NOX-2 activation

We have previously found that differentiating SW872 cells display an early ROS formation, at least in part attributable to NOX-2 activation [33]. By using DCF, a probe that fluoresces in response to various types of ROS [44], we recapitulated these findings and demonstrated that the ROS response obtained under these conditions is reduced by CLZ in a concentration-dependent fashion and suppressed at 15 μM (Fig. S2 and Fig. 2A). In addition, CLZ also suppressed the increased p47^{phox} phosphorylation detected at T3, as it can be well appreciated after visualization of the images obtained by confocal microscopy analysis (Fig. 2B). More specifically, phosphorylated p47^{phox}-derived fluorescence appeared brighter and organized in patterns extending from the perinuclear region, with a clear labelling of intracellular/nuclear membrane structures (arrows). The diffused labelling detected at T3 + CLZ was like

that detected at T0.

An identical outcome was provided by flow cytometric studies (representative cytometric profiles and their quantification are shown in Fig. 2C and D, respectively), which also indicated that this event takes place in the absence of significant changes in the overall p47^{phox} expression (Fig. 2E). Finally, a CLZ-sensitive increased expression of p67^{phox}, an additional NOX-2 subunit [54], was also detected at T3 (Fig. 2F).

These results, while further implicating NOX-2 activation in ROS formation occurring at the early stages of SW872 cell differentiation, indicate that this response is suppressed by CLZ as a likely consequence of its ability to cause NOX-2 inhibition.

3.3. Antioxidant activity of clozapine contributes to its suppressive effects on early ROS formation

As previously reported [23–25], CLZ displays an antioxidant activity
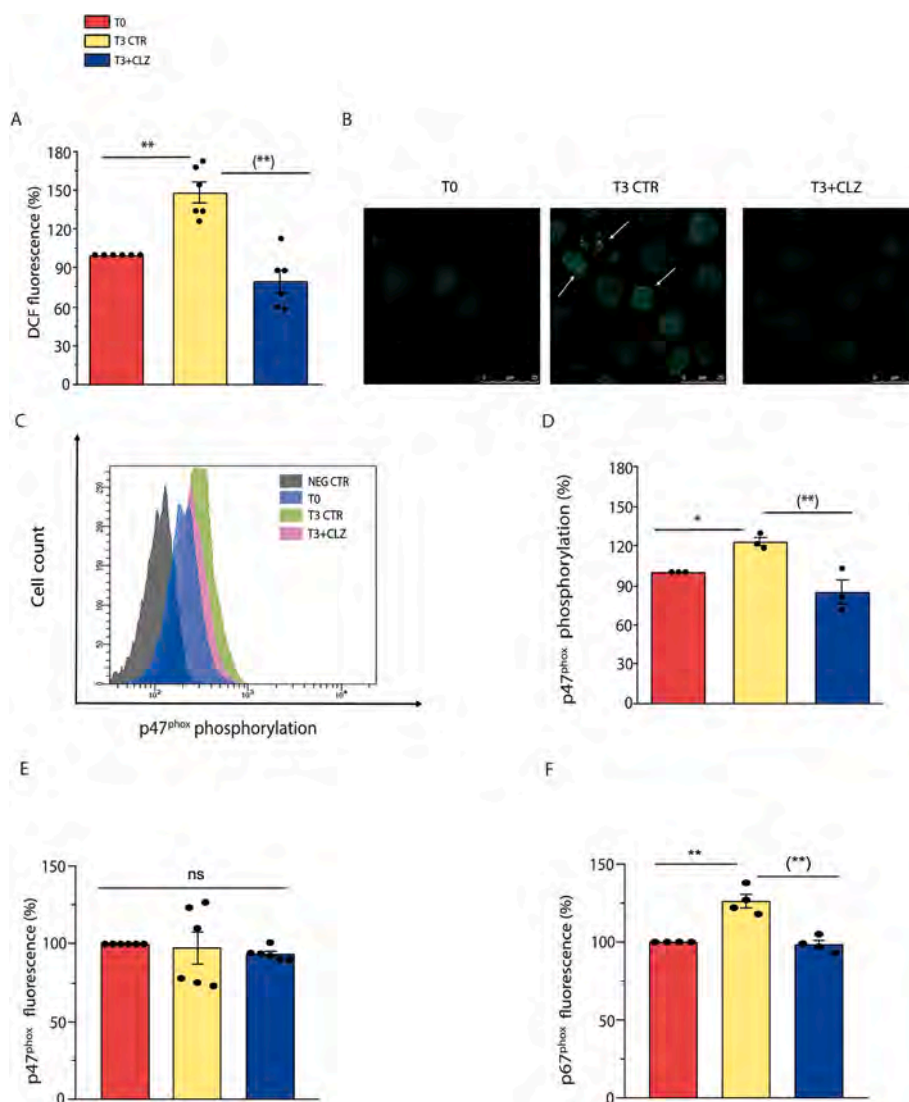
Fig. 2. Clozapine blunts NOX-2-dependent ROS in SW872 cells.
Confluent SW872 cells were induced to differentiate for 3 days with or without CLZ. (A) ROS formation detected with a flow cytometric assay using DCF. (B) Representative micrographs showing phosphorylated p47^{phox} localization (white arrows). In these experiments, the cells were fixed and analysed for immunocytochemical detection of phosphorylated p47^{phox} by confocal microscopy, with all three panels having identical excitation and exposure conditions. Magnification 60X; Scale bar represents 25 μm. (C) Representative flow cytometry histograms of phosphorylated p47^{phox} fluorescence. (D) Statistical analysis of the results obtained in (C). (E–F) Statistical analysis of flow cytometry histograms of p47^{phox} and p67^{phox} fluorescence. T3 CTR received DMSO alone. Data are expressed in % respect to T0 condition. Results represent the means ± SEM calculated from at least three independent determinations. *$p < 0.05$, **$p < 0.01$, as compared to T0; (**)$p < 0.01$, as compared to T3. ns: not significant (one-way ANOVA followed by Dunnett's test).

that might contribute to the observed inhibition of the ROS response. We therefore investigated NOX-2 inhibitory *vs* direct antioxidant effects of CLZ in a well-defined cellular system, i.e., promonocytic U937 cells, that have PMA-responsive NOX-2 activity [55,56]. In these experiments, the cells were initially exposed for 1 or 24 h to CLZ, treated for 15 min with either 0.162 μM PMA or 150 μM H_2O_2, and immediately processed to determine the DCF fluorescence. As indicated in Fig. 3, PMA and H_2O_2 promoted similar fluorescence responses that were suppressed by CLZ supplementation for both 1 (A) and 24 (B) h. These experiments were preceded by preliminary studies, not reported here for the sake of brevity, establishing the H_2O_2 concentration causing a DCF fluorescence response comparable with that elicited by PMA. We also determined that treatments with PMA or H_2O_2 fail to promote loss of membrane integrity and/or apoptotic DNA chromatin fragmentation/condensation (not shown).

We could not perform similar experiments in differentiating SW872 cells, as concomitant ROS formation and activation of various signalling and antioxidant pathways complicates the interpretation of the experimental results. We therefore used undifferentiated SW872 cells and obtained results in line with those from U937 cells. More specifically, the 1 (Fig. 3C) or 24 (Fig. 3D) h exposure protocol to CLZ suppressed the ROS response induced by both 0.162 μM PMA and 750 μM H_2O_2. Note that SW872 cells were particularly resistant to H_2O_2, and that a concentration of the oxidant five times greater than that used in U937 cells was needed to promote a fluorescence response like that mediated by PMA. These differences are not surprising, as remarkable variations in the susceptibility of different cell types have been previously reported by various laboratories and attributed to an array of variables, such as cell density, expression of antioxidant enzymes, growth conditions, etc. [57, 58].

We finally performed a luminol-chemiluminescent assay to determine whether, at T3, NOX-2-derived ROS are released in the

extracellular milieu and obtained negative results (Fig. S3B) under the same conditions in which as low as 2.5 μM H_2O_2 caused a clear catalase-sensitive signal (Fig. S3A). This is consistent with the notion, also supported by confocal microscopy images shown in Fig. 2B, that NOX-2 is largely compartmentalised in intracellular/nuclear membranes to mediate ROS-dependent signalling regulation.

The last set of experiments illustrated in this section addressed the issue of whether CLZ was capable of mediating antioxidant effects in the extracellular compartment, which turned out to be the case since the chemiluminescence signal emitted by increasing concentrations of H_2O_2 was dramatically reduced by 15 μM CLZ (Fig. S3C).

The results presented in this section are consistent with the possibility that the inhibitory effects mediated by CLZ on SW872 cell differentiation are paralleled by two different activities of the drug converging in suppression of the early ROS signalling, i.e., NOX-2 inhibition and ROS scavenging.

3.4. Clozapine prevents Nrf2 expression/activation and the ensuing antioxidant response

We analysed the consequences of the inhibitory effects of CLZ on early ROS formation and initially examined Nrf2 expression. Enhanced mRNA (Fig. 4A) and protein (Fig. 4B) Nrf2 expression was clearly detected in differentiating SW872 cells at T3, in parallel with the translocation of the transcription factor to the nuclei (Fig. 4C). Consistently with the notion that Nrf2 activation leads to enhanced expression of numerous antioxidant genes [59,60], we observed an increased expression of NQO1 (Fig. 4D). The increased levels of cellular GSH (Fig. 4E) are also linked to Nrf2, which controls the expression of glutamate-cysteine ligase (GCL), the rate limiting enzyme of GSH synthesis [61]. Likewise, T3 cells displayed increased expression of Trx-1 (Fig. 4F) and of the corresponding reductase (Fig. 4H), as well as an
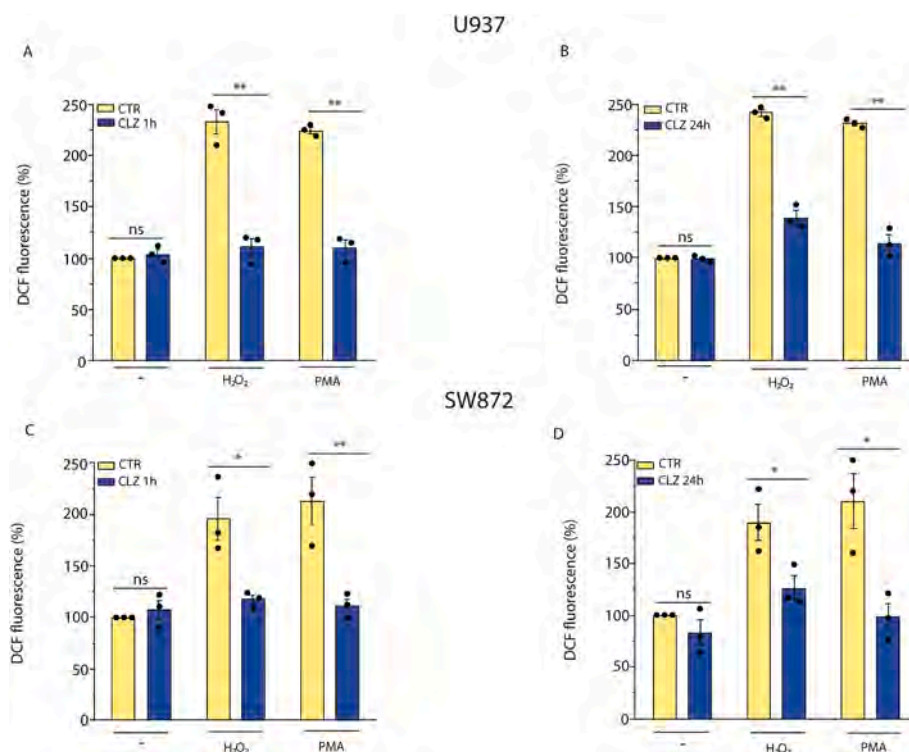

Fig. 3. Antioxidant *vs* NOX-2 inhibitory effects of clozapine in U937 and SW872 cells. U937 cells were treated for 1 h (A) or 24 h (B) with or without CLZ and then exposed for 15 min to either 150 μM H_2O_2 or 0.162 μM PMA. Undifferentiated SW872 cells (C and D) were also used in identical experiments, in which however the concentration of H_2O_2 employed was significantly greater, i.e., 750 μM (30 min) and the exposure time to PMA was 30 min. After treatments, the cells were analysed for DCF fluorescence. CTR samples received DMSO alone. Data are expressed in % respect to untreated CTR cells. Results represent the means ± SEM calculated from at least three independent determinations. *p < 0.05, **p < 0.01, as compared to CTR cells. ns: not significant (Unpaired *t*-test).
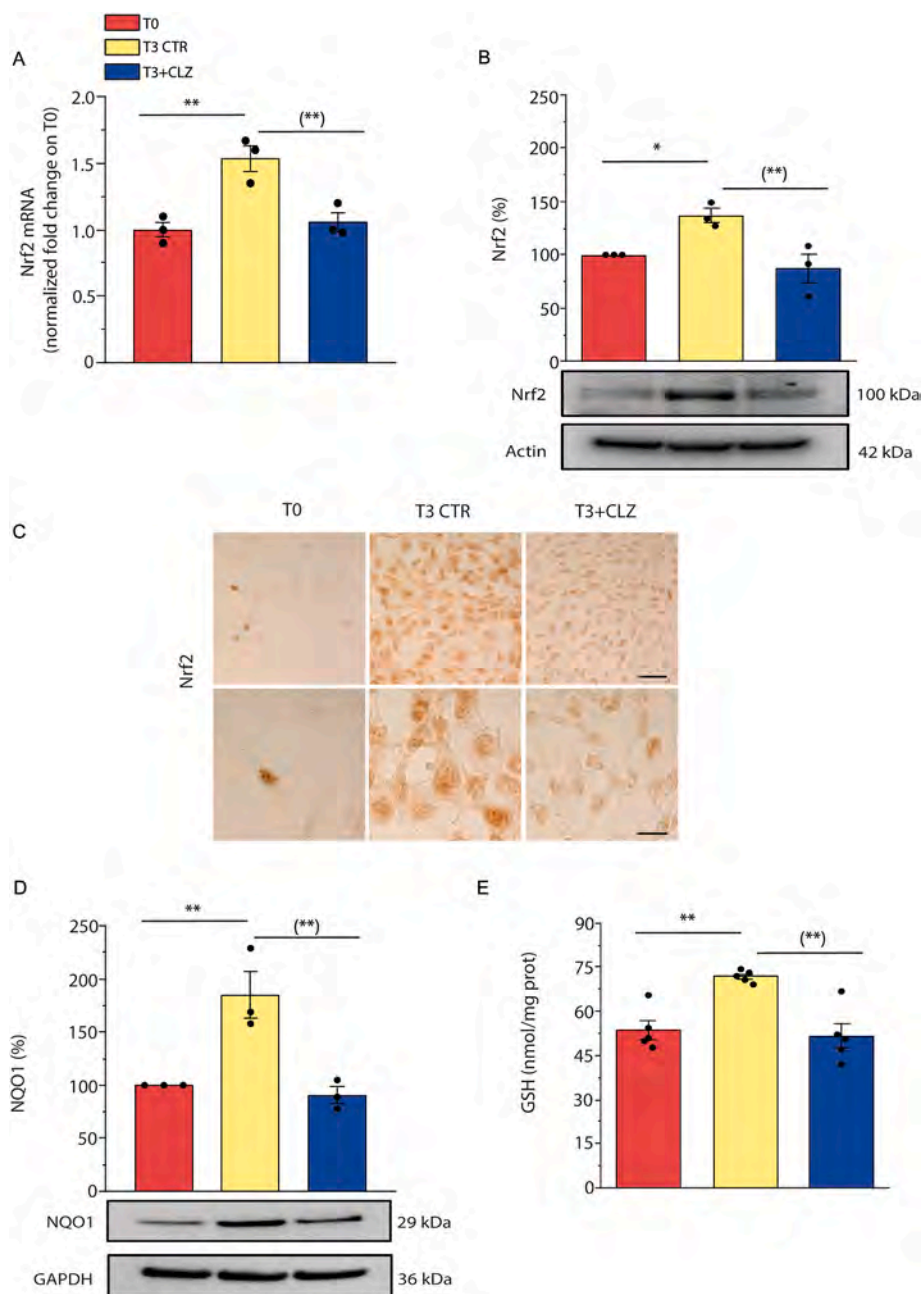
Fig. 4. Clozapine prevents Nrf2 expression and the ensuing antioxidant response in SW872 cells.
Confluent SW872 cells were induced to differentiate for 3 days with or without CLZ (15 μM). (A) Quantitative real time PCR of Nrf2 expression. The graph shows the normalized fold change compared to T0. GAPDH was used as housekeeping. (B) Western immunoblotting analysis of Nrf2 expression. Actin was used as loading control. (C) Immunocytochemical analysis of Nrf2 expression. Magnification 40X and 100X. Scale bars represent 40 and 20 μm. (D) Western immunoblotting analysis of NQO1 expression. GAPDH was used as loading control. (E) GSH content. (F) Western immunoblotting analysis of Trx-1 expression. Actin was used as loading control. (G) Trx-1 activity (expressed as the activity nmol active Trx-1 per mg total protein as inferred from a standard curve with recombinant human Trx-1). (H) Western immunoblotting analysis of TrxR-1 expression. GAPDH was used as loading control. (I) TrxR-1 activity (expressed as the activity pmol active TrxR-1 per mg total protein as inferred from a standard curve with recombinant human TrxR-1). T3 CTR received DMSO alone. Data in the panels B, D, F, and H are expressed in % respect to T0 condition. Results represent the means ± SEM calculated from at least three independent determinations. *$p < 0.05$, **$p < 0.01$, as compared to T0; (*) $p < 0.05$, (**)$p < 0.01$, as compared to T3 (one-way ANOVA followed by Dunnett's test).

increase in the activities of both Trx-1 (Fig. 4G) and TrxR-1 (Fig. 4I).

CLZ blunted Nrf2 expression and the above downstream responses (Fig. 4A–I). CLZ instead failed to directly affect the activity of the Trx system. This notion was established by testing the effect of increasing concentrations of the SGA on the activity of recombinant human TrxR-1 (Fig. S4A), which instead displayed collateral sensitivity to auranofin (Fig. S4B). A high concentration of CLZ (100 μM) also failed to affect

recombinant human Trx-1 activity (Fig. S4C).

Asking whether CLZ could redox cycle with the Trx system, similarly to that seen with the peroxidase mimic ebselen [62], we tested whether CLZ could promote the NADPH consumption of the Trx-1/TrxR-1 system *in vitro* in the presence of H_2O_2, which however was not the case (Figs. S5A and B).

Collectively, the results presented in this section indicate that CLZ,
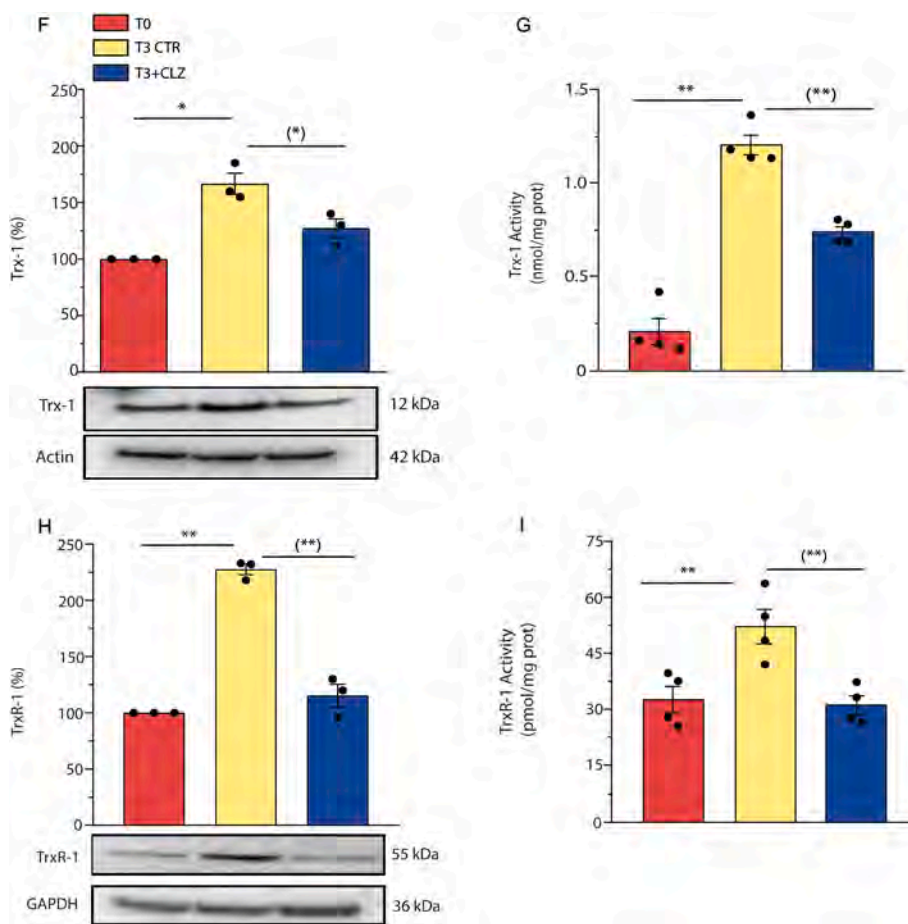
Fig. 4. (*continued*).

by virtue of its ability to inhibit the formation of NOX-2-derived ROS and to scavenge ROS, effectively blunts the Nrf2 signalling.

3.5. Clozapine promotes mitochondrial ROS formation and dysfunction

Adipogenic differentiation of SW872 cells is associated with a late formation of mitochondrial ROS, particularly significant at T10 [33]. CLZ, by blunting the early Nrf2 antioxidant signalling, could anticipate the formation of these ROS and thus distort the intracellular signalling events. On the other hand, the potent antioxidant effects of CLZ, if also displayed in the intramitochondrial compartment, might blunt mitochondrial ROS. These alternatives were next addressed.

To obtain an indication on the impact of the antioxidant activity of CLZ on mitochondrial ROS, we employed once again U937 cells grown for 1 or 24 h with or without CLZ, followed by a final 10 min treatment with 2.5 μM arsenite/100 μM ATP. This cocktail promotes the exclusive formation of mitochondrial superoxide [41] and, not surprisingly, elicited a significant MitoSOX-red fluorescence signal (Fig. 5A and B). This MitoSOX-red fluorescence response was not affected by the 1 h CLZ supplementation protocol (Fig. 5A). Furthermore, there was a significantly increased fluorescent signal in cells that had also received CLZ for 24 h (Fig. 5B).

This indicates that CLZ fails to scavenge mitochondrial ROS, or can even increase their levels, in contrast to the opposite effects in the cytosol shown above (Fig. 3). We thus also performed experiments using DCF, which detects ROS in the cytosol, upon the same 2.5 μM arsenite/100 μM ATP supplementation. Under these conditions, the DCF fluorescent signal should be due to cytosolic H_2O_2 derived from mitochondrial superoxide [41]. In contrast to the results obtained with MitoSOX-Red, CLZ completely suppressed the DCF fluorescence in this

case, in cells supplemented with the drug for 1 (Fig. 5C) or 24 (Fig. 5D) h, respectively.

Thus, CLZ is an effective scavenger of ROS in the cytosolic compartment, regardless of their origin, but not in the mitochondrial compartment. With this information in mind, we next moved to experiments investigating the impact of CLZ on mitochondrial ROS formation in differentiating SW872 cells. As expected, there was no difference in the percentage of MitoSOX-red positive cells at T0 *vs* T3 (Fig. 6A) as well as in the overall fluorescence response (Fig. 6B). Interestingly, however, CLZ significantly increased both effects.

Our findings are therefore consistent with the possibility that suppression of early NOX-2-derived ROS, and of the ensuing stimulation of the Nrf2 antioxidant response, lowers the efficiency of the mitochondrial antioxidant machinery, thereby fostering mitochondrial ROS formation.

To address the issue of the consequences of the early mitochondrial ROS formation, we focused on Trx-2, which, while Nrf2-independent, was increased at T3 in control cells *via* a mechanism sensitive to CLZ (Fig. 6C). Interestingly, under the same conditions CLZ also increased Trx-2 oxidation, as indicated by the outcome of Trx-2 redox state gel assays, using diamide as a positive control (Fig. 6D). However, CLZ did not affect human Trx-2 activity *in vitro* using pure enzyme systems (Fig. S4D).

Fig. 6E shows that CLZ blunts the increased NAO fluorescence detected at T3, indicative of an increased cardiolipin expression. This effect of CLZ is compatible with inhibition of mitochondrial biogenesis and with cardiolipin oxidation. Furthermore, confocal microscopy studies indicated that CLZ promotes mitochondrial fragmentation and a general disorganization of the mitochondrial network, which was not as evidently observed in the absence of CLZ (Fig. 6F and S6).

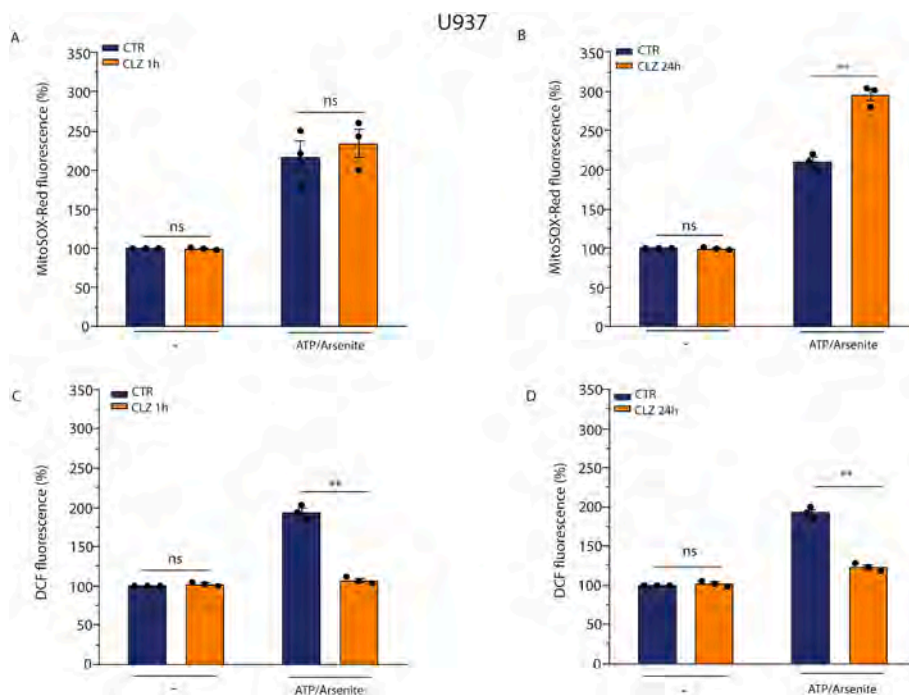Together, these results indicate that CLZ promotes an anticipated

Fig. 5. Clozapine fails to promote an antioxidant effect in the intramitochondrial compartment in U937 cells.
U937 cells were treated for 1 h (A and C) or 24 h (B and D) with or without CLZ and then exposed for 10 min to 100 μM ATP/2.5 μM arsenite. Cells were finally analysed for ROS formation with either MitoSOX-red (A and B) or DCF (C and D). CTR samples received DMSO alone. Data are expressed as % of untreated CTR cells. Results represent the means ± SEM calculated from at least three independent determinations. **p < 0.01 as compared to CTR cells; ns: not significant (Unpaired *t*-test). (For interpretation of the references to colour in this figure legend, the reader is referred to the Web version of this article.)

mitochondrial ROS formation and hence causes mitochondrial dysfunction during the early stages of SW872 cell adipogenic differentiation.

3.6. The effects of clozapine on primary mouse embryonic fibroblast adipogenic differentiation

We performed experiments to determine whether some of the key findings obtained with SW872 cells could be recapitulated in primary cells. For this purpose, we used MEFs, previously shown to undergo adipogenic differentiation when grown in an appropriate DM [63–67]. Adipogenic differentiation of these cells was measured at T3, to minimize the variables with the experiments performed in SW872 cells. We initially provided evidence of lipid accumulation using BODIPY (Fig. 7A–B) and NR (Fig. 7C–D), two fluorescent probes allowing visualization and quantification of LDs, by fluorescence microscopy and flow cytometry, respectively. Qualitative indication of adipogenic differentiation was then provided by ORO-staining experiments (Fig. 7E). Also note that the level of ORO-staining increased further at T4 (Fig. S7A).

Adipogenic differentiation of MEFs was also measured at the molecular level, by documenting an increased mRNA expression of relevant transcription factors (C/EBPβ, C/EBPδ, C/EBPα, PPARγ, GLUT4) at T3 (Fig. 7F) and their further increase at T4 (Fig. S7B). Moreover, C/EBPβ (Fig. 7G) and PPARγ (Fig. S7C) protein expression, respectively detected by WB and cytochemical analyses, as well as DCF fluorescence (Fig. 7H), were significantly increased at T3.

All together, the above results demonstrated that MEFs were grown under conditions leading to adipogenic differentiation and early ROS formation.

We therefore investigated the effects of CLZ (15 μM) and found that the SGA slowed down adipogenesis (Fig. 7), as detected with BODIPY (A and B) and NR-cytofluorimetric analysis (C and D), as well as with ORO-staining (E). CLZ also suppressed the increased mRNA expression of the main adipogenic transcription factors (Fig. 7F) and C/EBPβ protein

expression (Fig. 7G).

In other assays, we confirmed the ability of CLZ to blunt the DCF fluorescence response (Fig. 7H) and to anticipate mitochondrial ROS formation (Fig. 7I).

The last set of experiments was performed to address the issue of whether CLZ displays NOX-2 inhibitory/ROS scavenging effects also in undifferentiated MEFs. As reported in Fig. S8, the SGA suppressed the DCF fluorescence signal induced by 0.162 μM PMA or 100 μM H_2O_2, using both the 1 (A) and 24 (B) h exposure protocol. Note that all the above experiments were performed under conditions in which flow cytometric analysis failed to reveal sub-diploid peaks (Fig. S9A) and toxicity (Fig. S9B) in cells grown with or without CLZ.

It therefore appears that in the MEF model of adipogenic differentiation, CLZ promotes the same critical effects previously described in human SW872 cells, an observation that validates the conclusion of our investigation, i.e., that CLZ slows down adipogenesis and anticipates mitochondrial ROS formation and dysfunction because of the early prevention of formation/scavenging of cytosolic ROS.

4. Discussion

The notion that ROS are critically involved in the adipogenic process is well established [68–70]. In a previous study [33] using the same cells and conditions employed in the present investigation, we identified two separate mechanisms of ROS formation [33], with the first occurring early in differentiation (T3), attributable to NOX-2 activation, and the second one confined to a late phase (T10), in which mitochondria were actively involved.

The increased Nrf2 expression detected at T3 was coincidental with NOX-2-derived superoxide formation, thereby suggesting the existence of a cause-effect relationship. It is well established that mitochondrial superoxide readily dismutates to diffusible H_2O_2 [71], which can then promote extramitochondrial events leading to Nrf2 activation/increased expression. Indeed, the oxidant causes the dissociation of Keap1 from
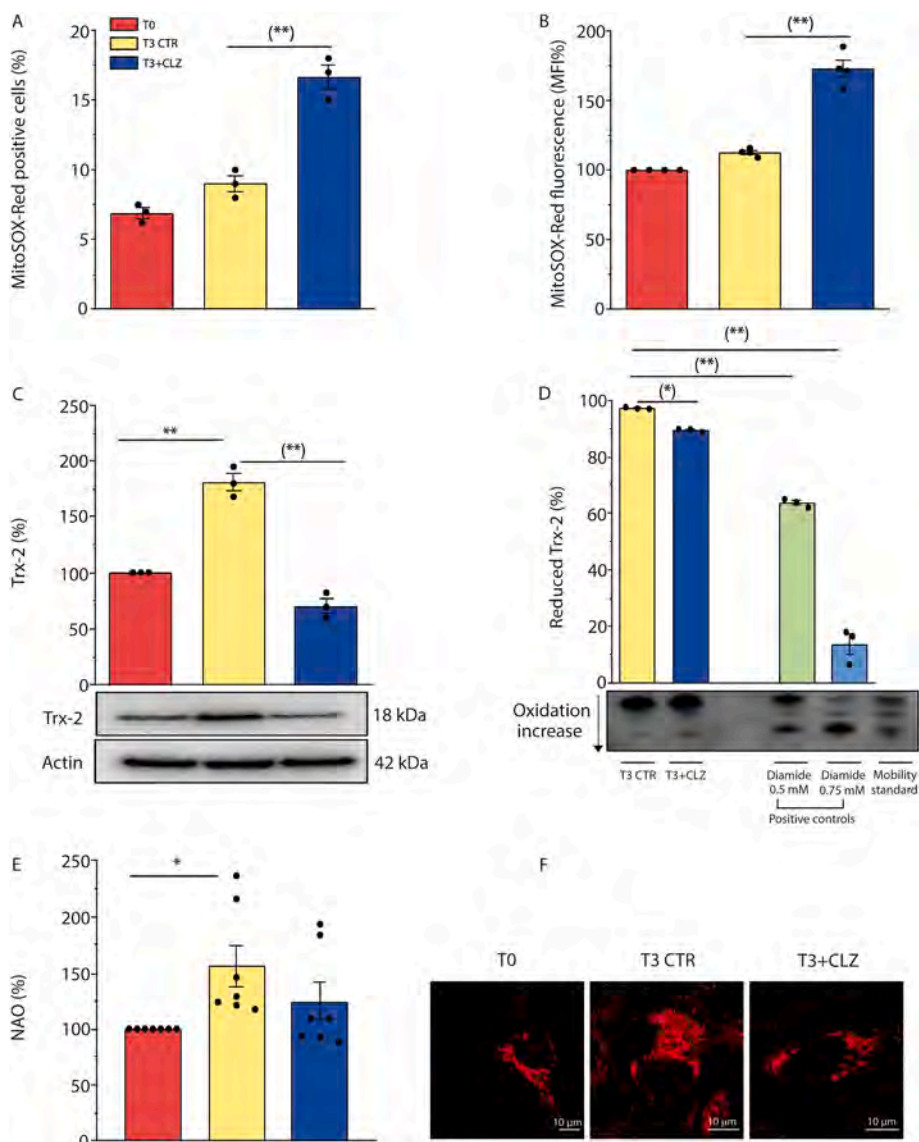
Fig. 6. Clozapine promotes mitochondrial ROS formation and dysfunction in SW872 cells.

Confluent SW872 cells were induced to differentiate for 3 days with or without CLZ. (A) % of MitoSOX-red positive cells (B) Statistical analysis of total MitoSOX-red fluorescence intensity. (C) Western immunoblotting analysis of Trx-2 expression. Actin was used as loading control. (D) Reduced, partially oxidized, and fully oxidized Trx-2 thiol groups. The redox state of Trx-2 was determined by urea polyacrylamide gel electrophoresis under non reducing conditions. Data are expressed as % of T3. (E) NAO analysis. (F) Representative micrographs of mitochondrial network and structural integrity. Images were obtained by confocal microscopy. Magnification 60X; scale bars represent 10 μm. T3 CTR received DMSO alone. Data in the panels B, C and E are expressed in % respect to T0 condition. Results represent the means ± SEM calculated from at least three independent determinations. *p < 0.05, **p < 0.01, as compared to T0; (*)p < 0.05, (**)p < 0.01, as compared to T3 (one-way ANOVA followed by Dunnett's test). (For interpretation of the references to colour in this figure legend, the reader is referred to the Web version of this article.)

Nrf2, either by direct oxidation of critical cysteines of Keap1 itself [72], or via phosphorylation mediated by a variety of kinases [72,73]. Subsequently, Nrf2 translocates to the nucleus thereby increasing the expression of an array of genes encoding proteins with diverse functions and activities, as antioxidant enzymes regulating the redox state in both the cytosolic and mitochondrial compartments [60].

Consistently with the above premise, we herein report evidence for an early increase in the expression and activity of Trx-1 and TrxR-1, expression of NQO1 and GSH levels, as a likely consequence of the increased expression of GCL, the rate limiting enzyme of GSH biosynthesis [61]. The observation that CLZ suppresses both NOX-2-derived ROS and Nrf2 expression, as well as the expression of Nrf2 dependent antioxidant enzymes, therefore suggests that these events are sequentially connected and causally linked. Consistently, we did not observe

direct inhibitory effects of CLZ on the activities of antioxidant enzymes as TrxR-1 or Trx-1.

We also obtained evidence for a similar relationship between NOX-2-derived ROS and progression of adipogenesis, since lipid accumulation was lower in T3 cells supplemented with CLZ, an effect paralleled by inhibition of the expression or nuclear translocation of C/EBPβ or PPARγ, respectively. Although more studies are necessary to univocally implicate Nrf2 in these processes, it is tempting to speculate that the effects of NOX-2-derived ROS on C/EBPβ and PPARγ are mediated by Nrf2, as recently proposed by others [74], which could explain the inhibitory effects of CLZ.

These results provide relevant information on the mechanism(s) involved in the regulation of adipogenic differentiation of SW872 cells. More specifically, it appears that ROS generated by NOX-2 critically
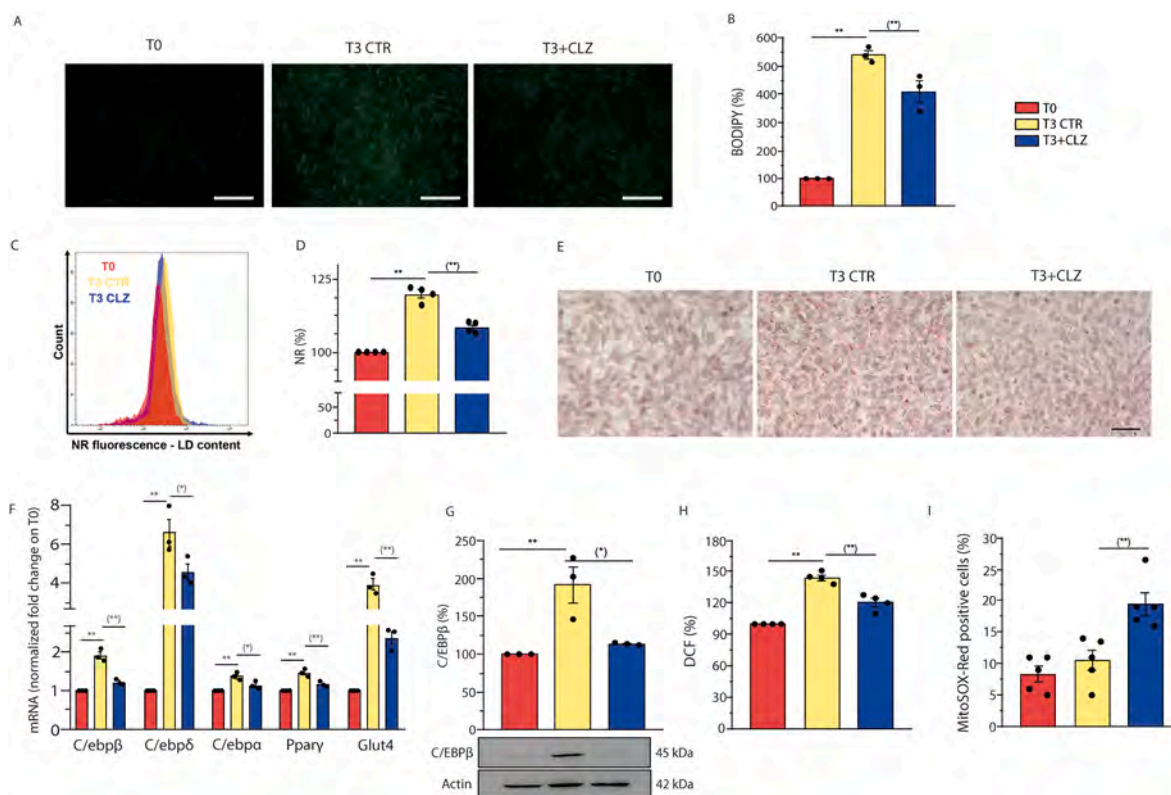
Fig. 7. Clozapine slows down adipogenesis and anticipates mitochondrial ROS formation and dysfunction in MEFs.
Confluent MEFs were induced to differentiate for 3 days with or without CLZ (15 μM). (A) Representative images (40X) of BODIPY-stained LDs in differentiating MEFs. Scale bar = 100 μm. (B) BODIPY fluorescence quantification of (A). (C) Representative flow cytometry histograms of NR-labelled cells in differentiating MEFs. (D) Statistical analysis of the results obtained from NR flow cytometry assays. (E) Representative images (40X) of ORO-stained LDs (red) and hematoxylin-stained nuclei (blue). Scale bar = 50 μm. (F) Quantitative real time PCR of CEBP/β, CEBP/δ, CEBP/α, PPARγ and GLUT4 mRNA expression. The graph shows the normalized fold change compared to T0. HPRT was used as housekeeping. (G) Western immunoblotting analysis of C/EBPβ. Actin was used as loading control. (H) ROS formation detected with a flow cytometric assay using DCF. (I) % of MitoSOX red positive cells. T3 CTR received DMSO alone. Data in panels B, D, G and H are expressed in % respect to T0 condition. Results represent the means ± SEM calculated from at least three independent determinations, **p < 0.01, as compared to T0; (*) p < 0.05, (**) p < 0.01, as compared to T3 (one-way ANOVA followed by Dunnett's test). (For interpretation of the references to colour in this figure legend, the reader is referred to the Web version of this article.)

mediate the triggering of early events regulating an amplification of the overall antioxidant defense and adipocyte differentiation.

We also addressed the mechanism(s) involved in the above effects of CLZ and obtained results suggesting the existence of a dual mechanism based on both NOX-2 inhibition and ROS scavenging.

The notion that CLZ inhibits NOX-2 activity has been previously documented [22,75]. We herein report that, at T3, the SGA suppresses the increased phosphorylation of p47[phox], mainly detected in intracellular membrane compartments, at variance with phagocytic cells, in which NOX-2 subunits mainly translocate to the plasma membrane compartment during activation [76].

CLZ inhibited p47[phox] phosphorylation in the absence of detectable changes in p47[phox] expression. p47[phox] phosphorylation on specific serine residues was previously documented, and this event has been recently associated with the effects of p67[phox] [54], which is transcriptionally regulated [77]. Consistently, a dramatic reduction in p47[phox] phosphorylation was observed in lymphocytes from p67[phox−/−] Chronic Granulomatous disease patients [54].

We found that, at T3, cells display an increased expression of p67[phox] and that this response is suppressed by CLZ, an observation providing a potential link between the decline in p47[phox] phosphorylation and the diminished p67[phox] expression.

We also tried to gather information on the antioxidant effects of CLZ and for this purpose employed promonocytic U937 cells, previously shown to respond to PMA with NOX-2-mediated ROS formation [55,56] and SW872 pre-adipocytes, obtaining similar ROS responses. The

outcome of these and other studies, in which PMA was replaced with reagent H_2O_2, provided clear evidence for an important and long-lasting antioxidant effect of CLZ, which, in concert with NOX-2 inhibition, may account for the observed effects of CLZ on early ROS signalling. In addition, we showed that CLZ is an effective potential scavenger of extracellular ROS, an effect of a yet undefined significance due to the apparent lack of extracellular ROS at T3, which appears to be consistent with the observed expression of the NOX-2 enzyme in intracellular membrane compartments of adipocytes.

We then addressed the issue of whether the powerful antioxidant effects of CLZ might conceal the expected consequences of prevention of the Nrf2-dependent amplification of antioxidant enzymes, with special reference to the mitochondrial compartment. Mitochondrial ROS formation should indeed take place under growth conditions causing an oversupply of electrons to the respiratory chain [78,79] and prevention of Nrf2 expression should anticipate the formation of these species and make cells more vulnerable to mitochondrial dysfunction. Indeed, Nrf2 is not only a master regulator of cellular redox homeostasis, since, as well summarised in Ref. [80], it also regulates critical mitochondrial functions, which include the efficiency for ATP synthesis, as well as mitochondrial biogenesis and integrity. In this perspective, Nrf2, while not directly involved in the regulation of Trx-2 expression, might nevertheless indirectly control its expression, an event readily observed in differentiating SW872 cells at T3.

In principle, the lipophilic nature of CLZ should be permissive for its mitochondrial uptake, thereby potentially allowing effective scavenging

of mitochondrial ROS, but apparently this might not the case, since CLZ failed to reduce the MitoSOX-red fluorescence response selectively induced by the cocktail ATP/arsenite in U937 or SW872 cells. This was an interesting observation, since under the same conditions CLZ instead scavenged mitochondrial ROS-derived H_2O_2 in the cytosolic compartment, in keeping with previous findings obtained in experiments using reagent H_2O_2.

Based on the above considerations, we were not surprised to observe that CLZ remarkably anticipates mitochondrial ROS formation at T3, with no evidence of cytosolic ROS, either mediated by NOX-2 or derived from mitochondrial ROS.

The obvious consequence of early mitochondrial ROS formation in cells made vulnerable by the impaired Nrf2 response was the induction of signs of mitochondrial dysfunction. We indeed demonstrated that these events were associated with a reorganization of the mitochondrial network with clear morphological evidence of fragmentation. At the biochemical level, these events were associated with Trx-2 oxidation, a well-established and critical intramitochondrial target [42]. At least in principle, the results obtained in experiments measuring cardiolipin expression are also suggestive of cardiolipin oxidation induced by mitochondrial ROS, an additional important mitochondrial target.

These findings are however of more complex interpretation as increased cardiolipin expression detected at T3 likely reflects increased mitochondrial biogenesis which accompanies adipogenesis [81]. The inhibitory effects of CLZ might therefore suggest that the SGA blunts mitochondrial biogenesis, which also represents a good explanation for our results on Trx-2 expression, increased at T3 *via* a CLZ-sensitive mechanism. Our results on Nrf2 expression are also consistent with the possibility that CLZ inhibits mitochondrial biogenesis, as Nrf2 is a positive regulator of this process [81]. Finally, confocal images shown in Fig. S6 are compatible with an increased mitochondrial biogenesis detected at T3, significantly reduced by CLZ.

Thus, we herein provide results showing that the anticipated mitochondrial ROS formation triggered by CLZ at T3 promotes some early signs of mitochondrial dysfunction. On the other hand, our results also suggest that CLZ inhibits mitochondrial biogenesis, an effect currently investigated in our laboratories. Impairment of mitochondrial biogenesis and mitochondrial disfunction are indeed strictly related processes in pathological adipogenesis, and critically connected with metabolic diseases and obesity [82].

As a final note, we could replicate the same critical effects described above in a different model of adipogenic differentiation, with different characteristics, i.e., MEFs, of murine origin unlike SW872 cells, which are human. Furthermore, MEFs are primary cells in contrast to SW872 cells, a continuous cell line derived from a liposarcoma.

Thus, the results presented in this study indicate that CLZ blunts early NOX-2 derived ROS, thereby preventing Nrf2 expression and activation, and slowing down adipogenesis. These conditions are then associated with a significantly anticipated formation of mitochondrial ROS, with the SGA displaying antioxidant properties restricted to the cytosolic compartment. CLZ therefore causes an early mitochondrial dysfunction in differentiating adipocytes, an event critically connected with metabolic syndrome associated pathologies.

Fig. 8 summarises this proposed scheme, which may help to explain how CLZ has its unique and sometimes grave adverse metabolic effects when used in the clinical setting.

Author contributions

MF, EA, and OC conceived and designed the study.

MF, G Blandino, G Buffi, BC, RDM, LC, AG, and MM conducted experimental work and data acquisition.

MF, G Blandino, G Buffi, RDM, BC, LC, AG, EA, and OC analysed and interpreted the results.
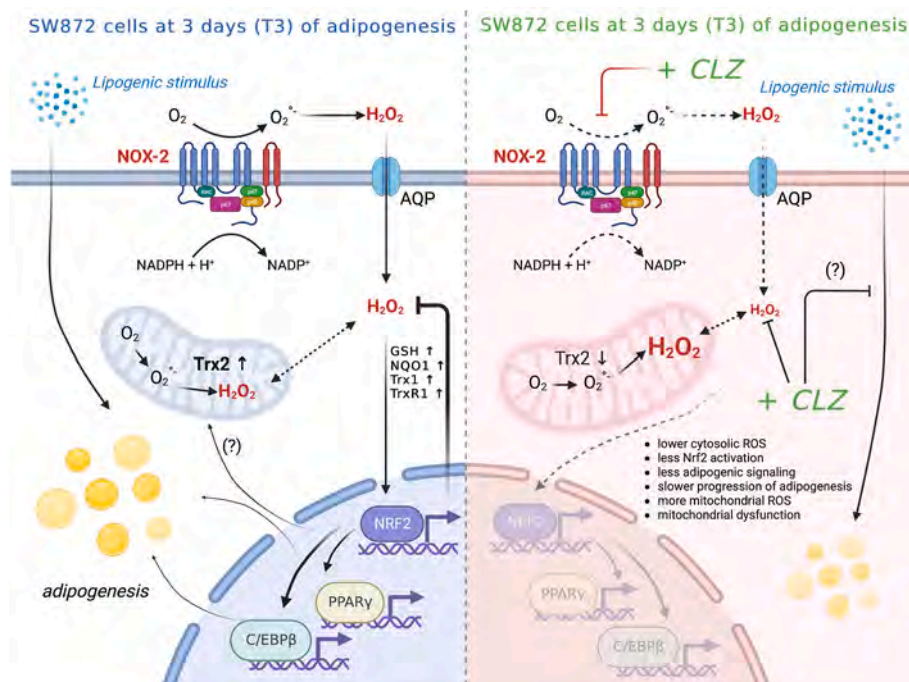

Fig. 8. Schematic summary of the proposed mechanism of clozapine on induction of early mitochondrial dysfunction.
Early adipogenic differentiation of human SW872 cells is accompanied by activation of NOX-2 and superoxide formation. In this scheme the components of NOX-2 enzyme are associated with the plasma membrane, although localization in other membranes (e.g., nuclear membrane) is also possible [83]. Dismutation of superoxide to H_2O_2 triggers Nrf2 activation and a plethora of downstream events associated with the amplification of the antioxidant machinery, maintenance of mitochondrial function and integrity and, possibly, stimulation of the adipogenic signalling. CLZ suppressed ROS formation by a dual mechanism, based on both NOX-2 inhibition and ROS scavenging restricted to the cytosolic compartment, thereby preventing Nrf2 activation and the above downstream events. These conditions were associated with mitochondrial ROS formation, resistant to the antioxidant effects of CLZ, and by signs of an early mitochondrial dysfunction. This figure was edited according to the licence agreement: "Created with BioRender.com".

MF and OC wrote the manuscript.

MF, EA, G Blandino, G Buffi, LC, and OC reviewed, wrote, and edited the final manuscript.

All authors discussed the results and contributed to the final manuscript.

Funding

Conflict of Interest disclosure: The authors declare no potential conflict of interest.

Declaration of competing interest

The authors declare that they have no known competing financial interests or personal relationships that could have appeared to influence the work reported in this paper.

Data availability

Data will be made available on request.

Appendix A. Supplementary data

Supplementary data to this article can be found online at https://doi.org/10.1016/j.redox.2023.102915.

References

[1] A.T. Raben, V.S. Marshe, A. Chintoh, I. Gorbovskaya, D.J. Muller, M.K. Hahn, The complex relationship between antipsychotic-induced weight gain and therapeutic benefits: a systematic review and implications for treatment, Front. Neurosci. 11 (2017) 741.

[2] E. Fernandez-Egea, C. Garcia-Rizo, B. Miller, E. Parellada, A. Justicia, M. Bernardo, B. Kirkpatrick, Testosterone in newly diagnosed, antipsychotic-naive men with nonaffective psychosis: a test of the accelerated aging hypothesis, Psychosom. Med. 73 (8) (2011) 643–647.

[3] P. Oriot, J.L. Feys, S. Mertens de Wilmars, A. Misson, L. Ayache, O. Fagnart, D. Gruson, A. Luts, J. Jamart, M.P. Hermans, M. Buysschaert, Insulin sensitivity, adjusted beta-cell function and adiponectinaemia among lean drug-naive schizophrenic patients treated with atypical antipsychotic drugs: a nine-month prospective study, Diabetes Metabol. 34 (5) (2008) 490–496.

[4] C.C. Chiu, K.P. Chen, H.C. Liu, M.L. Lu, The early effect of olanzapine and risperidone on insulin secretion in atypical-naive schizophrenic patients, J. Clin. Psychopharmacol. 26 (5) (2006) 504–507.

[5] J.W.Y. Yuen, D.D. Kim, R.M. Procyshyn, W.J. Panenka, W.G. Honer, A.M. Barr, A focused review of the metabolic side-effects of clozapine, Front. Endocrinol. 12 (2021), 609240.

[6] J.A. Lieberman, T.S. Stroup, J.P. McEvoy, M.S. Swartz, R.A. Rosenheck, D. O. Perkins, R.S. Keefe, S.M. Davis, C.E. Davis, B.D. Lebowitz, J. Severe, J.K. Hsiao, I. Clinical, Antipsychotic Trials of Intervention Effectiveness, Effectiveness of antipsychotic drugs in patients with chronic schizophrenia, N. Engl. J. Med. 353 (12) (2005) 1209–1223.

[7] H. Nasrallah, A review of the effect of atypical antipsychotics on weight, Psychoneuroendocrinology 28 (Suppl 1) (2003) 83–96.

[8] S. Leucht, C. Corves, D. Arbter, R.R. Engel, C. Li, J.M. Davis, Second-generation versus first-generation antipsychotic drugs for schizophrenia: a meta-analysis, Lancet 373 (9657) (2009) 31–41.

[9] A.H. Barnett, P. Mackin, I. Chaudhry, A. Farooqi, R. Gadsby, A. Heald, J. Hill, H. Millar, R. Peveler, A. Rees, V. Singh, D. Taylor, J. Vora, P.B. Jones, Minimising metabolic and cardiovascular risk in schizophrenia: diabetes, obesity and dyslipidaemia, J. Psychopharmacol. 21 (4) (2007) 357–373.

[10] J.L. Roerig, K.J. Steffen, J.E. Mitchell, Atypical antipsychotic-induced weight gain: insights into mechanisms of action, CNS Drugs 25 (12) (2011) 1035–1059.

[11] G. Tulipano, C. Rizzetti, I. Bianchi, A. Fanzani, P. Spano, D. Cocchi, Clozapine-induced alteration of glucose homeostasis in the rat: the contribution of hypothalamic-pituitary-adrenal axis activation, Neuroendocrinology 85 (2) (2007) 61–70.

[12] Y.E. Savoy, M.A. Ashton, M.W. Miller, F.M. Nedza, D.K. Spracklin, M.H. Hawthorn, H. Rollema, F.F. Matos, E. Hajos-Korcsok, Differential effects of various typical and atypical antipsychotics on plasma glucose and insulin levels in the mouse: evidence for the involvement of sympathetic regulation, Schizophr. Bull. 36 (2) (2010) 410–418.

[13] L. Benarroch, C. Kowalchuk, V. Wilson, C. Teo, M. Guenette, A. Chintoh, Y. Nesarajah, V. Taylor, P. Selby, P. Fletcher, G.J. Remington, M.K. Hahn, Atypical antipsychotics and effects on feeding: from mice to men, Psychopharmacology 233 (14) (2016) 2629–2653.

[14] C. Cuerda, J. Merchan-Naranjo, C. Velasco, A. Gutierrez, M. Leiva, M.J. de Castro, M. Parellada, M. Giraldez, I. Breton, M. Camblor, P. Garcia-Peris, E. Dulin, I. Sanz, M. Desco, C. Arango, Influence of resting energy expenditure on weight gain in adolescents taking second-generation antipsychotics, Clin. Nutr. 30 (5) (2011) 616–623.

[15] M.R. Baig, E. Navaira, M.A. Escamilla, H. Raventos, C. Walss-Bass, Clozapine treatment causes oxidation of proteins involved in energy metabolism in lymphoblastoid cells: a possible mechanism for antipsychotic-induced metabolic alterations, J. Psychiatr. Pract. 16 (5) (2010) 325–333.

[16] C. Walss-Bass, S.T. Weintraub, J. Hatch, J. Mintz, A.R. Chaudhuri, Clozapine causes oxidation of proteins involved in energy metabolism: a possible mechanism for antipsychotic-induced metabolic alterations, Int. J. Neuropsychopharmacol. 11 (8) (2008) 1097–1104.

[17] E.L. Streck, G.T. Rezin, L.M. Barbosa, L.C. Assis, E. Grandi, J. Quevedo, Effect of antipsychotics on succinate dehydrogenase and cytochrome oxidase activities in rat brain, N. Schmied. Arch. Pharmacol. 376 (1–2) (2007) 127–133.

[18] V. Contreras-Shannon, D.L. Heart, R.M. Paredes, E. Navaira, G. Catano, S.K. Maffi, C. Walss-Bass, Clozapine-induced mitochondria alterations and inflammation in brain and insulin-responsive cells, PLoS One 8 (3) (2013), e59012.

[19] P. Sangwung, K.F. Petersen, G.I. Shulman, J.W. Knowles, Mitochondrial dysfunction, insulin resistance, and potential genetic implications, Endocrinology 161 (4) (2020).

[20] J.A. Kim, Y. Wei, J.R. Sowers, Role of mitochondrial dysfunction in insulin resistance, Circ. Res. 102 (4) (2008) 401–414.

[21] H.Q. Tran, S.J. Park, E.J. Shin, T.V. Tran, N. Sharma, Y.J. Lee, J.H. Jeong, C. G. Jang, D.J. Kim, T. Nabeshima, H.C. Kim, Clozapine attenuates mitochondrial burdens and abnormal behaviors elicited by phencyclidine in mice via inhibition of p47 (phox); Possible involvements of phosphoinositide 3-kinase/Akt signaling, J. Psychopharmacol. 32 (11) (2018) 1233–1251.

[22] L. Jiang, X. Wu, S. Wang, S.H. Chen, H. Zhou, B. Wilson, C.Y. Jin, R.B. Lu, K. Xie, Q. Wang, J.S. Hong, Clozapine metabolites protect dopaminergic neurons through inhibition of microglial NADPH oxidase, J. Neuroinflammation 13 (1) (2016) 110.

[23] A. Dalla Libera, G. Scutari, R. Boscolo, M.P. Rigobello, A. Bindoli, Antioxidant properties of clozapine and related neuroleptics, Free Radic. Res. 29 (2) (1998) 151–157.

[24] I. Sadowska-Bartosz, S. Galiniak, G. Bartosz, M. Zuberek, A. Grzelak, A. Dietrich-Muszalska, Antioxidant properties of atypical antipsychotic drugs used in the treatment of schizophrenia, Schizophr. Res. 176 (2–3) (2016) 245–251.

[25] F.F. Brinholi, C.C. Farias, K.L. Bonifacio, L. Higachi, R. Casagrande, E.G. Moreira, D.S. Barbosa, Clozapine and olanzapine are better antioxidants than haloperidol, quetiapine, risperidone and ziprasidone in vitro models, Biomed. Pharmacother Biomedecine & pharmacotherapie 81 (2016) 411–415.

[26] B.R. Imhoff, J.M. Hansen, Differential redox potential profiles during adipogenesis and osteogenesis, Cell. Mol. Biol. Lett. 16 (1) (2011) 149–161.

[27] X. Wang, C. Hai, Redox modulation of adipocyte differentiation: hypothesis of "Redox Chain" and novel insights into intervention of adipogenesis and obesity, Free Radic. Biol. Med. 89 (2015) 99–125.

[28] X. Peng, A. Gimenez-Cassina, P. Petrus, M. Conrad, M. Ryden, E.S. Arner, Thioredoxin reductase 1 suppresses adipocyte differentiation and insulin responsiveness, Sci. Rep. 6 (2016), 28080.

[29] V. Ferreira, D. Grajales, A.M. Valverde, Adipose tissue as a target for second-generation (atypical) antipsychotics: a molecular view, Biochimica et biophysica acta, Mol. Cell Biol. Lipids 1865 (2) (2020), 158534.

[30] T. Tsubai, A. Yoshimi, Y. Hamada, M. Nakao, H. Arima, Y. Oiso, Y. Noda, Effects of clozapine on adipokine secretions/productions and lipid droplets in 3T3-L1 adipocytes, J. Pharmacol. Sci. 133 (2) (2017) 79–87.

[31] C.M. Cottingham, T. Patrick, M.A. Richards, K.D. Blackburn, Tricyclic antipsychotics promote adipogenic gene expression to potentiate preadipocyte differentiation in vitro, Hum. Cell 33 (3) (2020) 502–511.

[32] Y. Hu, E. Kutscher, G.E. Davies, Berberine inhibits SREBP-1-related clozapine and risperidone induced adipogenesis in 3T3-L1 cells, Phytother Res.: PTR 24 (12) (2010) 1831–1838.

[33] M. Fiorani, R. De Matteis, B. Canonico, G. Blandino, A. Mazzoli, M. Montanari, A. Guidarelli, O. Cantoni, Temporal correlation of morphological and biochemical changes with the recruitment of different mechanisms of reactive oxygen species formation during human SW872 cell adipogenic differentiation, Biofactors 47 (5) (2021) 837–851.

[34] S. Germani, A.C. Marchetti, A. Guidarelli, O. Cantoni, V. Sorrentino, E. Zito, Loss-of-rescue of Ryr1(I4895T)-related pathology by the genetic inhibition of the ER stress response mediator CHOP, Sci. Rep. 12 (1) (2022), 20632.

[35] E.S. Arner, A. Holmgren, Physiological functions of thioredoxin and thioredoxin reductase, Eur. J. Biochem. 267 (20) (2000) 6102–6109.

[36] Q. Cheng, E.S.J. Arner, Overexpression of recombinant selenoproteins in E. coli, Methods Mol. Biol. 1661 (2018) 231–240.

[37] G. Buffi, A. Diotallevi, M. Ceccarelli, F. Bruno, G. Castelli, F. Vitale, M. Magnani, L. Galluzzi, The host micro-RNA cfa-miR-346 is induced in canine leishmaniasis, BMC Vet. Res. 18 (1) (2022) 247.

[38] M.W. Pfaffl, A new mathematical model for relative quantification in real-time RT-PCR, Nucleic Acids Res. 29 (9) (2001) e45.

[39] M. Fiorani, A. Guidarelli, V. Capellacci, L. Cerioni, R. Crinelli, O. Cantoni, The dual role of mitochondrial superoxide in arsenite toxicity: signaling at the boundary between apoptotic commitment and cytoprotection, Toxicol. Appl. Pharmacol. 345 (2018) 26–35.

[40] E. Varone, D. Pozzer, S. Di Modica, A. Chernorudskiy, L. Nogara, M. Baraldo, M. Cinquanta, S. Fumagalli, R.N. Villar-Quiles, M.G. De Simoni, B. Blaauw, A. Ferreiro, E. Zito, SELENON (SEPN1) protects skeletal muscle from saturated fatty acid-induced ER stress and insulin resistance, Redox Biol. 24 (2019), 101176.

[41] A. Guidarelli, L. Cerioni, M. Fiorani, A. Catalani, O. Cantoni, Arsenite-induced mitochondrial superoxide formation: time and concentration requirements for the effects of the metalloid on the endoplasmic reticulum and mitochondria, J. Pharmacol. Exp. Therapeut. 373 (1) (2020) 62–71.

[42] A. Folda, A. Citta, V. Scalcon, T. Cali, F. Zonta, G. Scutari, A. Bindoli, M. P. Rigobello, Mitochondrial thioredoxin system as a modulator of cyclophilin D redox state, Sci. Rep. 6 (2016), 23071.

[43] M.E. Kauffman, M.K. Kauffman, K. Traore, H. Zhu, M.A. Trush, Z. Jia, Y.R. Li, MitoSOX-based flow cytometry for detecting mitochondrial ROS, Reactive oxygen species 2 (5) (2016) 361–370.

[44] A. Wojtala, M. Bonora, D. Malinska, P. Pinton, J. Duszynski, M.R. Wieckowski, Methods to monitor ROS production by fluorescence microscopy and fluorometry, Methods Enzymol. 542 (2014) 243–262.

[45] B. Canonico, E. Cesarini, M. Montanari, G. Di Sario, R. Campana, L. Galluzzi, F. Sola, O. Gundogdu, F. Luchetti, A. Diotallevi, W. Baffone, A. Giordano, S. Papa, Rapamycin Re-directs lysosome network, stimulates ER-remodeling, involving membrane CD317 and affecting exocytosis, in Campylobacter jejuni-lysate-infected U937 cells, Int. J. Mol. Sci. 21 (6) (2020).

[46] R.J. Baldessarini, F. Centorrino, J.G. Flood, S.A. Volpicelli, D. Huston-Lyons, B. M. Cohen, Tissue concentrations of clozapine and its metabolites in the rat, Neuropsychopharmacology: official publication of the American College of Neuropsychopharmacology 9 (2) (1993) 117–124.

[47] C. Iglesias Garcia, A. Iglesias Alonso, J. Bobes, Concentrations in plasma clozapine levels in schizophrenic and schizoaffective patients, Rev. Psiquiatía Salud Ment. 10 (4) (2017) 192–196.

[48] J. Lee, M.G. Kim, H.C. Jeong, K.H. Shin, Physiologically-based pharmacokinetic model for clozapine in Korean patients with schizophrenia, Translational and clinical pharmacology 29 (1) (2021) 33–44.

[49] G. Scaini, J. Quevedo, D. Velligan, D.L. Roberts, H. Raventos, C. Walss-Bass, Second generation antipsychotic-induced mitochondrial alterations: implications for increased risk of metabolic syndrome in patients with schizophrenia, Eur. Neuropsychopharmacol: the journal of the European College of Neuropsychopharmacology 28 (3) (2018) 369–380.

[50] A.L. Sertie, A.M. Suzuki, R.A. Sertie, S. Andreotti, F.B. Lima, M.R. Passos-Bueno, W. F. Gattaz, Effects of antipsychotics with different weight gain liabilities on human in vitro models of adipose tissue differentiation and metabolism, Progress in neuro-psychopharmacology & biological psychiatry 35 (8) (2011) 1884–1890.

[51] L. Guo, X. Li, Q.Q. Tang, Transcriptional regulation of adipocyte differentiation: a central role for CCAAT/enhancer-binding protein (C/EBP) beta, J. Biol. Chem. 290 (2) (2015) 755–761.

[52] E.D. Rosen, P. Sarraf, A.E. Troy, G. Bradwin, K. Moore, D.S. Milstone, B. M. Spiegelman, R.M. Mortensen, PPAR gamma is required for the differentiation of adipose tissue in vivo and in vitro, Mol. Cell 4 (4) (1999) 611–617.

[53] M.I. Lefterova, A.K. Haakonsson, M.A. Lazar, S. Mandrup, PPARgamma and the global map of adipogenesis and beyond, Trends Endocrinol. Metabol. 25 (6) (2014) 293–302.

[54] S.A. Belambri, V. Marzaioli, M. Hurtado-Nedelec, C. Pintard, S. Liang, Y. Liu, T. Boussetta, M.A. Gougerot-Pocidalo, R.D. Ye, P.M. Dang, J. El-Benna, Impaired p47phox phosphorylation in neutrophils from patients with p67phox-deficient chronic granulomatous disease, Blood 139 (16) (2022) 2512–2522.

[55] L.C. Pfefferkorn, P.M. Guyre, M.W. Fanger, Functional comparison of the inductions of NADPH oxidase activity and Fc gamma RI in IFN gamma-treated U937 cells, Mol. Immunol. 27 (3) (1990) 263–272.

[56] A. Guidarelli, M. Fiorani, S. Carloni, L. Cerioni, W. Balduini, O. Cantoni, The study of the mechanism of arsenite toxicity in respiration-deficient cells reveals that NADPH oxidase-derived superoxide promotes the same downstream events mediated by mitochondrial superoxide in respiration-proficient cells, Toxicol. Appl. Pharmacol. 307 (2016) 35–44.

[57] K.R. Martin, M.L. Failla, J.C. Smith, Differential susceptibility of CACO-2 and HEPG2 human cell lines to oxidative stress, J. Elisha Mitchell Sci. Soc. 113 (4) (1997) 149–162.

[58] M.S. Yang, H.W. Chan, L.C. Yu, Glutathione peroxidase and glutathione reductase activities are partially responsible for determining the susceptibility of cells to oxidative stress, Toxicology 226 (2–3) (2006) 126–130.

[59] L.E. Tebay, H. Robertson, S.T. Durant, S.R. Vitale, T.M. Penning, A.T. Dinkova-Kostova, J.D. Hayes, Mechanisms of activation of the transcription factor Nrf2 by redox stressors, nutrient cues, and energy status and the pathways through which it attenuates degenerative disease, Free Radic. Biol. Med. 88 (Pt B) (2015) 108–146.

[60] Q. Ma, Role of nrf2 in oxidative stress and toxicity, Annu. Rev. Pharmacol. Toxicol. 53 (2013) 401–426.

[61] S.C. Lu, Regulation of glutathione synthesis, Curr. Top. Cell. Regul. 36 (2000) 95–116.

[62] R. Zhao, H. Masayasu, A. Holmgren, Ebselen: a substrate for human thioredoxin reductase strongly stimulating its hydroperoxide reductase activity and a superfast thioredoxin oxidant, Proc. Natl. Acad. Sci. U.S.A. 99 (13) (2002) 8579–8584.

[63] L. Gatticchi, G. Petricciuolo, P. Scarpelli, L. Macchioni, L. Corazzi, R. Roberti, Tm7sf2 gene promotes adipocyte differentiation of mouse embryonic fibroblasts and improves insulin sensitivity, Biochim. Biophys. Acta Mol. Cell Res. 1868 (1) (2021), 118897.

[64] X. Peng, A. Giménez-Cassina, P. Petrus, M. Conrad, M. Rydén, E.S. Arnér, Thioredoxin reductase 1 suppresses adipocyte differentiation and insulin responsiveness, Sci. Rep. 6 (2016), 28080.

[65] J. Dufau, J.X. Shen, M. Couchet, T. De Castro Barbosa, N. Mejhert, L. Massier, E. Griseti, E. Mouisel, E.Z. Amri, V.M. Lauschke, M. Rydén, D. Langin, In vitro and ex vivo models of adipocytes, Am. J. Physiol. Cell Physiol. 320 (5) (2021) C822–c841.

[66] M. Al-Sayegh, H. Ali, M.H. Jamal, M. ElGindi, T. Chanyong, K. Al-Awadi, M. Abu-Farha, Mouse embryonic fibroblast adipogenic potential: a comprehensive transcriptome analysis, Adipocyte 10 (1) (2021) 1–20.

[67] K.H.T. Mau, D. Karimlou, D. Barneda, V. Brochard, C. Royer, B. Leeke, R.A. de Souza, M. Pailles, M. Percharde, S. Srinivas, A. Jouneau, M. Christian, V. Azuara, Dynamic enlargement and mobilization of lipid droplets in pluripotent cells coordinate morphogenesis during mouse peri-implantation development, Nat. Commun. 13 (1) (2022) 3861.

[68] A. Mehlem, C.E. Hagberg, L. Muhl, U. Eriksson, A. Falkevall, Imaging of neutral lipids by oil red O for analyzing the metabolic status in health and disease, Nat. Protoc. 8 (6) (2013) 1149–1154.

[69] C.E. Hagberg, Q. Li, M. Kutschke, D. Bhowmick, E. Kiss, I.G. Shabalina, M. J. Harms, O. Shilkova, V. Kozina, J. Nedergaard, J. Boucher, A. Thorell, K. L. Spalding, Flow cytometry of mouse and human adipocytes for the analysis of browning and cellular heterogeneity, Cell Rep. 24 (10) (2018) 2746–2756 e5.

[70] A. Asumendi, M.C. Morales, A. Alvarez, J. Arechaga, G. Perez-Yarza, Implication of mitochondria-derived ROS and cardiolipin peroxidation in N-(4-hydroxyphenyl) retinamide-induced apoptosis, Br. J. Cancer 86 (12) (2002) 1951–1956.

[71] K. Bedard, K.H. Krause, The NOX family of ROS-generating NADPH oxidases: physiology and pathophysiology, Physiol. Rev. 87 (1) (2007) 245–313.

[72] C. Yu, J.H. Xiao, The Keap1-Nrf2 system: a mediator between oxidative stress and aging, Oxid. Med. Cell. Longev. 2021 (2021), 6635460.

[73] H. Yuan, Y. Xu, Y. Luo, N.X. Wang, J.H. Xiao, Role of Nrf2 in cell senescence regulation, Mol. Cell. Biochem. 476 (1) (2021) 247–259.

[74] K.S. Schneider, J.Y. Chan, Emerging role of Nrf2 in adipocytes and adipose biology, Adv. Nutr. 4 (1) (2013) 62–66.

[75] X. Hu, H. Zhou, D. Zhang, S. Yang, L. Qian, H.M. Wu, P.S. Chen, B. Wilson, H. M. Gao, R.B. Lu, J.S. Hong, Clozapine protects dopaminergic neurons from inflammation-induced damage by inhibiting microglial overactivation, J. Neuroimmune Pharmacol.: the official journal of the Society on NeuroImmune Pharmacology 7 (1) (2012) 187–201.

[76] J.M. Li, A.M. Shah, Intracellular localization and preassembly of the NADPH oxidase complex in cultured endothelial cells, J. Biol. Chem. 277 (22) (2002) 19952–19960.

[77] H.T. Hsu, Y.T. Tseng, W.J. Wong, C.M. Liu, Y.C. Lo, Resveratrol prevents nanoparticles-induced inflammation and oxidative stress via downregulation of PKC-alpha and NADPH oxidase in lung epithelial A549 cells, BMC Compl. Alternative Med. 18 (1) (2018) 211.

[78] A. Jankovic, A. Korac, B. Buzadzic, V. Otasevic, A. Stancic, A. Daiber, B. Korac, Redox implications in adipose tissue (dys)function–A new look at old acquaintances, Redox Biol. 6 (2015) 19–32.

[79] K.E. Wellen, C.B. Thompson, Cellular metabolic stress: considering how cells respond to nutrient excess, Mol. Cell 40 (2) (2010) 323–332.

[80] A.T. Dinkova-Kostova, A.Y. Abramov, The emerging role of Nrf2 in mitochondrial function, Free Radic. Biol. Med. 88 (Pt B) (2015) 179–188.

[81] S. Heinonen, R. Jokinen, A. Rissanen, K.H. Pietiläinen, White adipose tissue mitochondrial metabolism in health and in obesity, Obes. Rev. 21 (2020), e12958.

[82] J.S. Bhatti, G.K. Bhatti, P.H. Reddy, Mitochondrial dysfunction and oxidative stress in metabolic disorders— a step towards mitochondria based therapeutic strategies, Biochim. Biophys. Acta 1863 (2017) 1066–1077.

[83] J.A. Sipkens, N. Hahn, C.S. van den Brand, C. Meischl, S.A. Cillessen, D.E. Smith, L. J. Juffermans, R.J. Musters, D. Roos, C. Jakobs, H.J. Blom, Y.M. Smulders, P. A. Krijnen, C.D. Stehouwer, J.A. Rauwerda, V.W. van Hinsbergh, H.W. Niessen, Homocysteine-induced apoptosis in endothelial cells coincides with nuclear NOX2 and peri-nuclear NOX4 activity, Cell Biochem. Biophys. 67 (2) (2013) 341–352.
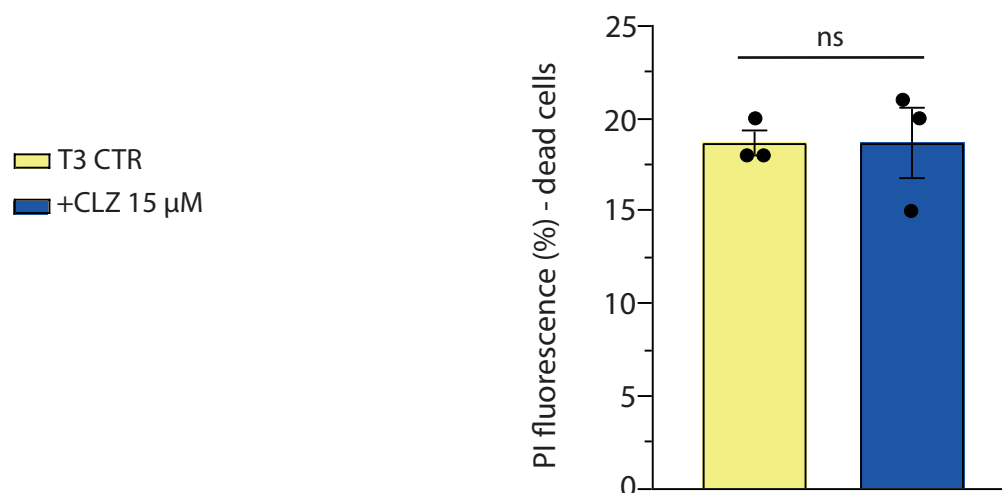
SUPPLEMENTARY DATA
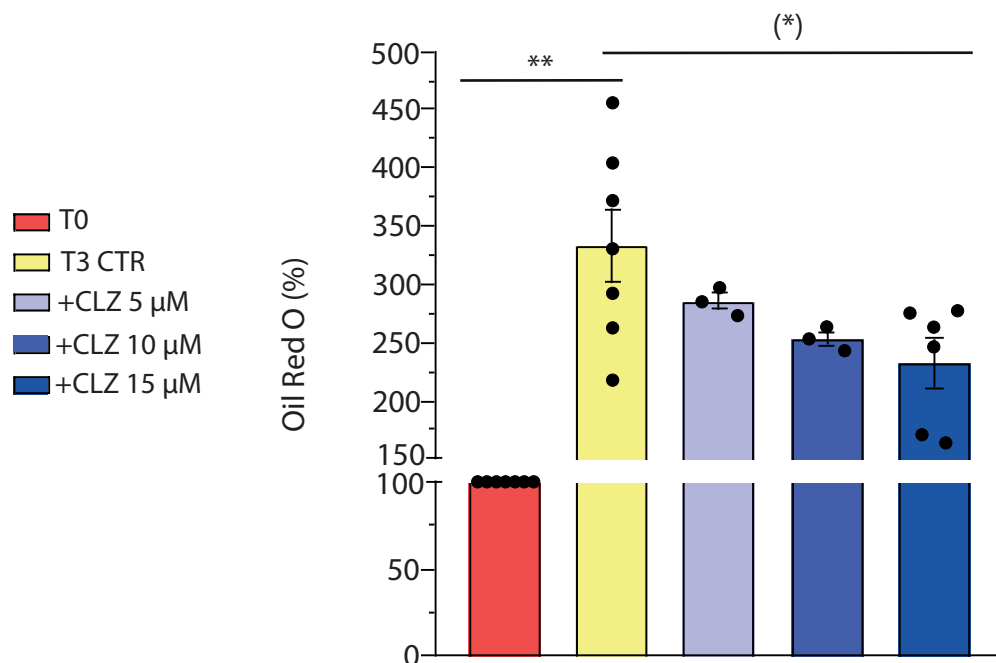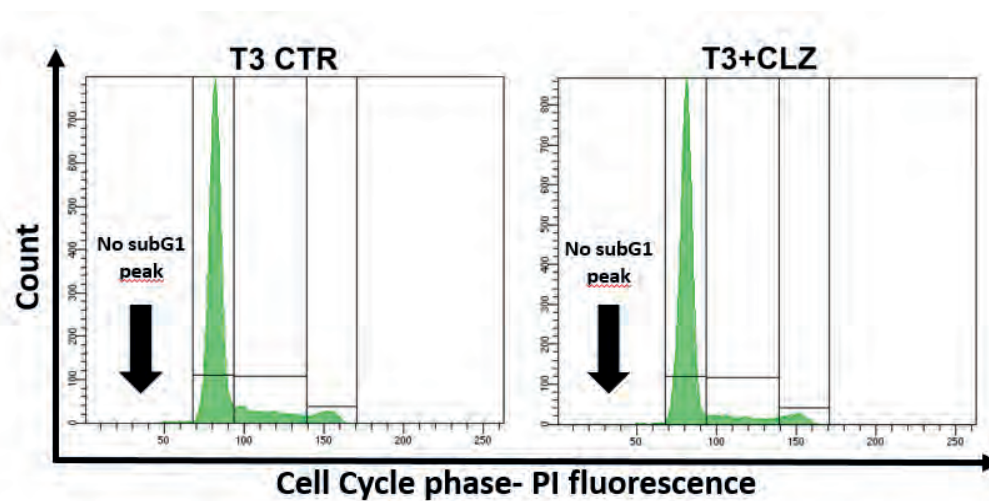
FIGURE S1. Concentration-dependence and toxicity of clozapine in SW872 cells.
(A) SW872 cells were grown for 3 days with increasing concentration of CLZ. LDs were quantified by ORO spectrophotometric analysis at 510 nm. Data are expressed in % respect to T0 condition. Results represent the means ± SEM calculated from at least three independent determinations, **$p < 0.01$, as compared to T0; (*) $p < 0.05$ as compared to T3 (one-way ANOVA followed by Dunnett's multiple comparisons). (B) Flow cytometric evaluation of DNA content showing the absence of sub diploid peaks in cells grown for 3 days with or without CLZ (15 µM). (C) Statistical analysis of the results obtained by PI labelling of fresh cells, for general viability assessment. T3 CTR received DMSO alone. Results represent the means ± SEM calculated from at least three independent determinations. ns: not significant.
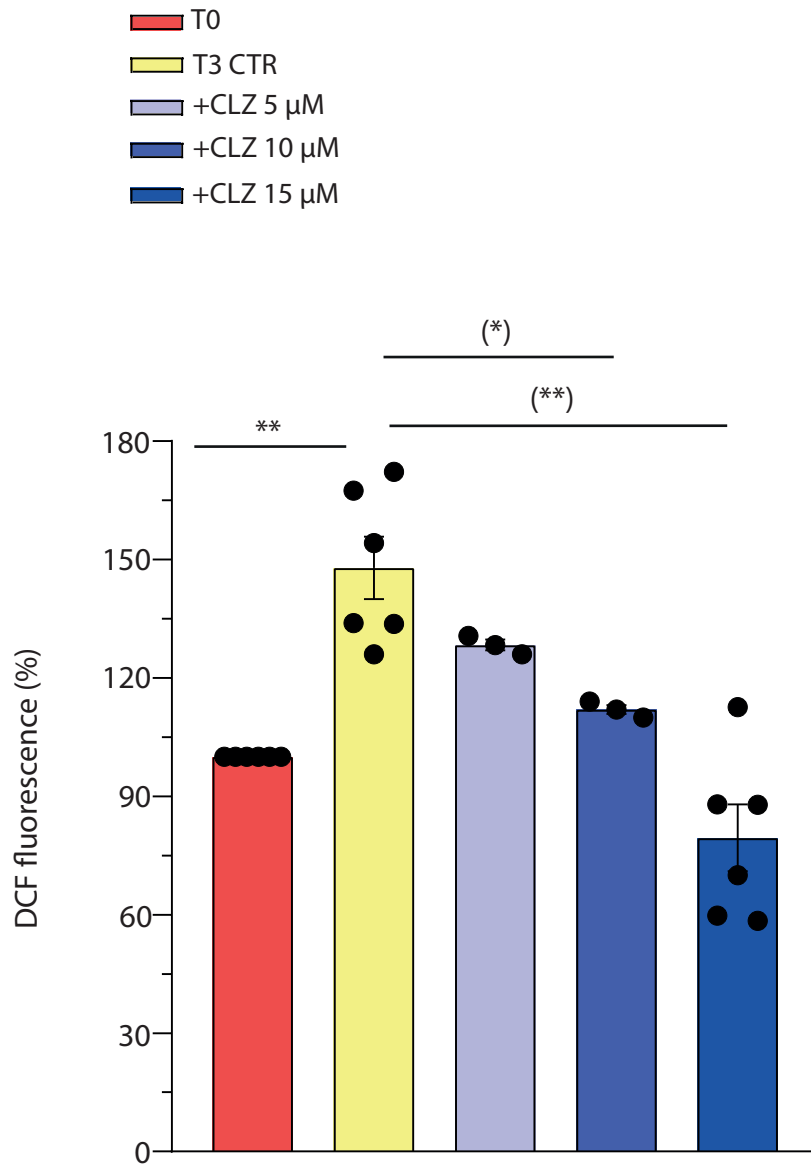
FIGURE S2. Clozapine reduces ROS formation in a dose-dependent manner in SW872 cells. SW872 cells were grown for 3 days with increasing concentration of CLZ. ROS were detected with a flow cytometric assay using DCF. T3 CTR received DMSO alone. Data are expressed in % respect to T0 condition. Results represent the means ± SEM calculated from at least three independent determinations. **p < 0.01, as compared to T0; (*) p < 0.05, (**) p < 0.01, as compared to T3 (one-way ANOVA followed by Dunnett's test).
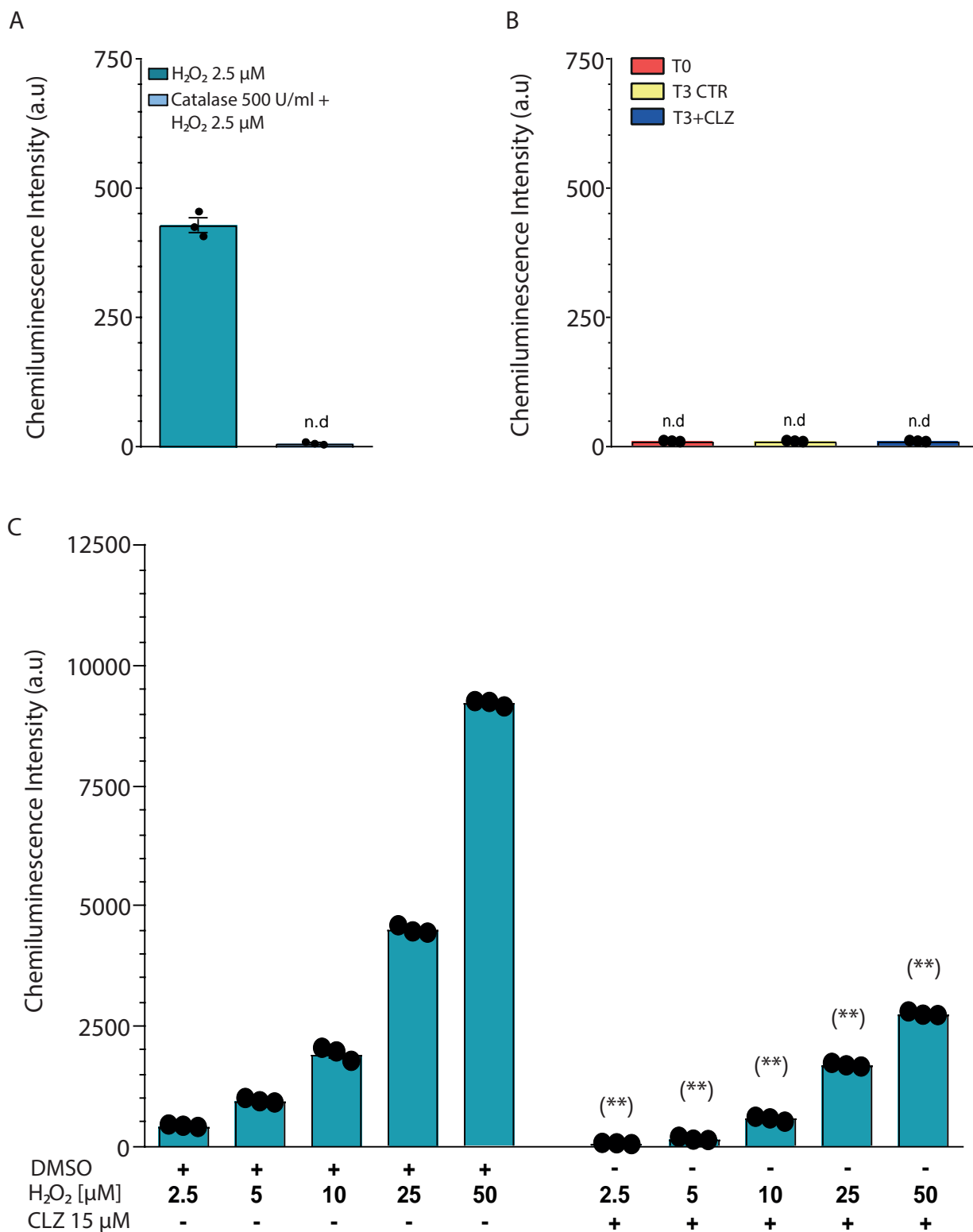
FIGURE S3. Luminol-peroxidase-dependent chemiluminescent assay of extracellular H_2O_2. (A) Addition of 2.5 μM H_2O_2 in PBS causes a detectable signal sensitive to catalase. The method employed was previously described in detail [H. Zhu, Z. Jia, M.A. Trush, Y.R. Li, A Highly Sensitive Chemiluminometric Assay for Real-Time Detection of Biological Hydrogen Peroxide Formation, Reactive oxygen species 1(3) (2016) 216-227]. Briefly, 100 μM luminol and HRP (0.03 U/ml) were added to the mixture (final volume of 200 μl) in a white 96-well plate and the chemiluminescence intensity was determined using a microplate reader (Spark, TECAN). (B) H_2O_2 concentration was measured in SW872 cell medium at T0 and T3 with or without CLZ. n.d., not detectable. T3 CTR received DMSO alone. (C) Effect of CLZ on chemiluminescence signal induced by increasing concentrations of H_2O_2 in PBS. Results represent the means ± SEM calculated from at least three independent determinations. (**) $p < 0.01$, as compared to samples without CLZ (Unpaired t-test).
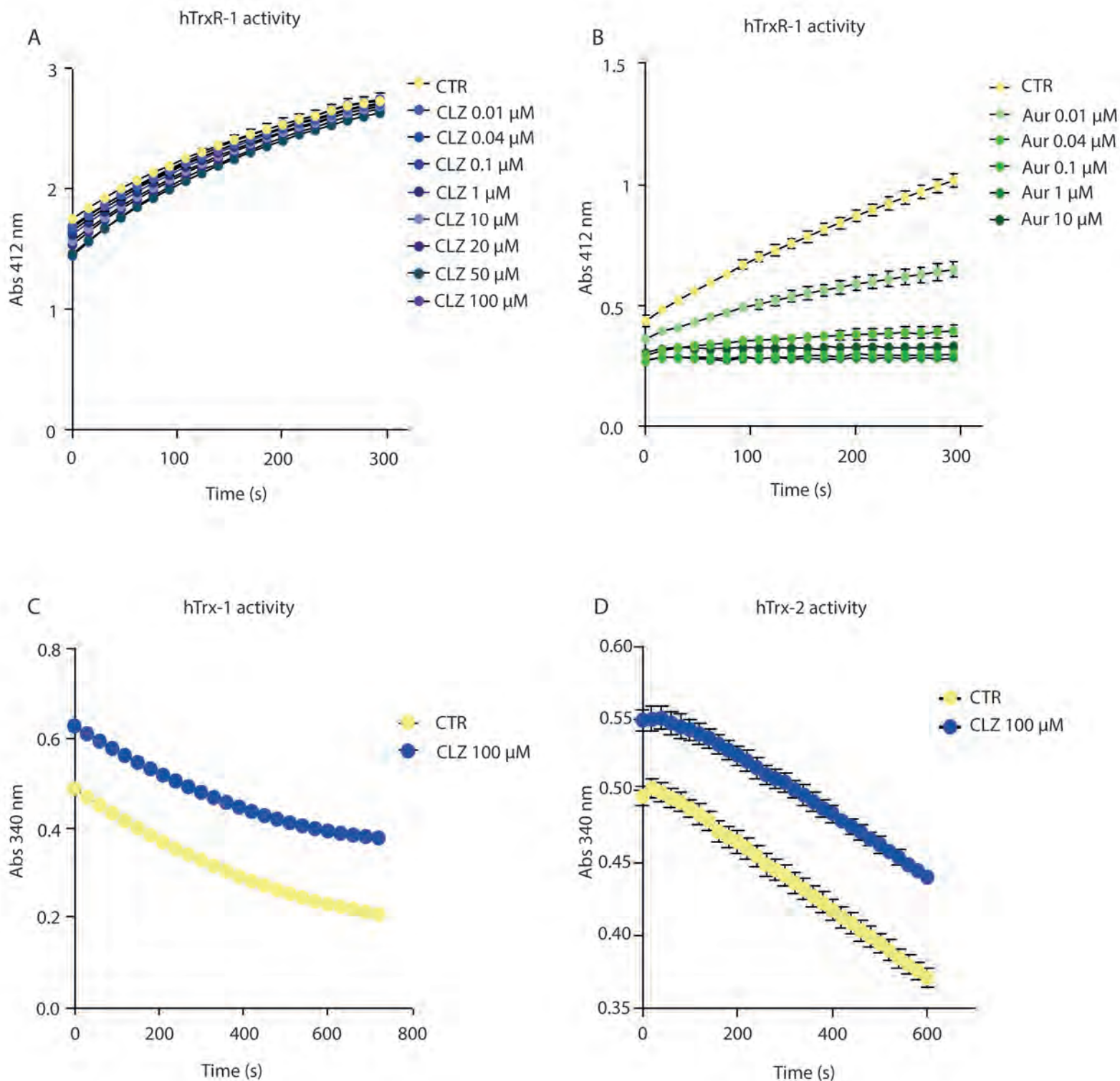
FIGURE S4. *In vitro* assays to determine the effects of Clozapine on hTrxR-1, hTrx-1 and hTrx-2 activities.

The effect of CLZ (A) and Auranofin (B) on the activity of hTrxR-1 was determined by using the DTNB assay [W.X. Koh, L. Coppo, A. Holmgren, J.W. Kong, W.K. Leong, Inhibition of Thioredoxin Reductase by Triosmium Carbonyl Clusters, Chemical research in toxicology 33(9) (2020) 2441-2445]. Briefly, 10 nM hTrxR-1 was incubated with increasing concentrations of CLZ or Auranofin for 30 min at RT in presence of 0.25 mM NADPH. DMSO was used as control. The reaction was started by adding 1 mM DTNB and the absorbance at 412 nm was followed for 5 min. All experiments were performed in quadruplicate. Results represent the mean ± SEM. The effect of CLZ on the activities of (C) hTrx-1 and (D) hTrx-2 was evaluated by Insulin Assay [R. Gencheva, Q. Cheng, E.S.J. Arner, Efficient selenocysteine-dependent reduction of toxoflavin by mammalian thioredoxin reductase, Biochimica et biophysica acta. General subjects 1862(11) (2018) 2511-2517.]. Briefly, 300 µM NADPH, 10 nM hTrxR-1, 1 µM hTrx-1 and 100 µM CLZ were mixed in the TE buffer, for 30 min at RT; DMSO was used as control. In the final step 0.16 mM insulin was added to the mixture and the absorbance at 340 nm was followed overtime (representing the NADPH consumption). The concentration of NADPH in the assay mixture was the same in all samples. The higher values recorded at 340 nm in CLZ-treated samples are due to the abs of CLZ, which however remained constant over all the time period of the analysis (not shown). All experiments were performed in quadruplicate. Results represent the mean ± SEM.
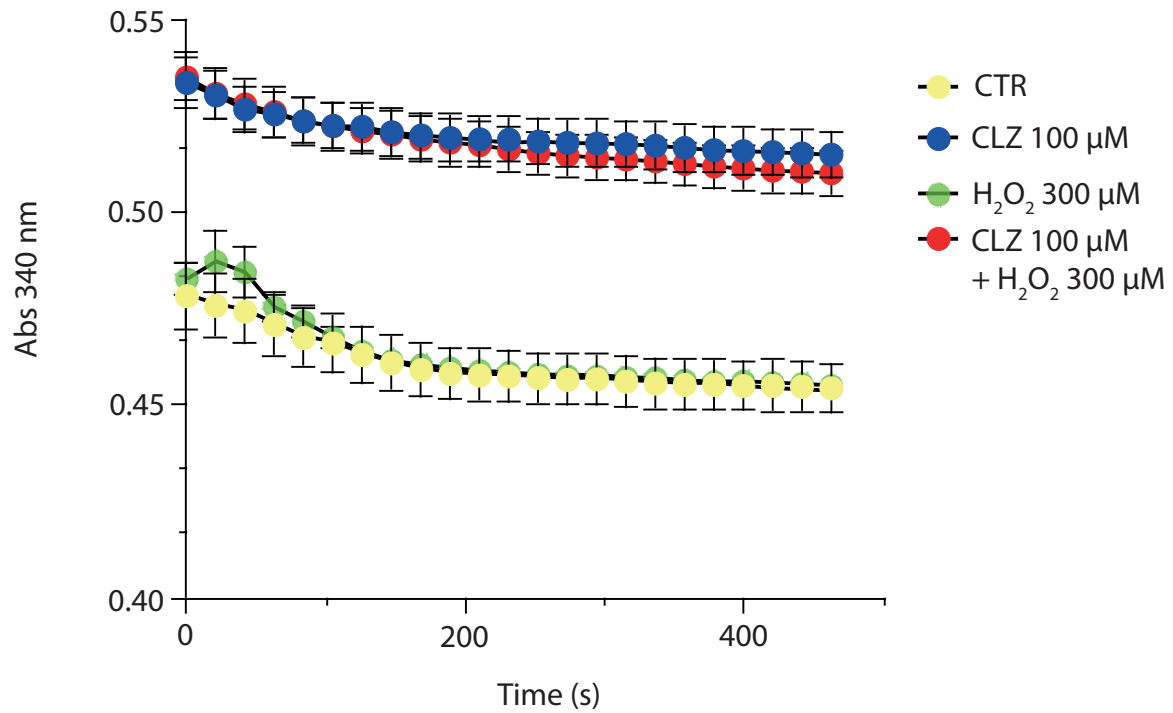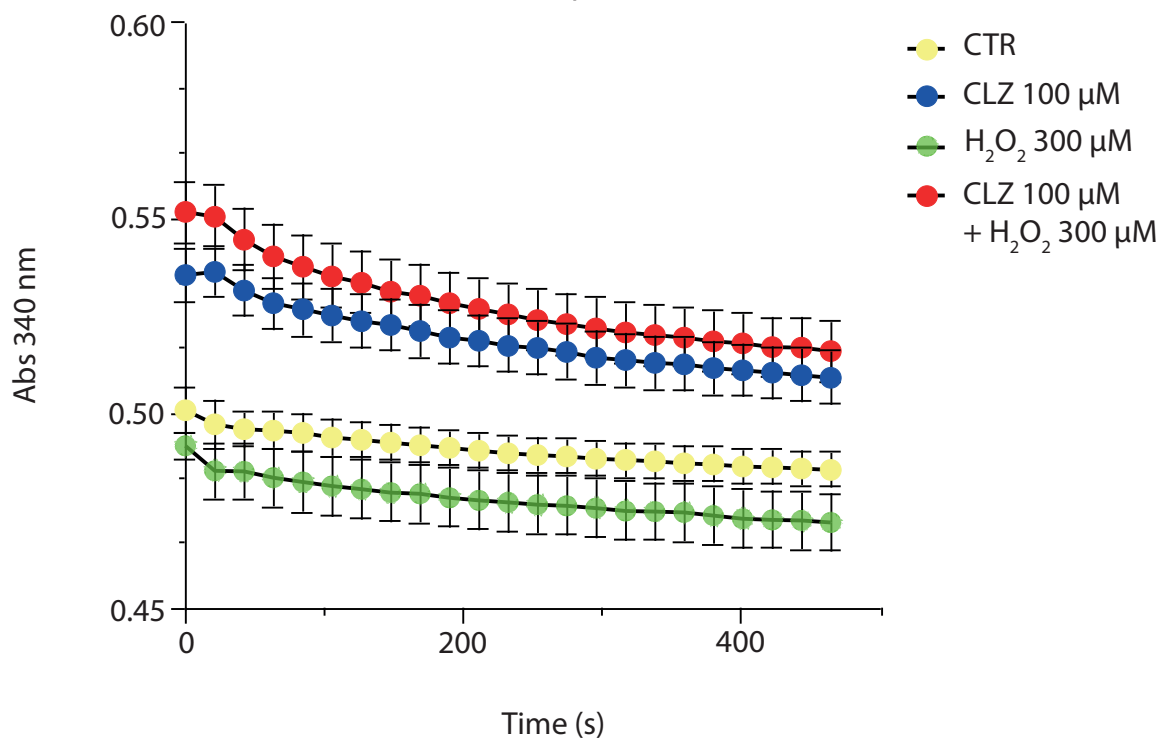
FIGURE S5. Clozapine is not a substrate for hTrxR-1 and hTrx-1.
The effect of 100 μM CLZ on hTrxR-1 and hTrx-1 activities was determined in the presence or absence of 300 μM H_2O_2. The consumption of NADPH was monitored measuring the abs at 340 nm overtime in presence of (A) 10 nM hTrxR-1 and 0.3 mM NADPH and plus (B) 1 μM hTrx-1, as described elsewhere [R. Gencheva, Q. Cheng, E.S.J. Arner, Efficient selenocysteine-dependent reduction of toxoflavin by mammalian thioredoxin reductase, Biochimica et biophysica acta. General subjects 1862(11) (2018) 2511-2517]. In the experiments with H_2O_2, CLZ was preincubated for 10 min at RT with H_2O_2. The concentration of NADPH in the assay mixture was the same in all samples. The higher values recorded at 340 nm in CLZ-treated samples are due to the abs of CLZ, which however remained constant over all the time period of the analysis (not shown). All experiments were performed in quadruplicate, DMSO was used as control. Results represent the mean ± SEM.

A) T0
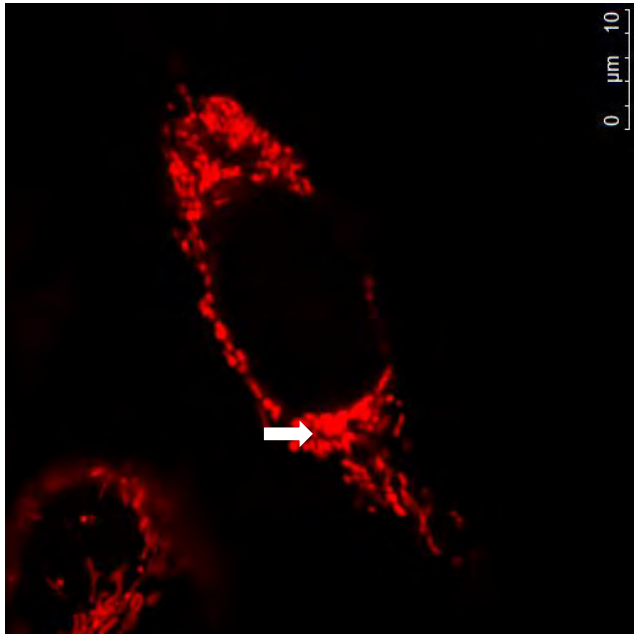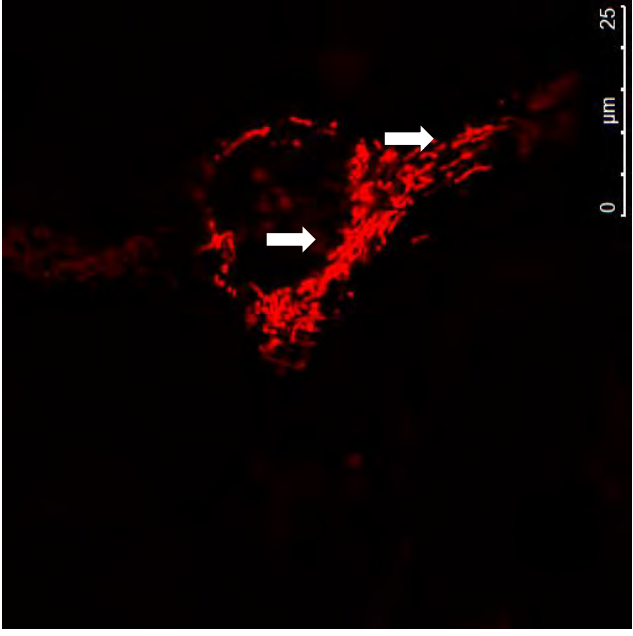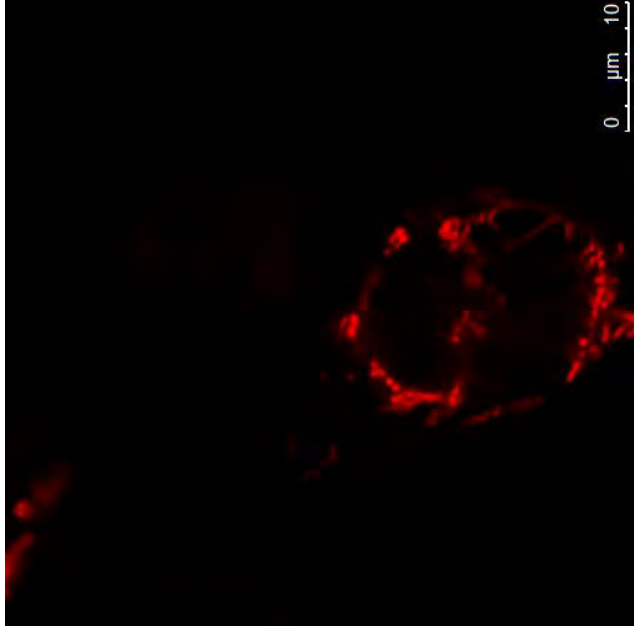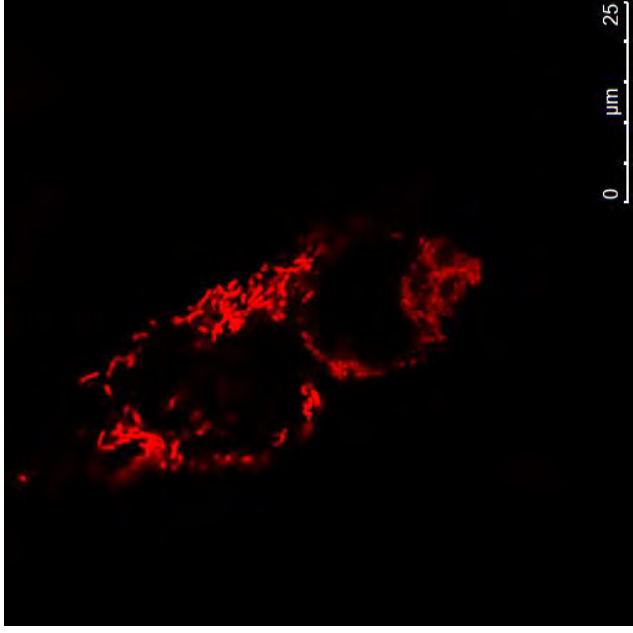
B) T3 CTR
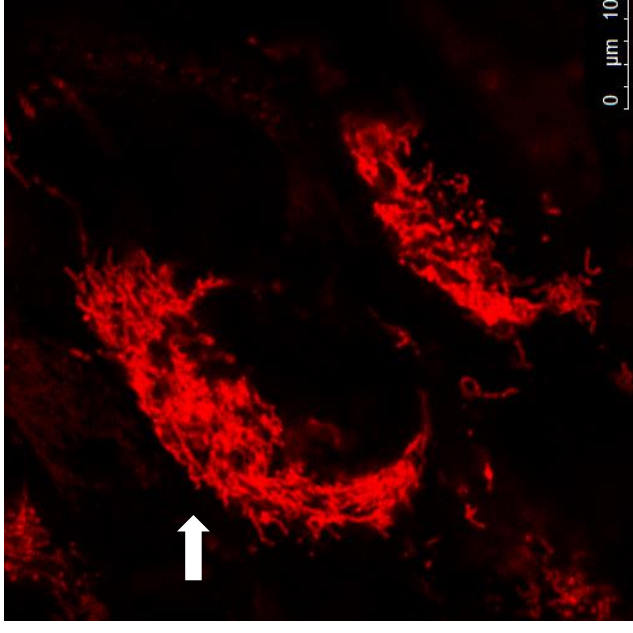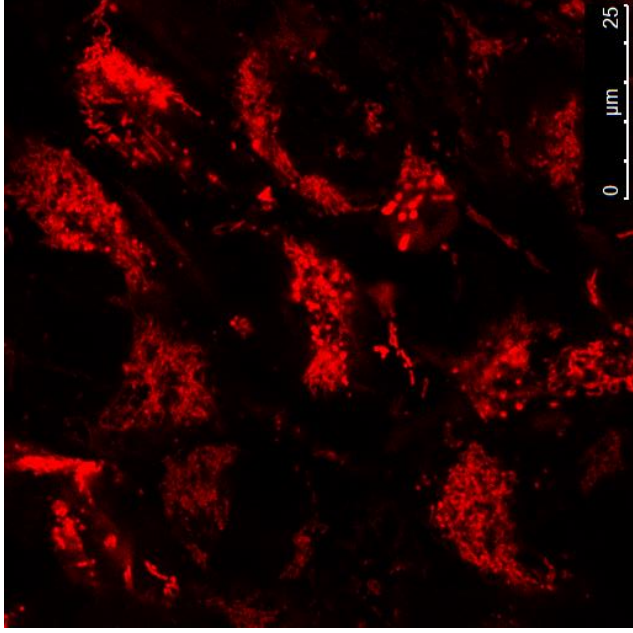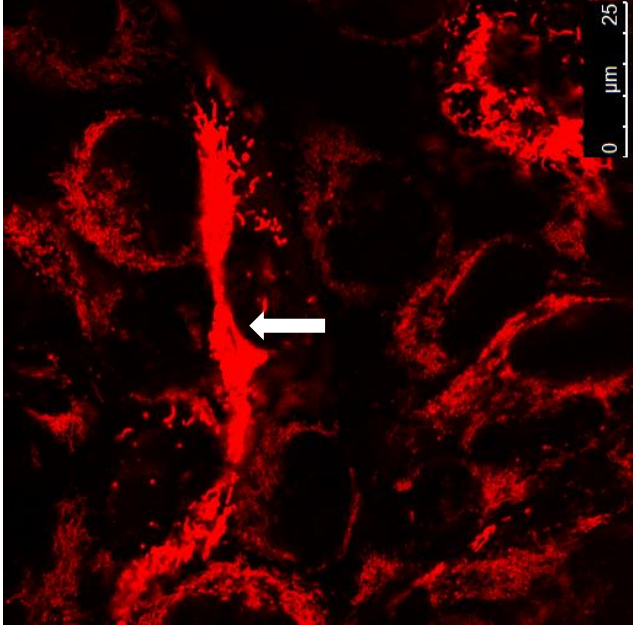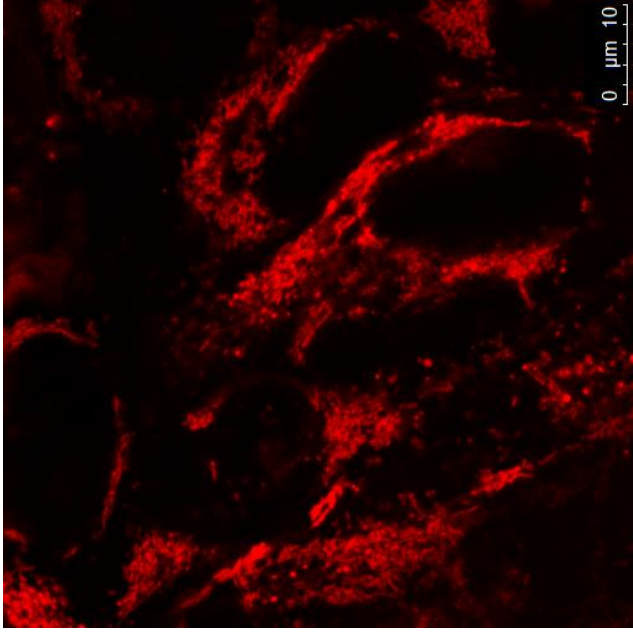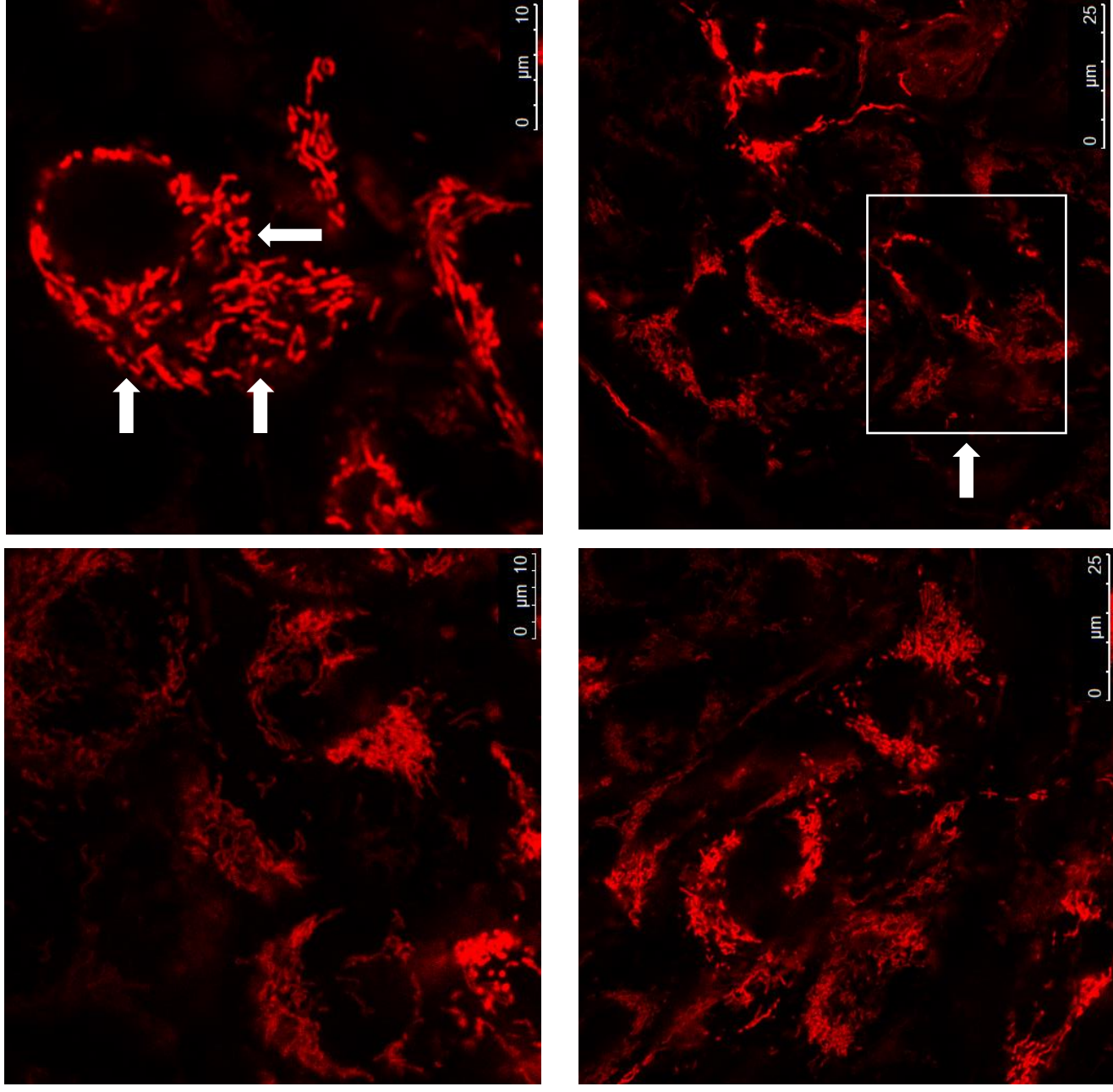
FIGURE S6. Representative micrographs of mitochondrial network and structural integrity in T3 SW872 cells grown with or without CLZ. Images were obtained by confocal microscopy. T0: mitochondrial network appears well organised, with elongated organelles (white arrows). T3: a brighter MitoTracker Deep red derived signal is emitted by these cells, a notion consistent with an increase in mitochondria mass/number (white arrow). An extensive mitochondria network is appreciable. T3+CLZ: white arrows highlight mitochondrial shape modifications with more rounded and less interrelated organelles in the network. The square white area is drawn around MitoTracker Deep red dim fluorescent mitochondria.

C) T3+CLZ
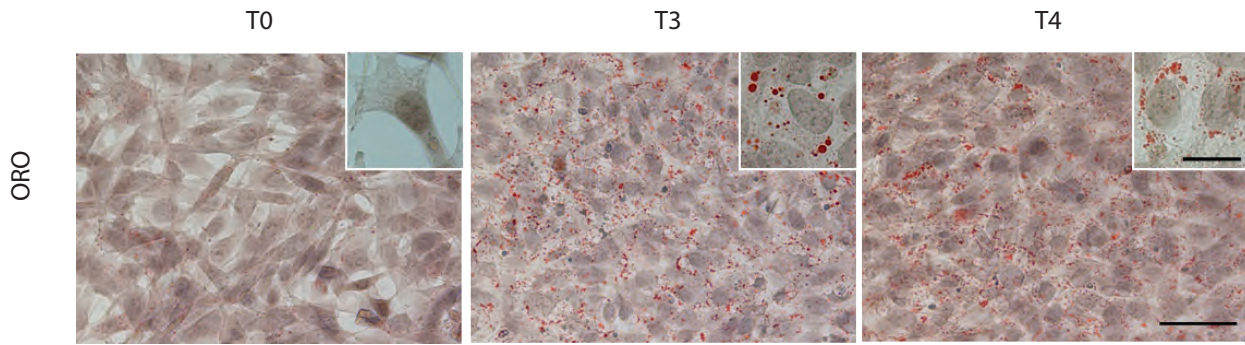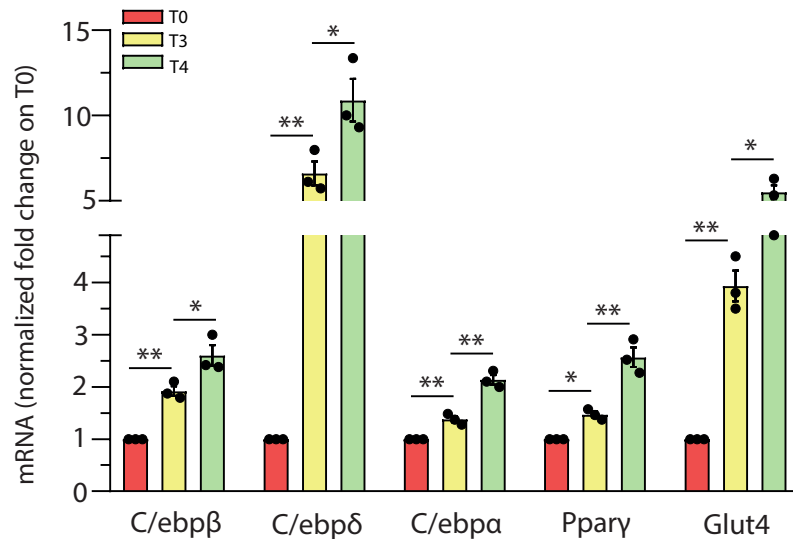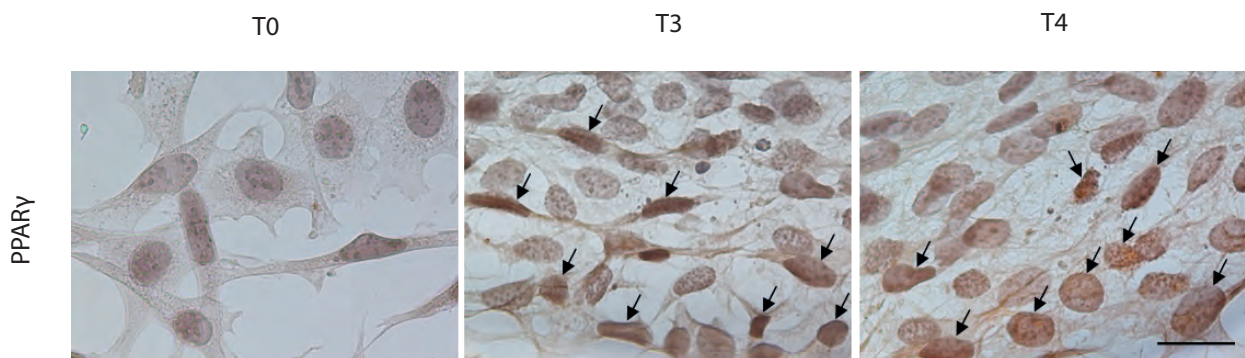
FIGURE S7. Lipid accumulation and adipogenic marker expression in differentiating MEFs. Confluent MEFs were induced to differentiate for 3 and 4 days. (A) Representative images (40X) of ORO-stained LDs and hematoxylin-stained nuclei. The higher enlargements (insets, 100X) allow better analysis of the different lipid accumulation in the cells. Scale bars = 50 μm; inset = 20 μm. (B) Quantitative real time PCR of CEBP/β, CEBP/δ, CEBP/α, PPARγ and GLUT4 mRNA expression. The graph shows the normalized fold change compared to T0. HPRT was used as housekeeping. Results represent the means ± SEM calculated from at least three independent determinations. *p < 0.05, **p < 0.01, as compared to the previous time point (one-way ANOVA followed by Dunnett's test). (C) Immunocytochemical analysis of PPARγ expression (100X). Arrows indicate PPARγ - positive nuclei. Scale bars = 20 μm.
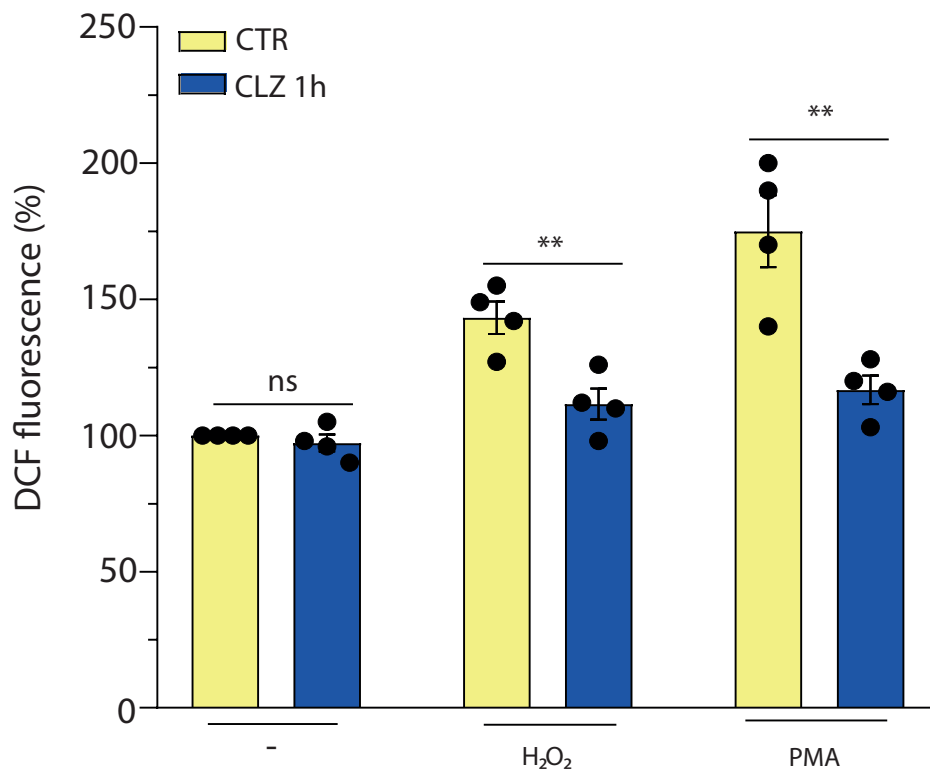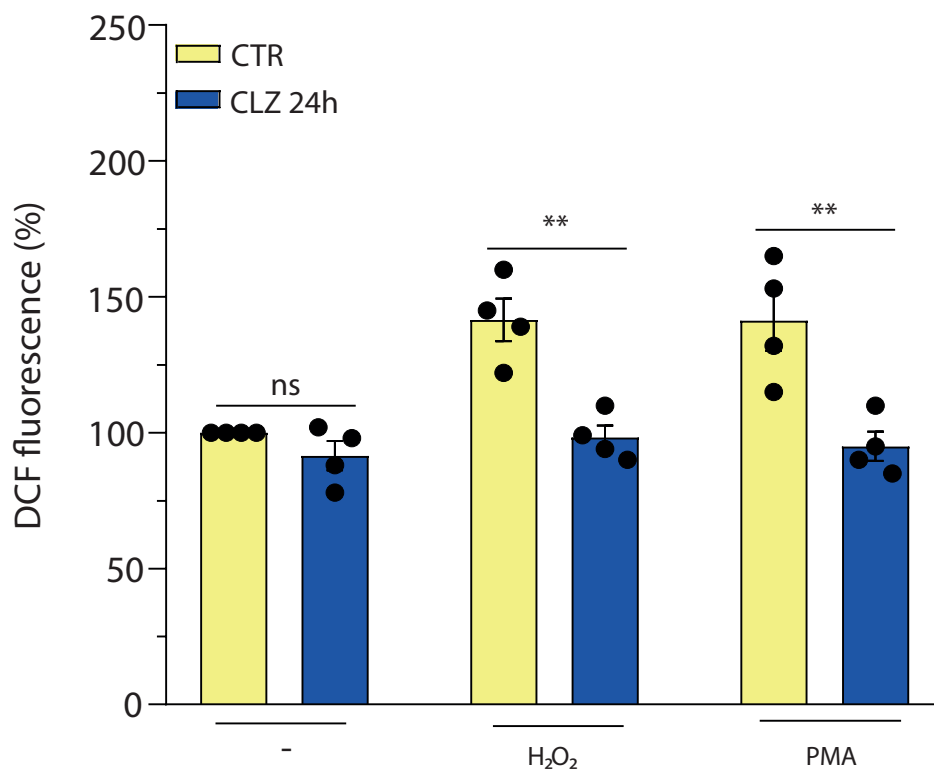
FIGURE S8. Antioxidant vs NOX-2 inhibitory effects of clozapine in MEFs.
MEFs were pre-exposed for 1 h (A) or 24 h (B) to CLZ and then treated for 15 min with either 100 μM H_2O_2 or 0.162 μM PMA. After treatments, the cells were analysed for DCF fluorescence. CTR samples received DMSO alone. Data are expressed in % respect to untreated CTR cells. Results represent the means ± SEM calculated from at least three independent determinations. **$p < 0.01$, as compared to CTR cells. ns: not significant (Unpaired t-test).
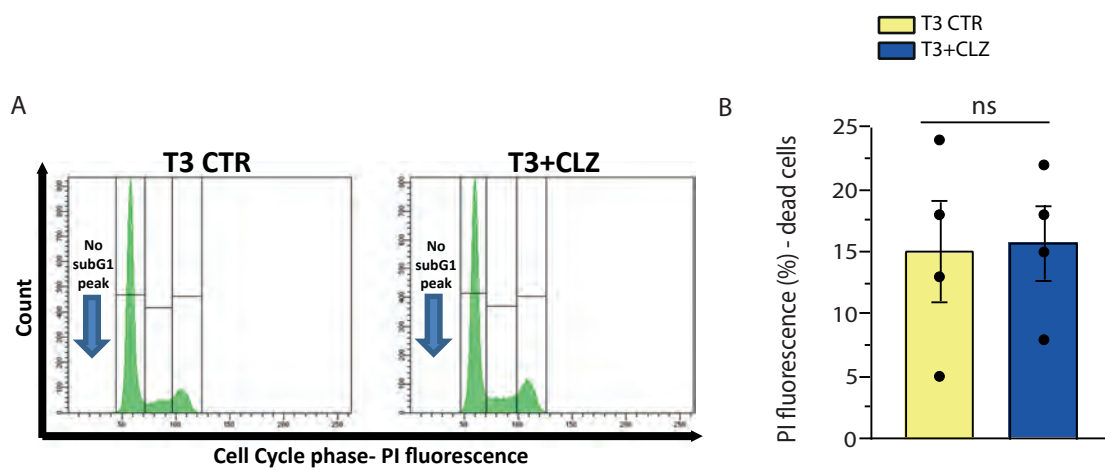
FIGURE S9. **CLZ does not exert any toxic effects in MEFs.**
Confluent MEFs were induced to differentiate for 3 days with or without CLZ (15 µM). (A) Flow cytometric evaluation of DNA content showing absence of subdiploid peaks. (B) Statistical analysis of the results obtained by PI labelling of fresh cells, for general viability assessment. Results represent the means ± SEM calculated from at least three independent determinations; ns: not significant (Unpaired t-test).

Table 1. Human qPCR primers

Gene	Primer forward (5'-3')	Primer reverse (5'-3')	Ref
C/ebpβ	CGA AGT TGA TGC AAT CGG TTT	TTA AGC GAT TAC TCA GGG CCC	[1]
Gapdh	CCA TGT TCG TCA TGG GTG TG	GGT GCT AAG CAG TTG GTG GTG	[1]
Nrf2	CCA TTC CTG AGT TAC AGT GTC TT	CAG TTT GGC TTC TGG ACT TGG	

C/ebpβ, Homo sapiens CCAAT/Enhancer Binding Protein (C/EBP), Beta; **Gapdh,** Homo sapiens Glyceraldehyde-3-Phosphate Dehydrogenase; **Nrf2,** Homo sapiens Nuclear Factor Erythroid-Derived 2-Like 2
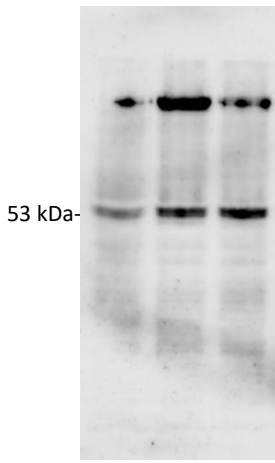
Table 2. Murine qPCR primers

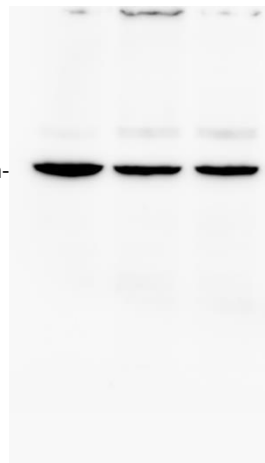| Gene	Primer forward (5'-3')	Primer reverse (5'-3')	Ref
C/ebpα	TGG ACA AGA ACA GCA ACG AG	TCA CTG GTC AAC TCC AGC AC	[2]
C/ebpβ	ACC GGG TTT CGG GAC TTG A	TTG CGT CAG TCC CGT GTC CA	[1]
C/ebpδ	TCC ACG ACT CCT GCC ATG TAC G	GTG GTT GCT GTT GAA GAG GTC G	[3]
Glut4	GCA ACG TGG CTG GGT AGG CA	CCC ACA GAG AAG ATG GCC ACG G	[4]
Hprt	CTC AGA CCG CTT TTT GCC G	GCT AAT CAC GAC GCT GGG A	
Pparγ	AGG CTC CAT AAA GTC ACC AAA G	CTG GCC TCC CTG ATG AAT AAA G	[5]

C/ebpα, Mus musculus CCAAT/Enhancer Binding Protein (C/EBP), Alpha; **C/ebpβ**, Mus musculus CCAAT/Enhancer Binding Protein (C/EBP), Beta; **C/ebpδ**, Mus musculus CCAAT/Enhancer Binding Protein (C/EBP), Delta; **Glut4**, Mus musculus Glucose Transporter Type 4, Insulin-Responsive; **Hprt**, Mus musculus Hypoxanthine Guanine Phosphoribosyl Transferase; **Pparγ,** Mus musculus Peroxisome Proliferator-Activated Receptor Gamma.
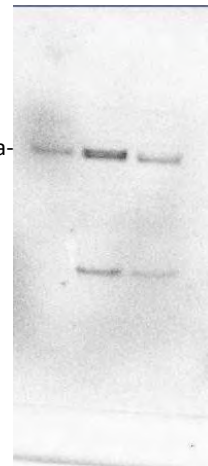
REFERENCES:

[1] L. Galluzzi, A. Diotallevi, M. De Santi, M. Ceccarelli, F. Vitale, G. Brandi, M. Magnani, Leishmania infantum Induces Mild Unfolded Protein Response in Infected Macrophages, PloS one 11(12) (2016) e0168339.
[2] Y. Chen, G.H. Cai, B. Xia, X. Wang, C.C. Zhang, B.C. Xie, X.C. Shi, H. Liu, J.F. Lu, R.X. Zhang, M.Q. Zhu, M. Liu, S.Z. Yang, D. Yang Zhang, X.Y. Chu, R. Khan, Y.L. Wang, J.W. Wu, Mitochondrial aconitase controls adipogenesis through mediation of cellular ATP production, FASEB J 34(5):6688-6702 (2020).
[3] P. Castillo, O. Aisagbonhi, C.C. Saenz, W.M. ElShamy, Novel insights linking BRCA1-IRIS role in mammary gland development to formation of aggressive PABCs: the case for longer breastfeeding, Am J Cancer Res. 12(1):396-426 (2022).
[4] L. Gatticchi, M. Petricciuolo, P. Scarpelli, L. Macchioni, L. Corazzi, R. Roberti, Tm7sf2 gene promotes adipocyte differentiation of mouse embryonic fibroblasts and improves insulin sensitivity, Biochim Biophys Acta Mol Cell Res 1868(1)(2021) 118897.
[5] V. Scalcon, A. Folda, M.G. Lupo, F. Tonolo, N. Pei, I. Battisti, N. Ferri, G. Arrigoni, A. Bindoli, A. Holmgren, L. Coppo, M.P. Rigobello, Mitochondrial depletion of glutaredoxin 2 induces metabolic dysfunction-associated fatty liver disease in mice, Redox Biol (51):102277 (2022).
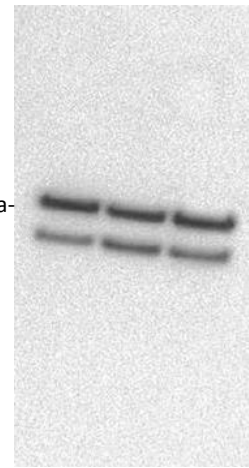
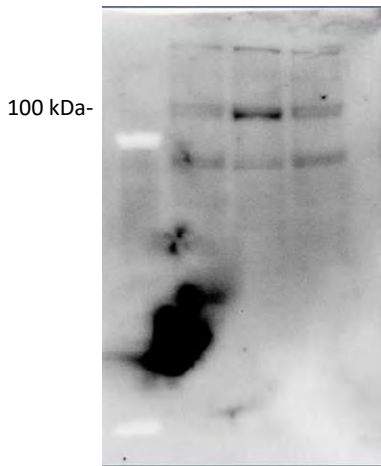**PPARγ**

53 kDa-

Actin

42 kDa-

C/EBPβ

45 kDa-

GAPDH

36 kDa-

Nrf2

100 kDa-

Actin

42 kDa-

NQO1

29 kDa-

GAPDH

36 kDa-

Trx-1

42 kDa-

12 kDa-

Actin

42 kDa-

TrxR-1

55 kDa-

GAPDH

36 kDa-
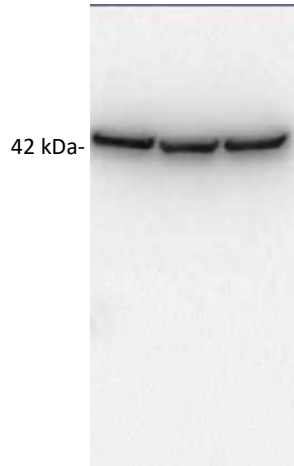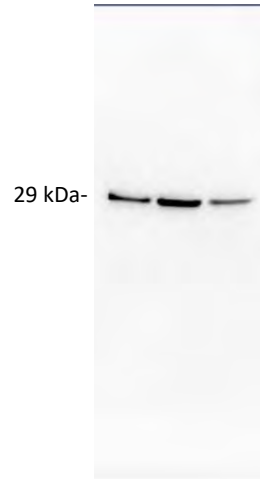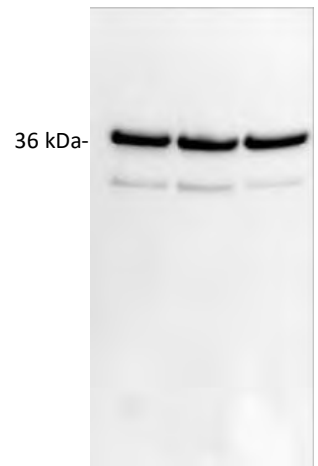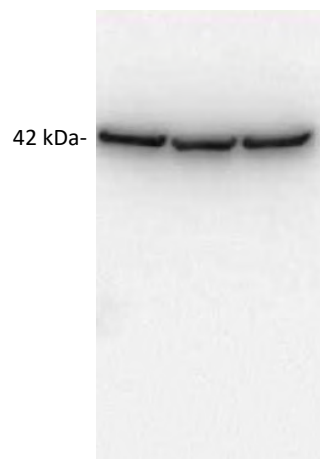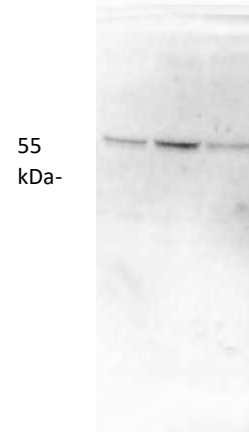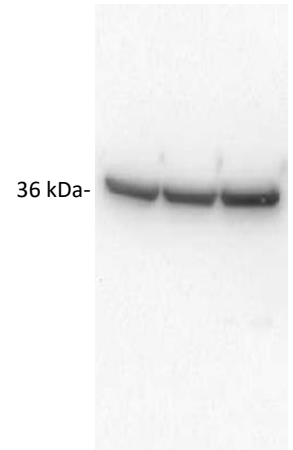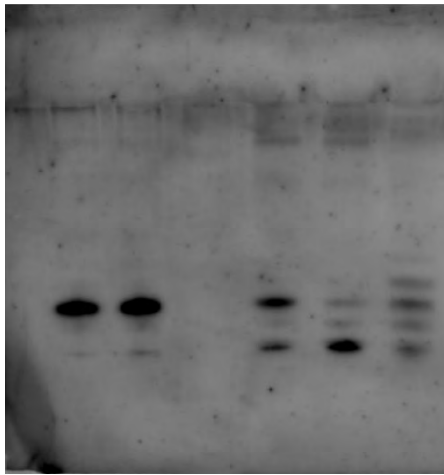
Redox Western Blot for Trx-2

18 kDa-

Trx-2

42 kDa-

Actin

45 kDa-

C/EBPβ

42 kDa-
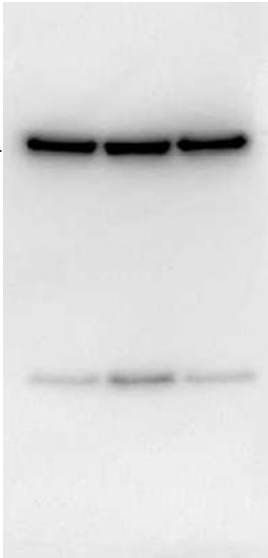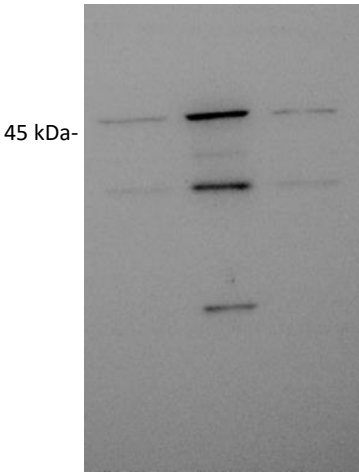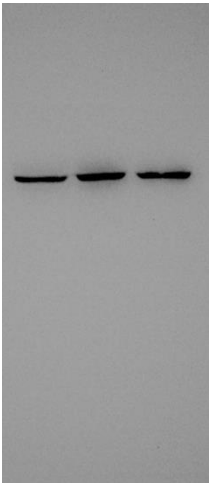
Actin

FIGURE S11. Uncut Western blots.
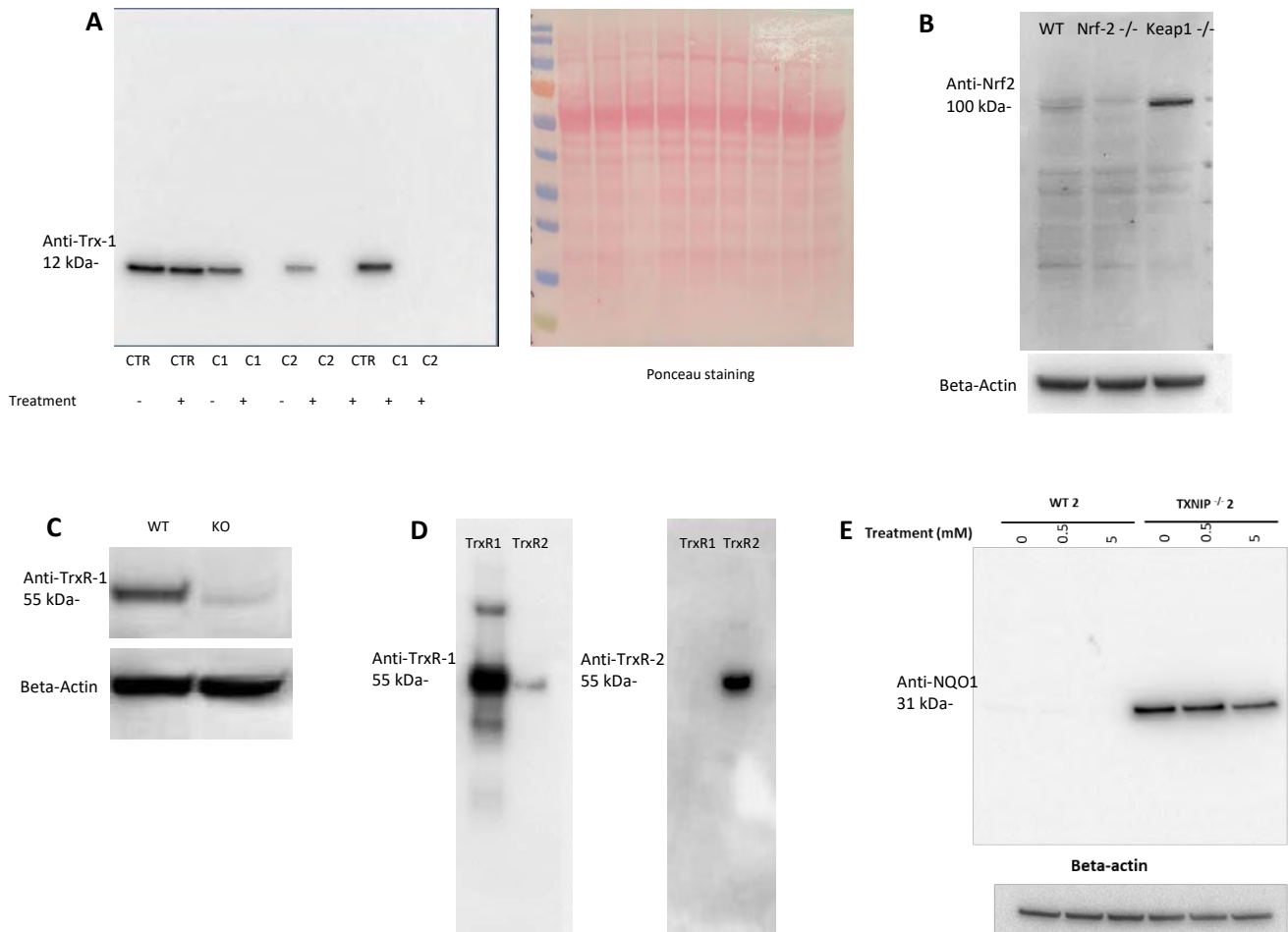
FIGURE S12. Validation of Trx-1, TrxR-1 and NQO1, Nrf2 and Keap1 WB analysis by using KO cells.
These cell lines were kindly provided by Drs. T. Dick (A), A. Wedell (B), M. Conrad (C) and V. Sayin (E) for inclusion in other collaborative projects and were here merely used for the purpose of helping to validate the primary antibodies used in the present study. (A) Trx-1 antibody: inducible KD for Trx-1 (gently provided by T, Dick's lab). Two of the shRNA constructs (C1 and C2) showed a strong down-regulation above 90% in the presence of treatment for 7 days. In the figure the parental cells (CTR) the C1 and C2 positive KD cells treated for 7 and 10 days with KD inducer. (B) Nrf2 antibody: Cells Nrf2 -/- and Keap1 -/- (gently from V. Sayin'lab) when Keap1 is absent, Nrf2 is constitutively upregulated. (C) TrxR-1 antibody: we validated the antibody using immortalized mouse embryonic fibroblasts (MEFs) lacking Txnrd1 (Txnrd1−/−) (gently provided by M.Conrad's lab) and cross reaction with TrxR-2 (D) using recombinant proteins. WT = Immortalized mouse embryonic fibroblasts; KO= Immortalized mouse embryonic fibroblasts Txnrd1−/−; TrxR-1 = recombinant human thioredoxin Reductase 1; TrxR-2 = recombinant human Thioredoxin Reductase 2. (E) NQO1 antibody: we validated the antibody in human myoblast (gently provided by A. Wedell's lab) to confirm the PCR results published here [Y. Katsu-Jiménez, C.Vázquez-Calvo, C. Maffezzini, M. Halldin, X. Peng, C. Freyer, A. Wredenberg, A. Giménez-Cassina, A. Wedell, E.S.J. Arnér, Absence of TXNIP in Humans Leads to Lactic Acidosis and Low Serum Methionine Linked to Deficient Respiration on Pyruvate, Diabetes. 68(4) (2019) 709-723], where the Txnip-/- patient 2 cells showed an overexpression of NQO1 that decreased upon treatment (WB are part of Shayida Maimaiti's doctoral theses performed on the same samples analysed with PCR in the published paper).

T0
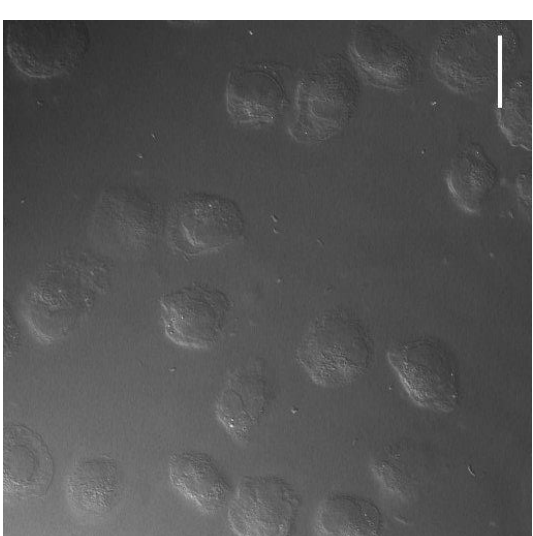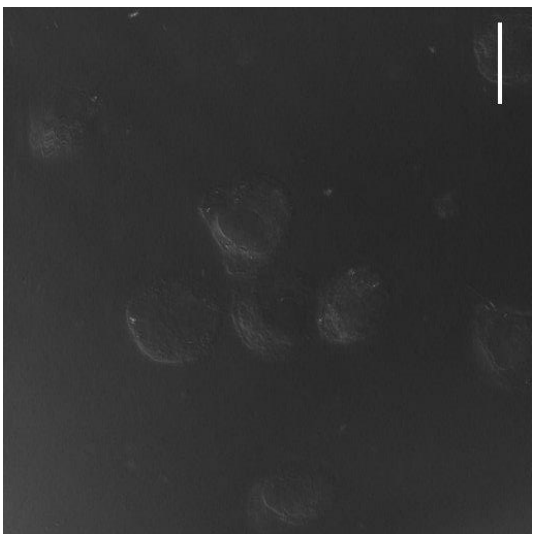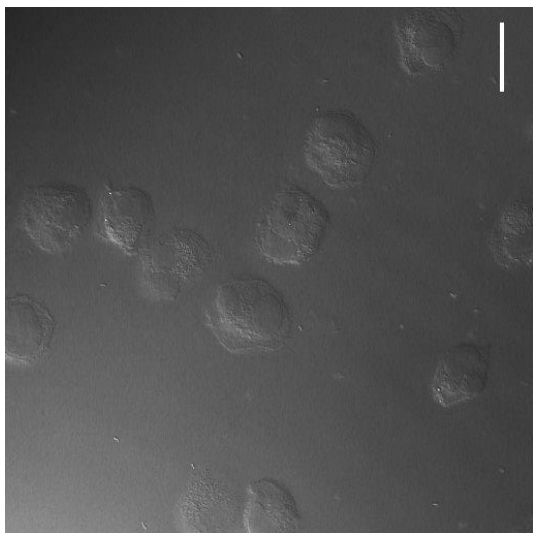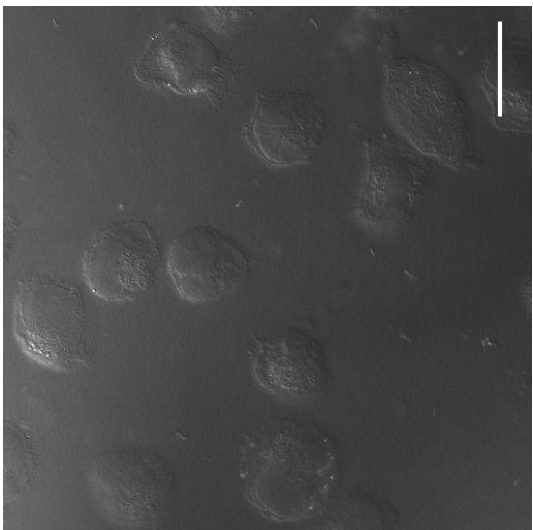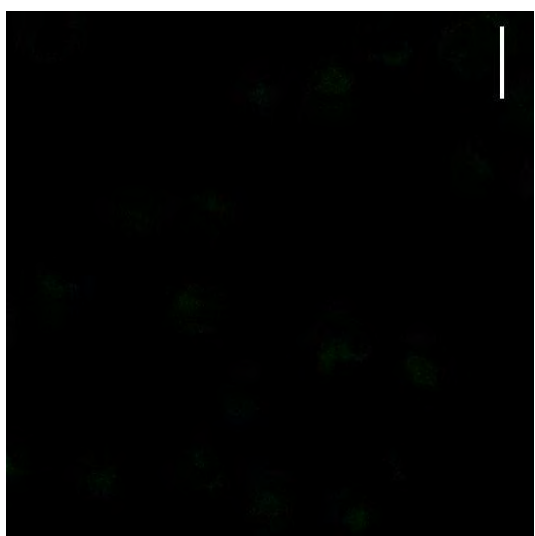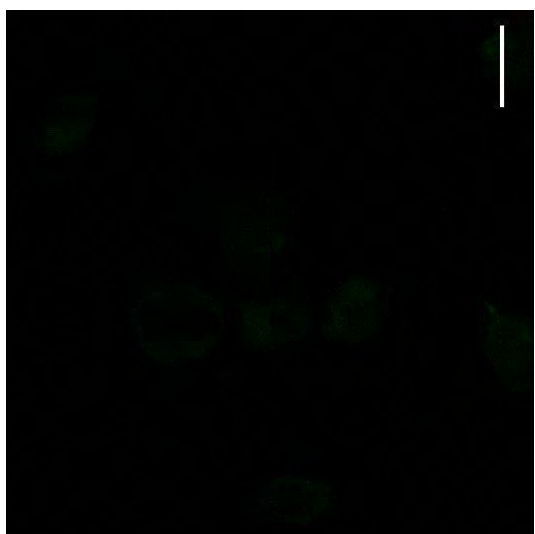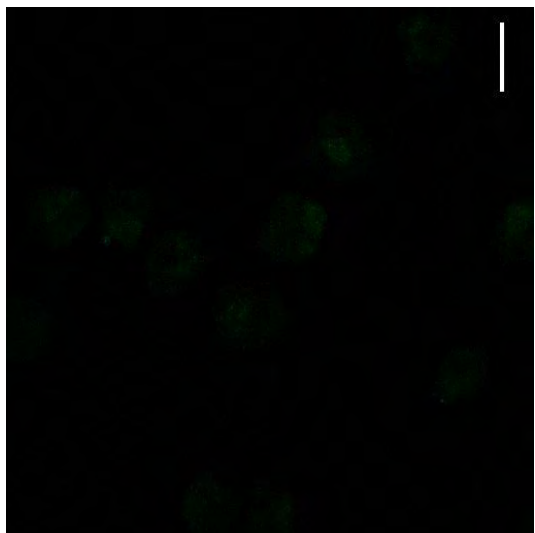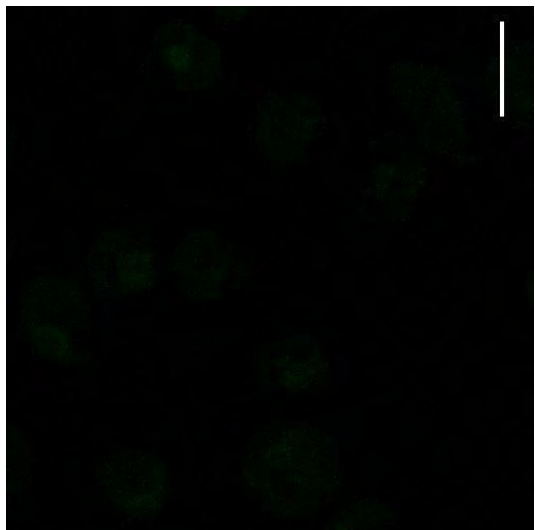
T3 CTR

T3 CTR
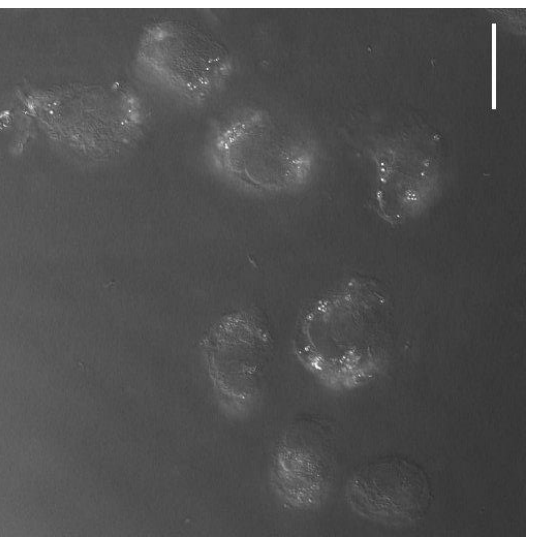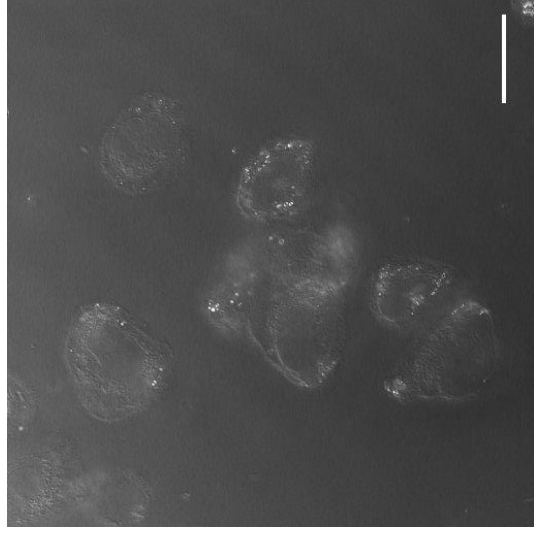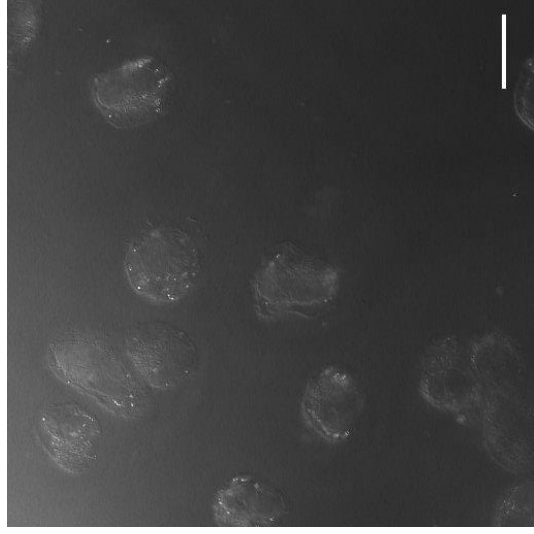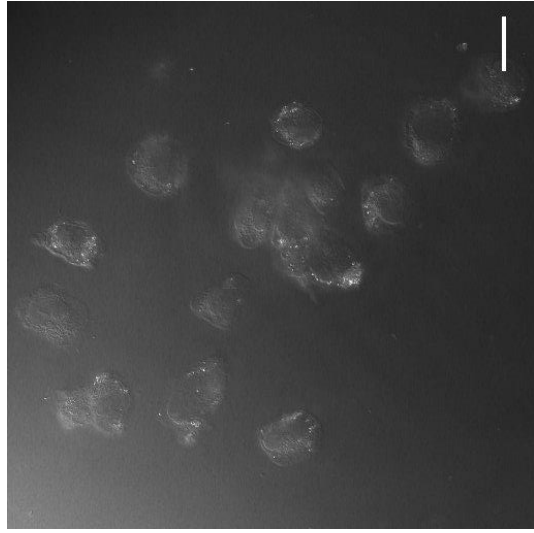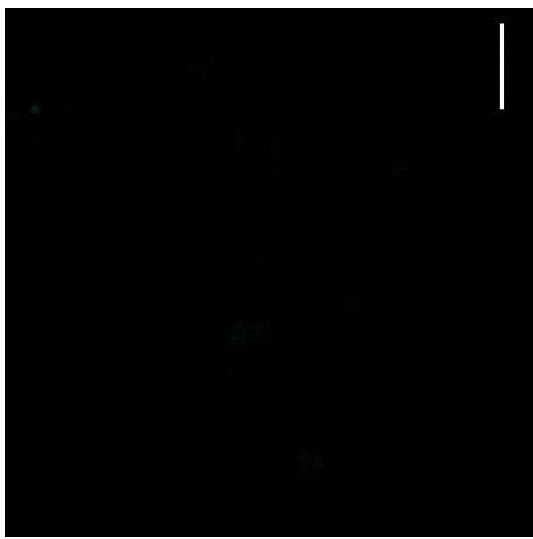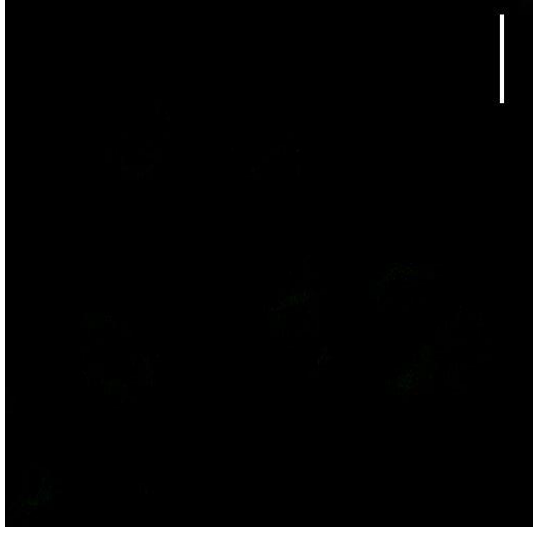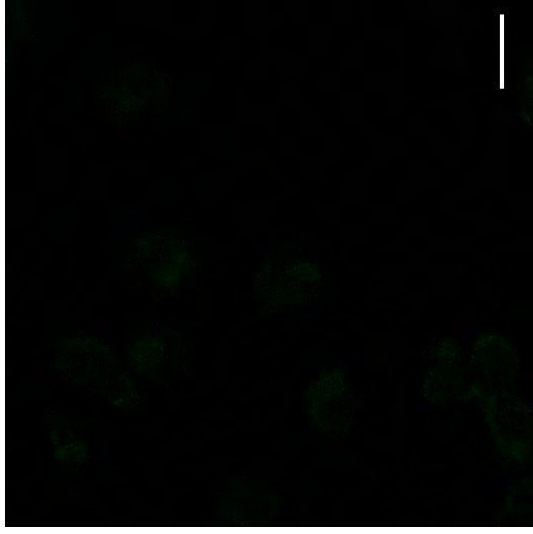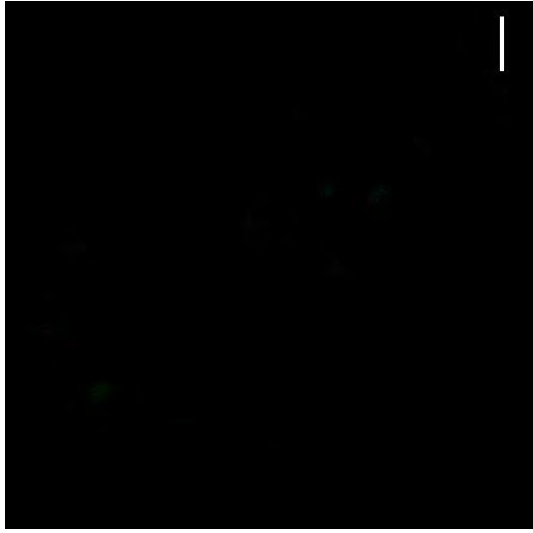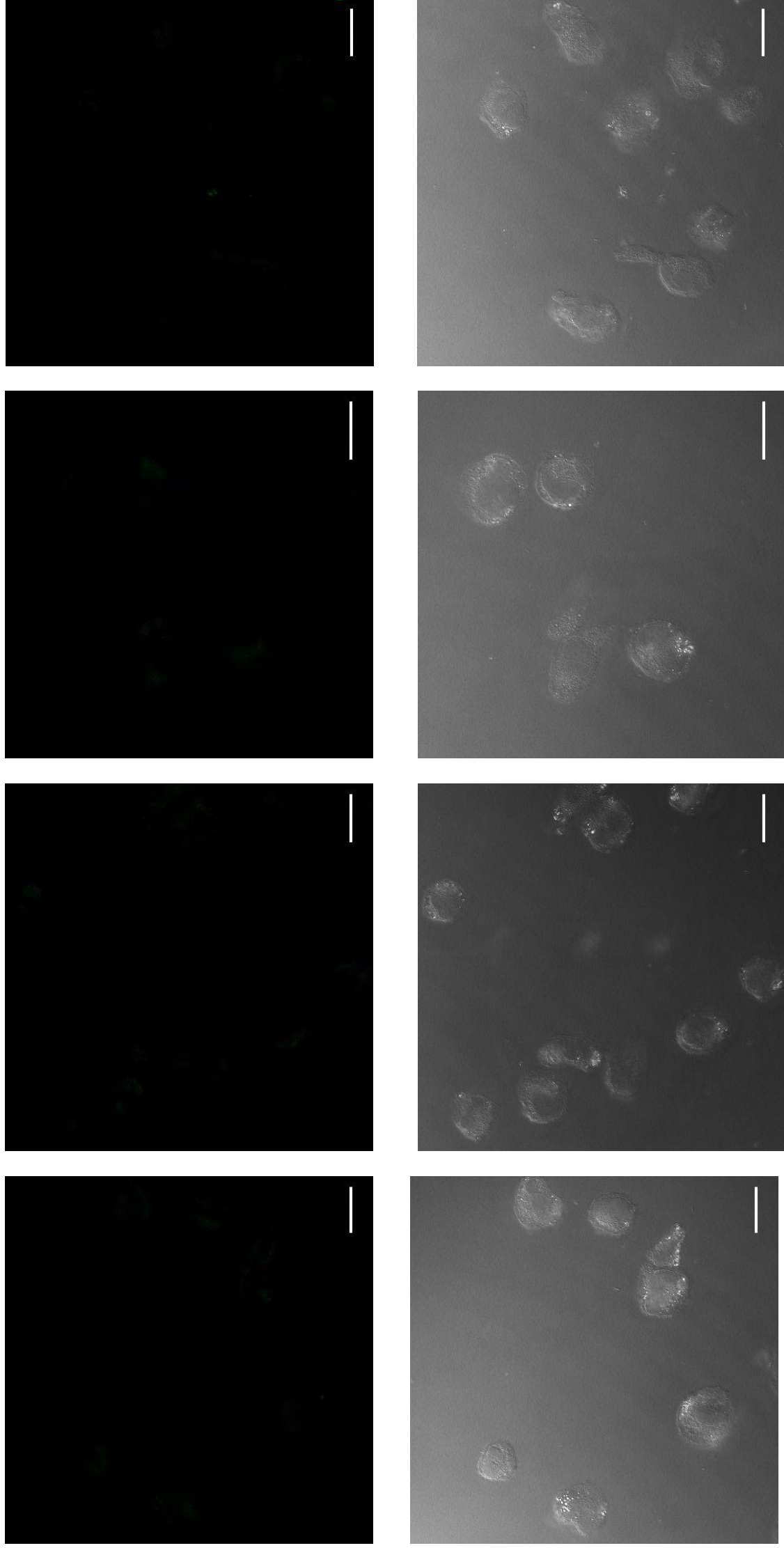
FIGURE S13. Negative controls for anti-phospho-p47^{phox} in SW872 cells. To exclude a non-specific binding with the secondary antibody, experiments like those reported in Fig 2B were carried out by omitting the primary antibody anti-phospho-p47^{phox}.

T3

T3+CLZ
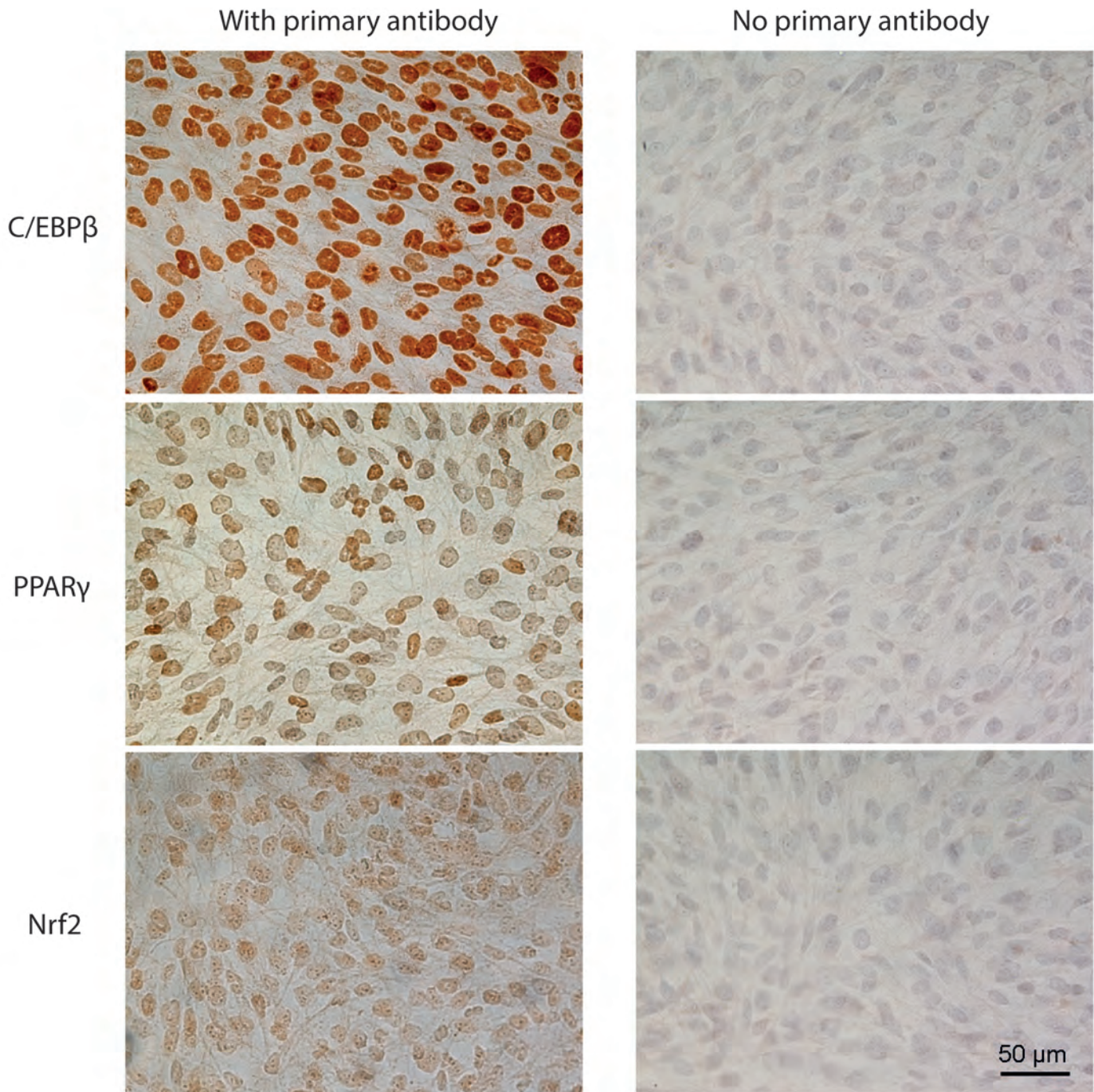
FIGURE S14. Negative controls for anti-C/EBPβ, PPARγ and Nrf2 in SW872 cells.
To exclude a non-specific binding with the secondary antibody, experiments like those reported in Figs 1F-G and 4C were carried out by omitting the primary antibodies anti-C/EBPβ, PPARγ and Nrf2 respectively; in grey the Nuclei counterstained with hematoxylin.

CHAPTER 3

Clozapine suppresses mitochondrial biogenesis, induces mitochondrial dysfunction and impairs glycolysis in differentiating SW872 cells (Unpublished data)

3.1 ABSTRACT

Clozapine (CLZ), a second-generation antipsychotic drug (SGA) is used for treating psychiatric disorders in patients resistant to other treatments, but, unfortunately, it can induce a series of metabolic side effects by virtually unknown mechanisms. Growing evidence suggests the involvement of mitochondrial ROS formation and subsequent mitochondrial dysfunction in CLZ-induced metabolic side effects.

Consistently with this notion, we found that in SW872 cells, CLZ, in the same conditions in which it slows down the adipogenic process [by blunting lipid accumulation and the early expression of key adipogenic transcription factors, i.e., CCAAT/enhancer-binding protein β (C/EBPβ) and peroxisome proliferator activated receptor γ (PPARγ)], anticipates mitochondrial ROS production, inhibits mitochondriogenesis and negatively impacts mitochondrial dynamics (fission and fusion).

As expected, the expression of some mitochondrial proteins such as 2-oxoglutarate carrier (2-OGC), increased at day 3 and was sensitive to CLZ treatment. However, the expression of some proteins belonging to respiratory chain complexes which also increased at day 3, was not reduced by CLZ, but rather increased.

We finally observed that undifferentiated cells are highly glycolytic and produce their ATP with very little, if any, contribution of oxidative phosphorylation. The increased ATP levels detected during the differentiation (T3), were instead mainly of mitochondrial origin and this contribution was lost after CLZ supplementation. CLZ also negatively impacted the compensatory glycolytic response observed after Rotenone supplementation (an inhibitor of Complex I).

In conclusion, it appears that the CLZ-induced slowing down of adipogenesis is accompanied by mitochondrial dysfunction associated with inhibition of mitochondrial biogenesis, unexpected increased expression of proteins of the mitochondrial respiratory chain, mitochondrial membrane hyperpolarization, and increased ROS formation.

Although still preliminary, these results could contribute to the understanding of the mechanisms by which CLZ induces metabolic adverse effects in patients treated with the drug.

3.2 INTRODUCTION

Second generation antipsychotics (SGAs), in particular CLZ, is extremely effective in the treatment of psychiatric disorders such as schizophrenia and bipolarism and it is widely used in patients resistant to first-line drugs [Swartz M.S. *et al.,* 2008; Remington G. *et al.,* 2017; Remington G. *et al.,* 2016; Lee L.H.N. *et al.,* 2018; Honer W.G. *et al.,* 2009].

Unfortunately, it can induce a series of metabolic side effects, e.g., weight gain, hyperlipidemia [Lamberti J.S. *et al.,* 2006; Allison and Casey, 2001], insulin resistance [Henderson D.C. *et al.,* 2000], as well as increased morbidity and mortality from cardiovascular diseases [Yuen J.W.Y. *et al.,* 2018; Kim D.D. *et al.,* 2018; Kim D.D. *et al.,* 2017].

While the molecular mechanisms mediating these effects remain largely unknown, growing experimental evidence suggests a correlation between dysfunctional adipose tissue and mitochondrial impairment.

Alteration of mitochondrial functions and homeostasis could be due to a deregulation of electron transport chain activities [Cikankova T. *et al.,* 2019] and/or an imbalance in mitochondrial fusion and fission ratio [Del Campo A. *et al.,* 2018]. Some studies propose that SGAs-induced mitochondrial dysfunction or mitochondrial dynamics disruption can be involved in the onset of metabolic disorders caused by these drugs [Contreras-Shannon V. *et al.,* 2013; Scaini G. *et al.,* 2018].

Consistently with this premise, we found that CLZ slows down adipogenesis in human liposarcoma SW872 cell line by reducing lipid droplet formation and the early (day 3) expression/translocation of critical transcription factors of adipogenesis, i.e., C/EBPβ and PPARγ. In addition, CLZ altered the cellular redox state through a mechanism associated with its ability to both inhibit NOX-2 (NADPH oxidase-2) and act as a ROS scavenger. Inhibition of this early ROS response, and of the ensuing nuclear factor erythroid 2-related factor 2 (Nrf2) expression/nuclear translocation and Nrf2-dependent antioxidant response, was then followed by anticipated mitochondrial ROS formation and early mitochondrial dysfunction [Blandino G. *et al.,* 2023].

In the present study we investigated the impact of CLZ on mitochondrial biogenesis, functionality and dynamics, focusing on the bioenergetic mechanisms which may help to shed light on the more detailed molecular mechanisms explaining some of the adverse metabolic effects of CLZ.

3.3 MATERIALS AND METHODS

3.3.1 Materials

Acrylamide 30%, glycine, sodium dodecyl sulphate (SDS), methanol, acetonitrile, insulin, dexamethasone, 3-isobutyl-1-methylxanthine (IBMX), DL-Dithiothreitol (DTT), oleic acid-albumin and linoleic acid albumin, Oil Red O (ORO), Glutathione (GSH), dithiobis-2- nitrobenzoic acid (DTNB), TWEEN 20, isopropanol, glacial meta-phosphoric acid as well as most of the reagent-grade chemicals were purchased from Merck Life Science s.r.l. (Milan, Italy). Sodium chloride, Na_2HPO_4, KH_2PO_4 and K_2HPO_4 were from Carlo Erba (Milan, Italy). WesternBright™ ECL (K-12045-D20) was from Advansta-Aurogenes s.r.l (Rome, Italy). Clarity Max was from Biorad Laboratories s.r.l. (Milan, Italy). CLZ (S2459) was purchased from Selleckchem (Planegg, Germany).

3.3.2. Cell culture condition and treatments

Human liposarcoma cells (SW872) were purchased from the American Type Colture Collection (ATCC HTB-92) and cultured in 75 cm^2 flasks in Dulbecco's Modified Eagle's Medium/Nutrient Mixture F-12 Ham culture medium (DMEM/F12), supplemented with 10% FBS, penicillin (100 U/ml), and streptomycin (100 μg/ml). Cells were kept in a cell culture incubator at 37°C and 5% CO_2.

SW872 cells were plated (250.000 cells/dish) in 35 mm dishes or six well plates.

The differentiation was induced by replacing culture medium with differentiation medium (DM), containing:

• 0.1 mM IBMX: prepared starting from 0.1 M stock solution in DMSO and then stored at -20°C.

• 1 μM Dexamethasone: prepared starting from 1 mM stock solution in 100% ethanol and stored at -20°C.

• Insulin (10 μg/ml)

• 30 μM BSA-conjugated Oleic/Linoleic acids.

The DM was replaced every 2 days. 5, 10 or 15 μM CLZ (starting from a 15 mM stock solution in DMSO) were added contextually to the DM and replaced with the DM.

For ATP and lactate assays, cells were treated until 4 hours with 1 µM Rotenone (ROT), starting from 1 mM stock solution dissolved in DMSO, in DMEM 1X supplemented with 3.15 g/L D-glucose; or with 2.5 mM 2-Deoxy-D-glucose (2-DG), starting from 500 mM stock solution dissolved in PBS, in DMEM 1X without D-glucose.

3.3.3. Extraction and quantification of mitochondrial DNA (mtDNA)

For DNA purification, SW872 cells were detached from dishes using trypsin and centrifuged for 3 minutes at 1260 rpm. The pellet is washed twice in PBS and optionally frozen at -20 °C until subsequent extraction. DNA extraction is performed using the QIAamp DNA Mini and Blood Mini Handbook kit (Qiagen, Hilden, Germany) following the specific protocol for cell cultures. DNA dosage was performed using Micro UV-Vis Spectrophotometer Nanoready spectrophotometer (Life Real, Hangzhou city, Zhejiang, China). Quantification of mtDNA was assessed by Real-Time PCR using TB Green PreMix ex Taq II Master Mix (Takara Bio Europe, France) and 200 nM primer (Table 1) in the RotorGene 6000 instrument (Corbett life science, Sydney, Australia). For the amplification of DNA (25 ng) the following conditions were used: 95°C for 10 minutes, 40 cycles at 95°C for 15 seconds and 60°C for 50 seconds. A duplicate non-template control was included for each primer pair reaction as negative control. To exclude the presence of non-specific products or primer dimers, at the end of each reaction, a Melting curve analysis was performed from 65°C to 95°C. To evaluate the mtDNA quantification, the ratio of the mitochondrial ND1 gene to nuclear 18s rRNA was determined and analysed by the instrument software.

Target	Forward sequence	Reverse sequence
PPARγ	GCCCAGGTTTGCTGAATGTG	TGAGGACTCAGGGTGGTTCA
C/EBPβ	CGAAGTTGATGCAATCGGTTT	TTAAGCGATTACTCAGGGCCC
18s rRNA	TGACTCAACACGGGAAACCT	GCTCCACCAACTAAGAACG
DRP1	TGCTTCCCAGAGGTACTGGA	TCTGCTTCCACCCCATTTTCT
FIS1	GAAGAAAGATGGACTCGTG	CGTCTCCTTCAGGATTTG
FOXO3a	TAATGGGAGGATCAGTCACACA	GTAAGCCATGGTGTCCTCTCC
GAPDH	CCATGTTCGTCATGGGTGTG	GGTGCTAAGCAGTTGGTGGTG
MFN1	CGAACAGCACACTATCAG	TTGGTCTTCCCTCTCTTC
MFN2	GAGACACATGGCTGAGGTGAA	TGCATTCCTGTACGTGTCTTC
ND1	ACGCCATAAAACTCTTCACCAAAG	TAGTAGAAGAGCGATGGTGAGAGCTA
NRF1	TTGAGTCTAATCCATCTATCCG	TACTTACGCACCACATTCTC
NRF2/GABPA	GGAACAGAACAGGAAACAATG	CTCATAGTTCATCGTAGGCTTA
PGC1-α	AAATCTGCGGGATGATGGAGAC	AGCAGCAAAAGCATCACAGG
OPA1	GATAGTTCTCGGGAGTTTG	GGTACAGCCTTCTTTCAC
TFAM	TCACAATGGATAGGCACAGG	TGGCAGAAGTCCATGAGCT
TFB2m	CCAAGGAAGGCGTCTAAGGC	CTTTCGAGCGCAACCACTTTG

Table 1. Primers list used for qPCR

3.3.4. RNA extraction and retro transcription

For RNA purification, cells were lysed directly with 700 µl of QIAzol® Lysis Reagent (Qiagen, Hilden, Germany). Total RNA extraction was performed with miRNeasy Mini Kit (Qiagen, Hilden, Germany) according to the kit's protocol. For RNA quantification, Micro UV-Vis Spectrophotometer Nanoready spectrophotometer (Life Real, Hangzhou city, Zhejiang, China) was used. 500 ng total RNA was retro transcribed using PrimeScript™ RT Master Mix (Perfect Real Time) (Takara Bio Inc., Otsu, Shiga, Japan) by incubation at 37°C for 15 min followed by 85°C for 15 sec in the GeneExplorer Thermal Cycler (Hangzhou Bioer Technology Co., Ltd). Samples are stored at -20°C until further analysis.

3.3.5. Quantitative Real Time PCR (qPCR)

Amplification reactions for gene expression analysis were performed in a final volume of 20 µl in duplicate, using TB Green PreMix ex Taq II Master Mix (Takara Bio Europe, France) and 200 nM primer (Table 1) in the RotorGene 6000 instrument (Corbett life sciences, Sydney, Australia). 2 ng of cDNA was loaded for each PCR tube. For all targets the following amplification conditions were used: 95°C for 10 minutes, 40 cycles at 95°C for 15 seconds and 60°C for 50 seconds, followed by a melting curve analysis at the end of each run from 65–95°C, to exclude the presence of non-specific products or primer dimers. A duplicate non-template control was included for each primer pair reaction as negative control. The relative expression levels were calculated by the 2−ΔΔCt method [Pfaffl M.W., 2001] using GAPDH as a reference gene.

3.3.6. Lactate production assay

250 µl of 30% Trichloroacetic acid (TCA) have been added to 500 µl of cell medium. The samples were kept for 30 min on ice, by vortexing every 5 min and then frozen at -20°C. Just before analysis, samples (blank: medium alone plus 30% TCA, 1 mM STD lactate solution and TCA-extracted medium) were centrifuged (14.000 rpm, 4°C, 20 min) and the surnatants used for the assay. The assay mixture contains 500 µl glycine hydrazine buffer (2 M Glycine, 0.8 M Hydrazine Sulfate, 0.01 M disodium EDTA); 200 µl 5 mM NAD^+; 10 or 20 µl sample/STD/blank; and water (final volume: 1 ml). The analysis was performed spectrophotometrically (340 nm; 37°C). When the absorption reached stable values, 10 µl of 2500 U/ml Lactate dehydrogenase (LDH) was added to each cuvette and the absorbance was recorded for 1h.

3.3.7. Evaluation of ATP content by HPLC assay

After removing the medium, cells were washed twice with PBS. After adding 300 μl of 5% $HClO_4$, cells were detached by scraping and the cell samples transferred to 1.5 ml tubes, vortexed and left on ice for 10 min. After centrifugation (13.000 rpm; 5 min; 4°C) supernatants were collected and stored at -80°C. Details of HPLC assay are reported elsewhere [Stocchi V. *et al.,* 1987].

3.3.8. Western Blot analysis

Protein samples were separated by SDS poly-acrylamide gel electrophoresis, blotted in PVDF membrane and then probed with Total OXPHOS Human WB Antibody Cocktail (Abcam ab110411) 1:1000; anti-COX IV (Abcam 33985) 1:1000; anti-GAPDH (Santa Cruz sc-47724) 1:2000; anti-SLC25A11 (Abcam ab155196) 1:1000; anti-Actin (Biorad VMA00048) 1:1000 and anti-PGC-1α (Sigma-Aldrich ST1202) 1:1000 in milk 5% TBS-T. After washing 3 times with TBS-T, membranes were further probed with m-IgGk BP-HRP (Santa Cruz sc-516102) 1:2000 or goat anti-rabbit IgG-HRP (Santa Cruz sc-2004) 1:2000 in milk 5% in TBS-T for 2h at RT. Bands were detected using the chemiluminescence system (WesternBright™ ECL). The density of the corresponding bands was measured quantitatively using National Institutes of Health (NIH) Image software (http://rsb.info.nih.gov/nih-image).

3.3.9. Flow cytometry

SW872 cells were analysed by flow cytometry using MitoTracker Green (MTG, 50 nM, 30 minutes), a fluorescent probe that binds mitochondrial proteins, to evaluate mitochondrial mass, and Tetramethylrhodamine ethyl ester (TMRE, 40 nM, 15 minutes) to evaluate mitochondrial membrane potential. To perform all cytometric analyses, FACSCanto II flow cytometer with argon laser (blue, Ex 488 nm), helium-neon laser (red, Ex 633 nm) and solid-state diode laser (purple, Ex 405 nm) was used. The results were analysed using FACSDiva™ software.

3.3.10. 3-(4, 5-dimethylthiazol-2-yl)-2, 5-diphenyltetrazolium bromide (MTT) assay

SW872 cells were incubated with 25 μg/ml MTT in a cell culture incubator and after removing the medium, 1 ml of DMSO was added in each sample and absorbance was recorded at 570 nm, as reported elsewhere [Guidarelli A. *et al.,* 2021].

3.3.11. Oil Red O (ORO) staining

SW872 cells were stained with 0.3% ORO working solution (1 h, RT), washed several times with PBS, and then quantification of lipid droplets was performed by eluting the dye with 100% isopropanol and measuring the absorption at 510 nm, as reported elsewhere [Fiorani M. *et al.,* 2021].

3.3.12. Statistical analysis

The data obtained in our experiments are expressed as mean ± SEM (standard error). Statistical analysis was conducted using One-way ANOVA, followed by Dunnett's, Unpaired t-test or Two-Way ANOVA followed by Dunnett's using GraphPad Prism 8.0.2 Software. Differences are considered statistically significant for p values < 0.05.

3.4 RESULTS AND DISCUSSION

3.4.1. Clozapine inhibits mitochondrial biogenesis in differentiating SW872 cells.

SW872 liposarcoma cells change morphology and progressively accumulate increasing amounts of lipids when grown for 10 days in DM [Fiorani M. *et al.,* 2021]. As recently reported [Blandino G. *et al.*, 2023] these changes, clearly detected at T3, are inhibited by 15 μM CLZ. The effect of the SGA was concentration-dependent (Fig. 1A) although, even at the highest concentration tested, i.e.15 μM, residual lipid accumulation remained significant.

Under the same conditions, mRNA levels of CEPBβ (Fig. 1B) and PPARγ (Fig. 1C), two key transcription factors involved in the regulation of adipogenic differentiation [Farmer S.R., 2006], were also increased at T3 *via* a mechanism dose-dependently inhibited by CLZ. These results are surprisingly similar to those obtained in experiments measuring the expression of PGC1α, a master regulator of mitochondrial biogenesis [Islam H. *et al.,* 2018], at both the mRNA (Fig.1D) and protein (Fig. 1E) levels. mRNA levels of other transcription factors controlling mitochondrial biogenesis, *e.g.*, FOXO3α and TFB2m, were also higher in comparison to preadipocytes (T0), and their expression was significantly reduced by 15 μM CLZ (Fig. 2). In other circumstances, even under conditions in which the increased mRNA expression was not detectable at T3, as is the case of NRF1, NRF2, and TFAM, CLZ lowered their levels below those found in preadipocytes (Fig. 2). These results indicate that CLZ inhibits the expression of critical transcription factors regulating mitochondrial biogenesis occurring at the early phases of SW872 cell adipogenic differentiation.
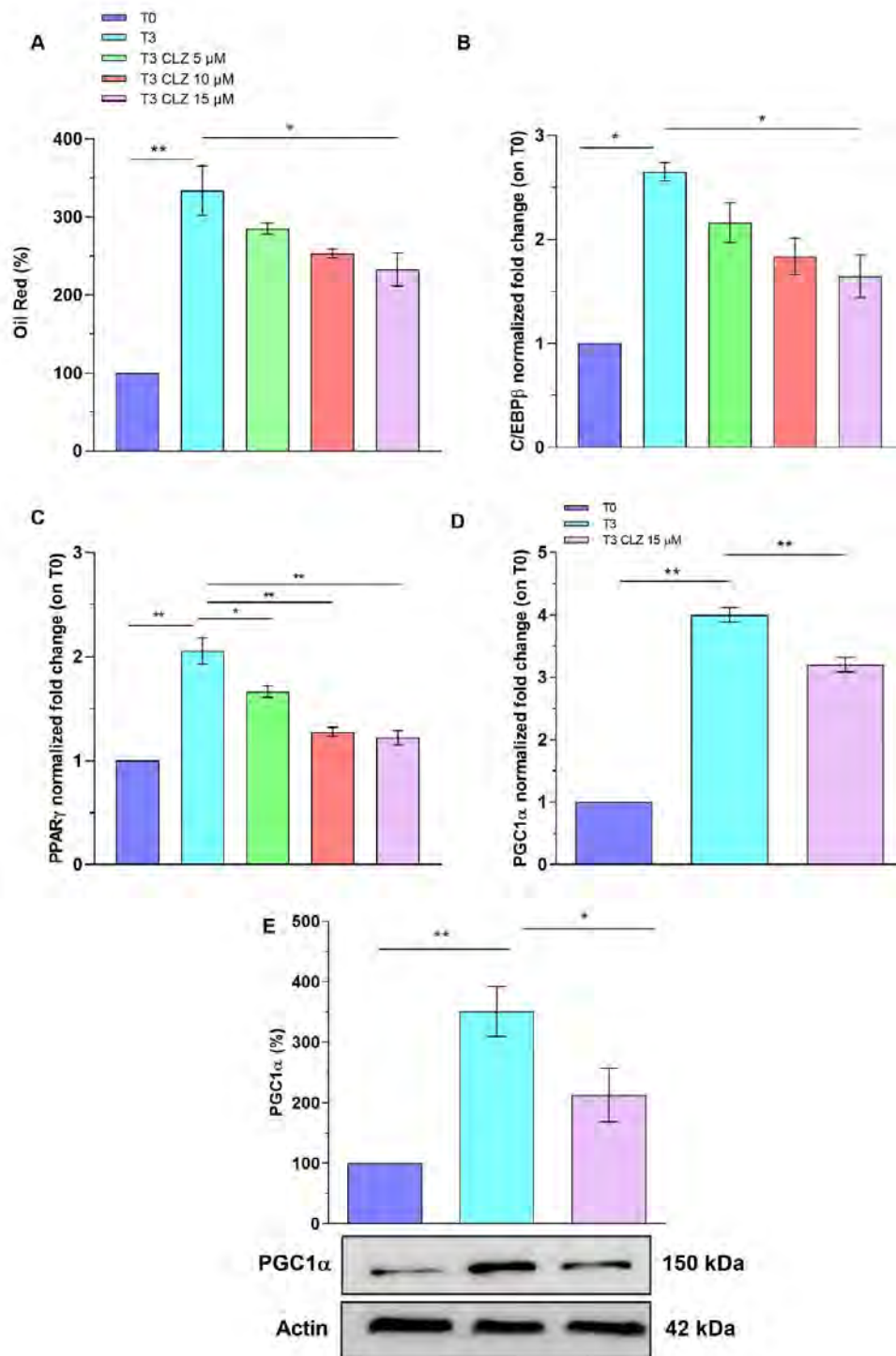
FIG.1. Clozapine slows down adipogenic differentiation and inhibits mitochondrial biogenesis during SW872 cell differentiation.

Lipid accumulation was quantified by ORO spectrophotometric analysis at 510 nm. Data are expressed in % respect to T0 (A). qPCR of C/EBPβ (B), PPARγ (C) and PGC1α (D) expression. The graphs show the normalised fold change compared to T0. GAPDH was used as housekeeping. Western immunoblotting analysis of PGC1α expression (E). Actin was used as loading control. Data are expressed in % respect to T0. Results represent the means ± SEM calculated from at least three independent determinations. *p<0.05; **p<0.01. One-Way ANOVA followed by Dunnett's test.
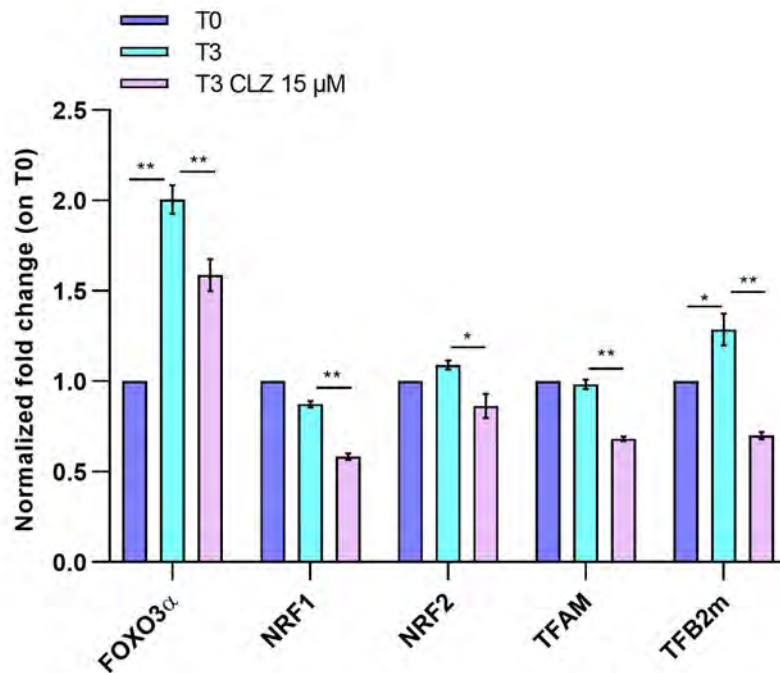
FIG. 2. Clozapine inhibits the expression of critical transcription factors regulating mitochondrial biogenesis during SW872 cell differentiation.

qPCR of FOXO3a, NRF1, NRF2/GABPA, TFAM, TFB2m expressions. The graph shows the normalised fold change compared to T0. GAPDH was used as housekeeping. Results represent the means ± SEM calculated from at least three independent determinations. *p<0.05; **p<0.01. One-Way ANOVA followed by Dunnett's test.

3.4.2. Clozapine inhibits mitochondrial biogenesis and induces opposite responses in the expression of specific mitochondrial proteins.

Mitochondrial biogenesis is associated with increased mitochondrial number and mass.

The results of our experiments show that mitochondrial DNA is significantly increased at T3 compared to T0, therefore providing an indication of a higher mitochondrial number (Fig. 3A). Importantly, this event was significantly inhibited by 15 µM CLZ, suggesting that the SGA might impact on mitochondriogenesis by reducing mitochondrial number.

In addition, cytofluorimetric analysis using the fluorescent probe MTG provided evidence also of increased mitochondrial mass at T3, that was once again sensitive to 15 µM CLZ (Fig. 3B).

Less and smaller mitochondria should be accompanied by reduced expression of all mitochondrial proteins, as it occurs in WAT from obese patients [Bournat and Brown., 2016]. In line with this premise, Fig. 3C and D show an increased expression, detected at T3, of the 2-oxoglutarate carrier (2-OGC), the mitochondrial transporter of 2-oxoglutarate [Monnè M. *et al.,* 2013]. Identical results were obtained measuring the expression of another representative mitochondrial protein, Thioredoxin 2 (Trx-2) [not shown, Blandino et al 2023], which participates in the mitochondrial antioxidant defence [Lu and Holmgren, 2014]. As expected, CLZ (15 µM) blunted all these responses.

Consistently with the enhancement in mitochondriogenesis during the differentiation process, the expression of cytochrome oxidase IV (COX IV) also increased at T3 (Figs. 3E and F). Surprisingly, in 15 µM CLZ-treated cells COX IV did not decrease -but rather further went up (Figs. 3E and F). Interestingly, the expression of different proteins of the respiratory chain complexes which, as other mitochondrial proteins was increased at T3, was further upregulated upon CLZ supplementation (Fig. 3G and H).

These findings provide evidence for a surprising and unique effect of CLZ on mitochondrial biogenesis, leading to decreased mitochondrial number and mass unexpectedly associated with an upregulation of proteins of the mitochondrial respiratory chain complexes.
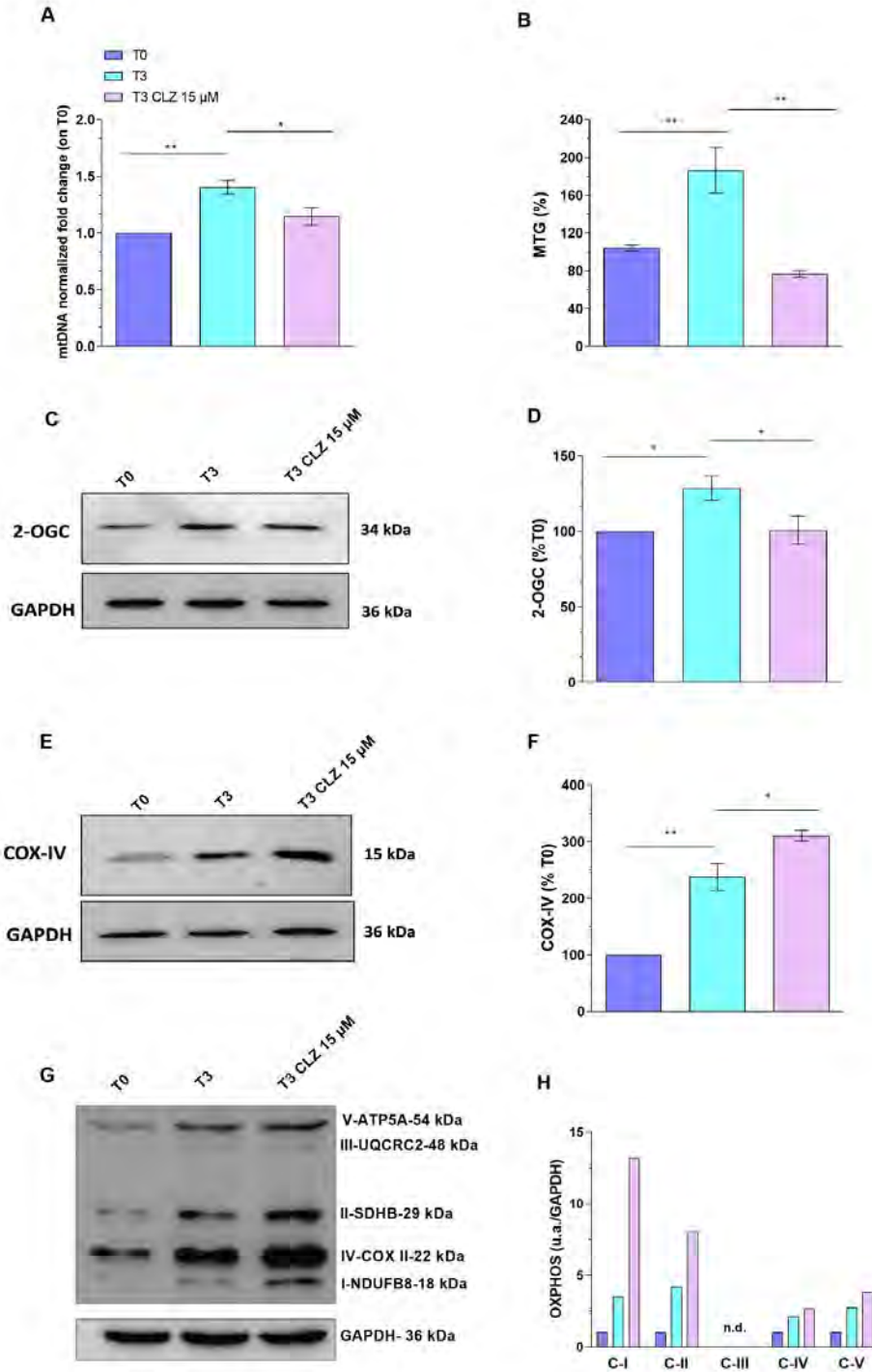
FIG. 3 Clozapine reduces mitochondrial mass and number and upregulates OXPHOS proteins during SW872 cell differentiation.

mtDNA quantification by real time PCR calculated by the ratio between ND1 mitochondrial gene and 18s RNA nuclear gene. The graph shows the normalised fold change compared to T0 (A). MTG-cytofluorimetric analysis of mitochondrial mass (B). Western immunoblotting analyses of 2-OGC (C), COX-IV (E) and OXPHOS (G) proteins. GAPDH was used as loading control. Histograms reported in D, F and H show the densitometry analyses of C, E and G respectively. Data in the panels B, D and F are expressed in % respect to T0. Results (A-F) represent the means ± SEM calculated from at least three independent determinations. *p<0.05; **p<0.01. One-Way ANOVA followed by Dunnett's test.

3.4.3. Effects of Clozapine on the residual mitochondria.

The above results indicate that CLZ blunts mitochondrial biogenesis during early adipogenic differentiation and affects the structure and organisation of the residual mitochondria, which, based on our previous findings, generate higher levels of ROS under the influence of the SGA [Blandino G. *et al.,* 2023].

Indeed, an increased formation of these reactive species was detected in CLZ supplemented cells by the MitoSOX Red fluorescence assay [Blandino G. *et al.,* 2023]. Next, we carried out experiments measuring mitochondrial membrane potential (TMRE) by cytofluorimetric technique and obtained evidence for an apparent increase at T3 (Fig. 4A), however no more detectable after normalisation to mitochondrial mass (Fig. 4B). Interestingly, CLZ did not inhibit, but rather increased further mitochondrial membrane potential (Fig. 4A), and normalisation to mitochondrial mass further amplified the data indicating that the SGA causes a dramatic mitochondrial hyperpolarization (Fig. 4B).

Measurement of MTT reduction provides an estimate of the activity of mitochondrial dehydrogenase activity [Huet O. *et al.,* 1991]. The conversion of MTT to formazan crystals, indicative of increased mitochondrial activity, was raised at day 3 and we found that CLZ further increased this response (Fig. 4C). A significant impact on the experimental outcome was obtained after normalisation to mitochondrial mass (not shown), similarly to that obtained in experiments measuring mitochondrial membrane potential.

In conclusion, results reported in this section indicate that under the same condition in which CLZ causes inhibition of mitochondrial biogenesis, displayed an increased expression of mitochondrial respiratory chain complexes. Most importantly, residual mitochondria exhibited higher activity of mitochondrial dehydrogenases as well as increased mitochondrial membrane potential and superoxide formation.
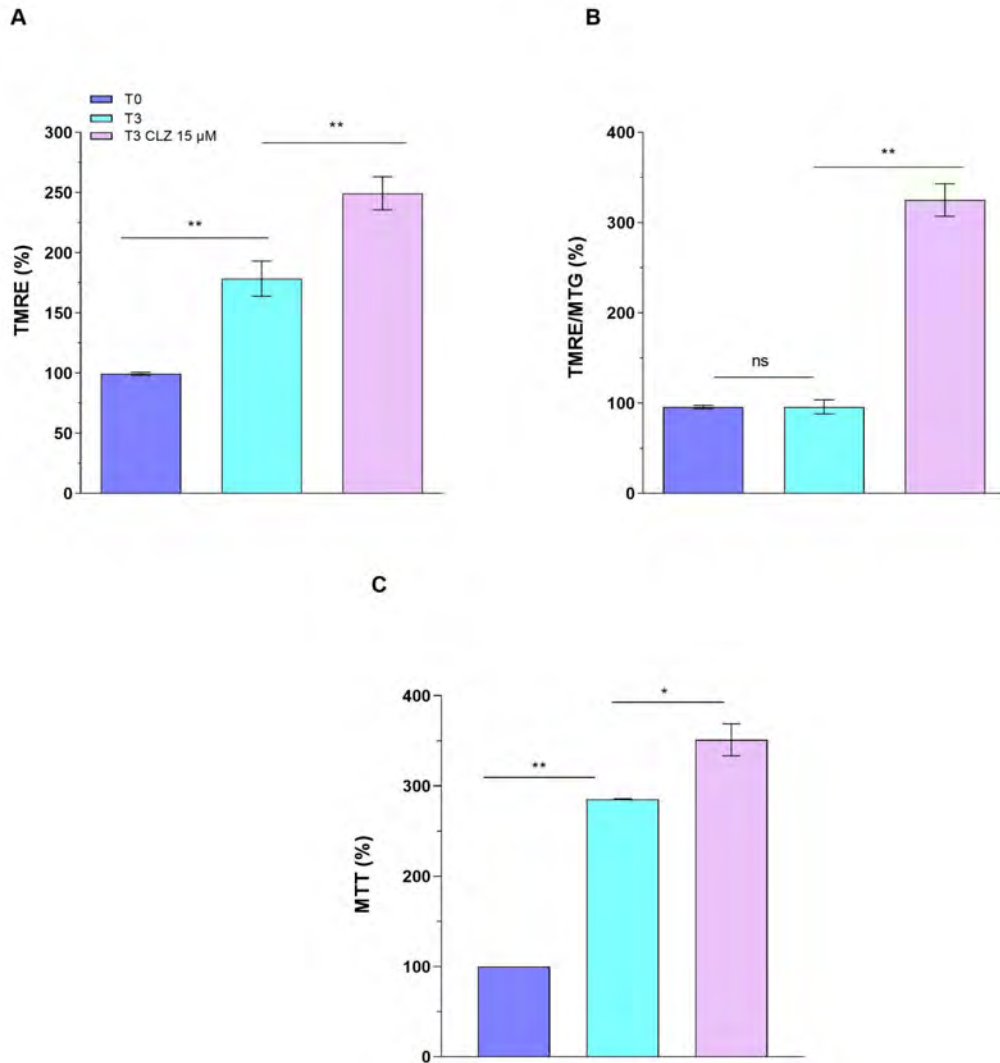
FIG. 4. Clozapine increases mitochondrial membrane potential and mitochondrial dehydrogenase activity during SW872 cell differentiation.

TMRE-cytofluorimetric analysis of mitochondrial membrane potential (A). TMRE and MTG ratio (B). Spectrophotometric analysis of MTT performed at 570 nm (C). Data are expressed in % respect to T0. Results represent the means ± SEM calculated from at least three independent determinations.*$p<0.05$; **$p<0.01$. One-Way ANOVA followed by Dunnett's test.

3.4.4. Effect of Clozapine on cellular bioenergetics.

Adipogenic process is associated with a metabolic switch from glycolysis to oxidative phosphorylation [Drehmer D.L *et al.,* 2016; Sánchez-Ramírez E. *et al.,* 2022]. The concept that preadipocytes are highly glycolytic is consistent with the results illustrated in Fig. 5, in which ATP levels (A-B) in preadipocytes (T0) remained unaffected after 1 or 4 h exposure to the complex I inhibitor ROT, employed under conditions associated with suppression of oxygen consumption (not shown). The glycolysis inhibitor 2-DG instead rapidly dropped off ATP levels (Fig. 5A and B).

Lactate is a classical byproduct of glucose metabolism, and the main lactate production pathway depends on glycolysis [Li X. *et al.,* 2022]. The measurement of L-lactate provides an indication of the glycolytic activity and also of the cellular metabolic status in general [Schmiedeknecht K. *et al.,* 2022].

Lactate formation increased linearly over the 4h observation period and ROT remarkably accelerated this process in the preadipocytes (T0) (Fig. 5C). The scenario changed significantly at T3, as the increased mitochondrial mass was associated with an increased ATP content (Fig. 5A and B). The observation that cellular ATP was reduced under conditions of ROT supplementation is suggestive of a more significant contribution of mitochondrial activity in ATP production (Fig. 5A and B). Consistently, T3 cells produced less lactate than T0 cells after 1 h of exposure to ROT, but after 4 h (Fig. 5D) they displayed the same rate of lactate release like that of preadipocytes (T0 cells). Thus, at T3, the compensatory glycolytic pathway associated with complex I inhibition was transiently retarded (at 1h), but nevertheless fully recovered after 4 h.

Finally, CLZ lowered basal ATP levels and ROT failed to affect this response (Fig. 5A and B), suggesting that ATP production in CLZ treated cells came mainly from glycolysis.

Interestingly, also the compensatory glycolytic response was lower in CLZ treated samples (Fig. 5E). This effect is particularly evident after 4 h exposure to ROT, as illustrated in Fig. 5E, in which the ability to release lactate is significantly reduced, suggesting that CLZ might have a negative impact on glycolytic recovery rate.
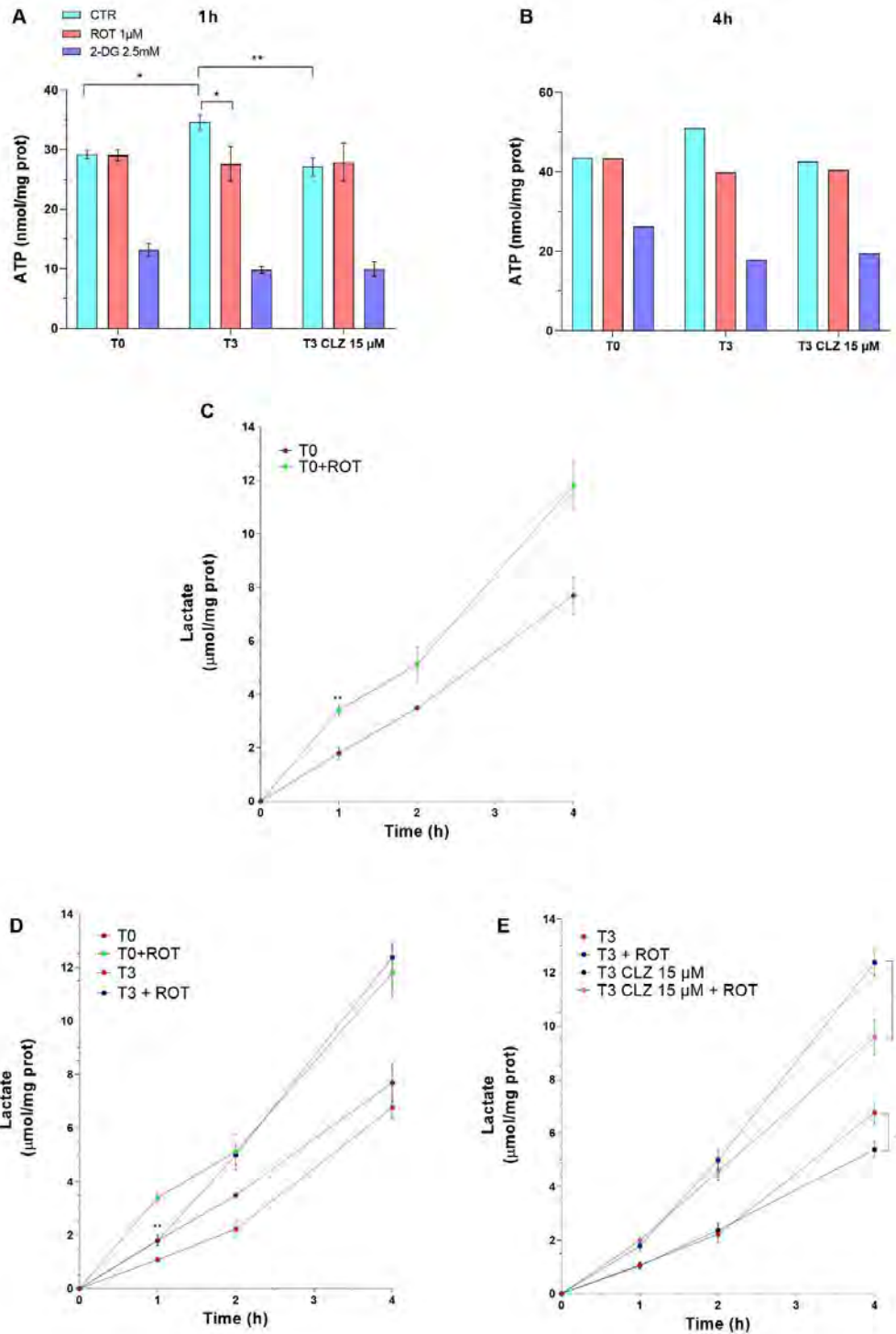
FIG. 5. Clozapine impairs the glycolytic compensatory capacity during SW872 cell differentiation.
HPLC analysis of ATP levels in differentiating SW872 cells exposed to 1 µM ROT or 2.5 mM 2-DG for 4 h. The ATP concentration was measured after 1 h (A) and 4 h (B). Spectrophotometric analysis of lactate production measured in SW872 cells exposed to 1 µM ROT for 4 h (C-D-E). Results (A, C, D, E) represent the means ± SEM calculated from at least three independent determinations. $*p<0.05$; $**p<0.01$. Unpaired t-test; Two-way ANOVA followed by Dunnett's test.

3.4.5. Effect of Clozapine on mitochondrial dynamics.

Mitochondrial dynamics is a delicate physiological process that involves the balance of two events, fission and fusion, essential for proper mitochondrial functionality [Westermann B., 2010; Wai and Langer., 2016].

The process of mitochondrial fusion is regulated by mitofusin-1 (MFN1) and mitofusin-2 (MFN2) for the outer mitochondrial membrane and optic atrophy 1 (OPA1) for the inner mitochondrial membrane, respectively [Song Z. *et al.,* 2009].

An appropriate mitochondrial fusion maintains the genetic homogeneity of these organelles, controls the production of mROS and the repolarization of the membrane [Scaini G. *et al.,* 2018; Bach D. *et al.,* 2003].

The fission process is controlled by two proteins, dynamin-related protein 1 (DRP1) and fission protein 1 (FIS1), which are located in the cytosol and in the mitochondrial outer membrane, respectively [Shaw and Nunnari., 2002]. DRP1 resides in the cytosol until recruited to mitochondria by FIS1 [Zhao J. *et al.,* 2013]. DRP1 further undergoes oligomerization to form a helical structure in the outer membrane which encircles, constricts, and cleaves the mitochondrion into two daughter mitochondria.

Recent studies have highlighted that dysregulated mitochondrial dynamics negatively affects mitochondrial functionality, leading to excessive ROS production, altered mitochondrial enzyme activities and calcium homeostasis, reduced ATP production and systemic energy perturbation [Bhatti J.S. *et al.,* 2017]. In turn, this imbalance is associated with the pathophysiology of metabolic diseases such as obesity and T2DM [Wada and Nakatsuka., 2016].

The effect of CLZ in mitochondrial dynamics was evaluated by analysing the expression of several genes involved in this process.

There are no differences in mRNA levels between preadipocytes (T0 cells) and T3 cells (Fig. 6), underlining that fission and fusion are not modulated during the early phases of the adipogenic process. On the contrary, a significant downregulation of all these targets was detected in CLZ-treated cells.

Although the role of mitochondrial dynamics in adipocyte metabolism and dysfunction has not been thoroughly elucidated, recent studies support the idea that a dysregulated mitochondrial dynamics might have a critical role in the pathophysiology of metabolic disorders; such as insulin resistance, obesity, and T2DM. In line with these findings, our results could contribute to shed light on the mechanism by which CLZ, by inducing dysfunctional mitochondria, can predispose to metabolic disorders.
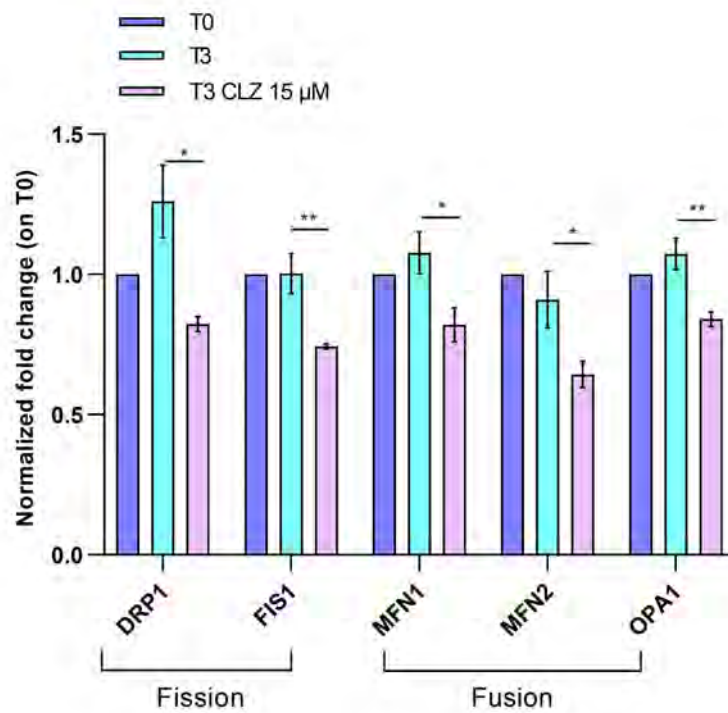
FIG. 6. Clozapine affects the mitochondrial dynamics during SW872 cell differentiation.

qPCR of DRP1, FIS1, MFN1, MFN2 and OPA1 expressions. GAPDH was used as housekeeping. The graph shows the normalised fold change compared to T0. Results represent the means ± SEM calculated from at least three independent determinations. *$p < 0.05$; **$p < 0.01$. One-Way ANOVA followed by Dunnett's test.

CONCLUSIONS

ROS critically regulate both physiological and pathological processes associated with adipogenesis through yet poorly defined mechanisms [Masschelin P.M. *et al.,* 2020; de Villiers D. *et al.,* 2018].

To address this issue in my thesis work, I initially characterised the adipogenic differentiation of human liposarcoma SW872 cells grown in a milieu enriched with various nutrients and supplements. Two different mechanisms of ROS formation were identified under these conditions. The first one was detected at the early phase of differentiation (T3) and was entirely mediated by NOX-2 activation. The second mechanism was instead associated with late events (T10) enforcing the mitochondrial formation of species leading to mitochondrial dysfunction.

Next, I demonstrated that these sequential mechanisms were in fact interconnected and postulated a physiological role of NOX-2 derived ROS in the regulation of events affecting adipogenesis and mitochondrial homeostasis. More specifically, I hypothesise that NOX-2-derived ROS could stimulate the Nrf2 dependent antioxidant response, thereby delaying mitochondrial ROS emission. In these experiments, I used CLZ, an antipsychotic favouring the onset of metabolic syndrome, which displays both antioxidant and NOX-2 inhibitory properties. Interestingly, the antioxidant effects of the drug were restricted to the cytosolic compartments, with no apparent effect in the mitochondrial compartment. Thus, to make a long story short, I could demonstrate that the Nrf2 dependent antioxidant response was critically involved in the buffering of early mitochondrial ROS, which in fact were detected only late in adipogenesis. CLZ, by suppressing early ROS formation, therefore delayed adipogenesis and remarkably anticipated the onset of mitochondrial ROS formation and dysfunction.

It is well established that adipogenesis and mitochondrial biogenesis are intertwined processes [Wilson-Fritch L. *et al.,* 2003]. By keeping in mind this notion, I could recapitulate numerous events documenting an increased mitochondrial biogenesis at T3, and soon realised that CLZ had a significant impact on these processes. Thus, CLZ suppressed mitochondrial biogenesis, anticipated ROS formation in residual mitochondria, and caused mitochondrial dysfunction. These findings are compatible with the possibility that CLZ has an important impact on the energetic status of the cells. In this direction, I could identify important effects in residual mitochondria, e.g., increased mitochondrial membrane potential, expression of specific respiratory chain complexes, oxygen consumption rate, etc., suggesting the involvement of compensatory mechanisms to support energy production, and providing a mechanism for mitochondrial ROS formation. In this last part of my work, I could demonstrate that CLZ hampers glycolysis stimulated by inhibition of electron transport in the respiratory chain. This effect might therefore contribute to the above effects of the antipsychotic converging in the induction of adipose tissue dysfunction.

REFERENCES

- Ago T, Nunoi H, Ito T, Sumimoto H. Mechanism for phosphorylation-induced activation of the phagocyte NADPH oxidase protein p47(phox). Triple replacement of serines 303, 304, and 328 with aspartates disrupts the SH3 domain-mediated intramolecular interaction in p47(phox), thereby activating the oxidase. J Biol Chem. 1999 Nov 19;274(47):33644-53. doi: 10.1074/jbc.274.47.33644. PMID: 10559253.
- Akl MG, Fawzy E, Deif M, Farouk A, Elshorbagy AK. Perturbed adipose tissue hydrogen peroxide metabolism in centrally obese men: Association with insulin resistance. PLoS One. 2017 May 18;12(5):e0177268. doi: 10.1371/journal.pone.0177268. PMID: 28545081; PMCID: PMC5436683.
- Alberti KG, Zimmet P, Shaw J; IDF Epidemiology Task Force Consensus Group. The metabolic syndrome--a new worldwide definition. Lancet. 2005 Sep 24-30;366(9491):1059-62. doi: 10.1016/S0140-6736(05)67402-8. PMID: 16182882.
- Alcázar-Fabra M, Navas P, Brea-Calvo G. Coenzyme Q biosynthesis and its role in the respiratory chain structure. Biochim Biophys Acta. 2016 Aug;1857(8):1073-1078. doi: 10.1016/j.bbabio.2016.03.010. Epub 2016 Mar 10. PMID: 26970214.
- Aleksunes LM, Reisman SA, Yeager RL, Goedken MJ, Klaassen CD. Nuclear factor erythroid 2-related factor 2 deletion impairs glucose tolerance and exacerbates hyperglycemia in type 1 diabetic mice. J Pharmacol Exp Ther. 2010 Apr;333(1):140-51. doi: 10.1124/jpet.109.162271. Epub 2010 Jan 19. PMID: 20086057; PMCID: PMC2846027.
- Ali AT, Hochfeld WE, Myburgh R, Pepper MS. Adipocyte and adipogenesis. Eur J Cell Biol. 2013 Jun-Jul;92(6-7):229-36. doi: 10.1016/j.ejcb.2013.06.001. Epub 2013 Jun 14. PMID: 23876739.
- Allison DB, Casey DE. Antipsychotic-induced weight gain: a review of the literature. J Clin Psychiatry. 2001;62 Suppl 7:22-31. PMID: 11346192.
- Anderson EJ, Lustig ME, Boyle KE, Woodlief TL, Kane DA, Lin CT, Price JW 3rd, Kang L, Rabinovitch PS, Szeto HH, Houmard JA, Cortright RN, Wasserman DH, Neufer PD. Mitochondrial H2O2 emission and cellular redox state link excess fat intake to insulin resistance in both rodents and humans. J Clin Invest. 2009 Mar;119(3):573-81. doi: 10.1172/JCI37048. Epub 2009 Feb 2. PMID: 19188683; PMCID: PMC2648700.
- Babior BM. NADPH oxidase. Curr Opin Immunol. 2004 Feb;16(1):42-7. doi: 10.1016/j.coi.2003.12.001. PMID: 14734109.
- Bach D, Pich S, Soriano FX, Vega N, Baumgartner B, Oriola J, Daugaard JR, Lloberas J, Camps M, Zierath JR, Rabasa-Lhoret R, Wallberg-Henriksson H, Laville M, Palacín M, Vidal H, Rivera F, Brand M, Zorzano A. Mitofusin-2 determines mitochondrial network architecture and mitochondrial metabolism. A novel regulatory mechanism altered in obesity. J Biol Chem. 2003 May 9;278(19):17190-7. doi: 10.1074/jbc.M212754200. Epub 2003 Feb 21. PMID: 12598526.
- Baig MR, Navaira E, Escamilla MA, Raventos H, Walss-Bass C. Clozapine treatment causes oxidation of proteins involved in energy metabolism in lymphoblastoid cells: a possible mechanism for antipsychotic-induced metabolic alterations. J Psychiatr Pract. 2010 Sep;16(5):325-33. doi: 10.1097/01.pra.0000388627.36781.6a. PMID: 20859109.
- Bánfi B, Molnár G, Maturana A, Steger K, Hegedûs B, Demaurex N, Krause KH. A Ca(2+)-activated NADPH oxidase in testis, spleen, and lymph nodes. J Biol Chem. 2001 Oct 5;276(40):37594-601. doi: 10.1074/jbc.M103034200. Epub 2001 Aug 1. PMID: 11483596.
- Barshad G, Marom S, Cohen T, Mishmar D. Mitochondrial DNA Transcription and Its Regulation: An Evolutionary Perspective. Trends Genet. 2018 Sep;34(9):682-692. doi: 10.1016/j.tig.2018.05.009. Epub 2018 Jun 23. PMID: 29945721.
- Bedard K, Krause KH. The NOX family of ROS-generating NADPH oxidases: physiology and pathophysiology. Physiol Rev. 2007 Jan;87(1):245-313. doi: 10.1152/physrev.00044.2005. PMID: 17237347.
- Berger JP, Akiyama TE, Meinke PT. PPARs: therapeutic targets for metabolic disease. Trends Pharmacol Sci. 2005 May;26(5):244-51. doi: 10.1016/j.tips.2005.03.003. PMID: 15860371.
- Bhatti JS, Bhatti GK, Reddy PH. Mitochondrial dysfunction and oxidative stress in metabolic disorders - A step towards mitochondria based therapeutic strategies. Biochim Biophys Acta Mol Basis Dis. 2017 May;1863(5):1066-1077. doi: 10.1016/j.bbadis.2016.11.010. Epub 2016 Nov 9. PMID: 27836629; PMCID: PMC5423868.
- Blakely RD, Wages SA, Justice JB, Herndon JG, Neill DB. Neuroleptics increase striatal catecholamine metabolites but not ascorbic acid in dialyzed perfusate. Brain Res. 1984 Aug 6;308(1):1-8. doi: 10.1016/0006-8993(84)90910-7. PMID: 6206916.
- Blandino G, Fiorani M, Canonico B, De Matteis R, Guidarelli A, Montanari M, Buffi G, Coppo L, Arnér ESJ, Cantoni O. Clozapine suppresses NADPH oxidase activation, counteracts cytosolic H2O2, and triggers early

onset mitochondrial dysfunction during adipogenesis of human liposarcoma SW872 cells. Redox Biol. 2023 Oct 12;67:102915. doi: 10.1016/j.redox.2023.102915. Epub ahead of print. PMID: 37866162.

- Bolonna AA, Kerwin RW. Partial agonism and schizophrenia. Br J Psychiatry. 2005 Jan;186:7-10. doi: 10.1192/bjp.186.1.7. PMID: 15630117.

- Bournat JC, Brown CW. Mitochondrial dysfunction in obesity. Curr Opin Endocrinol Diabetes Obes. 2010 Oct;17(5):446-52. doi: 10.1097/MED.0b013e32833c3026. PMID: 20585248; PMCID: PMC5001554.

- Boveris A, Chance B. The mitochondrial generation of hydrogen peroxide. General properties and effect of hyperbaric oxygen. Biochem J. 1973 Jul;134(3):707-16. doi: 10.1042/bj1340707. PMID: 4749271; PMCID: PMC1177867.

- Boyda HN, Procyshyn RM, Pang CC, Barr AM. Peripheral adrenoceptors: the impetus behind glucose dysregulation and insulin resistance. J Neuroendocrinol. 2013 Mar;25(3):217-28. doi: 10.1111/jne.12002. PMID: 23140239.

- Brandes RP, Weissmann N, Schröder K. Nox family NADPH oxidases: Molecular mechanisms of activation. Free Radic Biol Med. 2014 Nov;76:208-26. doi: 10.1016/j.freeradbiomed.2014.07.046. Epub 2014 Aug 23. PMID: 25157786.

- Bravo EL. Metabolic factors and the sympathetic nervous system. Am J Hypertens. 1989 Dec;2(12 Pt 2):339S-344S. doi: 10.1093/ajh/2.12.339s. PMID: 2688691.

- Brinholi FF, Farias CC, Bonifácio KL, Higachi L, Casagrande R, Moreira EG, Barbosa DS. Clozapine and olanzapine are better antioxidants than haloperidol, quetiapine, risperidone and ziprasidone in in vitro models. Biomed Pharmacother. 2016 Jul;81:411-415. doi: 10.1016/j.biopha.2016.02.047. Epub 2016 Apr 27. PMID: 27261620.

- Brookes PS. Mitochondrial H(+) leak and ROS generation: an odd couple. Free Radic Biol Med. 2005 Jan 1;38(1):12-23. doi: 10.1016/j.freeradbiomed.2004.10.016. PMID: 15589367.

- Calzadilla P, Sapochnik D, Cosentino S, Diz V, Dicelio L, Calvo JC, Guerra LN. N-acetylcysteine reduces markers of differentiation in 3T3-L1 adipocytes. Int J Mol Sci. 2011;12(10):6936-51. doi: 10.3390/ijms12106936. Epub 2011 Oct 19. PMID: 22072928; PMCID: PMC3211019.

- Cantó C, Auwerx J. PGC-1alpha, SIRT1 and AMPK, an energy sensing network that controls energy expenditure. Curr Opin Lipidol. 2009 Apr;20(2):98-105. doi: 10.1097/MOL.0b013e328328d0a4. PMID: 19276888; PMCID: PMC3627054.

- Cao Z, Umek RM, McKnight SL. Regulated expression of three C/EBP isoforms during adipose conversion of 3T3-L1 cells. Genes Dev. 1991 Sep;5(9):1538-52. doi: 10.1101/gad.5.9.1538. PMID: 1840554.

- Caruso G, Grasso M, Fidilio A, Tascedda F, Drago F, Caraci F. Antioxidant Properties of Second-Generation Antipsychotics: Focus on Microglia. Pharmaceuticals (Basel). 2020 Dec 12;13(12):457. doi: 10.3390/ph13120457. PMID: 33322693; PMCID: PMC7764768.

- Casquero-Veiga M, García-García D, MacDowell KS, Pérez-Caballero L, Torres-Sánchez S, Fraguas D, Berrocoso E, Leza JC, Arango C, Desco M, Soto-Montenegro ML. Risperidone administered during adolescence induced metabolic, anatomical and inflammatory/oxidative changes in adult brain: A PET and MRI study in the maternal immune stimulation animal model. Eur Neuropsychopharmacol. 2019 Jul;29(7):880-896. doi: 10.1016/j.euroneuro.2019.05.002. Epub 2019 Jun 20. PMID: 31229322.

- Castro JP, Grune T, Speckmann B. The two faces of reactive oxygen species (ROS) in adipocyte function and dysfunction. Biol Chem. 2016 Aug 1;397(8):709-24. doi: 10.1515/hsz-2015-0305. PMID: 27031218.

- Chang CC, Lin KY, Peng KY, Day YJ, Hung LM. Resveratrol exerts anti-obesity effects in high-fat diet obese mice and displays differential dosage effects on cytotoxicity, differentiation, and lipolysis in 3T3-L1 cells. Endocr J. 2016;63(2):169-78. doi: 10.1507/endocrj.EJ15-0545. Epub 2015 Dec 23. PMID: 26698690.

- Chang YC, Yu YH, Shew JY, Lee WJ, Hwang JJ, Chen YH, Chen YR, Wei PC, Chuang LM, Lee WH. Deficiency of NPGPx, an oxidative stress sensor, leads to obesity in mice and human. EMBO Mol Med. 2013 Aug;5(8):1165-79. doi: 10.1002/emmm.201302679. Epub 2013 Jul 4. Update in: EMBO Mol Med. 2013 Aug;5(8):1147-8. PMID: 23828861; PMCID: PMC3944459.

- Cho KJ, Moon HE, Moini H, Packer L, Yoon DY, Chung AS. Alpha-lipoic acid inhibits adipocyte differentiation by regulating pro-adipogenic transcription factors via mitogen-activated protein kinase pathways. J Biol Chem. 2003 Sep 12;278(37):34823-33. doi: 10.1074/jbc.M210747200. Epub 2003 Jun 30. PMID: 12837769.

- Chung SS, Kim M, Youn BS, Lee NS, Park JW, Lee IK, Lee YS, Kim JB, Cho YM, Lee HK, Park KS. Glutathione peroxidase 3 mediates the antioxidant effect of peroxisome proliferator-activated receptor gamma in human skeletal muscle cells. Mol Cell Biol. 2009 Jan;29(1):20-30. doi: 10.1128/MCB.00544-08. Epub 2008 Oct 20. PMID: 18936159; PMCID: PMC2612482.

- Chutkow WA, Birkenfeld AL, Brown JD, Lee HY, Frederick DW, Yoshioka J, Patwari P, Kursawe R, Cushman SW, Plutzky J, Shulman GI, Samuel VT, Lee RT. Deletion of the alpha-arrestin protein Txnip in mice promotes adiposity and adipogenesis while preserving insulin sensitivity. Diabetes. 2010 Jun;59(6):1424-34. doi: 10.2337/db09-1212. Epub 2010 Mar 18. PMID: 20299477; PMCID: PMC2874703.

- Chutkow WA, Lee RT. Thioredoxin regulates adipogenesis through thioredoxin-interacting protein (Txnip) protein stability. J Biol Chem. 2011 Aug 19;286(33):29139-29145. doi: 10.1074/jbc.M111.267666. Epub 2011 Jun 24. PMID: 21705327; PMCID: PMC3190721.
- Cicolari S, Dacrema M, Tsetegho Sokeng AJ, Xiao J, Atchan Nwakiban AP, Di Giovanni C, Santarcangelo C, Magni P, Daglia M. Hydromethanolic Extracts from *Adansonia digitata* L. Edible Parts Positively Modulate Pathophysiological Mechanisms Related to the Metabolic Syndrome. Molecules. 2020 Jun 21;25(12):2858. doi: 10.3390/molecules25122858. PMID: 32575811; PMCID: PMC7356617.
- Cikánková T, Fišar Z, Bakhouche Y, Ľupták M, Hroudová J. In vitro effects of antipsychotics on mitochondrial respiration. Naunyn Schmiedebergs Arch Pharmacol. 2019 Oct;392(10):1209-1223. doi: 10.1007/s00210-019-01665-8. Epub 2019 May 19. PMID: 31104106.
- Contreras-Shannon V, Heart DL, Paredes RM, Navaira E, Catano G, Maffi SK, Walss-Bass C. Clozapine-induced mitochondria alterations and inflammation in brain and insulin-responsive cells. PLoS One. 2013;8(3):e59012. doi: 10.1371/journal.pone.0059012. Epub 2013 Mar 20. PMID: 23527073; PMCID: PMC3604003.
- Cooney SJ, Bermudez-Sabogal SL, Byrnes KR. Cellular and temporal expression of NADPH oxidase (NOX) isotypes after brain injury. J Neuroinflammation. 2013 Dec 17;10:155. doi: 10.1186/1742-2094-10-155. PMID: 24344836; PMCID: PMC3878417.
- Dang PM, Cross AR, Babior BM. Assembly of the neutrophil respiratory burst oxidase: a direct interaction between p67PHOX and cytochrome b558. Proc Natl Acad Sci U S A. 2001 Mar 13;98(6):3001-5. doi: 10.1073/pnas.061029698. PMID: 11248021; PMCID: PMC30596.
- Davies MJ. Protein oxidation and peroxidation. Biochem J. 2016 Apr 1;473(7):805-25. doi: 10.1042/BJ20151227. PMID: 27026395; PMCID: PMC4819570.
- Del Campo A, Bustos C, Mascayano C, Acuña-Castillo C, Troncoso R, Rojo LE. Metabolic Syndrome and Antipsychotics: The Role of Mitochondrial Fission/Fusion Imbalance. Front Endocrinol (Lausanne). 2018 Apr 23;9:144. doi: 10.3389/fendo.2018.00144. PMID: 29740394; PMCID: PMC5924798.
- de Villiers D, Potgieter M, Ambele MA, Adam L, Durandt C, Pepper MS. The Role of Reactive Oxygen Species in Adipogenic Differentiation. Adv Exp Med Biol. 2018;1083:125-144. doi: 10.1007/5584_2017_119. PMID: 29139087.
- Dietrich-Muszalska A, Kopka J, Kwiatkowska A. The effects of ziprasidone, clozapine and haloperidol on lipid peroxidation in human plasma (in vitro): comparison. Neurochem Res. 2013 Jul;38(7):1490-5. doi: 10.1007/s11064-013-1050-z. Epub 2013 Apr 26. PMID: 23619559.
- Dinkova-Kostova AT, Liby KT, Stephenson KK, Holtzclaw WD, Gao X, Suh N, Williams C, Risingsong R, Honda T, Gribble GW, Sporn MB, Talalay P. Extremely potent triterpenoid inducers of the phase 2 response: correlations of protection against oxidant and inflammatory stress. Proc Natl Acad Sci U S A. 2005 Mar 22;102(12):4584-9. doi: 10.1073/pnas.0500815102. Epub 2005 Mar 14. PMID: 15767573; PMCID: PMC555528.
- Dominko K, Đikić D. Glutathionylation: a regulatory role of glutathione in physiological processes. Arh Hig Rada Toksikol. 2018 Mar 1;69(1):1-24. doi: 10.2478/aiht-2018-69-2966. PMID: 29604197.
- Dominy JE Jr, Lee Y, Gerhart-Hines Z, Puigserver P. Nutrient-dependent regulation of PGC-1alpha's acetylation state and metabolic function through the enzymatic activities of Sirt1/GCN5. Biochim Biophys Acta. 2010 Aug;1804(8):1676-83. doi: 10.1016/j.bbapap.2009.11.023. Epub 2009 Dec 11. PMID: 20005308; PMCID: PMC2886158.
- Drehmer DL, de Aguiar AM, Brandt AP, Petiz L, Cadena SM, Rebelatto CK, Brofman PR, Filipak Neto F, Dallagiovanna B, Abud AP. Metabolic switches during the first steps of adipogenic stem cells differentiation. Stem Cell Res. 2016 Sep;17(2):413-421. doi: 10.1016/j.scr.2016.09.001. Epub 2016 Sep 7. PMID: 27653462.
- Dutchak PA, Katafuchi T, Bookout AL, Choi JH, Yu RT, Mangelsdorf DJ, Kliewer SA. Fibroblast growth factor-21 regulates PPARγ activity and the antidiabetic actions of thiazolidinediones. Cell. 2012 Feb 3;148(3):556-67. doi: 10.1016/j.cell.2011.11.062. PMID: 22304921; PMCID: PMC3273727.
- Eseberri I, Miranda J, Lasa A, Churruca I, Portillo MP. Doses of Quercetin in the Range of Serum Concentrations Exert Delipidating Effects in 3T3-L1 Preadipocytes by Acting on Different Stages of Adipogenesis, but Not in Mature Adipocytes. Oxid Med Cell Longev. 2015;2015:480943. doi: 10.1155/2015/480943. Epub 2015 Jun 9. PMID: 26180590; PMCID: PMC4477249.
- Esen-Danaci A, Sarandöl A, Taneli F, Yurtsever F, Ozlen N. Effects of second generation antipsychotics on leptin and ghrelin. Prog Neuropsychopharmacol Biol Psychiatry. 2008 Aug 1;32(6):1434-8. doi: 10.1016/j.pnpbp.2008.03.015. Epub 2008 Apr 1. PMID: 18579280.
- Eslam M, Newsome PN, Sarin SK, Anstee QM, Targher G, Romero-Gomez M, Zelber-Sagi S, Wai-Sun Wong V, Dufour JF, Schattenberg JM, Kawaguchi T, Arrese M, Valenti L, Shiha G, Tiribelli C, Yki-Järvinen H, Fan JG, Grønbæk H, Yilmaz Y, Cortez-Pinto H, Oliveira CP, Bedossa P, Adams LA, Zheng MH, Fouad Y, Chan WK, Mendez-Sanchez N, Ahn SH, Castera L, Bugianesi E, Ratziu V, George J. A new definition for metabolic dysfunction-associated fatty liver disease: An international expert consensus statement. J Hepatol. 2020 Jul;73(1):202-209. doi: 10.1016/j.jhep.2020.03.039. Epub 2020 Apr 8. PMID: 32278004.

- Esterbauer H, Schaur RJ, Zollner H. Chemistry and biochemistry of 4-hydroxynonenal, malonaldehyde and related aldehydes. Free Radic Biol Med. 1991;11(1):81-128. doi: 10.1016/0891-5849(91)90192-6. PMID: 1937131.
- Farmer SR. Transcriptional control of adipocyte formation. Cell Metab. 2006 Oct;4(4):263-73. doi: 10.1016/j.cmet.2006.07.001. PMID: 17011499; PMCID: PMC1958996.
- Fazakerley DJ, Minard AY, Krycer JR, Thomas KC, Stöckli J, Harney DJ, Burchfield JG, Maghzal GJ, Caldwell ST, Hartley RC, Stocker R, Murphy MP, James DE. Mitochondrial oxidative stress causes insulin resistance without disrupting oxidative phosphorylation. J Biol Chem. 2018 May 11;293(19):7315-7328. doi: 10.1074/jbc.RA117.001254. Epub 2018 Mar 29. PMID: 29599292; PMCID: PMC5950018.
- Fex M, Nicholas LM, Vishnu N, Medina A, Sharoyko VV, Nicholls DG, Spégel P, Mulder H. The pathogenetic role of β-cell mitochondria in type 2 diabetes. J Endocrinol. 2018 Mar;236(3):R145-R159. doi: 10.1530/JOE-17-0367. PMID: 29431147.
- Findeisen HM, Gizard F, Zhao Y, Qing H, Jones KL, Cohn D, Heywood EB, Bruemmer D. Glutathione depletion prevents diet-induced obesity and enhances insulin sensitivity. Obesity (Silver Spring). 2011 Dec;19(12):2429-32. doi: 10.1038/oby.2011.298. Epub 2011 Sep 29. PMID: 21959341.
- Fiorani M, De Matteis R, Canonico B, Blandino G, Mazzoli A, Montanari M, Guidarelli A, Cantoni O. Temporal correlation of morphological and biochemical changes with the recruitment of different mechanisms of reactive oxygen species formation during human SW872 cell adipogenic differentiation. Biofactors. 2021 Sep;47(5):837-851. doi: 10.1002/biof.1769. Epub 2021 Jul 14. PMID: 34260117; PMCID: PMC8597007.
- Freytag SO, Paielli DL, Gilbert JD. Ectopic expression of the CCAAT/enhancer-binding protein alpha promotes the adipogenic program in a variety of mouse fibroblastic cells. Genes Dev. 1994 Jul 15;8(14):1654-63. doi: 10.1101/gad.8.14.1654. PMID: 7958846.
- Frogley C, Taylor D, Dickens G, Picchioni M. A systematic review of the evidence of clozapine's anti-aggressive effects. Int J Neuropsychopharmacol. 2012 Oct;15(9):1351-71. doi: 10.1017/S146114571100201X. Epub 2012 Feb 20. PMID: 22339930.
- Furukawa S, Fujita T, Shimabukuro M, Iwaki M, Yamada Y, Nakajima Y, Nakayama O, Makishima M, Matsuda M, Shimomura I. Increased oxidative stress in obesity and its impact on metabolic syndrome. J Clin Invest. 2004 Dec;114(12):1752-61. doi: 10.1172/JCI21625. PMID: 15599400; PMCID: PMC535065.
- Gabig TG, Babior BM. The O2(-) -forming oxidase responsible for the respiratory burst in human neutrophils. Properties of the solubilized enzyme. J Biol Chem. 1979 Sep 25;254(18):9070-4. PMID: 479180.
- Galic S, Oakhill JS, Steinberg GR. Adipose tissue as an endocrine organ. Mol Cell Endocrinol. 2010 Mar 25;316(2):129-39. doi: 10.1016/j.mce.2009.08.018. Epub 2009 Aug 31. PMID: 19723556.
- Garfield AS. Derivation of primary mouse embryonic fibroblast (PMEF) cultures. Methods Mol Biol. 2010;633:19-27. doi: 10.1007/978-1-59745-019-5_2. PMID: 20204617.
- Garruti G, Ricquier D. Analysis of uncoupling protein and its mRNA in adipose tissue deposits of adult humans. Int J Obes Relat Metab Disord. 1992 May;16(5):383-90. PMID: 1319974.
- Gaulin BD, Markowitz JS, Caley CF, Nesbitt LA, Dufresne RL. Clozapine-associated elevation in serum triglycerides. Am J Psychiatry. 1999 Aug;156(8):1270-2. doi: 10.1176/ajp.156.8.1270. PMID: 10450273.
- Glazer WM, Dickson RA. Clozapine reduces violence and persistent aggression in schizophrenia. J Clin Psychiatry. 1998;59 Suppl 3:8-14. PMID: 9541332.
- Green H, Meuth M. An established pre-adipose cell line and its differentiation in culture. Cell. 1974 Oct;3(2):127-33. doi: 10.1016/0092-8674(74)90116-0. PMID: 4426090.
- Gregoire FM, Smas CM, Sul HS. Understanding adipocyte differentiation. Physiol Rev. 1998 Jul;78(3):783-809. doi: 10.1152/physrev.1998.78.3.783. PMID: 9674695.
- Gregoire FM. Adipocyte differentiation: from fibroblast to endocrine cell. Exp Biol Med (Maywood). 2001 Dec;226(11):997-1002. doi: 10.1177/153537020122601106. PMID: 11743135.
- Grek CL, Zhang J, Manevich Y, Townsend DM, Tew KD. Causes and consequences of cysteine S-glutathionylation. J Biol Chem. 2013 Sep 13;288(37):26497-504. doi: 10.1074/jbc.R113.461368. Epub 2013 Jul 16. PMID: 23861399; PMCID: PMC3772197.
- Grimsrud PA, Xie H, Griffin TJ, Bernlohr DA. Oxidative stress and covalent modification of protein with bioactive aldehydes. J Biol Chem. 2008 Aug 8;283(32):21837-41. doi: 10.1074/jbc.R700019200. Epub 2008 Apr 29. PMID: 18445586; PMCID: PMC2494933.
- Groemping Y, Lapouge K, Smerdon SJ, Rittinger K. Molecular basis of phosphorylation-induced activation of the NADPH oxidase. Cell. 2003 May 2;113(3):343-55. doi: 10.1016/s0092-8674(03)00314-3. PMID: 12732142.
- Grundy SM. Metabolic syndrome update. Trends Cardiovasc Med. 2016 May;26(4):364-73. doi: 10.1016/j.tcm.2015.10.004. Epub 2015 Oct 31. PMID: 26654259.
- Grundy SM. Obesity, metabolic syndrome, and cardiovascular disease. J Clin Endocrinol Metab. 2004 Jun;89(6):2595-600. doi: 10.1210/jc.2004-0372. PMID: 15181029.
- Guidarelli A, Catalani A, Spina A, Varone E, Fumagalli S, Zito E, Fiorani M, Cantoni O. Functional organization of the endoplasmic reticulum dictates the susceptibility of target cells to arsenite-induced mitochondrial

superoxide formation, mitochondrial dysfunction and apoptosis. Food Chem Toxicol. 2021 Oct;156:112523. doi: 10.1016/j.fct.2021.112523. Epub 2021 Aug 25. PMID: 34453993.

- Halliwell B. Reactive species and antioxidants. Redox biology is a fundamental theme of aerobic life. Plant Physiol. 2006 Jun;141(2):312-22. doi: 10.1104/pp.106.077073. PMID: 16760481; PMCID: PMC1475431.

- Hansen JB, Kristiansen K. Regulatory circuits controlling white versus brown adipocyte differentiation. Biochem J. 2006 Sep 1;398(2):153-68. doi: 10.1042/BJ20060402. PMID: 16898874; PMCID: PMC1550312.

- Hausman GJ, Basu U, Wei S, Hausman DB, Dodson MV. Preadipocyte and adipose tissue differentiation in meat animals: influence of species and anatomical location. Annu Rev Anim Biosci. 2014 Feb;2:323-51. doi: 10.1146/annurev-animal-022513-114211. PMID: 25384146.

- Hayes JD, Flanagan JU, Jowsey IR. Glutathione transferases. Annu Rev Pharmacol Toxicol. 2005;45:51-88. doi: 10.1146/annurev.pharmtox.45.120403.095857. PMID: 15822171.

- Heiser P, Sommer O, Schmidt AJ, Clement HW, Hoinkes A, Hopt UT, Schulz E, Krieg JC, Dobschütz E. Effects of antipsychotics and vitamin C on the formation of reactive oxygen species. J Psychopharmacol. 2010 Oct;24(10):1499-504. doi: 10.1177/0269881109102538. Epub 2009 Mar 12. PMID: 19282419.

- Henderson DC, Cagliero E, Gray C, Nasrallah RA, Hayden DL, Schoenfeld DA, Goff DC. Clozapine, diabetes mellitus, weight gain, and lipid abnormalities: A five-year naturalistic study. Am J Psychiatry. 2000 Jun;157(6):975-81. doi: 10.1176/appi.ajp.157.6.975. PMID: 10831479.

- Henderson DC, Nguyen DD, Copeland PM, Hayden DL, Borba CP, Louie PM, Freudenreich O, Evins AE, Cather C, Goff DC. Clozapine, diabetes mellitus, hyperlipidemia, and cardiovascular risks and mortality: results of a 10-year naturalistic study. J Clin Psychiatry. 2005 Sep;66(9):1116-21. doi: 10.4088/jcp.v66n0905. PMID: 16187768.

- Hendouei N, Farnia S, Mohseni F, Salehi A, Bagheri M, Shadfar F, Barzegar F, Hoseini SD, Charati JY, Shaki F. Alterations in oxidative stress markers and its correlation with clinical findings in schizophrenic patients consuming perphenazine, clozapine and risperidone. Biomed Pharmacother. 2018 Jul;103:965-972. doi: 10.1016/j.biopha.2018.04.109. Epub 2018 Apr 25. PMID: 29710513.

- Henriksen EJ, Diamond-Stanic MK, Marchionne EM. Oxidative stress and the etiology of insulin resistance and type 2 diabetes. Free Radic Biol Med. 2011 Sep 1;51(5):993-9. doi: 10.1016/j.freeradbiomed.2010.12.005. Epub 2010 Dec 13. PMID: 21163347; PMCID: PMC3071882.

- Höhn A, König J, Grune T. Protein oxidation in aging and the removal of oxidized proteins. J Proteomics. 2013 Oct 30;92:132-59. doi: 10.1016/j.jprot.2013.01.004. Epub 2013 Jan 18. PMID: 23333925.

- Honer WG, Procyshyn RM, Chen EY, MacEwan GW, Barr AM. A translational research approach to poor treatment response in patients with schizophrenia: clozapine-antipsychotic polypharmacy. J Psychiatry Neurosci. 2009 Nov;34(6):433-42. PMID: 19949719; PMCID: PMC2783434.

- Hou Y, Xue P, Bai Y, Liu D, Woods CG, Yarborough K, Fu J, Zhang Q, Sun G, Collins S, Chan JY, Yamamoto M, Andersen ME, Pi J. Nuclear factor erythroid-derived factor 2-related factor 2 regulates transcription of CCAAT/enhancer-binding protein β during adipogenesis. Free Radic Biol Med. 2012 Jan 15;52(2):462-72. doi: 10.1016/j.freeradbiomed.2011.10.453. Epub 2011 Oct 28. PMID: 22138520; PMCID: PMC3307524.

- Hubert HB, Feinleib M, McNamara PM, Castelli WP. Obesity as an independent risk factor for cardiovascular disease: a 26-year follow-up of participants in the Framingham Heart Study. Circulation. 1983 May;67(5):968-77. doi: 10.1161/01.cir.67.5.968. PMID: 6219830.

- Hudemann C, Lönn ME, Godoy JR, Zahedi Avval F, Capani F, Holmgren A, Lillig CH. Identification, expression pattern, and characterization of mouse glutaredoxin 2 isoforms. Antioxid Redox Signal. 2009 Jan;11(1):1-14. doi: 10.1089/ars.2008.2068. PMID: 18707224.

- Huet O, Petit JM, Ratinaud MH, Julien R. NADH-dependent dehydrogenase activity estimation by flow cytometric analysis of 3-(4,5-dimethylthiazolyl-2-yl)-2,5-diphenyltetrazolium bromide (MTT) reduction. Cytometry. 1992;13(5):532-9. doi: 10.1002/cyto.990130513. PMID: 1633732.

- Hurd TR, Costa NJ, Dahm CC, Beer SM, Brown SE, Filipovska A, Murphy MP. Glutathionylation of mitochondrial proteins. Antioxid Redox Signal. 2005 Jul-Aug;7(7-8):999-1010. doi: 10.1089/ars.2005.7.999. PMID: 15998254.

- Innamorato NG, Rojo AI, García-Yagüe AJ, Yamamoto M, de Ceballos ML, Cuadrado A. The transcription factor Nrf2 is a therapeutic target against brain inflammation. J Immunol. 2008 Jul 1;181(1):680-9. doi: 10.4049/jimmunol.181.1.680. PMID: 18566435.

- Islam H, Edgett BA, Gurd BJ. Coordination of mitochondrial biogenesis by PGC-1α in human skeletal muscle: A re-evaluation. Metabolism. 2018 Feb;79:42-51. doi: 10.1016/j.metabol.2017.11.001. Epub 2017 Nov 8. PMID: 29126696.

- Ji B, La Y, Gao L, Zhu H, Tian N, Zhang M, Yang Y, Zhao X, Tang R, Ma G, Zhou J, Meng J, Ma J, Zhang Z, Li H, Feng G, Wang Y, He L, Wan C. A comparative proteomics analysis of rat mitochondria from the cerebral cortex and hippocampus in response to antipsychotic medications. J Proteome Res. 2009 Jul;8(7):3633-41. doi: 10.1021/pr800876z. PMID: 19441803.

- Jiang L, Wu X, Wang S, Chen SH, Zhou H, Wilson B, Jin CY, Lu RB, Xie K, Wang Q, Hong JS. Clozapine metabolites protect dopaminergic neurons through inhibition of microglial NADPH oxidase. J Neuroinflammation. 2016 May 16;13(1):110. doi: 10.1186/s12974-016-0573-z. PMID: 27184631; PMCID: PMC4869380.
- Jornayvaz FR, Shulman GI. Regulation of mitochondrial biogenesis. Essays Biochem. 2010;47:69-84. doi: 10.1042/bse0470069. PMID: 20533901; PMCID: PMC3883043.
- Kahn BB, Alquier T, Carling D, Hardie DG. AMP-activated protein kinase: ancient energy gauge provides clues to modern understanding of metabolism. Cell Metab. 2005 Jan;1(1):15-25. doi: 10.1016/j.cmet.2004.12.003. PMID: 16054041.
- Kang I, Kim Y, Tomás-Barberán FA, Espín JC, Chung S. Urolithin A, C, and D, but not iso-urolithin A and urolithin B, attenuate triglyceride accumulation in human cultures of adipocytes and hepatocytes. Mol Nutr Food Res. 2016 May;60(5):1129-38. doi: 10.1002/mnfr.201500796. Epub 2016 Apr 13. PMID: 26872561.
- Kapur S, Seeman P. Does fast dissociation from the dopamine d(2) receptor explain the action of atypical antipsychotics?: A new hypothesis. Am J Psychiatry. 2001 Mar;158(3):360-9. doi: 10.1176/appi.ajp.158.3.360. PMID: 11229973.
- Kim DD, Barr AM, Fredrikson DH, Honer WG, Procyshyn RM. Association between Serum Lipids and Antipsychotic Response in Schizophrenia. Curr Neuropharmacol. 2019;17(9):852-860. doi: 10.2174/1570159X17666190228113348. PMID: 30819084; PMCID: PMC7052836.
- Kim DD, Barr AM, Honer WG, Procyshyn RM. Reversal of Dopamine Supersensitivity as a Mechanism of Action of Clozapine. Psychother Psychosom. 2018;87(5):306-307. doi: 10.1159/000491700. Epub 2018 Jul 19. PMID: 30025405.
- Kim DD, Barr AM, Lu C, Stewart SE, White RF, Honer WG, Procyshyn RM. Clozapine-Associated Obsessive-Compulsive Symptoms and Their Management: A Systematic Review and Analysis of 107 Reported Cases. Psychother Psychosom. 2020;89(3):151-160. doi: 10.1159/000505876. Epub 2020 Feb 11. PMID: 32045914.129
- Kim DD, Barr AM, White RF, Honer WG, Procyshyn RM. Clozapine-induced obsessive–compulsive symptoms: mechanisms and treatment. J Psychiatry Neurosci. 2019 Jan 1;44(1):71-72. doi: 10.1503/jpn.180087. PMID: 30565908; PMCID: PMC6306284.
- Kim DD, Lang DJ, Warburton DER, Woodward ML, White RF, Barr AM, Honer WG, Procyshyn RM. Heart-rate response to alpha$_2$-adrenergic receptor antagonism by antipsychotics. Clin Auton Res. 2017 Dec;27(6):407-410. doi: 10.1007/s10286-017-0444-4. Epub 2017 Jul 3. PMID: 28674870.
- Kim DD, White RF, Barr AM, Honer WG, Procyshyn RM. Clozapine, elevated heart rate and QTc prolongation. J Psychiatry Neurosci. 2018 Jan;43(1):71-72. doi: 10.1503/jpn.170135. PMID: 29252168; PMCID: PMC5747540.
- Kim JR, Ryu HH, Chung HJ, Lee JH, Kim SW, Kwun WH, Baek SH, Kim JH. Association of anti-obesity activity of N-acetylcysteine with metallothionein-II down-regulation. Exp Mol Med. 2006 Apr 30;38(2):162-72. doi: 10.1038/emm.2006.20. PMID: 16672770.
- Klemettilä JP, Kampman O, Seppälä N, Viikki M, Hämäläinen M, Moilanen E, Leinonen E. Cytokine and adipokine alterations in patients with schizophrenia treated with clozapine. Psychiatry Res. 2014 Aug 30;218(3):277-83. doi: 10.1016/j.psychres.2014.04.049. Epub 2014 May 9. PMID: 24837425.
- Klemettilä JP, Kampman O, Seppälä N, Viikki M, Hämäläinen M, Moilanen E, Leinonen E. Resistin as an inflammatory marker in patients with schizophrenia treated with clozapine. Nord J Psychiatry. 2017 Feb;71(2):89-95. doi: 10.1080/08039488.2016.1230649. Epub 2016 Sep 23. PMID: 27658459.
- Kobayashi H, Matsuda M, Fukuhara A, Komuro R, Shimomura I. Dysregulated glutathione metabolism links to impaired insulin action in adipocytes. Am J Physiol Endocrinol Metab. 2009 Jun;296(6):E1326-34. doi: 10.1152/ajpendo.90921.2008. Epub 2009 Apr 14. PMID: 19366877.
- Krause KH. Tissue distribution and putative physiological function of NOX family NADPH oxidases. Jpn J Infect Dis. 2004 Oct;57(5):S28-9. PMID: 15507765.
- Kroeze WK, Hufeisen SJ, Popadak BA, Renock SM, Steinberg S, Ernsberger P, Jayathilake K, Meltzer HY, Roth BL. H1-histamine receptor affinity predicts short-term weight gain for typical and atypical antipsychotic drugs. Neuropsychopharmacology. 2003 Mar;28(3):519-26. doi: 10.1038/sj.npp.1300027. PMID: 12629531.
- Kühlbrandt W. Structure and function of mitochondrial membrane protein complexes. BMC Biol. 2015 Oct 29;13:89. doi: 10.1186/s12915-015-0201-x. PMID: 26515107; PMCID: PMC4625866.
- Kwak MK, Wakabayashi N, Itoh K, Motohashi H, Yamamoto M, Kensler TW. Modulation of gene expression by cancer chemopreventive dithiolethiones through the Keap1-Nrf2 pathway. Identification of novel gene clusters for cell survival. J Biol Chem. 2003 Mar 7;278(10):8135-45. doi: 10.1074/jbc.M211898200. Epub 2002 Dec 27. PMID: 12506115.
- Lamberti JS, Olson D, Crilly JF, Olivares T, Williams GC, Tu X, Tang W, Wiener K, Dvorin S, Dietz MB. Prevalence of the metabolic syndrome among patients receiving clozapine. Am J Psychiatry. 2006 Jul;163(7):1273-6. doi: 10.1176/ajp.2006.163.7.1273. PMID: 16816234.

- Lambeth JD, Neish AS. Nox enzymes and new thinking on reactive oxygen: a double-edged sword revisited. Annu Rev Pathol. 2014;9:119-45. doi: 10.1146/annurev-pathol-012513-104651. Epub 2013 Sep 13. PMID: 24050626.
- Lambeth JD. NOX enzymes and the biology of reactive oxygen. Nat Rev Immunol. 2004 Mar;4(3):181-9. doi: 10.1038/nri1312. PMID: 15039755.
- Landry P, Dimitri E, Tessier S, Légaré N. Efficacy of lipid-lowering medications in patients treated with clozapine: a naturalistic study. J Clin Psychopharmacol. 2008 Jun;28(3):348-9. doi: 10.1097/JCP.0b013e3181727592. PMID: 18480696.
- Lau SL, Muir C, Assur Y, Beach R, Tran B, Bartrop R, McLean M, Caetano D. Predicting Weight Gain in Patients Treated With Clozapine: The Role of Sex, Body Mass Index, and Smoking. J Clin Psychopharmacol. 2016 Apr;36(2):120-4. doi: 10.1097/JCP.0000000000000476. PMID: 26872115.
- Lee H, Lee YJ, Choi H, Ko EH, Kim JW. Reactive oxygen species facilitate adipocyte differentiation by accelerating mitotic clonal expansion. J Biol Chem. 2009 Apr 17;284(16):10601-9. doi: 10.1074/jbc.M808742200. Epub 2009 Feb 23. PMID: 19237544; PMCID: PMC2667747.
- Lee LHN, Procyshyn RM, White RF, Woodward TS, Honer WG, Barr AM. Antipsychotic prescribing patterns on admission to and at discharge from a tertiary care program for treatment-resistant psychosis. PLoS One. 2018 Aug 10;13(8):e0199758. doi: 10.1371/journal.pone.0199758. PMID: 30096136; PMCID: PMC6086406.
- Lee MJ, Fried SK. Optimal protocol for the differentiation and metabolic analysis of human adipose stromal cells. Methods Enzymol. 2014;538:49-65. doi: 10.1016/B978-0-12-800280-3.00004-9. PMID: 24529433; PMCID: PMC4336794.
- Lefterova MI, Lazar MA. New developments in adipogenesis. Trends Endocrinol Metab. 2009 Apr;20(3):107-14. doi: 10.1016/j.tem.2008.11.005. Epub 2009 Mar 9. PMID: 19269847.
- Li X, Yang Y, Zhang B, Lin X, Fu X, An Y, Zou Y, Wang JX, Wang Z, Yu T. Lactate metabolism in human health and disease. Signal Transduct Target Ther. 2022 Sep 1;7(1):305. doi: 10.1038/s41392-022-01151-3. Erratum in: Signal Transduct Target Ther. 2022 Oct 31;7(1):372. PMID: 36050306; PMCID: PMC9434547.
- Lipinski B. Hydroxyl radical and its scavengers in health and disease. Oxid Med Cell Longev. 2011;2011:809696. doi: 10.1155/2011/809696. Epub 2011 Jul 17. PMID: 21904647; PMCID: PMC3166784.
- Lönn ME, Hudemann C, Berndt C, Cherkasov V, Capani F, Holmgren A, Lillig CH. Expression pattern of human glutaredoxin 2 isoforms: identification and characterization of two testis/cancer cell-specific isoforms. Antioxid Redox Signal. 2008 Mar;10(3):547-57. doi: 10.1089/ars.2007.1821. PMID: 18092940.
- Lu J, Holmgren A. The thioredoxin antioxidant system. Free Radic Biol Med. 2014 Jan;66:75-87. doi: 10.1016/j.freeradbiomed.2013.07.036. Epub 2013 Jul 27. PMID: 23899494.
- Lu SC. Glutathione synthesis. Biochim Biophys Acta. 2013 May;1830(5):3143-53. doi: 10.1016/j.bbagen.2012.09.008. Epub 2012 Sep 17. PMID: 22995213; PMCID: PMC3549305.
- Ma ZA, Zhao Z, Turk J. Mitochondrial dysfunction and β-cell failure in type 2 diabetes mellitus. Exp Diabetes Res. 2012;2012:703538. doi: 10.1155/2012/703538. Epub 2011 Nov 9. PMID: 22110477; PMCID: PMC3216264.
- MacLeod AK, McMahon M, Plummer SM, Higgins LG, Penning TM, Igarashi K, Hayes JD. Characterization of the cancer chemopreventive NRF2-dependent gene battery in human keratinocytes: demonstration that the KEAP1-NRF2 pathway, and not the BACH1-NRF2 pathway, controls cytoprotection against electrophiles as well as redox-cycling compounds. Carcinogenesis. 2009 Sep;30(9):1571-80. doi: 10.1093/carcin/bgp176. Epub 2009 Jul 16. PMID: 19608619; PMCID: PMC3656619.
- Mahadev K, Motoshima H, Wu X, Ruddy JM, Arnold RS, Cheng G, Lambeth JD, Goldstein BJ. The NAD(P)H oxidase homolog Nox4 modulates insulin-stimulated generation of H2O2 and plays an integral role in insulin signal transduction. Mol Cell Biol. 2004 Mar;24(5):1844-54. doi: 10.1128/MCB.24.5.1844-1854.2004. PMID: 14966267; PMCID: PMC350558.
- Martyn KD, Frederick LM, von Loehneysen K, Dinauer MC, Knaus UG. Functional analysis of Nox4 reveals unique characteristics compared to other NADPH oxidases. Cell Signal. 2006 Jan;18(1):69-82. doi: 10.1016/j.cellsig.2005.03.023. Epub 2005 May 31. PMID: 15927447.
- Masand PS, Culpepper L, Henderson D, Lee S, Littrell K, Newcomer JW, Rasgon N. Metabolic and endocrine disturbances in psychiatric disorders: a multidisciplinary approach to appropriate atypical antipsychotic utilization. CNS Spectr. 2005 Oct;10(10):suppl14 1-15. PMID: 16404802.
- Masschelin PM, Cox AR, Chernis N, Hartig SM. The Impact of Oxidative Stress on Adipose Tissue Energy Balance. Front Physiol. 2020 Jan 22;10:1638. doi: 10.3389/fphys.2019.01638. PMID: 32038305; PMCID: PMC6987041.
- Maurer I, Zierz S, Möller H. Evidence for a mitochondrial oxidative phosphorylation defect in brains from patients with schizophrenia. Schizophr Res. 2001 Mar 1;48(1):125-36. doi: 10.1016/s0920-9964(00)00075-x. PMID: 11278159.

- McClung JP, Roneker CA, Mu W, Lisk DJ, Langlais P, Liu F, Lei XG. Development of insulin resistance and obesity in mice overexpressing cellular glutathione peroxidase. Proc Natl Acad Sci U S A. 2004 Jun 15;101(24):8852-7. doi: 10.1073/pnas.0308096101. Epub 2004 Jun 7. PMID: 15184668; PMCID: PMC428436.
- Mijovic A, MacCabe JH. Clozapine-induced agranulocytosis. Ann Hematol. 2020 Nov;99(11):2477-2482. doi: 10.1007/s00277-020-04215-y. Epub 2020 Aug 20. PMID: 32815018; PMCID: PMC7536144.
- Monné M, Miniero DV, Iacobazzi V, Bisaccia F, Fiermonte G. The mitochondrial oxoglutarate carrier: from identification to mechanism. J Bioenerg Biomembr. 2013 Feb;45(1-2):1-13. doi: 10.1007/s10863-012-9475-7. Erratum in: J Bioenerg Biomembr. 2013 Feb;45(1-2):175. Iacobazzi, Vito [added]. PMID: 23054077.
- Mouche S, Mkaddem SB, Wang W, Katic M, Tseng YH, Carnesecchi S, Steger K, Foti M, Meier CA, Muzzin P, Kahn CR, Ogier-Denis E, Szanto I. Reduced expression of the NADPH oxidase NOX4 is a hallmark of adipocyte differentiation. Biochim Biophys Acta. 2007 Jul;1773(7):1015-27. doi: 10.1016/j.bbamcr.2007.03.003. Epub 2007 Mar 19. PMID: 17553579.
- Mueller E, Drori S, Aiyer A, Yie J, Sarraf P, Chen H, Hauser S, Rosen ED, Ge K, Roeder RG, Spiegelman BM. Genetic analysis of adipogenesis through peroxisome proliferator-activated receptor gamma isoforms. J Biol Chem. 2002 Nov 1;277(44):41925-30. doi: 10.1074/jbc.M206950200. Epub 2002 Aug 27. PMID: 12200443.
- Mulder H, Ling C. Mitochondrial dysfunction in pancreatic beta-cells in Type 2 diabetes. Mol Cell Endocrinol. 2009 Jan 15;297(1-2):34-40. doi: 10.1016/j.mce.2008.05.015. Epub 2008 Jul 7. PMID: 18606489.
- Murphy MP. How mitochondria produce reactive oxygen species. Biochem J. 2009 Jan 1;417(1):1-13. doi: 10.1042/BJ20081386. PMID: 19061483; PMCID: PMC2605959.
- Nakanishi A, Imajoh-Ohmi S, Fujinawa T, Kikuchi H, Kanegasaki S. Direct evidence for interaction between COOH-terminal regions of cytochrome b558 subunits and cytosolic 47-kDa protein during activation of an O(2-)-generating system in neutrophils. J Biol Chem. 1992 Sep 25;267(27):19072-4. PMID: 1326544.
- Nasrallah H. A review of the effect of atypical antipsychotics on weight. Psychoneuroendocrinology. 2003 Jan;28 Suppl 1:83-96. doi: 10.1016/s0306-4530(02)00114-2. PMID: 12504074.
- Nathan C, Cunningham-Bussel A. Beyond oxidative stress: an immunologist's guide to reactive oxygen species. Nat Rev Immunol. 2013 May;13(5):349-61. doi: 10.1038/nri3423. PMID: 23618831; PMCID: PMC4250048.
- Nazari B, Jaquet V, Krause KH. NOX family NADPH oxidases in mammals: Evolutionary conservation and isoform-defining sequences. Redox Biol. 2023 Oct;66:102851. doi: 10.1016/j.redox.2023.102851. Epub 2023 Aug 12. PMID: 37595375; PMCID: PMC10458973.
- Newcomer JW. Antipsychotic medications: metabolic and cardiovascular risk. J Clin Psychiatry. 2007;68 Suppl 4:8-13. PMID: 17539694.
- Nguyen T, Sherratt PJ, Pickett CB. Regulatory mechanisms controlling gene expression mediated by the antioxidant response element. Annu Rev Pharmacol Toxicol. 2003;43:233-60. doi: 10.1146/annurev.pharmtox.43.100901.140229. Epub 2002 Jan 10. PMID: 12359864.
- Ntambi JM, Young-Cheul K. Adipocyte differentiation and gene expression. J Nutr. 2000 Dec;130(12):3122S-3126S. doi: 10.1093/jn/130.12.3122S. PMID: 11110885.
- Okabe Y, Shimada T, Horikawa T, Kinoshita K, Koyama K, Ichinose K, Aburada M, Takahashi K. Suppression of adipocyte hypertrophy by polymethoxyflavonoids isolated from Kaempferia parviflora. Phytomedicine. 2014 May 15;21(6):800-6. doi: 10.1016/j.phymed.2014.01.014. Epub 2014 Mar 11. PMID: 24629599.
- Olivieri C, Ruzza M, Tolaj F, DaDalt L, Magni P. Molecular and Functional Characterization of SW872 Adipocytes as a Model System for Testing Nutraceutical Products. Biology ad Life Sciences Forum. 2022, 12(1)19; https://doi.org/10.3390/IECN2022-12370
- Ouchi N, Parker JL, Lugus JJ, Walsh K. Adipokines in inflammation and metabolic disease. Nat Rev Immunol. 2011 Feb;11(2):85-97. doi: 10.1038/nri2921. Epub 2011 Jan 21. PMID: 21252989; PMCID: PMC3518031.
- Paredes RM, Quinones M, Marballi K, Gao X, Valdez C, Ahuja SS, Velligan D, Walss-Bass C. Metabolomic profiling of schizophrenia patients at risk for metabolic syndrome. Int J Neuropsychopharmacol. 2014 Aug;17(8):1139-48. doi: 10.1017/S1461145714000157. Epub 2014 Feb 25. PMID: 24565079.
- Parvez S, Long MJC, Poganik JR, Aye Y. Redox Signaling by Reactive Electrophiles and Oxidants. Chem Rev. 2018 Sep 26;118(18):8798-8888. doi: 10.1021/acs.chemrev.7b00698. Epub 2018 Aug 27. Erratum in: Chem Rev. 2019 Mar 27;119(6):4464-4469. PMID: 30148624; PMCID: PMC6158072.
- Patel R, Apostolatos A, Carter G, Ajmo J, Gali M, Cooper DR, You M, Bisht KS, Patel NA. Protein kinase C δ (PKCδ) splice variants modulate apoptosis pathway in 3T3L1 cells during adipogenesis: identification of PKCδII inhibitor. J Biol Chem. 2013 Sep 13;288(37):26834-46. doi: 10.1074/jbc.M113.482638. Epub 2013 Jul 31. PMID: 23902767; PMCID: PMC3772230.
- Pearson KJ, Lewis KN, Price NL, Chang JW, Perez E, Cascajo MV, Tamashiro KL, Poosala S, Csiszar A, Ungvari Z, Kensler TW, Yamamoto M, Egan JM, Longo DL, Ingram DK, Navas P, de Cabo R. Nrf2 mediates cancer protection but not prolongevity induced by caloric restriction. Proc Natl Acad Sci U S A. 2008 Feb 19;105(7):2325-30. doi: 10.1073/pnas.0712162105. Epub 2008 Feb 19. PMID: 18287083; PMCID: PMC2268135.

- Peng X, Giménez-Cassina A, Petrus P, Conrad M, Rydén M, Arnér ES. Thioredoxin reductase 1 suppresses adipocyte differentiation and insulin responsiveness. Sci Rep. 2016 Jun 27;6:28080. doi: 10.1038/srep28080. PMID: 27346647; PMCID: PMC4921861.
- Petersen RK, Madsen L, Pedersen LM, Hallenborg P, Hagland H, Viste K, Døskeland SO, Kristiansen K. Cyclic AMP (cAMP)-mediated stimulation of adipocyte differentiation requires the synergistic action of Epac- and cAMP-dependent protein kinase-dependent processes. Mol Cell Biol. 2008 Jun;28(11):3804-16. doi: 10.1128/MCB.00709-07. Epub 2008 Apr 7. PMID: 18391018; PMCID: PMC2423297.
- Pfaffl MW. A new mathematical model for relative quantification in real-time RT-PCR. Nucleic Acids Res. 2001 May 1;29(9):e45. doi: 10.1093/nar/29.9.e45. PMID: 11328886; PMCID: PMC55695.
- Pi J, Leung L, Xue P, Wang W, Hou Y, Liu D, Yehuda-Shnaidman E, Lee C, Lau J, Kurtz TW, Chan JY. Deficiency in the nuclear factor E2-related factor-2 transcription factor results in impaired adipogenesis and protects against diet-induced obesity. J Biol Chem. 2010 Mar 19;285(12):9292-300. doi: 10.1074/jbc.M109.093955. Epub 2010 Jan 20. PMID: 20089859; PMCID: PMC2838347.
- Pisani DF, Djedaini M, Beranger GE, Elabd C, Scheideler M, Ailhaud G, Amri EZ. Differentiation of Human Adipose-Derived Stem Cells into "Brite" (Brown-in-White) Adipocytes. Front Endocrinol (Lausanne). 2011 Nov 29;2:87. doi: 10.3389/fendo.2011.00087. PMID: 22654831; PMCID: PMC3356055.
- Polydoro M, Schröder N, Lima MN, Caldana F, Laranja DC, Bromberg E, Roesler R, Quevedo J, Moreira JC, Dal-Pizzol F. Haloperidol- and clozapine-induced oxidative stress in the rat brain. Pharmacol Biochem Behav. 2004 Aug;78(4):751-6. doi: 10.1016/j.pbb.2004.05.018. PMID: 15301931.
- Poulos SP, Dodson MV, Hausman GJ. Cell line models for differentiation: preadipocytes and adipocytes. Exp Biol Med (Maywood). 2010 Oct;235(10):1185-93. doi: 10.1258/ebm.2010.010063. Epub 2010 Sep 23. PMID: 20864461.
- Prasun P. Mitochondrial dysfunction in metabolic syndrome. Biochim Biophys Acta Mol Basis Dis. 2020 Oct 1;1866(10):165838. doi: 10.1016/j.bbadis.2020.165838. Epub 2020 May 16. PMID: 32428560.
- Procyshyn RM, Wasan KM, Thornton AE, Barr AM, Chen EY, Pomarol-Clotet E, Stip E, Williams R, Macewan GW, Birmingham CL, Honer WG; Clozapine and Risperidone Enhancement Study Group. Changes in serum lipids, independent of weight, are associated with changes in symptoms during long-term clozapine treatment. J Psychiatry Neurosci. 2007 Sep;32(5):331-8. PMID: 17823649; PMCID: PMC1963353.
- Quincozes-Santos A, Bobermin LD, Tonial RP, Bambini-Junior V, Riesgo R, Gottfried C. Effects of atypical (risperidone) and typical (haloperidol) antipsychotic agents on astroglial functions. Eur Arch Psychiatry Clin Neurosci. 2010 Sep;260(6):475-81. doi: 10.1007/s00406-009-0095-0. Epub 2009 Dec 30. PMID: 20041330.
- Rajalin AM, Micoogullari M, Sies H, Steinbrenner H. Upregulation of the thioredoxin-dependent redox system during differentiation of 3T3-L1 cells to adipocytes. Biol Chem. 2014 Jun;395(6):667-77. doi: 10.1515/hsz-2014-0102. PMID: 24516001.
- Ray PD, Huang BW, Tsuji Y. Reactive oxygen species (ROS) homeostasis and redox regulation in cellular signaling. Cell Signal. 2012 May;24(5):981-90. doi: 10.1016/j.cellsig.2012.01.008. Epub 2012 Jan 20. PMID: 22286106; PMCID: PMC3454471.
- Reddy NM, Suryanarayana V, Kalvakolanu DV, Yamamoto M, Kensler TW, Hassoun PM, Kleeberger SR, Reddy SP. Innate immunity against bacterial infection following hyperoxia exposure is impaired in NRF2-deficient mice. J Immunol. 2009 Oct 1;183(7):4601-8. doi: 10.4049/jimmunol.0901754. Epub 2009 Sep 4. PMID: 19734219; PMCID: PMC2820249.
- Reinke A, Martins MR, Lima MS, Moreira JC, Dal-Pizzol F, Quevedo J. Haloperidol and clozapine, but not olanzapine, induces oxidative stress in rat brain. Neurosci Lett. 2004 Nov 30;372(1-2):157-60. doi: 10.1016/j.neulet.2004.09.032. PMID: 15531108.
- Remington G, Addington D, Honer W, Ismail Z, Raedler T, Teehan M. Guidelines for the Pharmacotherapy of Schizophrenia in Adults. Can J Psychiatry. 2017 Sep;62(9):604-616. doi: 10.1177/0706743717720448. Epub 2017 Jul 13. PMID: 28703015; PMCID: PMC5593252.
- Remington G, Lee J, Agid O, Takeuchi H, Foussias G, Hahn M, Fervaha G, Burton L, Powell V. Clozapine's critical role in treatment resistant schizophrenia: ensuring both safety and use. Expert Opin Drug Saf. 2016 Sep;15(9):1193-203. doi: 10.1080/14740338.2016.1191468. Epub 2016 Jun 1. PMID: 27207070.
- Ribaudo G, Bortoli M, Pavan C, Zagotto G, Orian L. Antioxidant Potential of Psychotropic Drugs: From Clinical Evidence to In Vitro and In Vivo Assessment and toward a New Challenge for in Silico Molecular Design. Antioxidants (Basel). 2020 Aug 6;9(8):714. doi: 10.3390/antiox9080714. PMID: 32781750; PMCID: PMC7465375.
- Roberts RC. Postmortem studies on mitochondria in schizophrenia. Schizophr Res. 2017 Sep;187:17-25. doi: 10.1016/j.schres.2017.01.056. Epub 2017 Feb 9. PMID: 28189530; PMCID: PMC5550365.
- Rosen ED, Hsu CH, Wang X, Sakai S, Freeman MW, Gonzalez FJ, Spiegelman BM. C/EBPalpha induces adipogenesis through PPARgamma: a unified pathway. Genes Dev. 2002 Jan 1;16(1):22-6. doi: 10.1101/gad.948702. PMID: 11782441; PMCID: PMC155311.

- Rosen ED, MacDougald OA. Adipocyte differentiation from the inside out. Nat Rev Mol Cell Biol. 2006 Dec;7(12):885-96. doi: 10.1038/nrm2066. PMID: 17139329.
- Rosen ED, Walkey CJ, Puigserver P, Spiegelman BM. Transcriptional regulation of adipogenesis. Genes Dev. 2000 Jun 1;14(11):1293-307. PMID: 10837022.
- Ruiz S, Pergola PE, Zager RA, Vaziri ND. Targeting the transcription factor Nrf2 to ameliorate oxidative stress and inflammation in chronic kidney disease. Kidney Int. 2013 Jun;83(6):1029-41. doi: 10.1038/ki.2012.439. Epub 2013 Jan 16. PMID: 23325084; PMCID: PMC3633725.
- Ruiz-Ojeda FJ, Aguilera CM, Rupérez AI, Gil Á, Gomez-Llorente C. An analogue of atrial natriuretic peptide (C-ANP4-23) modulates glucose metabolism in human differentiated adipocytes. Mol Cell Endocrinol. 2016 Aug 15;431:101-8. doi: 10.1016/j.mce.2016.05.011. Epub 2016 May 13. PMID: 27181211.
- Ruiz-Ojeda FJ, Gomez-Llorente C, Aguilera CM, Gil A, Rupérez AI. Impact of 3-Amino-1,2,4-Triazole (3-AT)-Derived Increase in Hydrogen Peroxide Levels on Inflammation and Metabolism in Human Differentiated Adipocytes. PLoS One. 2016 Mar 29;11(3):e0152550. doi: 10.1371/journal.pone.0152550. PMID: 27023799; PMCID: PMC4811533.
- Ruiz-Ojeda FJ, Rupérez AI, Gomez-Llorente C, Gil A, Aguilera CM. Cell Models and Their Application for Studying Adipogenic Differentiation in Relation to Obesity: A Review. Int J Mol Sci. 2016 Jun 30;17(7):1040. doi: 10.3390/ijms17071040. PMID: 27376273; PMCID: PMC4964416.
- Ruwanpura SM, McLeod L, Lilja AR, Brooks G, Dousha LF, Seow HJ, Bozinovski S, Vlahos R, Hertzog PJ, Anderson GP, Jenkins BJ. Non-essential role for TLR2 and its signaling adaptor Mal/TIRAP in preserving normal lung architecture in mice. PLoS One. 2013 Oct 29;8(10):e78095. doi: 10.1371/journal.pone.0078095. PMID: 24205107; PMCID: PMC3812132.
- Rybak LP, Mukherjea D, Jajoo S, Kaur T, Ramkumar V. siRNA-mediated knock-down of NOX3: therapy for hearing loss? Cell Mol Life Sci. 2012 Jul;69(14):2429-34. doi: 10.1007/s00018-012-1016-3. Epub 2012 May 5. PMID: 22562580; PMCID: PMC5441545.
- Sadowska-Bartosz I, Galiniak S, Bartosz G, Zuberek M, Grzelak A, Dietrich-Muszalska A. Antioxidant properties of atypical antipsychotic drugs used in the treatment of schizophrenia. Schizophr Res. 2016 Oct;176(2-3):245-251. doi: 10.1016/j.schres.2016.07.010. Epub 2016 Jul 20. PMID: 27449251.
- Saeed H, Taipaleenmäki H, Aldahmash AM, Abdallah BM, Kassem M. Mouse embryonic fibroblasts (MEF) exhibit a similar but not identical phenotype to bone marrow stromal stem cells (BMSC). Stem Cell Rev Rep. 2012 Jun;8(2):318-28. doi: 10.1007/s12015-011-9315-x. PMID: 21927803.
- Saitoh Y, Xiao L, Mizuno H, Kato S, Aoshima H, Taira H, Kokubo K, Miwa N. Novel polyhydroxylated fullerene suppresses intracellular oxidative stress together with repression of intracellular lipid accumulation during the differentiation of OP9 preadipocytes into adipocytes. Free Radic Res. 2010 Sep;44(9):1072-81. doi: 10.3109/10715762.2010.499905. PMID: 20815770
- Sánchez-Ramírez E, Ung TPL, Alarcón Del Carmen A, del Toro-Ríos X, Fajardo-Orduña GR, Noriega LG, Cortés-Morales VA, Tovar AR, Montesinos JJ, Orozco-Solís R, Stringari C, Aguilar-Arnal L. Coordinated metabolic transitions and gene expression by NAD+ during adipogenesis. J Cell Biol. 2022 Dec 5;221(12):e202111137. doi: 10.1083/jcb.202111137. Epub 2022 Oct 5. PMID: 36197339; PMCID: PMC9538974.
- Sautin YY, Nakagawa T, Zharikov S, Johnson RJ. Adverse effects of the classic antioxidant uric acid in adipocytes: NADPH oxidase-mediated oxidative/nitrosative stress. Am J Physiol Cell Physiol. 2007 Aug;293(2):C584-96. doi: 10.1152/ajpcell.00600.2006. Epub 2007 Apr 11. Erratum in: Am J Physiol Cell Physiol. 2010 Sep;299(3):C726. PMID: 17428837.
- Scaini G, Quevedo J, Velligan D, Roberts DL, Raventos H, Walss-Bass C. Second generation antipsychotic-induced mitochondrial alterations: Implications for increased risk of metabolic syndrome in patients with schizophrenia. Eur Neuropsychopharmacol. 2018 Mar;28(3):369-380. doi: 10.1016/j.euroneuro.2018.01.004. Epub 2018 Feb 12. PMID: 29449054.
- Scalcon V, Folda A, Lupo MG, Tonolo F, Pei N, Battisti I, Ferri N, Arrigoni G, Bindoli A, Holmgren A, Coppo L, Rigobello MP. Mitochondrial depletion of glutaredoxin 2 induces metabolic dysfunction-associated fatty liver disease in mice. Redox Biol. 2022 May;51:102277. doi: 10.1016/j.redox.2022.102277. Epub 2022 Mar 2. PMID: 35290904; PMCID: PMC89213
- Scarpulla RC, Vega RB, Kelly DP. Transcriptional integration of mitochondrial biogenesis. Trends Endocrinol Metab. 2012 Sep;23(9):459-66. doi: 10.1016/j.tem.2012.06.006. Epub 2012 Jul 18. PMID: 22817841; PMCID: PMC3580164.
- Schatz G. Mitochondrial oxidative phosphorylation. Angew Chem Int Ed Engl. 1967 Dec;6(12):1035-46. doi: 10.1002/anie.196710351. PMID: 4965486.
- Scherer PE. Adipose tissue: from lipid storage compartment to endocrine organ. Diabetes. 2006 Jun;55(6):1537-45. doi: 10.2337/db06-0263. PMID: 16731815.

- Schmiedeknecht K, Kaufmann A, Bauer S, Venegas Solis F. L-lactate as an indicator for cellular metabolic status: An easy and cost-effective colorimetric L-lactate assay. PLoS One. 2022 Jul 22;17(7):e0271818. doi: 10.1371/journal.pone.0271818. PMID: 35867690; PMCID: PMC9307176.
- Schröder K, Wandzioch K, Helmcke I, Brandes RP. Nox4 acts as a switch between differentiation and proliferation in preadipocytes. Arterioscler Thromb Vasc Biol. 2009 Feb;29(2):239-45. doi: 10.1161/ATVBAHA.108.174219. Epub 2008 Dec 4. PMID: 19057021.
- Seeman P. Atypical antipsychotics: mechanism of action. Can J Psychiatry. 2002 Feb;47(1):27-38. PMID: 11873706.
- Shaw JM, Nunnari J. Mitochondrial dynamics and division in budding yeast. Trends Cell Biol. 2002 Apr;12(4):178-84. doi: 10.1016/s0962-8924(01)02246-2. PMID: 11978537; PMCID: PMC3785940.
- Shin H, Kim J, Song JH. Clozapine and olanzapine inhibit proton currents in BV2 microglial cells. Eur J Pharmacol. 2015 May 15;755:74-9. doi: 10.1016/j.ejphar.2015.03.003. Epub 2015 Mar 11. PMID: 25771455.
- Shin S, Wakabayashi N, Misra V, Biswal S, Lee GH, Agoston ES, Yamamoto M, Kensler TW. NRF2 modulates aryl hydrocarbon receptor signaling: influence on adipogenesis. Mol Cell Biol. 2007 Oct;27(20):7188-97. doi: 10.1128/MCB.00915-07. Epub 2007 Aug 20. PMID: 17709388; PMCID: PMC2168916.
- Singh OP, Chakraborty I, Dasgupta A, Datta S. A comparative study of oxidative stress and interrelationship of important antioxidants in haloperidol and olanzapine treated patients suffering from schizophrenia. Indian J Psychiatry. 2008 Jul;50(3):171-6. doi: 10.4103/0019-5545.43627. PMID: 19742187; PMCID: PMC2738368.
- Siskind DJ, Leung J, Russell AW, Wysoczanski D, Kisely S. Metformin for Clozapine Associated Obesity: A Systematic Review and Meta-Analysis. PLoS One. 2016 Jun 15;11(6):e0156208. doi: 10.1371/journal.pone.0156208. PMID: 27304831; PMCID: PMC4909277.
- Siskind DJ, Russell AW, Gamble C, Winckel K, Mayfield K, Hollingworth S, Hickman I, Siskind V, Kisely S. Treatment of clozapine-associated obesity and diabetes with exenatide in adults with schizophrenia: A randomized controlled trial (CODEX). Diabetes Obes Metab. 2018 Apr;20(4):1050-1055. doi: 10.1111/dom.13167. Epub 2017 Dec 19. PMID: 29194917.
- Soberman RJ. The expanding network of redox signaling: new observations, complexities, and perspectives. J Clin Invest. 2003 Mar;111(5):571-4. doi: 10.1172/JCI18099. Erratum in: J Clin Invest. 2003 Apr;111(7):1093. PMID: 12618508; PMCID: PMC151913.
- Song Z, Ghochani M, McCaffery JM, Frey TG, Chan DC. Mitofusins and OPA1 mediate sequential steps in mitochondrial membrane fusion. Mol Biol Cell. 2009 Aug;20(15):3525-32. doi: 10.1091/mbc.e09-03-0252. Epub 2009 May 28. PMID: 19477917; PMCID: PMC2719570.
- Spinelli JB, Haigis MC. The multifaceted contributions of mitochondria to cellular metabolism. Nat Cell Biol. 2018 Jul;20(7):745-754. doi: 10.1038/s41556-018-0124-1. Epub 2018 Jun 27. PMID: 29950572; PMCID: PMC6541229.
- Sporn MB, Liby KT. NRF2 and cancer: the good, the bad and the importance of context. Nat Rev Cancer. 2012 Jul 19;12(8):564-71. doi: 10.1038/nrc3278. PMID: 22810811; PMCID: PMC3836441.
- Stadtman ER, Levine RL. Protein oxidation. Ann N Y Acad Sci. 2000;899:191-208. doi: 10.1111/j.1749-6632.2000.tb06187.x. PMID: 10863540.
- Starkov AA. The role of mitochondria in reactive oxygen species metabolism and signaling. Ann N Y Acad Sci. 2008 Dec;1147:37-52. doi: 10.1196/annals.1427.015. PMID: 19076429; PMCID: PMC2869479.
- Stępnicki P, Kondej M, Kaczor AA. Current Concepts and Treatments of Schizophrenia. Molecules. 2018 Aug 20;23(8):2087. doi: 10.3390/molecules23082087. PMID: 30127324; PMCID: PMC6222385.
- Stocchi V, Cucchiarini L, Canestrari F, Piacentini MP, Fornaini G. A very fast ion-pair reversed-phase HPLC method for the separation of the most significant nucleotides and their degradation products in human red blood cells. Anal Biochem. 1987 Nov 15;167(1):181-90. doi: 10.1016/0003-2697(87)90150-3. PMID: 2829656.
- Streck EL, Rezin GT, Barbosa LM, Assis LC, Grandi E, Quevedo J. Effect of antipsychotics on succinate dehydrogenase and cytochrome oxidase activities in rat brain. Naunyn Schmiedebergs Arch Pharmacol. 2007 Oct;376(1-2):127-33. doi: 10.1007/s00210-007-0178-2. Epub 2007 Aug 3. PMID: 17673979.
- Styner M, Sen B, Xie Z, Case N, Rubin J. Indomethacin promotes adipogenesis of mesenchymal stem cells through a cyclooxygenase independent mechanism. J Cell Biochem. 2010 Nov 1;111(4):1042-50. doi: 10.1002/jcb.22793. PMID: 20672310; PMCID: PMC3627539.
- Suh YA, Arnold RS, Lassegue B, Shi J, Xu X, Sorescu D, Chung AB, Griendling KK, Lambeth JD. Cell transformation by the superoxide-generating oxidase Mox1. Nature. 1999 Sep 2;401(6748):79-82. doi: 10.1038/43459. PMID: 10485709.
- Sun F, Zhou Q, Pang X, Xu Y, Rao Z. Revealing various coupling of electron transfer and proton pumping in mitochondrial respiratory chain. Curr Opin Struct Biol. 2013 Aug;23(4):526-38. doi: 10.1016/j.sbi.2013.06.013. Epub 2013 Jul 16. PMID: 23867107.
- Swartz MS, Stroup TS, McEvoy JP, Davis SM, Rosenheck RA, Keefe RS, Hsiao JK, Lieberman JA. What CATIE found: results from the schizophrenia trial. Psychiatr Serv. 2008 May;59(5):500-6. doi: 10.1176/ps.2008.59.5.500. PMID: 18451005; PMCID: PMC5033643.

- Tanaka Y, Aleksunes LM, Yeager RL, Gyamfi MA, Esterly N, Guo GL, Klaassen CD. NF-E2-related factor 2 inhibits lipid accumulation and oxidative stress in mice fed a high-fat diet. J Pharmacol Exp Ther. 2008 May;325(2):655-64. doi: 10.1124/jpet.107.135822. Epub 2008 Feb 15. PMID: 18281592.
- Tang QQ, Lane MD. Adipogenesis: from stem cell to adipocyte. Annu Rev Biochem. 2012;81:715-36. doi: 10.1146/annurev-biochem-052110-115718. Epub 2012 Mar 29. PMID: 22463691.
- Tentolouris N, Argyrakopoulou G, Katsilambros N. Perturbed autonomic nervous system function in metabolic syndrome. Neuromolecular Med. 2008;10(3):169-78. doi: 10.1007/s12017-008-8022-5. Epub 2008 Jan 26. PMID: 18224460.
- Thimmulappa RK, Lee H, Rangasamy T, Reddy SP, Yamamoto M, Kensler TW, Biswal S. Nrf2 is a critical regulator of the innate immune response and survival during experimental sepsis. J Clin Invest. 2006 Apr;116(4):984-95. doi: 10.1172/JCI25790. PMID: 16585964; PMCID: PMC1421348.
- Tomlinson JJ, Boudreau A, Wu D, Atlas E, Haché RJ. Modulation of early human preadipocyte differentiation by glucocorticoids. Endocrinology. 2006 Nov;147(11):5284-93. doi: 10.1210/en.2006-0267. Epub 2006 Jul 27. PMID: 16873539.
- Tontonoz P, Hu E, Spiegelman BM. Stimulation of adipogenesis in fibroblasts by PPAR gamma 2, a lipid-activated transcription factor. Cell. 1994 Dec 30;79(7):1147-56. doi: 10.1016/0092-8674(94)90006-x. Erratum in: Cell 1995 Mar 24;80(6):following 957. PMID: 8001151.
- Tse L, Procyshyn RM, Fredrikson DH, Boyda HN, Honer WG, Barr AM. Pharmacological treatment of antipsychotic-induced dyslipidemia and hypertension. Int Clin Psychopharmacol. 2014 May;29(3):125-37. doi: 10.1097/YIC.0000000000000014. PMID: 24169026.
- Turrens JF, Alexandre A, Lehninger AL. Ubisemiquinone is the electron donor for superoxide formation by complex III of heart mitochondria. Arch Biochem Biophys. 1985 Mar;237(2):408-14. doi: 10.1016/0003-9861(85)90293-0. PMID: 2983613.
- Uchida K. 4-Hydroxy-2-nonenal: a product and mediator of oxidative stress. Prog Lipid Res. 2003 Jul;42(4):318-43. doi: 10.1016/s0163-7827(03)00014-6. PMID: 12689622.
- Valle I, Alvarez-Barrientos A, Arza E, Lamas S, Monsalve M. PGC-1alpha regulates the mitochondrial antioxidant defense system in vascular endothelial cells. Cardiovasc Res. 2005 Jun 1;66(3):562-73. doi: 10.1016/j.cardiores.2005.01.026. Epub 2005 Feb 25. PMID: 15914121.
- Vega RB, Huss JM, Kelly DP. The coactivator PGC-1 cooperates with peroxisome proliferator-activated receptor alpha in transcriptional control of nuclear genes encoding mitochondrial fatty acid oxidation enzymes. Mol Cell Biol. 2000 Mar;20(5):1868-76. doi: 10.1128/MCB.20.5.1868-1876.2000. PMID: 10669761; PMCID: PMC85369.
- Vermot A, Petit-Härtlein I, Smith SME, Fieschi F. NADPH Oxidases (NOX): An Overview from Discovery, Molecular Mechanisms to Physiology and Pathology. Antioxidants (Basel). 2021 Jun 1;10(6):890. doi: 10.3390/antiox10060890. PMID: 34205998; PMCID: PMC8228183.
- Wada J, Nakatsuka A. Mitochondrial Dynamics and Mitochondrial Dysfunction in Diabetes. Acta Med Okayama. 2016 Jun;70(3):151-8. doi: 10.18926/AMO/54413. PMID: 27339203.
- Wai T, Langer T. Mitochondrial Dynamics and Metabolic Regulation. Trends Endocrinol Metab. 2016 Feb;27(2):105-117. doi: 10.1016/j.tem.2015.12.001. Epub 2016 Jan 2. PMID: 26754340.
- Wallace DC. Mitochondrial genetic medicine. Nat Genet. 2018 Dec;50(12):1642-1649. doi: 10.1038/s41588-018-0264-z. Epub 2018 Oct 29. PMID: 30374071.
- Walss-Bass C, Weintraub ST, Hatch J, Mintz J, Chaudhuri AR. Clozapine causes oxidation of proteins involved in energy metabolism: a possible mechanism for antipsychotic-induced metabolic alterations. Int J Neuropsychopharmacol. 2008 Dec;11(8):1097-104. doi: 10.1017/S1461145708008882. Epub 2008 May 9. PMID: 18466668.
- Wang B, Williamson G. Detection of a nuclear protein which binds specifically to the antioxidant responsive element (ARE) of the human NAD(P) H:quinone oxidoreductase gene. Biochim Biophys Acta. 1994 Nov 22;1219(3):645-52. doi: 10.1016/0167-4781(94)90223-2. PMID: 7948021.
- Wang X, Hai C. Redox modulation of adipocyte differentiation: hypothesis of "Redox Chain" and novel insights into intervention of adipogenesis and obesity. Free Radic Biol Med. 2015 Dec;89:99-125. doi: 10.1016/j.freeradbiomed.2015.07.012. Epub 2015 Jul 14. PMID: 26187871.
- Wang X, Tao L, Hai CX. Redox-regulating role of insulin: the essence of insulin effect. Mol Cell Endocrinol. 2012 Feb 26;349(2):111-27. doi: 10.1016/j.mce.2011.08.019. Epub 2011 Aug 24. PMID: 21878367.
- Wassef H, Bernier L, Davignon J, Cohn JS. Synthesis and secretion of apoC-I and apoE during maturation of human SW872 liposarcoma cells. J Nutr. 2004 Nov;134(11):2935-41. doi: 10.1093/jn/134.11.2935. PMID: 15514255.
- Watt IN, Montgomery MG, Runswick MJ, Leslie AG, Walker JE. Bioenergetic cost of making an adenosine triphosphate molecule in animal mitochondria. Proc Natl Acad Sci U S A. 2010 Sep 28;107(39):16823-7. doi: 10.1073/pnas.1011099107. Epub 2010 Sep 16. PMID: 20847295; PMCID: PMC2947889.

- Westermann B. Mitochondrial fusion and fission in cell life and death. Nat Rev Mol Cell Biol. 2010 Dec;11(12):872-84. doi: 10.1038/nrm3013. PMID: 21102612.
- Whitney Z, Procyshyn RM, Fredrikson DH, Barr AM. Treatment of clozapine-associated weight gain: a systematic review. Eur J Clin Pharmacol. 2015 Apr;71(4):389-401. doi: 10.1007/s00228-015-1807-1. Epub 2015 Jan 28. PMID: 25627831.
- Wilson-Fritch L, Burkart A, Bell G, Mendelson K, Leszyk J, Nicoloro S, Czech M, Corvera S. Mitochondrial biogenesis and remodeling during adipogenesis and in response to the insulin sensitizer rosiglitazone. Mol Cell Biol. 2003 Feb;23(3):1085-94. doi: 10.1128/MCB.23.3.1085-1094.2003. PMID: 12529412; PMCID: PMC140688.
- Wolins NE, Quaynor BK, Skinner JR, Tzekov A, Park C, Choi K, Bickel PE. OP9 mouse stromal cells rapidly differentiate into adipocytes: characterization of a useful new model of adipogenesis. J Lipid Res. 2006 Feb;47(2):450-60. doi: 10.1194/jlr.D500037-JLR200. Epub 2005 Nov 30. PMID: 16319419.
- Wu Z, Bucher NL, Farmer SR. Induction of peroxisome proliferator-activated receptor gamma during the conversion of 3T3 fibroblasts into adipocytes is mediated by C/EBPbeta, C/EBPdelta, and glucocorticoids. Mol Cell Biol. 1996 Aug;16(8):4128-36. doi: 10.1128/MCB.16.8.4128. PMID: 8754811; PMCID: PMC231409.
- Yeh WC, Cao Z, Classon M, McKnight SL. Cascade regulation of terminal adipocyte differentiation by three members of the C/EBP family of leucine zipper proteins. Genes Dev. 1995 Jan 15;9(2):168-81. doi: 10.1101/gad.9.2.168. PMID: 7531665.
- Yuen JWY, Kim DD, Procyshyn RM, Panenka WJ, Honer WG, Barr AM. A Focused Review of the Metabolic Side-Effects of Clozapine. Front Endocrinol (Lausanne). 2021 Feb 25;12:609240. doi: 10.3389/fendo.2021.609240. PMID: 33716966; PMCID: PMC7947876.
- Yuen JWY, Kim DD, Procyshyn RM, White RF, Honer WG, Barr AM. Clozapine-Induced Cardiovascular Side Effects and Autonomic Dysfunction: A Systematic Review. Front Neurosci. 2018 Apr 4;12:203. doi: 10.3389/fnins.2018.00203. PMID: 29670504; PMCID: PMC5893810.
- Zhang J, Fu M, Cui T, Xiong C, Xu K, Zhong W, Xiao Y, Floyd D, Liang J, Li E, Song Q, Chen YE. Selective disruption of PPARgamma 2 impairs the development of adipose tissue and insulin sensitivity. Proc Natl Acad Sci U S A. 2004 Jul 20;101(29):10703-8. doi: 10.1073/pnas.0403652101. Epub 2004 Jul 12. PMID: 15249658; PMCID: PMC489998.
- Zhang JW, Klemm DJ, Vinson C, Lane MD. Role of CREB in transcriptional regulation of CCAAT/enhancer-binding protein beta gene during adipogenesis. J Biol Chem. 2004 Feb 6;279(6):4471-8. doi: 10.1074/jbc.M311327200. Epub 2003 Oct 30. PMID: 14593102.
- Zhang X, Shan P, Jiang G, Cohn L, Lee PJ. Toll-like receptor 4 deficiency causes pulmonary emphysema. J Clin Invest. 2006 Nov;116(11):3050-9. doi: 10.1172/JCI28139. Epub 2006 Oct 19. PMID: 17053835; PMCID: PMC1616193.
- Zhang Y, Dallner OS, Nakadai T, Fayzikhodjaeva G, Lu YH, Lazar MA, Roeder RG, Friedman JM. A noncanonical PPARγ/RXRα-binding sequence regulates leptin expression in response to changes in adipose tissue mass. Proc Natl Acad Sci U S A. 2018 Jun 26;115(26):E6039-E6047. doi: 10.1073/pnas.1806366115. Epub 2018 Jun 11. PMID: 29891714; PMCID: PMC6042069.
- Zhao L, Yagiz Y, Xu C, Lu J, Chung S, Marshall MR. Muscadine grape seed oil as a novel source of tocotrienols to reduce adipogenesis and adipocyte inflammation. Food Funct. 2015 Jul;6(7):2293-302. doi: 10.1039/c5fo00261c. PMID: 26073057.
- Zhao J, Lendahl U, Nistér M. Regulation of mitochondrial dynamics: convergences and divergences between yeast and vertebrates. Cell Mol Life Sci. 2013 Mar;70(6):951-76. doi: 10.1007/s00018-012-1066-6. Epub 2012 Jul 18. PMID: 22806564; PMCID: PMC3578726.
- Zhu H, Itoh K, Yamamoto M, Zweier JL, Li Y. Role of Nrf2 signaling in regulation of antioxidants and phase 2 enzymes in cardiac fibroblasts: protection against reactive oxygen and nitrogen species-induced cell injury. FEBS Lett. 2005 Jun 6;579(14):3029-36. doi: 10.1016/j.febslet.2005.04.058. PMID: 15896789.
- Zorzano A, Liesa M, Palacín M. Role of mitochondrial dynamics proteins in the pathophysiology of obesity and type 2 diabetes. Int J Biochem Cell Biol. 2009 Oct;41(10):1846-54. doi: 10.1016/j.biocel.2009.02.004. Epub 2009 Feb 20. PMID: 19703653.

Appendix A: PAPER 3

Research paper

ERO1α primes the ryanodine receptor to respond to arsenite with concentration dependent Ca²⁺ release sequentially triggering two different mechanisms of ROS formation

Andrea Guidarelli [1], Andrea Spina [1], Gloria Buffi, Giulia Blandino, Mara Fiorani, Orazio Cantoni[*]

Department of Biomolecular Sciences, University of Urbino Carlo Bo, Urbino, Italy

ARTICLE INFO

ABSTRACT

A 6 h exposure of U937 cells to 2.5 μM arsenite stimulates low Ca²⁺ release from the inositol 1, 4, 5-triphosphate receptor (IP₃R), causing a cascade of causally connected events, i.e., endoplasmic reticulum oxidoreductin-1α (ERO1α) expression, activation of the ryanodine receptor (RyR), mitochondrial Ca²⁺ accumulation, mitochondrial superoxide formation and further ERO1α expression.

At greater arsenite concentrations, the release of the cation from the IP₃R and the ensuing ERO1α expression remained unchanged but were nevertheless critical to sequentially promote concentration-dependent increases in Ca²⁺ release from the RyR, NADPH oxidase activation and a third mechanism of ERO1α expression which, in analogy to the one driven by mitochondrial superoxide, was also mediated by reactive oxygen species (ROS) and devoid of effects on Ca²⁺ homeostasis.

Thus, concentration-independent stimulation of Ca²⁺ release from the IP₃R is of pivotal importance for the effects of arsenite on Ca²⁺ homeostasis. It stimulates the expression of a fraction of ERO1α that primes the RyR to respond to the metalloid with concentration-dependent Ca²⁺-release, triggering the formation of superoxide in the mitochondrial respiratory chain and *via* NADPH oxidase activation. The resulting dose-dependent ROS formation was associated with a progressive increase in ERO1α expression, which however failed to affect Ca²⁺ homeostasis, thereby suggesting that ROS, unlike IP₃R-dependent Ca²⁺ release, promote ERO1α expression in sites distal from the RyR.

1. Introduction

Human exposure to arsenic, a naturally occurring toxic metalloid, is associated with an increased incidence of an array of adverse effects, which include various types of cancers, cardiovascular pathologies, diabetes, and other diseases associated with organ toxicity (e.g., liver, skin, kidney, etc.) [1–3]. Inorganic trivalent arsenic (Na₂AsO₃, arsenite),

one of the most common forms of the metalloid present in nature, promotes the above toxic effects *via* multiple mechanisms, which can be directly triggered by its binding to protein thiols [4,5] and/or mediated by reactive oxygen species (ROS) [1,2,6].

There are two main mechanisms whereby arsenite promotes ROS formation, respectively taking place in the mitochondrial respiratory chain [7,8] and in the cytosolic compartment *via* NADPH oxidase

activation [9,10]. Since both mechanisms share the important feature of being Ca^{2+} dependent [11,12], it follows that ROS formation is strictly connected with the ability of the metalloid to mobilize the cation from the endoplasmic reticulum (ER) and to increase its concentration in the mitochondria or in cytosolic domains relevant for NADPH oxidase activation. This notion is particularly important in the case of the first mechanism, as close contact sites between the ER and mitochondria are necessary to allow Ca^{2+} transfer through the low affinity mitochondrial Ca^{2+} uniporter (MCU) [13]. High local Ca^{2+} levels (10–20 μM) indeed occur only under conditions in which the cation is released in the proximity of the MCU.

With these considerations in mind, we initially showed that low micromolar concentrations of arsenite directly stimulate Ca^{2+} release from the inositol-1,4,5-triphosphate receptor (IP_3R) [14], causing endoplasmic reticulum oxidoreductin-1α (ERO1α) expression and ERO1α-dependent activation of the ryanodine receptor (RyR) [15], critical to increase the mitochondrial Ca^{2+} concentration ($[Ca^{2+}]_m$) and promote mitochondrial superoxide (mitoO_2^-) formation [15] as well as additional expression of ERO1α which however failed to impact on Ca^{2+} homeostasis [16].

Thus, the effects mediated by the metalloid on Ca^{2+} homeostasis are not explained by a conventional Ca^{2+}-induced Ca^{2+}-release event, since the mobilization of the cation from the RyR requires IP_3R-dependent expression of ERO1α. However, it remains to be established whether RyR activation, besides being ERO1α-dependent, involves additional requirements such as the direct binding of arsenite to critical thiols. It is indeed well documented that oxidation of specific –SH groups of the RyR promotes its sensitization [17,18] and arsenite binding might promote a similar response. This issue appears important also for the comprehension of the effects mediated by greater concentrations of arsenite, failing to increase further Ca^{2+} release from the IP_3R [19] and, possibly, the downstream ERO1α expression, but nevertheless promoting a progressive increase in the release of the cation from the RyR and triggering a second mechanism of ROS formation based on NADPH oxidase activation [20]. It is therefore important to address the question of whether the mechanisms whereby concentrations of arsenite greater than 2.5 μM cause RyR activation are also ERO1α-dependent and eventually learn more about the mechanism(s) regulating the expression of the fraction (s) of ERO1α involved in the regulation of Ca^{2+} homeostasis.

We herein report that arsenite causes concentration-dependent induction of ERO1α expression and ERO1α-dependent ROS formation initially mediated by electron leakage in the respiratory chain and then by activation of NADPH oxidase. Inhibition of each, or both, of these mechanisms, reduced ERO1α expression with no consequence on ERO1α-dependent regulation of Ca^{2+} mobilization from the IP_3R or RyR, thereby implicating the IP_3R-dependent mechanism of ERO1α expression in RyR sensitization at both low and high concentrations of arsenite. Thus, an identical fraction of ERO1α primes the RyR to respond to increasing concentrations of arsenite with increasing levels of Ca^{2+} release, as a likely consequence of its direct binding to the RyR itself.

2. Materials and Methods

2.1. Chemicals

Sodium arsenite, 2-aminoethoxydiphenyl borate (2-APB), ryanodine (Ry), rotenone, apocynin, catalase, diphenyleneiodonium (DPI), hydrogen peroxide (H_2O_2), phorbol-12-myristate-13-acetate (PMA) as well most of the reagent end chemicals were purchased from Sigma-Aldrich (Milan, Italy). ISRIB and EN460 were obtained from Calbiochem (San Diego, CA). Dihydrorhodamine 123 (DHR), Fluo-4-acetoxymethyl ester and MitoSOX red were purchased from Thermo Fisher Scientific (Milan, Italy).

Sodium arsenite was prepared as 1 mM stock solution in saline A (8.182 g/l NaCl, 0.372 g/l KCl, 0.336 g/l $NaHCO_3$, and 0.9 g/l glucose, pH 7.4).

2.2. Antibodies

The antibody against β-actin (VMA00048) was purchased from Bio-Rad (Hercules, CA). Primary mouse monoclonal anti-ERO1α (sc-365526), mouse monoclonal anti-P47^{phox} (sc-17844), horseradish peroxidase-conjugated mouse secondary (sc-516102) and fluorescein isothiocyanate (FITC)-conjugated polyclonal goat anti-mouse (sc-2010) antibodies were purchased from Santa Cruz Biotechnology (Santa Cruz, CA).

2.3. Cell culture

U937 cells (pro-monocytic human myeloid leukaemia), herein defined as respiration-proficient (RP)-U937 cells, were cultured in RPMI 1640 medium (Sigma-Aldrich) supplemented with 10% foetal bovine serum (FBS, Euroclone, Celbio Biotecnologie, Milan, Italy).

Respiration deficient (RD)-U937 cells were cultured in RPMI medium containing 110 μg/ml pyruvate, 5 μg/ml uridine and 400 ng/ml ethidium bromide for 4 days, with medium change after two days, as indicated in Ref. [21].

C2C12, mouse myoblast, Wild Type (WT) and ERO1α knockout (KO) were cultured in high-glucose D-MEM (6546-Sigma-Aldrich) supplemented with 10% heat-inactivated FBS and 2 mM L-glutamine (Euroclone). Differentiation to myotubes (WT D-C2C12 and ERO1α KO D-C2C12) was performed at 80–90% of confluence in D-MEM with 1% heat-inactivated serum for four days. Details on the generation of ERO1α KO C2C12 cells are provided in Ref. [22].

All cells were cultured with penicillin (100 units/ml) and streptomycin (100 μg/ml) (Euroclone) at 37 °C in T-75 tissue culture flasks (Corning Inc., Corning, NY) gassed with an atmosphere of 95% air-5% CO_2.

2.4. Western blot analysis

Cells were lysed with RIPA buffer (Thermo Fisher Scientific) with the addition of 1 mM dithiothreitol, 1 mM Na_3VO_4, 1 mM NaF, 350 mM phenylmethylsulfonyl fluoride, 1% protease inhibitor complex, pH 7.5. Lysates were incubated on ice for 20 min and centrifuged (13,000 rpm, 10 min, 4 °C) to remove cellular debris. Protein concentrations were determined with the Bradford reagent (Bio-Rad) in SPECTRA Fluor Plus Microplate Reader Tecan (Tecan, Swiss). 30 μg of proteins for each condition were subjected to SDS-PAGE electrophoresis. Proteins were separated by polyacrylamide gel vertical electrophoresis and transferred to polyvinylidene difluoride membranes. The membranes were blocked in 5% milk and probed with primary antibodies overnight, at 4 °C. Membranes were washed 3 times for 10 min/each in Tween-Tris-buffered saline and probed with secondary antibodies anti-mouse diluted in 5% milk Tween-Tris-buffered saline for 1 h at room temperature. Antibodies against β-actin were used to assess the equal loading of the lanes. Membranes were visualized with ChemiDoc MP Imaging System (Bio-Rad) and relative amounts of proteins were quantified by densitometric analysis using Image J software.

2.5. Measurement of cytosolic Ca^{2+} levels

Cells were cultured on a cover slip in 35 mm tissue culture dishes. 4 μM Fluo-4-acetoxymethyl ester was added to the cultures in the last 30 min of arsenite exposure. After the treatments, the cells were washed three times with a phosphate buffer saline (PBS, 136 mM NaCl, 10 mM Na_2HPO_4, 1.5 mM KH_2PO_4, 3 mM KCl; pH 7.4) and examined under a BX-51 microscope (Olympus, Milan, Italy). The fluorescence intensity of oxidized Fluo-4 in cells was captured with a ToupCam (Optical Systems & Technological Instruments, Milan, Italy) using an Olympus LCAch 40 × /0.55 objective lens. The excitation and emission wavelengths were 488 and 515 nm with a 5-nm slit width for both emission and excitation. Images were collected with exposure times of 100–400 ms and
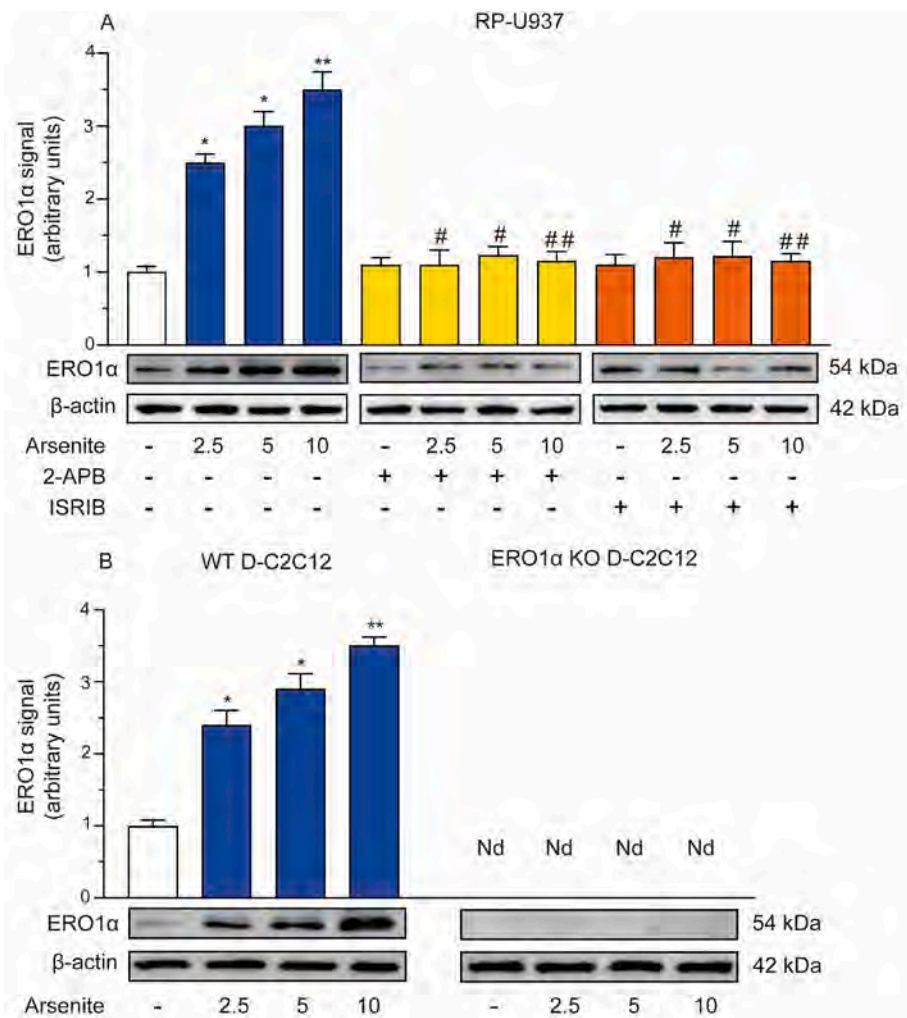
Fig. 1. Arsenite enhances the expression of ERO1α *via* concentration-dependent mechanisms.

RP-U937 (A) were exposed for 6 h to increasing concentrations of arsenite with or without 50 μM 2-APB or 0.2 μM ISRIB, as detailed in the methods section. In other experiments, WT D-C2C12 and ERO1α KO D-C2C12 (B) were exposed for 6 h to increasing concentrations of arsenite. After treatments, the cells were analyzed for ERO1α expression using a Western blot assay. Anti-β-actin antibody was used as a loading control. Results represent the means ± SD calculated from three separate experiments. (Nd, not detectable). *P < 0.05; **P < 0.01 compared with untreated cells. #P < 0.05; ##P < 0.01 compared with arsenite treated cells. (ANOVA followed by Dunnett's test).

fluorescence determination was evaluated at the single-cell level using the ImageJ software. Mean fluorescence values were determined by averaging the fluorescence values of at least 50 cells/treatment condition/experiment.

2.6. DHR and MitoSOX red fluorescence assays

Cells were cultured on a cover slip in 35 mm tissue culture dishes. Cells were then treated with arsenite and supplemented in the last 30 min with either 10 μM DHR or 5 μM MitoSOX red. In some experiments, the cells were incubated for 30 min with DHR, washed twice with PBS, and finally treated with H_2O_2 or PMA. The cells were then washed three times with PBS and fluorescence images were captured with a fluorescence microscope as previously described. The excitation and emission wavelengths were 488 and 515 nm (DHR) and 510 and 580 nm (Mito-SOX red) with a 5-nm slit width for both emission and excitation. Mean fluorescence values were determined by averaging the fluorescence values of at least 50 cells/treatment condition/experiment.

2.7. Immunofluorescence analysis

Cells were cultured on a cover slip and, after the treatments, were fixed for 1 min with 95% ethanol/5% acetic acid, washed with PBS and blocked for 30 min at room temperature with PBS-containing 2% (w/v) bovine serum albumin (BSA). The cells were then incubated overnight at 4 °C with primary anti-P47[phox] antibodies (1:100) and subsequently incubated for 3 h in the dark with fluorescently conjugated secondary

antibodies, FITC (1:100). Images were captured using a fluorescence microscope.

2.8. Statistical analysis

All the results were reported as mean ± standard deviation (SD). Statistical differences were analyzed by one-way ANOVA followed by Dunnett's test for multiple comparisons. GraphPad Prism software version 6.01 (GraphPad Software Inc., La Jolla, CA) was used for creating graphs and data analysis. The P value of <0.05 indicated statistical significance.

3. Results

3.1. Arsenite induces ERO1α expression in a concentration-dependent fashion

In our initial experiments, RP-U937 cells were exposed for 6 h to 2.5–10 μM arsenite and immediately analyzed for ERO1α expression. Interestingly, ERO1α immunoreactivity progressively increased in cells treated with increasing concentrations of the metalloid *via* a mechanism suppressed by ISRIB, an inhibitor of eukaryotic translation initiation factor 2α phosphorylation [23], or 2-APB, an IP3R antagonist [24] (Fig. 1A). Under identical conditions, arsenite also increased ERO1α expression in a concentration-dependent fashion in WT ERO1α D-C2C12 (Fig. 1B), with no evidence of ERO1α expression in both untreated and treated ERO1α KO D-C2C12 (Fig. 1B).
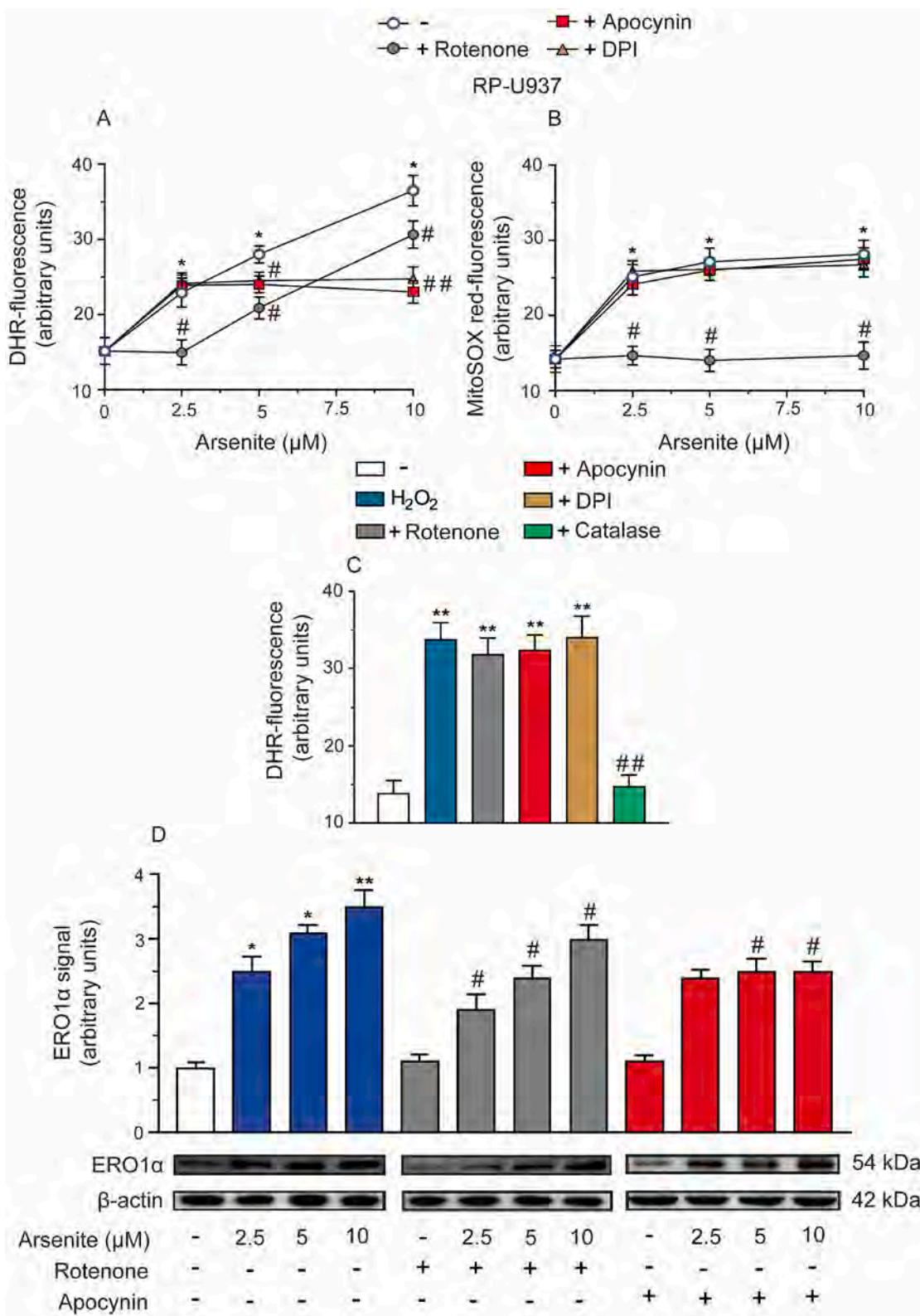
Fig. 2. Arsenite increases ERO1α expression *via* a ROS-independent and two different ROS-dependent mechanisms.
RP-U937 (A–D) or RD-U937 (E, F) were incubated for 6 h with increasing concentrations of arsenite in the absence or presence of the various addition indicated in the figure panels. After treatments, the cells were analyzed for DHR- (A, E) or MitoSOX red- (B, inset in E) fluorescence and ERO1α protein expression (D, F), as detailed in the Materials and Methods section. Anti-β-actin antibody was used as a loading control. In other experiments, RP-U937 (C) were incubated for 15 min with 100 μM H_2O_2, alone or associated with other additions, and analyzed for DHR-fluorescence. Results represent the means ± SD calculated from three separate experiments. *P < 0.05; **P < 0.01 compared with untreated cells. #P < 0.05; ##P < 0.01 compared with treated cells. (ANOVA followed by Dunnett's test).

Fig. 2. (*continued*).

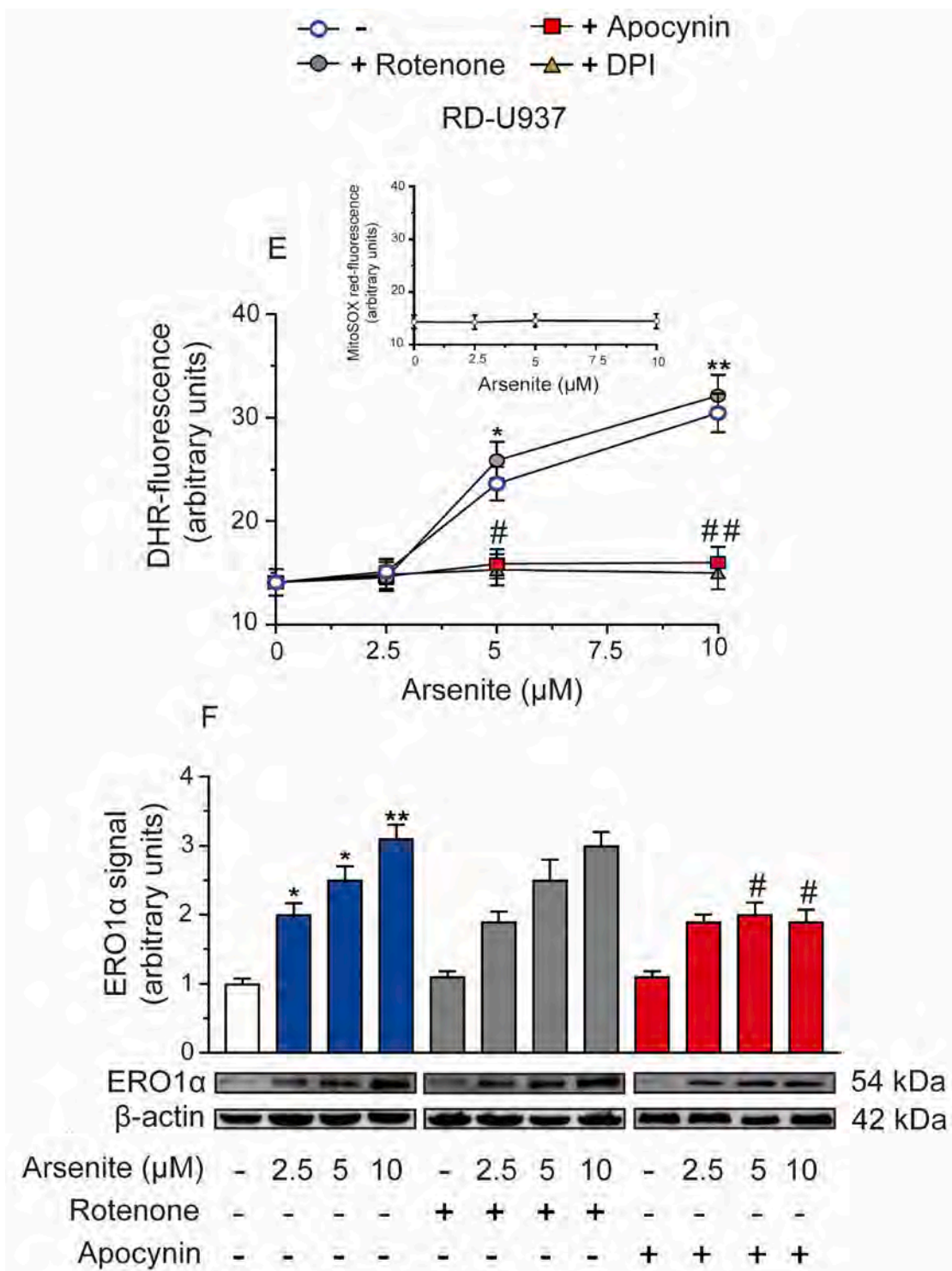These results indicate that arsenite induces a concentration-dependent increase in ERO1α expression in two remarkably different cell types. Furthermore, based on these and our previous findings [15], this response likely involves multiple mechanisms triggered by an initial stimulation of Ca^{2+} release from the IP_3R directly mediated by the metalloid [16]. The recent observation that 2.5 μM arsenite promotes ERO1α expression *via* both a ROS-dependent and -independent mechanisms [16], is consistent with the possibility that a ROS-dependent mechanism accounts for the progressive increase in ERO1α expression detected at high arsenite concentrations.

3.2. Arsenite induces ERO1α expression via three separate and sequential mechanisms: the third one is mediated by NADPH oxidase-derived ROS

The first set of experiments was performed in RP-U937 cells exposed for 6 h to increasing concentrations of arsenite. Using identical conditions, we previously showed that the formation of mitochondrial ROS saturates at 2.5 μM arsenite [25] and that increasing levels of ROS are then generated by greater concentrations of the metalloid *via* NADPH-oxidase activation [20].

In these experiments, we used DHR, a probe sensitive to H_2O_2 and
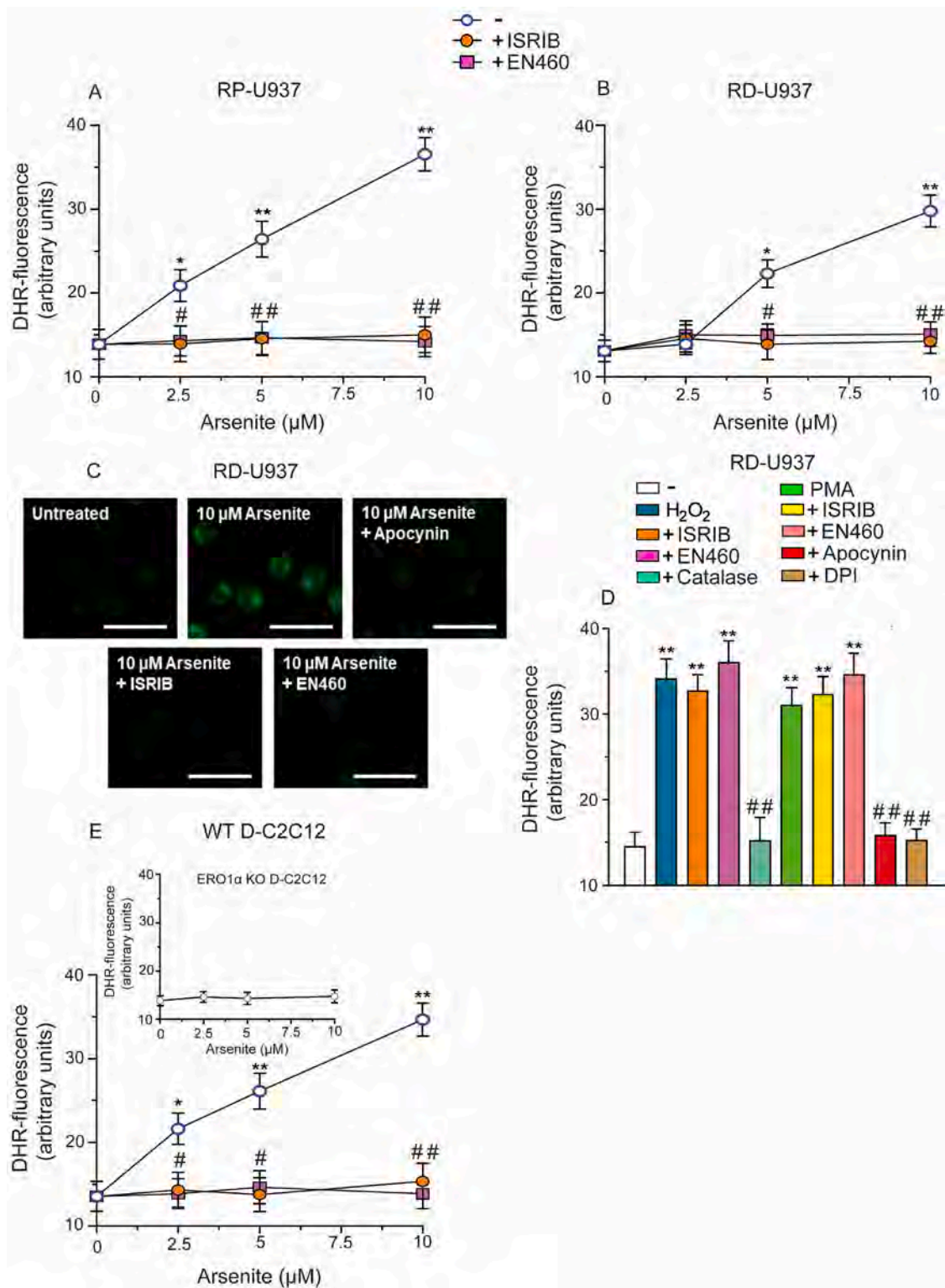
Fig. 3. Inhibition of expression/activity, or genetic deletion, of ERO1α suppresses mitochondrial as well as NADPH oxidase derived $O_2^{\bullet-}$ formation induced by increasing concentrations of arsenite.

RP-U937 (A), RD-U937 (B), WT-D C2C12 (E) and ERO1α KO D-C2C12 (inset to panel E) were exposed for 6 h to increasing concentrations of arsenite, with or without the indicated additions. After treatments, the cells were analyzed for DHR-fluorescence. Representative micrographs indicative of p47^{phox} phosphorylation in RD-cells exposed for 6 h to 10 μM arsenite in the absence or presence of the indicated additions (C). After treatments the cells were fixed and processed for the immunocytochemical detection of phosphorylated p47^{phox}. Scale bar represents 20 μm. In other experiments, RD-U937 were exposed for 15 min to 100 μM H_2O_2 or 0.162 μM PMA, in the absence or presence of the additions indicated in panel D. After treatments, the cells were analyzed for DHR-fluorescence. Results represent the means ± SD calculated from three separate experiments. *P < 0.05; **P < 0.01 compared with untreated cells. #P < 0.05; ##P < 0.01 compared with treated cells. (ANOVA followed by Dunnett's test).

various other ROS [26] released in different subcellular compartments, which include the mitochondria, since mitoO$_2^-$ readily dismutates to diffusible H$_2$O$_2$ [12]. Consistently, the DHR fluorescence response induced by 2.5 μM arsenite was suppressed by the complex I inhibitor rotenone (0.5 μM, [27]), which therefore partially inhibited also the DHR fluorescence response induced by greater arsenite concentrations (Fig. 2A). Instead two different inhibitors of NADPH oxidase, apocynin (10 μM) or DPI (1 μM) [11], blunted the rotenone resistant DHR fluorescence response, thereby providing identical residual fluorescence responses at the three different arsenite concentrations.

We also performed similar experiments in which DHR was replaced with MitoSOX red, a probe selectively detecting mitoO$_2^-$ [28]. Under these conditions, the fluorescence response was maximally induced by 2.5 μM arsenite and was both sensitive to rotenone and insensitive to the NADPH oxidase inhibitors (Fig. 2B).

As a final note, rotenone, apocynin or DPI failed to affect the DHR fluorescence response induced by a 15 min exposure to 100 μM H$_2$O$_2$, instead suppressed by 10 sigma units/ml catalase (Fig. 2C). The responses illustrated in Fig. 2A–C collectively suggest that, at least under the conditions employed in our experiments, the inhibitory effects mediated by rotenone, or the NADPH oxidase inhibitors, are not attributable to confounding iron chelating and/or antioxidant activities. Further indication in this direction is provided below.

With the above information in mind, we moved to other experiments aimed at establishing the role of mitochondrial and NADPH-derived ROS in the regulation of ERO1α expression. The results illustrated in Fig. 2D show that rotenone only marginally reduces the extent of ERO1α expression mediated by each of the concentrations of the metalloid tested. Under identical conditions, apocynin blunted the expression of ERO1α mediated by 5 or 10 μM arsenite, so that the expression of the protein was identical after exposure to the three different concentrations of the metalloid. As a final note, there was a residual ROS-independent mechanism induced by arsenite in a concentration-independent fashion which, based on the sensitivity to 2-APB (Fig. 1A), appears to be critically connected with the initial stimulation of Ca^{2+} release from the IP$_3$R.

To corroborate the above findings, we used RD-U937 cells, i.e., cells devoid of a functional respiratory chain. These cells therefore failed to respond to arsenite with the formation of mitoO$_2^-$ and the resulting DHR fluorescence was insensitive to rotenone (Fig. 2E) and like that obtained in RP-U937 cells treated with the metalloid in the presence of rotenone (Fig. 2A). Furthermore, under identical conditions, there was no detectable increase in MitoSOX red fluorescence (inset to Fig. 2E). Most importantly, the DHR fluorescence response induced by arsenite in RD-U937 cells was suppressed by apocynin, or DPI (Fig. 2E).

Consistently with the previous results obtained in RP-U937 cells, arsenite induced a concentration-dependent increase in ERO1α expression also in RD-U937 cells and this response was insensitive to rotenone and significantly inhibited by apocynin (Fig. 2F). More specifically, identical levels of ERO1α expression were detected in cells treated with the three different concentrations of arsenite. As a final note, evidence for the same ROS-independent mechanism of ERO1α expression previously observed in RP-U937 cells (Fig. 2D) was also obtained in RD-U937 cells.

The results presented in this section, obtained using respiration proficient and deficient cells as well as various inhibitors employed under strictly controlled conditions, indicate that arsenite induces a concentration-dependent expression of ERO1α via three different mechanisms. The first one, which is ROS independent, is indeed followed by a mechanism initiated by mitoO$_2^-$ and by an additional mechanism driven by NADPH-oxidase-derived O$_2^-$.

3.3. ERO1α dependence of the two mechanisms of ROS formation induced by arsenite

Having previously demonstrated that the formation of mitochondrial
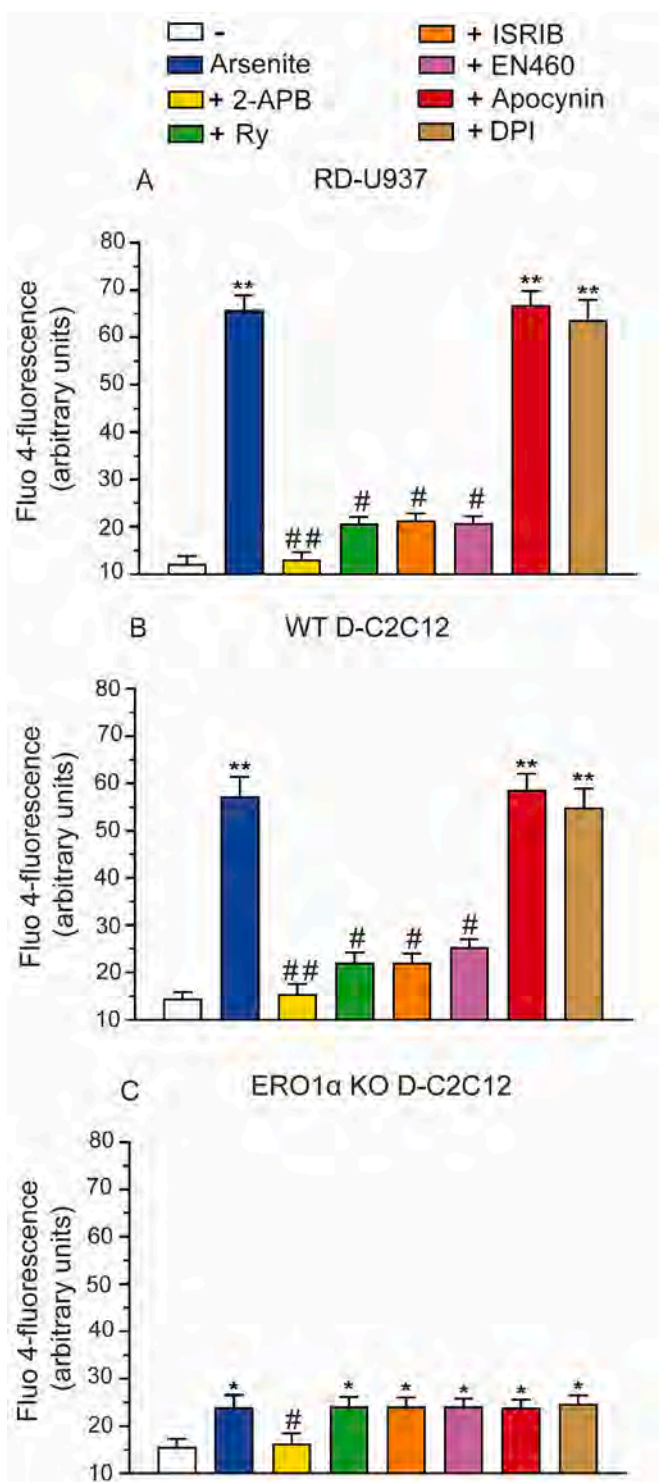
Fig. 4. The fraction of ERO1α generated by NADPH oxidase-derived ROS fails to affect the Ca^{2+} response mediated by arsenite.

RD-U937 (A), WT D-C2C12 (B) and ERO1α KO D-C2C12 (C) were exposed for 6 h to 10 μM arsenite, with or without the indicated additions. After treatments, the cells were analyzed for Fluo 4-fluorescence. Results represent the means ± SD calculated from three separate experiments. *P < 0.05; **P < 0.01 compared with untreated cells. #P < 0.05; ##P < 0.01 compared with arsenite treated cells. (ANOVA followed by Dunnett's test).

ROS induced by arsenite is ERO1α-dependent [15], we wondered whether the same was also true for NADPH-derived ROS. We therefore recapitulated our previous findings [16,29] indicating that mitochondrial ROS formation induced by 2.5 μM arsenite is blunted by ISRIB as well as EN460, an inhibitor of ERO1α [30]. Interestingly, both inhibitors also suppressed the DHR fluorescence response induced by increasing concentrations of arsenite in RP- (Fig. 3A) and RD- (Fig. 3B) U937 cells. The results illustrated in Fig. 3C provide immunocytochemical evidence of NADPH oxidase activation after treatment of RD-U937 cells with 10 μM arsenite. NADPH oxidase activity was suppressed by apocynin, ISRIB or EN460.

Inhibitors of ERO1α activity or expression instead failed to affect the catalase sensitive DHR fluorescence response induced by a 15 min exposure to 100 μM H_2O_2 (Fig. 3D), thereby supporting the notion that their effects are specifically linked to inhibition or ERO1α activity or expression. This notion was also corroborated by the demonstration that EN460 and ISRIB also failed to affect the PMA (0.162 μM)-dependent DHR fluorescence response, instead suppressed by apocynin or DPI.

These results argue in favor of the specificity of the effects mediated by the above inhibitors (Fig. 3A–C).

We finally performed experiments using WT D-C2C12, which responded to increasing concentrations of arsenite with DHR fluorescence responses suppressed by both EN460 and ISRIB (Fig. 3E), as observed in RP- (Fig. 3A) or RD- (Fig. 3B) cells. In addition, there was no detectable fluorescent signal in ERO1α KO D-C2C12 cells exposed to increasing concentrations of arsenite (inset to Fig. 3E).

The above results indicate that inhibitors of ERO1α activity or expression, as the genetic deletion of ERO1α, suppress both mitochondrial· and NADPH oxidase derived $O_2^{\cdot-}$ formation mediated by arsenite. These findings are therefore consistent with the notion that ROS formation induced by increasing concentrations of arsenite through two different mechanisms is ERO1α dependent.

3.4. ROS dependent mechanisms of ERO1α expression bear no consequences on Ca^{2+} homeostasis

The results presented above might suggest the existence of a positive amplification loop in which ERO1α expression is both the cause and the consequence of ROS formation mediated by two distinct mechanisms sequentially triggered by increasing concentrations of arsenite. However, ROS formation is Ca^{2+}-dependent, and we previously described two mechanisms of ERO1α expression [16] bearing different consequences on Ca^{2+} homeostasis and hence on ROS formation.

We therefore performed studies using RD-U937 cells exposed to 10 μM arsenite, which exclusively produce $O_2^{\cdot-}$ via NADPH oxidase activation, with the aim of assessing the role of the ROS-independent and NADPH derived ROS-dependent fractions of ERO1α on Ca^{2+} homeostasis. We found that, under these conditions, arsenite significantly and concentration-dependently elevates the cytosolic Ca^{2+} concentrations ($[Ca^{2+}]_c$) via a mechanism suppressed by 2-APB (Fig. 4A). In addition, the observed Ca^{2+} responses were partially and similarly inhibited by Ry (20 μM), an antagonist of the RyR [31], EN460 or ISRIB, thereby suggesting that increasing arsenite concentrations ERO1α targets the RyR to promote increasing levels of Ca^{2+} release. Interestingly, however, apocynin and DPI, used under the same conditions previously shown to suppress NADPH-derived ROS formation (Fig. 2A), failed to affect the Ca^{2+} response mediated by arsenite and, more specifically, to affect the amount of the cation released by the RyR. Thus, these results confirm the involvement of the ROS-independent mechanism of ERO1α expression in Ca^{2+} mobilization from the RyR and indicate that the fraction of ERO1α generated by NADPH oxidase-dependent mechanism fails to affect Ca^{2+} homeostasis, as previously observed for the mitoO$_2^{\cdot-}$-dependent mechanism [16].

Experiments using WT and ERO1α KO D-C2C12 provided consistent outcomes. Indeed, WT D-C2C12 responded to 10 μM arsenite with an increased $[Ca^{2+}]_c$ similarly inhibited by Ry, EN460 or ISRIB and

unaffected by apocynin or DPI (Fig. 4B). ERO1α KO D-C2C12 cells instead responded to the metalloid with a small increase in the $[Ca^{2+}]_c$ insensitive to all the above inhibitors (Fig. 4C). Finally, 2-APB suppressed the increase in $[Ca^{2+}]_c$ in both cell types (Fig. 4B and C).

Taken together, the above results indicate that the ROS independent mechanism of ERO1α expression maximally induced by 2.5 μM arsenite is critically connected with the concentration-dependent activation of the RyR. This observation is therefore compatible with the notion that ERO1α sensitizes the RyR to the direct effects of arsenite, presumably mediated by its direct binding to critical thiols. Instead, as we previously found for the mitoO$_2^{\cdot-}$-dependent mechanism of ERO1α expression [16], the NADPH oxidase mediated ERO1α expression, induced by arsenite in a concentration-dependent fashion, fails to promote a detectable effect on RyR activity, and more generally on Ca^{2+} homeostasis.

4. Discussion

Arsenite promotes the formation of ROS in the mitochondrial respiratory chain [19] and via stimulation of NADPH oxidase activity [20], i.e., two different mechanisms induced under specific conditions in which the $[Ca^{2+}]$ requirements are met in defined microdomains. The first mechanism is triggered by low concentrations of the metalloid in cells expressing both the IP$_3$R and RyR, with the second channel being in close apposition with the mitochondria [19] to generate high Ca^{2+} microdomains required for low affinity transport of the cation through the MCU [13]. Importantly, RyR activation was regulated by an initial direct stimulation of the IP$_3$R [14] and by the ensuing ER stress response associated with increased ERO1α expression [15]. Moreover, the resulting mitoO$_2^{\cdot-}$ formation caused a further expression of ERO1α with no apparent impact on Ca^{2+} homeostasis [16].

Our interpretation of these findings is that local ER stress responses promote the formation of ERO1α in sub-cellular microdomains which either do (the one driven by IP$_3$R-released Ca^{2+}), or do not, (the one driven by mitoO$_2^{\cdot-}$) impact on RyR activity. The first mechanism therefore leads to ERO1α accumulation in the close vicinity of the RyR, most likely in the mitochondria-associated endoplasmic reticulum membranes (MAMs), since the RyR itself appears to be expressed in close apposition with the mitochondria.

Indirect evidence for this specific localization of the RyR was previously obtained in the same U937 cells employed in this study, so that the fraction of Ca^{2+} taken up by the mitochondria was always derived from this channel, also after agonist stimulation of the IP$_3$R [19]. IP$_3$R-derived Ca^{2+} was instead directly cleared by the mitochondria in the same cell type after RyR downregulation [19]. Consistently, C2C12-derived myotubes which gain RyR expression with differentiation [32,33] responded to IP$_3$ releasing agonists, or arsenite, as U937 cells [19]. In contrast, IP$_3$R-derived Ca^{2+} was directly taken up by the mitochondria in C2C12 myoblasts as well as in other cell types devoid of RyR, after agonist stimulation, with hardly any effect being detected with arsenite.

An important observation from our previous work [19], in part recapitulated in the present study, is that increasing levels of arsenite promote concentration-dependent increases in the $[Ca^{2+}]_c$, entirely derived from the RyR and associated with ROS formation via NADPH oxidase activation, which implies the existence of mechanisms of concentration-dependent regulation of RyR activity. Thus, a simple explanation would be that arsenite promotes concentration-dependent stimulation of the IP$_3$R, and of the associated ER stress response-dependent ERO1α expression, thereby increasing the fraction of the oxidoreductase in the close vicinity of the RyR. This hypothesis, however, conflicts with our previous findings indicating that arsenite stimulation of the IP$_3$R is not concentration-dependent, and in fact saturates at the same low arsenite concentrations promoting maximal mitoO$_2^{\cdot-}$ formation [19].

On the other hand, ERO1α expression was increased by arsenite in a concentration-dependent fashion, with the involvement of the two
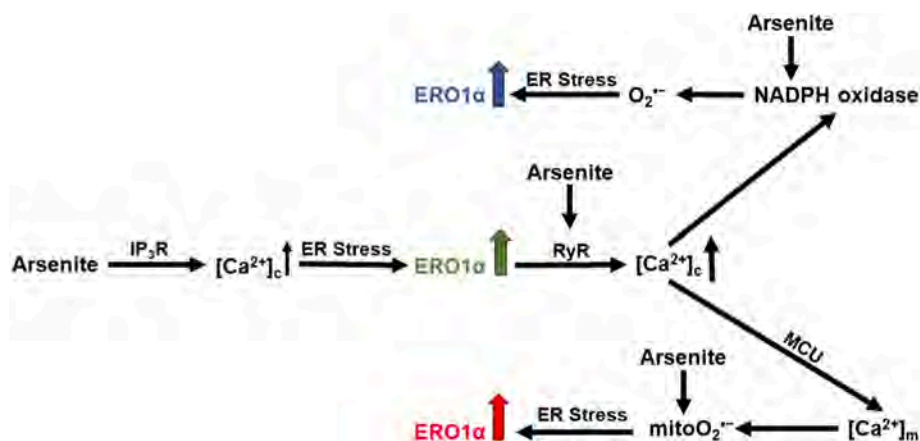
Fig. 5. Mechanisms regulating the interplay among various effects observed at increasing arsenite concentrations, namely ERO1α expression, Ca^{2+} mobilization/mitochondrial accumulation and regulation of two different mechanisms of ROS formation.

Arsenite directly stimulates the IP_3R *via* a mechanism saturating at low concentrations. The resulting limited Ca^{2+} release was causally linked to the triggering of an ER stress dependent accumulation of ERO1α (green arrow). ERO1α expression/activity mediated by this mechanism represents a condition necessary but not sufficient for promoting further Ca^{2+} release from the RyR, an event requiring direct effects mediated by the metalloid on the channel. The amount of the cation released by the RyR was a direct function of the arsenite concentrations. Low Ca^{2+} release from the RyR stimulated by the low concentrations of arsenite fails to promote NADPH oxidase activation, but nevertheless leads to the mitochondrial accumulation of the cation, thereby promoting, in conjunction with the direct effects of arsenite in mitochondria, ROS formation in the mitochondrial respiratory chain. This response was maximally induced at low arsenite concentrations. Importantly, this mechanism of ROS formation drives a second mechanism of ERO1α expression (red arrow), which however fails to impact on the regulation of Ca^{2+} homeostasis. At greater arsenite concentrations, ROS formation increases dose-dependently consequently to Ca^{2+}-dependent NADPH oxidase activation. Under these conditions, a second mechanism of ROS dependent ERO1α expression (blue arrow) ensues, which, as the previous one indicated by the red arrow, is devoid of effects of Ca^{2+} homeostasis.

previously mentioned mechanisms as well as of a third one, exclusively driven by the high concentrations of arsenite. In principle, this last mechanism could be triggered by RyR-derived Ca^{2+}, thereby fostering a positive feed-back mechanism in which Ca^{2+} promotes further Ca^{2+} release *via* ERO1α dependent RyR sensitization. The outcome of our experiments, however, was not entirely consistent with this hypothesis since RyR activation failed to directly cause ERO1α expression. However, RyR derived Ca^{2+} was nevertheless critically connected with ERO1α expression, since an increased $[Ca^{2+}]_c$ is required for NADPH oxidase activation, which in fact triggers the third mechanism of ERO1α expression *via* the resulting ROS formation.

Most importantly, we also found that inhibition of this ROS response had no consequence on Ca^{2+} homeostasis, as previously shown for the mitoO$_2^-$ driven ERO1α expression [16], an observation suggesting that ROS, regardless of whether generated in the mitochondria or in the cytosol, cause an ER stress response leading to ERO1α expression in compartments distal to the RyR and hence unable to affect Ca^{2+} release from this channel.

The observation that ROS stimulate ERO1α expression is not surprising, as the ability of these species to increase this response has been previously documented [34]. On the other hand, it is interesting to observe that, in the arsenite toxicity paradigm under investigation, ERO1α expression linearly increases in response to ROS generated in mitochondria (i.e., in the respiratory chain) and in other membrane bound compartments (i.e., by NADPH oxidase). Although the diffusible nature of H_2O_2 is compatible with the induction of distal effects, it makes sense to hypothesize that mitochondria and NADPH oxidase are in the close vicinity of specific sites of the ER in which local ROS-dependent ER stress responses lead to ERO1α expression. These same sites, however, are apparently distal from the RyR, which would explain why the activity of this channel is not regulated by the fraction of ERO1α generated *via* the ROS-dependent mechanisms.

Thus, the overall interpretation of the above results is that the fraction of ERO1α expressed *via* the ROS-independent mechanism, i.e., in response to IP_3R derived Ca^{2+} release, while maximally induced by the low arsenite concentrations, is nevertheless critically connected with RyR stimulation and mitochondrial Ca^{2+} accumulation required for the formation of mitoO$_2^-$ [16] as well as with the amplification of the Ca^{2+} response leading to concentration-dependent NADPH oxidase activation.

In conclusion, we herein provide experimental results indicative of

an effect of ERO1α on the RyR, necessary but not sufficient to promote Ca^{2+} release from this channel. However, RyR sensitization is mediated by a fraction of ERO1α, most likely localized in the MAMs, generated by IP_3R dependent Ca^{2+} release saturating at low concentrations of the metalloid. The increasing levels of Ca^{2+} release from the RyR induced at increasing arsenite concentrations are therefore likely regulated by a priming effect of ERO1α in conjunction with the binding of the metalloid to specific thiols of the RyR. The mitochondrial and NADPH oxidase dependent mechanisms of ROS release recruited at increasing concentrations of the metalloid instead promote ERO1α expression in compartments of the ER different from the MAMs, failing to affect RyR activity and, more generally, Ca^{2+} homeostasis. A scheme summarizing the molecular mechanisms involved in the arsenite-induced dose-dependent regulation of ERO1α expression, Ca^{2+} mobilization from the IP_3R and RyR, O$_2^-$ formation in mitochondria or through NADPH oxidase activation, as well as in the interplay among these mechanisms is provided in Fig. 5.

CRediT authorship contribution statement

Andrea Guidarelli: Investigation, coordinated the experiments, contributed to the design of the study, data curation, reviewed the manuscript, funding acquisition. Andrea Spina: Investigation, data curation. Gloria Buffi: Investigation, data curation. Giulia Blandino: Investigation, data curation. Mara Fiorani: Investigation, data curation, reviewed the manuscript. Orazio Cantoni: Project administration, contributed to the design of the study, wrote, reviewed, and edited the manuscript.

Declaration of competing interest

The authors declare that they have no known competing financial interests or personal relationships that could have appeared to influence the work reported in this paper.

Data availability

Data will be made available on request.

References

[1] S.J. Flora, Arsenic-induced oxidative stress and its reversibility, Free Radic. Biol. Med. 51 (2) (2011) 257–281.
[2] K. Jomova, Z. Jenisova, M. Feszterova, S. Baros, J. Liska, D. Hudecova, C.J. Rhodes, M. Valko, Arsenic: toxicity, oxidative stress and human disease, J. Appl. Toxicol. 31 (2) (2011) 95–107.
[3] B.C. Minatel, A.P. Sage, C. Anderson, R. Hubaux, E.A. Marshall, W.L. Lam, V. D. Martinez, Environmental arsenic exposure: from genetic susceptibility to pathogenesis, Environ. Int. 112 (2018) 183–197.
[4] Y.Y. Chang, T.C. Kuo, C.H. Hsu, D.R. Hou, Y.H. Kao, R.N. Huang, Characterization of the role of protein-cysteine residues in the binding with sodium arsenite, Arch. Toxicol. 86 (6) (2012) 911–922.
[5] S. Shen, X.F. Li, W.R. Cullen, M. Weinfeld, X.C. Le, Arsenic binding to proteins, Chem. Rev. 113 (10) (2013) 7769–7792.
[6] Y. Hu, J. Li, B. Lou, R. Wu, G. Wang, C. Lu, H. Wang, J. Pi, Y. Xu, The role of reactive oxygen species in arsenic toxicity, Biomolecules 10 (2) (2020).
[7] S.X. Liu, M.M. Davidson, X. Tang, W.F. Walker, M. Athar, V. Ivanov, T.K. Hei, Mitochondrial damage mediates genotoxicity of arsenic in mammalian cells, Cancer Res. 65 (8) (2005) 3236–3242.
[8] S. Wei, T. Qiu, X. Yao, N. Wang, L. Jiang, X. Jia, Y. Tao, Z. Wang, P. Pei, J. Zhang, Y. Zhu, G. Yang, X. Liu, S. Liu, X. Sun, Arsenic induces pancreatic dysfunction and ferroptosis via mitochondrial ROS-autophagy-lysosomal pathway, J. Hazard Mater. 384 (2020), 121390.
[9] A. Lemarie, E. Bourdonnay, C. Morzadec, O. Fardel, L. Vernhet, Inorganic arsenic activates reduced NADPH oxidase in human primary macrophages through a Rho kinase/p38 kinase pathway, J. Immunol. 180 (9) (2008) 6010–6017.
[10] A.C. Straub, K.A. Clark, M.A. Ross, A.G. Chandra, S. Li, X. Gao, P.J. Pagano, D. B. Stolz, A. Barchowsky, Arsenic-stimulated liver sinusoidal capillarization in mice requires NADPH oxidase-generated superoxide, J. Clin. Invest. 118 (12) (2008) 3980–3989.
[11] R.P. Brandes, N. Weissmann, K. Schroder, Nox family NADPH oxidases: molecular mechanisms of activation, Free Radic. Biol. Med. 76 (2014) 208–226.
[12] D.B. Zorov, M. Juhaszova, S.J. Sollott, Mitochondrial reactive oxygen species (ROS) and ROS-induced ROS release, Physiol. Rev. 94 (3) (2014) 909–950.
[13] Y. Kirichok, G. Krapivinsky, D.E. Clapham, The mitochondrial calcium uniporter is a highly selective ion channel, Nature 427 (6972) (2004) 360–364.
[14] A. Guidarelli, M. Fiorani, O. Cantoni, Low concentrations of arsenite target the intraluminal inositol 1, 4, 5-trisphosphate receptor/ryanodine receptor crosstalk to significantly elevate intracellular Ca^{2+}, J. Pharmacol. Exp. Therapeut. 367 (1) (2018) 184–193.
[15] A. Spina, A. Guidarelli, M. Fiorani, E. Varone, A. Catalani, E. Zito, O. Cantoni, Crosstalk between ERO1alpha and ryanodine receptor in arsenite-dependent mitochondrial ROS formation, Biochem. Pharmacol. 198 (2022), 114973.
[16] A. Guidarelli, A. Spina, M. Fiorani, E. Zito, O. Cantoni, Arsenite enhances ERO1alpha expression via ryanodine receptor dependent and independent mechanisms, Environ. Toxicol. Pharmacol. 98 (2023), 104080.
[17] K. Anzai, K. Ogawa, T. Ozawa, H. Yamamoto, Oxidative modification of ion channel activity of ryanodine receptor, Antioxidants Redox Signal. 2 (1) (2000) 35–40.
[18] Q.A. Sun, B. Wang, M. Miyagi, D.T. Hess, J.S. Stamler, Oxygen-coupled redox regulation of the skeletal muscle ryanodine receptor/Ca2+ release channel (RyR1): sites and nature of oxidative modification, J. Biol. Chem. 288 (32) (2013) 22961–22971.
[19] A. Guidarelli, A. Catalani, A. Spina, E. Varone, S. Fumagalli, E. Zito, M. Fiorani, O. Cantoni, Functional organization of the endoplasmic reticulum dictates the susceptibility of target cells to arsenite-induced mitochondrial superoxide formation, mitochondrial dysfunction and apoptosis, Food Chem. Toxicol. 156 (2021), 112523.
[20] A. Guidarelli, M. Fiorani, L. Cerioni, O. Cantoni, The compartmentalised nature of the mechanisms governing superoxide formation and scavenging in cells exposed to arsenite, Toxicol. Appl. Pharmacol. 384 (2019), 114766.
[21] A. Guidarelli, M. Fiorani, S. Carloni, L. Cerioni, W. Balduini, O. Cantoni, The study of the mechanism of arsenite toxicity in respiration-deficient cells reveals that NADPH oxidase-derived superoxide promotes the same downstream events mediated by mitochondrial superoxide in respiration-proficient cells, Toxicol. Appl. Pharmacol. 307 (2016) 35–44.
[22] E. Varone, D. Pozzer, S. Di Modica, A. Chernorudskiy, L. Nogara, M. Baraldo, M. Cinquanta, S. Fumagalli, R.N. Villar-Quiles, M.G. De Simoni, B. Blaauw, A. Ferreiro, E. Zito, SELENON (SEPN1) protects skeletal muscle from saturated fatty acid-induced ER stress and insulin resistance, Redox Biol. 24 (2019), 101176.
[23] C. Sidrauski, A.M. McGeachy, N.T. Ingolia, P. Walter, The small molecule ISRIB reverses the effects of eIF2alpha phosphorylation on translation and stress granule assembly, Elife 4 (2015).
[24] M.J. Berridge, The inositol trisphosphate/calcium signaling pathway in health and disease, Physiol. Rev. 96 (4) (2016) 1261–1296.
[25] A. Guidarelli, L. Cerioni, M. Fiorani, A. Catalani, O. Cantoni, Arsenite-induced mitochondrial superoxide formation: time and concentration requirements for the effects of the metalloid on the endoplasmic reticulum and mitochondria, J. Pharmacol. Exp. Therapeut. 373 (1) (2020) 62–71.
[26] A. Gomes, E. Fernandes, J.L. Lima, Fluorescence probes used for detection of reactive oxygen species, J. Biochem. Biophys. Methods 65 (2–3) (2005) 45–80.
[27] M. Degli Esposti, Inhibitors of NADH-ubiquinone reductase: an overview, Biochim. Biophys. Acta 1364 (2) (1998) 222–235.
[28] P. Mukhopadhyay, M. Rajesh, G. Hasko, B.J. Hawkins, M. Madesh, P. Pacher, Simultaneous detection of apoptosis and mitochondrial superoxide production in live cells by flow cytometry and confocal microscopy, Nat. Protoc. 2 (9) (2007) 2295–2301.
[29] A. Guidarelli, A. Spina, M. Fiorani, E. Zito, O. Cantoni, Inhibition of activity/expression, or genetic deletion, of ERO1alpha blunts arsenite geno- and cyto-toxicity, Food Chem. Toxicol. 168 (2022), 113360.
[30] J.D. Blais, K.T. Chin, E. Zito, Y. Zhang, N. Heldman, H.P. Harding, D. Fass, C. Thorpe, D. Ron, A small molecule inhibitor of endoplasmic reticulum oxidation 1 (ERO1) with selectively reversible thiol reactivity, J. Biol. Chem. 285 (27) (2010) 20993–21003.
[31] G. Meissner, The structural basis of ryanodine receptor ion channel function, J. Gen. Physiol. 149 (12) (2017) 1065–1089.
[32] J.A. Airey, M.D. Baring, J.L. Sutko, Ryanodine receptor protein is expressed during differentiation in the muscle cell lines BC3H1 and C2C12, Dev. Biol. 148 (1) (1991) 365–374.
[33] P. Tarroni, D. Rossi, A. Conti, V. Sorrentino, Expression of the ryanodine receptor type 3 calcium release channel during development and differentiation of mammalian skeletal muscle cells, J. Biol. Chem. 272 (32) (1997) 19808–19813.
[34] G. Li, C. Scull, L. Ozcan, I. Tabas, NADPH oxidase links endoplasmic reticulum stress, oxidative stress, and PKR activation to induce apoptosis, J. Cell Biol. 191 (6) (2010) 1113–1125.